INELASTIC DEFORMATION AND FAILURE ANALYSIS OF FILAMENT-WOUND COMPOSITE STRUCTURES

Final Report

By Wan-Lee Yin, Gerald A. Wempner and Zhizhong Fei

October 1991

U.S. ARMY RESEARCH OFFICE

CONTRACT NUMBER: DAAL03-88-K-0071

GEORGIA INSTITUTE OF TECHNOLOGY

ATLANTA, GEORGIA

MASTER COPY KEEP THIS COPY FOR REPRODUCTION PURPOSES

REPORT DOCUMENTATION PAGE

Form Approved
OMB No 0704-0188

1. AGENCY USE ONLY (Leave blank)	2. REPORT DATE	3. REPORT TYPE AND DATES COVERED
	October 1991	Final, 1 May 88 - 31 August 91

4. TITLE AND SUBTITLE
Inelastic Deformation and Failure Analysis of Filament-Wound Composite Structure

5. FUNDING NUMBERS
DAAL03-88-K-0071

6. AUTHOR(S)
Wan-Lee Yin, Gerald A. Wempner and Zhizhong Fei

7. PERFORMING ORGANIZATION NAME(S) AND ADDRESS(ES)
Georgia Institute Of Technology
School of Civil Engineering
Atlanta, GA 30332

8. PERFORMING ORGANIZATION REPORT NUMBER

9. SPONSORING/MONITORING AGENCY NAME(S) AND ADDRESS(ES)
U. S. Army Research Office
P. O. Box 12211
Research Triangle Park, NC 27709-2211

10. SPONSORING/MONITORING AGENCY REPORT NUMBER
ARO 25460.7-EG

11. SUPPLEMENTARY NOTES
The view, opinions and/or findings contained in this report are those of the author(s) and should not be construed as an official Department of the Army position, policy, or decision, unless so designated by other documentation.

12a. DISTRIBUTION/AVAILABILITY STATEMENT
Approved for public release; distribution unlimited.

12b. DISTRIBUTION CODE

13. ABSTRACT (Maximum 200 words)

Several fundamental problems associated with the mechanical behavior and failure of filament-wound composite structures are studied. Available experimental results on pressure testing of filament-wound composite tubes are analyzed to formulate the incremental constitutive relations of a filament layer under deformations with a large shear strain, and to correlate the intrinsic strain paths preceding the failure of the filament layer with the various failure modes of the structure. Implication of the results to the analysis of filament-wound structures is described. Micromechanical analyses using the boundary element method are conducted to determine the composite gross elastic moduli in terms of the constituent properties, and to study the fracture mechanics problems associated with fiber-matrix debonding and oblique matrix crack between adjacent fibers. Analytical models of delamination failure in filament-wound structures and composite laminates are proposed and the separation and postbuckling problems of helical and two-dimensional delaminations are extensively investigated. A variational method using stress functions is developed to obtain efficient and accurate solutions of free-edge interlaminar stresses in composite structures.

14. SUBJECT TERMS
Filament-wound structure, composites, constitutive equations, inelastic behavior, failure, micromechanics, boundary elements, delamination, interlaminar stress

15. NUMBER OF PAGES
267

16. PRICE CODE

17. SECURITY CLASSIFICATION OF REPORT	18. SECURITY CLASSIFICATION OF THIS PAGE	19. SECURITY CLASSIFICATION OF ABSTRACT	20. LIMITATION OF ABSTRACT
UNCLASSIFIED	UNCLASSIFIED	UNCLASSIFIED	UL

INELASTIC DEFORMATION AND FAILURE ANALYSIS OF FILAMENT-WOUND COMPOSITE STRUCTURES

Final Report

By Wan-Lee Yin, Gerald A. Wempner and Zhizhong Fei

October 1991

U.S. ARMY RESEARCH OFFICE

CONTRACT NUMBER: DAAL03-88-K-0071

GEORGIA INSTITUTE OF TECHNOLOGY

ATLANTA, GEORGIA

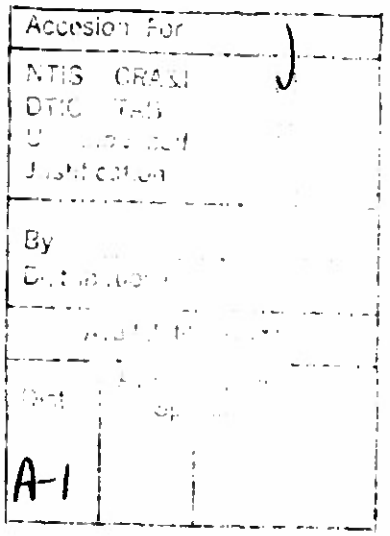

ACKNOWLEDGMENTS

The principal investigators deeply appreciate the encouragement and assistance received from the technical personnel in the U.S. Army Missile Command, Redstone, Alabama. Messrs. Dean Christensen and Troy Smith, in particular, provided exceedingly valuable suggestions and experimental results. Greater achievements in the conduct of this project were made possible thanks to the support and understanding of the project monitors Drs. Robert Singleton and Gary Anderson, and to a contract extension granted by the Army Research Office.

A. STATEMENT OF THE PROBLEM STUDIED

Fundamental problems involving the mechanical response and failure of filament-wound composite structures are studied. The issues include the linear and nonlinear constitutive equations of a filament layer, micro-mechanical analysis of composite behavior and fracture, failure modes and analysis, as well as end and edge effects in filament-wound structures and composite laminates.

B. SUMMARY OF THE MOST IMPORTANT RESULTS

See pages 2 to 4 of the report (under the title: I. An Outline of the Research Results).

C. LIST OF ALL PUBLICATIONS AND TECHNICAL REPORTS

1. Wan-Lee Yin and Lin Yang, "Lamina Constitutive Equations Based on the Mechanical Behavior of a Pressurized Composite Tube," Abstract of the Paper presented in the 8th International Conference on Composite Materials (July 1991, Honolulu, Hawaii).

2. Wan-Lee Yin, "Separation Failure of a Helical Delamination in a Filament-

Wound Composite Tube," Developments in Theoretical and Applied Mechanics Vol. XV (Proceedings of the 15th Southeastern Conference on Theoretical and Applied Mechanics, March, 1990, Atlanta, CA), pp. 440-447.

3. Wan-Lee Yin and K.C. Jane, "Refined Buckling and Postbuckling Analysis of Two-Dimensional Delaminations: Part I -- Analysis and Validation," International Journal of Solids and Structures, In Press.

4. K.C. Jane and Wan-Lee Yin, "Refined Buckling and Postbuckling Analysis of Two-Dimensional Delaminations: Part II -- Results for Anisotropic Laminates and Conclusion," International Journal of Solids and Structures, In Press.

5. Wan-Lee Yin, "Free-Edge Effects in Laminates Under Extension, Bending and Twisting, Part I: A Stress Function Approach," Proceedings AIAA/ASME/ ASCE/AHS/ASC 32nd Structures, Structural Dynamics and Materials Conference, April, 1991, Baltimore, MD, pp. 985-995.

6. Wan-Lee Yin, "Thermal Stresses and Free-Edge Effects in Laminated Beams: A Variational Approach Using Stress Functions," ASME Journal of Electronic Packaging, Vol. 113, pp. 68-75 (1991).

7. Wan-Lee Yin, "Refined Variational Solutions of the Interfacial Thermal Stresses in a Laminated Beam," ASME Paper, Winter Annual Meeting, December, 1991, Atlanta, GA.

8. Cerald A. Wempner and Wan-Lee Yin, six Progress Reports on "Inelastic Deformation and Failure Analysis of Filament-Wound Composite Structures," U.S. Army Research Office Contract DAAL03-88-K-0071, dated January 1989, July 1989, January 1990, July 1990, January 1991 and July, 1991.

D. LIST OF ALL PARTICIPATING SCIENTIFIC PERSONNEL

Dr. Gerald A. Wempner, Co-Principal Investigator. Former Professor, School of Civil Engineering, Georgia Institute of Technology. Dr. Wempner was

Project Director. During the contract period he interacted with the technical personnel in the U.S. Army Missile Command, Redstone Arsenal, Alabama. He provided guidance to the scientific personnel involved in the project, and contributed many seminal ideas.

Dr. Wan-Lee Yin, Co-Principal Investigator. Professor, School of Civil Engineering, Ceorgia Institute of Technology. Dr. Yin was responsible for the over-all conduct of the research, initiated and contributed to the various tasks of the project, and was the author of the final report.

Zhizhong Fei, Research Engineer II, Georgia Institute of Technology. Professor Fei collaborated with Dr. Yin on the tasks reported in Part III and portions of Part IV (Secs. 5, 6 and 7) of the report. He was responsible for developing the computer codes and generating numerical solutions for the boundary-element analysis of micromechanical problems in Part IV and Appendix A.

Dr. K.C. Jane, received Ph.D. degree in Engineering Science and Mechanics, Georgia Institute of Technology, in June 1989. Dr. Jane was a coauthor of two papers on delamination problems in Appendices D and E.

Lin Yang, received M.S. degree in Engineering Science and Mechanics, Georgia Institute of Technology, in September 1990. Mr. Yang made very substantial contributions to the research tasks summarized in Part II of the report.

Bao Han, Graduate Student in Engineering Science and Mechanics, School of Civil Engineering, Ceorgia Institute of Technology. Mr. Han assisted in the computational tasks of Part II, and contributed many figures in the report.

Douglas A. Bruttomesso, Craduate Student in Engineering Science and Mechanics, School of Civil Engineering, Ceorgia Institute of Technology. Mr. Bruttomesso assisted in the computer programming tasks involved in Part IV of the report.

TABLE OF CONTENTS

I. An Outline of the Research Results

The present report summarizes the research findings on several fundamental problems associated with the mechanical behavior and failure of filament-wound composite structures. The main body of the investigation and its conclusions are based on the available experimental results of filament-wound tubes of composite material systems tested under an internal pressure load. Depending on the winding geometry, the end conditions of the tubes, and other factors, different failure modes are observed and are preceded by widely different strain paths. In most cases, significant deviations from linear strain-pressure relations are found at moderate or even low levels of the applied pressure load. A basic problem in characterizing and analyzing the nonlinear behavior of a filament-wound structure is the determination of the (incremental) constitutive equations of a generic filament layer. However, even the formulation of the in-situ linearly elastic constitutive relation of the layer from the experimental results of tubes subjected to small deformations is not without ambiguity because, due to the variations in the process parameters (such as the resin content, fiber misalignment and waviness), the elastic moduli of the filament layer as calculated from different tube specimens show appreciable, and sometimes even substantial, discrepancies. The initial elastic modulus of the filament layer along the fiber direction is often found to be lower than the prediction of the micromechanical analysis based on the elastic moduli of the constituents. In the range of deformation where the composite behavior deviates significantly from linearity, the experimental results suggest strong coupling between the transverse extensional deformation and the shear deformation (associated with the directions parallel and perpendicular to the fibers). This coupling effect may seriously affect the solutions of filament-wound structures in the nolinear and inelastic range of deformation, but has not been sufficiently recognized in the past.

Depending on the winding geometry, material systems, and the nature of loading, filament layers in a composite tube may undergo significantly different strain paths in the intrinsic strain space. Failure initiation may occur at a low or moderate level of the pressure load, and the specimen may experience progressive damage and degradation of stiffness before ultimate failure in a

particular failure mode. Each distinct failure mode requires a specific methodology of failure analysis, which may involve empirical failure criteria, incremental macromechanical analysis involving stiffness degradation, micromechanical modeling and analysis, and failure criteria of fracture mechanics.

The report includes unpublished material presented in Parts II to V of the main text, and published or presented papers attached as Appendices B through H. Several important results obtained in the present study are summarized in the following.

(1) A kinematical analysis of the finite deformation of a long layered tube, with emphasis on the intrinsic strain measures referred to the material axes of the filament layers, is presented in Secs. 2.1 an 2.2 of Part II.

(2) A discussion of the scissoring action at the fiber cross-over points is given in Sec. 2.3. The effect yields a distributed couple moment acting between two adjacent filament layers and causes the non-symmetry of the in-plane shearing stresses.

(3) An incremental formulation for the axisymmetric deformation of a long, thick, layered composite tube, containing the incremental compliances of the successive layers as parameters, is presented in Secs. 2.4 and 2.5. A simple solution algorithm is given for the initial linear elasticity problem (Sec. 3).

(4) Analytical relations involving the winding angle, the intrinsic incremental compliance coefficients of the filament layer and the experimental data of the strains and the pressure are established in Secs. 4.1 to 4.3. These relations may be used to evaluate the initial elastic moduli in the range of small strain (Sec. 4.4) and to investigate the incremental shear modulus and other incremental stiffness parameters in subsequent large deformation (Sec. 4.4).

(5) A constitutive model for large deformation of a filament layer, including the coupling effect between the shear strain and the extensional strain perpendicular to the filament direction, is proposed. It is shown that the model reconciles the significant difference in the shear stress/shear strain relation between the experimental results of the open-end and the closed-end tubes with the $\pm 45^\circ$ winding angle (Sec. 4.5 to 4.8).

(6) An analysis scheme is given for the incremental solution of nonlinear problems of filament-wound structures, based on the presently proposed nonlinear

constitutive model of the filament layer (Sec. 4.9).

(7) A theoretical analysis is presented which demonstrates that, for a unidirectional composite consisting of isotropic matrix and transversely isotropic fibers, the micromechanical problems for determining the gross elastic moduli from the constituent properties can be transformed to plane-strain, two-phase elasticity problems involving a fictitious isotropic fiber region, with possible discontinuous displacement data across the interfaces (Part III, Secs. 1 to 5).

(8) A two-dimensional boundary-element method is developed for efficient and accurate solutions of the transformed, two-phase elasticity problems associated with the determination of gross composite moduli, based on the existing two-dimensional boundary-element-analysis computer codes for a single isotropic elastic medium. A unique and appealing feature of the solution scheme is that all boundary conditions, symmetry conditions and interface continuity and jump conditions are treated in a unified and systematic way, allowing significant simplification in the implementation of the boundary-element method (Secs. 6 to 8). A FORTRAN program MICROBEM is written and listed in Appendix A of this report.

(9) Numerical results of gross composite moduli are obtained by the boundary-element method and found to be in excellent agreement with existing elasticity solutions using serious expansions. The effects of the fiber-volume fraction and of the Poisson's ratio of the resin material are investigated (Sec. 9). Suggestions for further research on the problems of nonlinear composite behavior are mentioned (Sec. 10).

(10) Experimental data on the failure processes of filament-wound tubes with different winding angles and end conditions are reduced to plots of the intrinsic strains and the areal expansion ratio of the filament layer versus the pressure load (Sec. 4, Part IV). Two broad categories of failure processes, corresponding to the shear and expansion modes of failure, are identified. Various failure mechanisms that may operate in each mode are associated with the different types of strain histories preceding the final failure (Sec. 3). An analysis of the deformation of the fiber net without the resin material yields useful suggestions concerning the nature of the failure process (Sec. 2).

(11) Micromechanical analyses of fiber-matrix debonding are conducted by using a simplified, plane-strain analytical model considering the fibers as rigid media. Solutions to the problems of transverse strain and shearing strain,

corresponding respectively to relative displacements of two neighboring fibers in the transverse and axial directions, are obtained by the boundary-element method. A boundary-element code is developed for the present class of problems which uses linear shape functions in the elements and exact elementwise integration. The displacements on the crack boundary are solved and the strain-energy-release rates associated with disbond growth are calculated by the method of crack-closure integrals (Sec. 5).

(12) Similar micromechanical analysis is conducted for an oblique matrix crack between two adjacent fibers. Boundary-element solutions are computed for cracks with the inclination angle varying from 15° to 75°. For each inclination angle, the strain-energy-release rates are evaluated and compared between the two cases depending on whether the fiber-matrix interface has or has not a short disbond at the reentrant corner where the interface intersects the oblique matrix crack (Sec. 6).

(13) An analysis of a possible failure mode due to the separation and growth of a helical face layer from the interior surface of the filament-wound tube is mentioned in Sec. 7, and with details presented in a published paper attached as Appendix C. The work provides an analysis of an apparently puzzling mode of failure observed in pressure testing of certain filament wound tubes under the open-end condition.

(14) A general analysis of buckling and postbuckling deformation and growth of a thin, two-dimensional delaminated layer in a composite laminate is presented in a sequence of two papers attached as Appendices D and E. Delamination is a prevalent mode of failure in composite laminates and filament-wound structures are prone to local delamination failure in regions subjected to compressive service loads.

(15) A stress-function based, variational analysis of the free-edge interlaminar stress problems associated with the ends and openings of a composite structure is introduced in Part V. The methods of analysis and the analytical results are developed for the case of mechanical loading in a paper attached as Appendix F, and suggested for the case of thermal loading in the two papers attached as Appendices G and H. Free edge interlaminar stresses in layered composite structures can initiate delamination failure. The present analysis method yields highly efficient solutions with an accuracy comparable to elaborate finite-element solutions using refined mesh.

II. Linear and Nonlinear Behavior of a Filament-Wound Composite Tube

1. Introduction

In producing a filament-wound composite structural component, continuous filaments are laid down upon a rotating rigid mandrel by a feeding head which traverses back and forth along the axial direction. In some cases the mandrel undergoes both rotational and axial motion while the feeding head remains stationary. In each pass of the feeding head, a thin band of filaments is laid upon the surface of the partially finished product in a direction making an angle α with respect to the meridional direction. For a general axisymmetric filament-wound component, the angle α varies continuously during the forward or backward pass. In the special case of a circular cylinder, α remains constant in each pass but undergoes a discontinuous change when the relative axial motion reverses the direction. Cylinders may be formed of only filaments wound at $\pm\alpha$ angle, or they may have additional circumferential and longitudinal windings to enhance the strength for various cases of loading.

The band of filaments laid down in a single pass of the feeding head often consists of more than one layer of filaments in the thickness direction. Within the band the parallel filaments form a helical pattern and are more or less evenly distributed. This is ensured by applying a suitable tension in the filaments and, in the production of large components, by feeding the filaments through a series of rollers to produce desired wide tapes of uniform quality.

For several filament-wound structural components composed of the same filament-resin material system and produced under the same winding process, the fundamental structural unit for the analysis of the mechanical response is the thin band of resin-impregnated filaments laid in a single pass of the feeding

head. These thin bands are analogous to the unidirectional laminae in a laminate of fiber-reinforced composite. The mechanical behavior of the thin band and its strength is determined by the material system and the winding and curing process. When these bands are laid at predesigned angles to from the filament-wound structure, the response behavior and the strength of the structure can be calculated in terms of the properties of a generic band and the geometry of winding.

One complicating factor in the case of a filament-wound composite, when compared to a laminate formed by unidirectional laminae, is that the cross-over of two adjacent bands with different winding angles can produce local effects on the stresses in a filament-wound structure. However, if there are a large number of band layers across the thickness of the structure, and if the winding process ensures a fairly uniform distribution of the cross-over regions within the structure, then the local stresses due to the cross over of thin bands have insignificant effect on the gross stiffness properties of the composite structure, although they may have significant effects on its strength. In such a case, the filament-wound structure may be modeled analytically as a curved laminate, which is neatly divided into a sequence of thin laminae or layers. Each layer is actually patched up from parallel bands of resin-impregnated filaments introduced in the same or different passes of the feeding head. The layer has a winding angle α different from the two adjacent layers (which often have the winding angle $-\alpha$), and α is either constant or changes continuously on the surface of the layer. In fact, this simplified model is almost universally adapted in the existing analytical studies of filament-wound structures.

However, in the analysis of a filament-wound structure, the mechanical properties of a layer is often less consistent than those of a lamina in a

laminate. Due to the nature of the winding process, it is more difficult to avoid misalignment and uneven distribution of fibers, variations in the resin content and the degree of fiber waviness, as well as the curing residual stresses in filaments and the resin material. The constitutive relation of a filament layer as determined from the properties of the filament and the resin phases by a micromechanical analysis may be, and has been found to be, significantly different from the in situ behavior of the layer in the composite, because the micromechanical analysis usually ignores the deviation from perfect geometry and the effects of the residual stresses. These deviations and the variations of the process parameters are more significant in the products produced by filament winding, than in the laminates made of unidirectional coupons.

A program to directly determine the in situ constitutive behavior of a filament layer from the experimental testing of filament-wound tubes is attractive because the test results implicitly include the effects of certain process variables which are not easy to identify or to evaluate and which may significantly affect the final product. Such experiments are, furthermore, the only means to investigate the various failure modes and failure processes of filament-wound components. For simplicity of analysis and testing, long tubes with open or closed ends and consisting of alternating $+\alpha$ and $-\alpha$ filament layers are tested under an increasing internal pressure load, with or without using a rubber liner to contain the leakage of fluid from the tube wall. Analysis of the experimental results indicates that most tubes begin to behave nonlinearly at a relatively low pressure load. This is followed by several different deformation patterns, depending essentially on the winding angle and the end condition of testing, which lead to different modes of failure. The nonlinear response of the tube in an early stage of pressure loading has important implications for the

design of filament-wound structures. The nonlinearity is largely, but not entirely, associated with the large shear deformation of the resin material between neighboring filaments. Small or moderate tensile strain of a filament layer in the direction transverse to the fiber direction may cause microcracking of the resin material and thereby progressively degradate the stiffness of the layer.

An analysis of the existing experimental data indicates that the testing results of thin filament-wound tubes with different winding angles under different end conditions may yield different in-situ elastic stress-strain relations of a filament layer under infinitesimal deformation. This is not surprising because in at least two comprehensive and detailed sets of experimental results (Hull, D., Legg, M.J. and Spencer, B., "Failure of glass/polyester filament wound pipe," Composites, Vol. 9, pp. 17-24, 1978 and Spencer, B. and Hull, D., "Effect of winding angle on the failure of filament wound pipe," Composites, Vol. 9, pp.263-271, 1978; Uemura, M. and Fukunaga, H., "Probabilistic Burst Strength of Filament-Wound Cylinders Under Internal Pressure," J. Composite Materials, Vol. 15, pp. 462-480), there are appreciable and even substantial discrepancies in both the measured axial strain and the measured circumferential strains among supposedly identical tube specimens under the same pressure load. While other reports sometimes claim good agreement between the test results and the prediction of the elastic response of a filament layer from constituent elastic properties, such reports do not include sufficient test data (corresponding to tubes with identical or different winding angles under both the closed-end and the open-end conditions) to show the consistency of prediction. The apparently significant variations in the specimen and the resulting differences in the elastic properties of the filament layer suggest

that, for a particular type of filament-wound structure, the constitutive properties of a generic filament layer can be ascertained only to within an appreciable margin of error by repeating experiments on several specimens and calculating the average properties and their standard deviations.

The response of the filament layer in the nonlinear range of deformation is characterized by the dependence of the intrinsic stress components relative to the filament and transverse directions, σ_1, σ_2 and τ_{12}, upon the history of the corresponding intrinsic strain components ϵ_1, ϵ_2 and γ_{12}. Because of the limited types and ranges of deformation histories attainable in tube experiments, such experiments cannot provided the complete information of the material behavior needed to formulate the general inelastic constitutive equations of a filament layer. However, the experimental data may be used to provided constitutive equations with a limited range of applicability, i.e., intended for those applications in which the filament layers in a structure are subjected to deformation histories similar to those experienced in tube tests. It is with this objective in mind that we investigate, in this chapter of the present work, the kinematics and mechanics of deformation of a filament-wound tube which generally involve large intrinsic shear deformation of a filament layer. It is found that the experimental results of a tube with $\pm 45°$ winding angles provided sufficient information for determining the initial intrinsic shear modulus G_{12} referred to the material axes of the layer, as well as the incremental modulus in the subsequent states of deformation. The results also provide an additional relation among the initial or incremental compliances $1/E_1$, $1/E_2$ and ν_{12}/E_1. Additional relations among the initial compliance coefficients may be obtained from the experimental data of tubes with different winding angles or different end conditions. Assuming linearity of the layer response in the filament

direction, one may use the experimental data of filament-wound tubes to formulate an empirical constitutive equation involving two nonlinear material functions, and it is found that the test results under the open and closed end conditions yield material functions that are in approximate agreement.

Once the nonlinear or incremental constitutive equations of the filament layer have been formulated by a combination of theory and experiment, the equations can be applied to filament-wound structures to predict its response to external loads. Integration of the expressions of the incremental stresses (in terms of the incremental strain field in each filament layer) across the thickness of a filament-wound structure yields the dependence of the incremental force and moment resultants on the increments of the middle-surface strains and the curvatures of the composite shell These incremental relations are updated in each stage of the solution process to obtain the solution for the next step in terms of the results of the preceding step and the incremental load.

2. Deformation of a filament-wound tube under internal pressure

2.1 Finite deformation of a filament-wound tube

Consider a thin filament-wound tube with alternating layers of filaments oriented at $+\alpha_o$ and $-\alpha_o$ angles with respect to the longitudinal axis of the tube. Assume that the tube is subjected to a uniform internal pressure p, with or without an accompanying axial load, so that the stress and strain in the tube are independent of the axial and circumferential coordinates z and θ, at least in a section of the tube away from the two ends. In each layer of filament, we define (local) orthogonal material axes 1 and 2 along and perpendicular to the tangential direction of the filament. Then the extensional strain along the filament direction, ϵ_1 , is small if the longitudinal elastic modulus of the

filament is significantly greater than the elastic moduli of the resin material.

In this section, we restrict our attention to the special case in which the tube deforms without twisting, so that the longitudinal and circumferential material lines are mapped into the corresponding lines of the deformed tube. This condition is approximately valid if the tube has an equal number of layers with $+\alpha$ and $-\alpha$ winding angles and if it is subjected to no twisting moment. More general deformations including the twisting effect are considered in Sec. 2.2.

A pair of neighboring filaments in a filament layer with the winding angle $+\alpha_o$, and another pair of neighboring filaments in a layer with the winding angle $-\alpha_o$, form a rhombus. In the undeformed state, the diagonal length of the rhombus along the axial direction of the tube is $2L \cos \alpha_o$, and the diagonal length along the circumferential direction is $2L \sin \alpha_o$. After deformation, these diagonal lengths change to $2L(1+\epsilon_1)\cos \alpha$ and $2L(1+\epsilon_1)\sin \alpha$, respectively, where α is the winding angle in the deformed state (Fig. 1). The stretches (i.e., the ratio of the deformed curve length to the initial curve length) in the axial and circumferential directions of the tube are given by

$$\lambda_z = (2L(1+\epsilon_1) \cos \alpha)/(2L \cos \alpha_o) = (1+\epsilon_1) \cos \alpha / \cos \alpha_o \ ,$$

$$\lambda_\theta = (2L(1+\epsilon_1) \sin \alpha)/(2L \sin \alpha_o) = (1+\epsilon_1) \sin \alpha / \sin \alpha_o \ . \quad (2.1)$$

Hence the ratio of the deformed area of the rhombus to the initial area is

$$\lambda_z \lambda_\theta = (1+\epsilon_1)^2 \sin 2\alpha / \sin 2\alpha_o \ . \quad (2.2)$$

This area ratio must be equal to the product of the stretch along the filament direction, $1+\epsilon_1$, and the stretch along the perpendicular direction, $1+\epsilon_2$. It follows that

$$1+\epsilon_2 = (1+\epsilon_1) \sin 2\alpha / \sin 2\alpha_o \ . \quad (2.3)$$

While the extensional strains ϵ_1 and ϵ_2 are usually small in the states of deformation before failure of the tube, the resin matrix between two neighboring

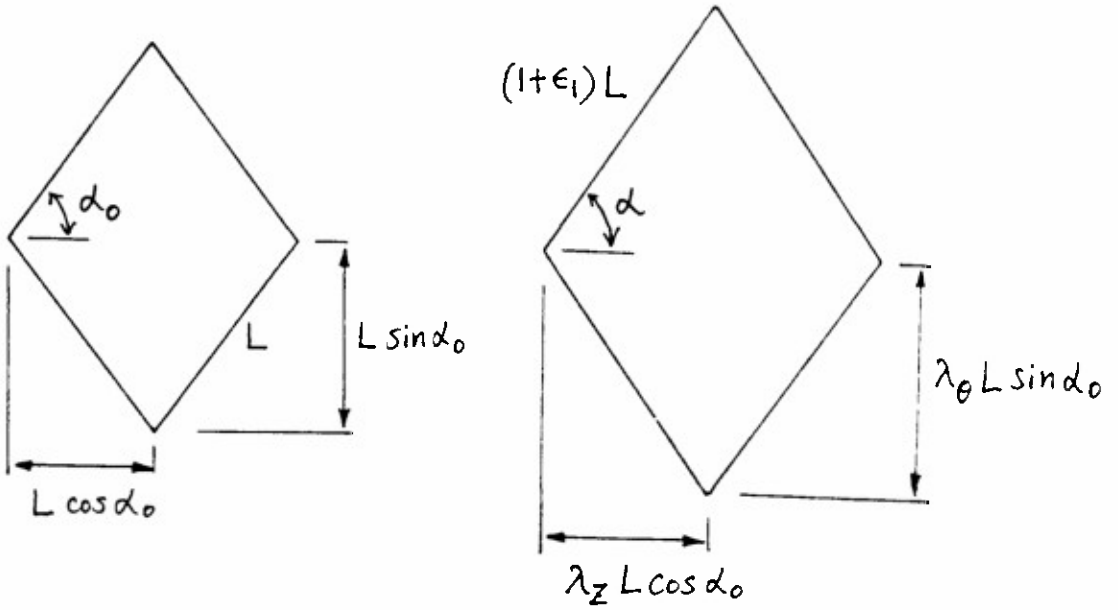

Fig. 1: Deformation of a Diamond-shaped element of a filament layer

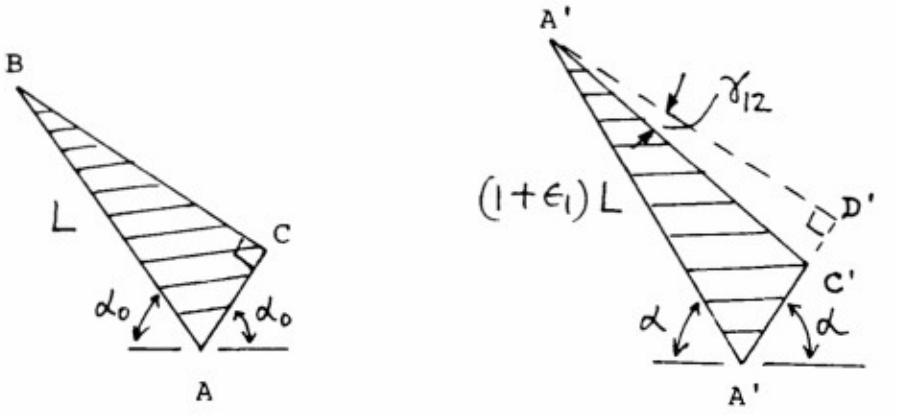

Fig. 2: Change of the angle between two material lines initially parallel and perpendicular to the fibers

fibers may be subjected to a very large shear deformation. In a filament-wound layer, material lines initially perpendicular to the filaments become non-orthogonal to the deformed filaments. The reduction in angle, γ_{12} , may be determined by considering the deformation of the right triangle ABC in Fig. 2a into the triangle A'B'C' in Fig. 2b. Here the undeformed material lines AB and AC are along two adjacent sides of an undeformed rhombus, and the deformed material lines A'B' and A'C' are along the corresponding sides of the deformed rhombus. Using the relations

$$A'C' = (1+\epsilon_1)\, AC, \qquad A'B' = (1+\epsilon_1)\, AB, \qquad AC = AB \cos(\pi-2\alpha_o),$$

$$A'D' = A'B' \cos(\pi-2\alpha), \qquad B'D' = A'B' \sin(\pi-2\alpha),$$

where D' is the orthogonal projection of the point B' on the line A'C', we obtain

$$C'D' = A'D'-A'C' = (1+\epsilon_1)\, AB \{\cos(\pi-2\alpha) - \cos(\pi-2\alpha_o)\}$$

$$- A'B' \{\cos 2\alpha_o - \cos 2\alpha\},$$

Substitution into $\tan \gamma_{12} = C'D'/B'D'$ yields the following result

$$\tan \gamma_{12} = (\cos 2\alpha_o - \cos 2\alpha)/\sin 2\alpha \ . \tag{2.4}$$

Although γ_{12} is not a tensorial component of a finite strain tensor with respect to the orthogonal axes 1 and 2, it may be used as a measure of the in-plane shear deformation of the filament layer. Equation (2.4) indicates that, for the type of deformation considered here (without twisting and uniform in each r-θ surface), γ_{12} depends only on the initial and deformed winding angles α_o.

From Eq. (2.1) we obtain

$$\lambda_z^2 \cos^2 o_o + \lambda_\theta^2 \sin^2\alpha_o = (1+\epsilon_1)^2 \ .$$

Hence the extensional strains ϵ_1 and ϵ_2 are given by

$$\epsilon_1 = (\lambda_z^2 \cos^2 o_o + \lambda_\theta^2 \sin^2\alpha_o)^{1/2} - 1 \ , \tag{2.5}$$

$$\epsilon_2 = \lambda_z\lambda_\theta/(1+\epsilon_1) - 1 = \lambda_z\lambda_\theta(\lambda_z^2 \cos^2\alpha_o + \lambda_\theta^2 \sin^2\alpha_o)^{-1/2} - 1$$

$$= (\lambda_z^2 \cos^2\alpha_o + \lambda_\theta^2 \sin^2\alpha_o)^{1/2} (\sin 2\alpha \,/\, \sin 2\alpha_o) - 1 \ . \tag{2.6}$$

The expressions on the right hand sides of Eqs. (2.4)-(2.6) involve only the axial and circumferential stretches, λ_z and λ_θ , and the initial and deformed winding angles. The constant axial stretch λ_z in the tube and the values of α and λ_θ on the exterior surface of the tube may be directly measured in tube experiments. If the thickness-to-radius ratio of the tube is small, then α and λ_θ vary only slightly across the thickness of the tube, so that the values of these quantities in the interior region of the tube may be approximated by the measured values on the exterior surface.

From eliminating $(1+\epsilon_1)$ from Eqs. (2.1) and (2.2), we obtain

$$(\lambda_z \cos \alpha_o)^2 + (\lambda_\theta \sin \alpha_o)^2 - \lambda_z\lambda_\theta \sin 2\alpha_o/\sin 2\alpha = 0.$$

This relation among the three measurable quantities λ_z, λ_θ and α is a consequence of the assumption that the tube experiences no twisting deformation. If this assumption is removed, then λ_z, λ_θ and α become independent kinematical variables.

The measured data of α, λ_z and λ_θ determine the intrinsic strains of a filament layer with respect to the material axes of the layer according to Eqs. (2.4)-(2.6), and the latter strains determine the intrinsic components of stress through the (generally nonlinear and inelastic) constitutive equations of the layer. The constitutive equations are needed to solve the successive states of deformation and stress in the tube under increasing loads. Conversely, experimental data of the relation between the load and deformation may be used to infer the constitutive equations of a filament layer referred to the intrinsic axes 1 and 2. A major concern in the following analysis is the determination of the constitutive behavior, both in linear and nonlinear range, of a filament layer from the experimental data of filament wound tubes with various winding angles.

2.2 The strain field

In a thick tube of mean radius R^* and thickness t, subjected to a uniform internal pressure load, the stress components depend on the radial coordinate r, but are independent of the coordinates z and θ (Fig. 3). In the absence of body force, the equilibrium equations reduce to

$$d(r\,\sigma_r)/dr = \sigma_\theta, \qquad d(r^2\,\tau_{r\theta})/dr = 0, \qquad d(r\,\tau_{rz}) = 0. \tag{2.7}$$

The last two equilibrium equations together with the traction boundary conditions $\tau_{r\theta} = \tau_{rz} = 0$ on the outer surface $r = R^*+t/2$ yield the following result in the entire tube:

$$\tau_{r\theta} = \tau_{rz} = 0. \tag{2.8}$$

This implies that the radial direction is a principal direction of stress. Since the layers are composed of orthotropic material and the radial direction is an axis of orthotropy, it follows that the same direction is also a principal direction of strain. While the validity of this conclusion requires the orthotropy of layers, it is not dependent on the material response being elastic or linear.

Since the radial direction is a principal direction of strain, and the intrinsic components of strain are independent of the coordinates z and θ, the deformation of the tube is characterized by a finite strain field whose right Cauchy-Green tensor (for the definition of this tensor see Truesdell, C. and Noll, W., Non-Liner Field Theories of Mechanics, Encyclopedia of Physics, Vol. III/3, Springer-Verlag, New York, 1965, p. 53) has the form

$$\mathbf{C} = \lambda_r^2\,\mathbf{i}_r\,\mathbf{i}_r + \lambda_z^2\,\mathbf{k}\,\mathbf{k} + \lambda_\theta^2\,\mathbf{i}_\theta\,\mathbf{i}_\theta + \mu\,(\mathbf{i}_\theta\,\mathbf{k} + \mathbf{k}\,\mathbf{i}_\theta), \tag{2.9}$$

where $(\mathbf{i}_r,\ \mathbf{i}_\theta,\ \mathbf{k})$ is the orthonormal set of cylindrical base vectors at the undeformed position of a material element.

The cylindrical surfaces r = constant are material surfaces. That is,

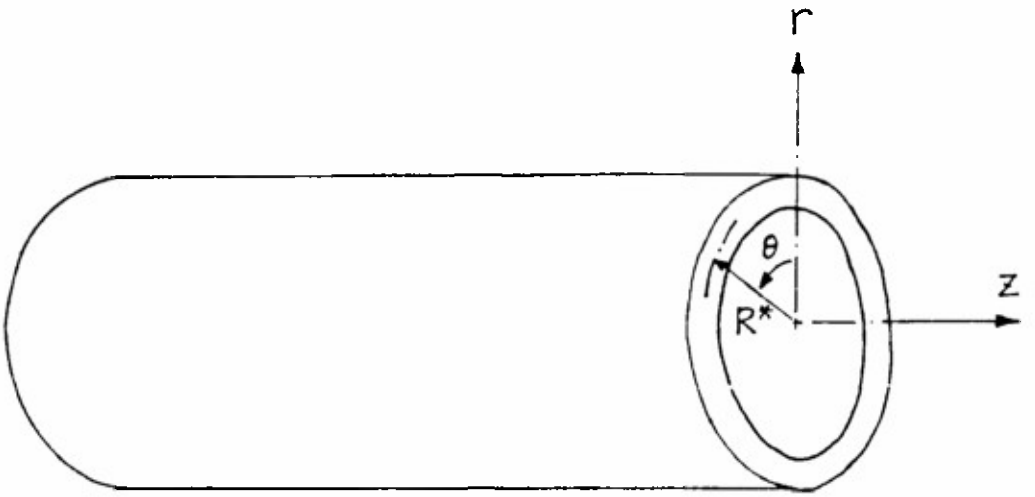

Fig. 3: Coordinate system for a composite tube

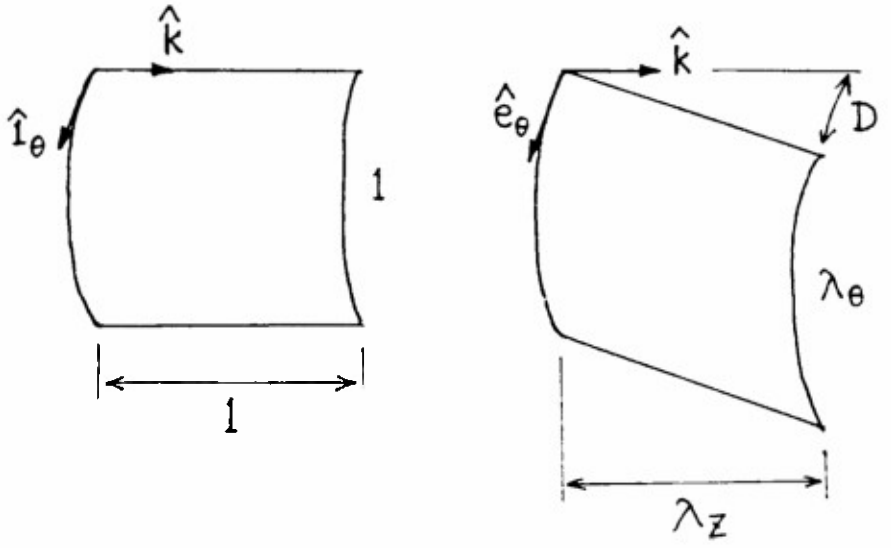

Fig. 4: Finite deformation of a surface element

filament sheets of initial radius R deform into cylindrical surface of radius r = f(R). We have

$$\lambda_\theta = r/R = f(R)/R\ , \qquad \lambda_r = dr/dR = f'(R). \tag{2.10}$$

A region in an undeformed filament layer bounded by a pair of axial material lines and an orthogonal pair of circumferential lines deforms into a region bounded by two intersecting pairs of helices in the deformed filament layer (Fig. 4). For a complete tube, the uniqueness of the axial displacement (i.e., the axial displacement at $\theta = 0$ must agree with that at $\theta = 2\pi$) requires that the deformation maps circumferential material lines in an undeformed filament layer into circumferential material lines in the deformed filament layer. Hence the deformation gradient tensor has the form

$$\begin{aligned} \mathbf{F} &= \lambda_r\, \mathbf{e}_r\, \mathbf{i}_r + \lambda_z\, \mathbf{k}\, \mathbf{k} + \lambda_\theta\, \mathbf{e}_\theta\, \mathbf{i}_\theta + D\, \mathbf{e}_\theta\, \mathbf{k}, \\ &= f'(R)\, \mathbf{e}_r\, \mathbf{i}_r + \lambda_z\, \mathbf{k}\, \mathbf{k} + (f(r)/R)\, \mathbf{e}_\theta\, \mathbf{i}_\theta + D\, \mathbf{e}_\theta\, \mathbf{k}, \end{aligned} \tag{2.11}$$

where $(\mathbf{e}_r,\ \mathbf{e}_\theta,\ \mathbf{k})$ is the orthonormal set of cylindrical base vectors at the deformed position. The last equation characterizes the finite deformation of the tube in terms of the deformation parameters $\lambda_z = 1+\epsilon_z$ and D and the radial deformation function $r = f(R)$.

Notice that while the analysis of Sec. 2.1 was based on the assumption of vanishing twisting deformation, the finite deformations considered in this section are not subjected to that restriction.

2.3 Scissoring action between the filaments of alternating layers

In the preceding analysis, we obtained kinematical results referring to the deformation of the tube as a homogeneous continuum. The kinematical tensor $\mathbf{C}$ and $\mathbf{F}$ given Eqs. (2.9) and (2.10) are macromechanical quantities that characterize the averaged deformation of the fiber phase and the matrix phase in

a volume element of the composite material. The actual deformation of the two phases at the micromechanical level is very complex. The macroscopic shear deformation γ_{12} is often contributed largely by severe shearing in the narrow matrix region between adjacent filaments on the same cylindrical surface r = constant. Likewise, the macroscopic strain ϵ_2 generally has uneven contributions from the fiber and matrix phases. These considerations are important for understanding the physical factors affecting the gross response of the composite material. However, most aspects of the deformation at the micromechanical level need not be scrutinized if the objective is to formulate gross constitutive equations of the composite material using a phenomenological approach, and if the two phases constituting the composite are distributed in a regular or continuous pattern in a volume element of the size comparable to a finite element for subsequent macromechanical analysis.

In filament-wound structures, the density and orientation of the filaments is either constant or varies continuous within certain strips of each filament layer. Across the thickness direction of a filament-wound vessel, the orientation of the fibers has a sequence of discontinuous changes. Therefore, while macroscopic averaging of the stresses and strains of the two phases is legitimate with respect to the in-plane coordinates of a filament sheet, it should be examined and used more carefully with regard to the thickness direction. In fact, if two adjacent filament layers have initial winding angles $\pm \alpha_o$ and deformed winding angles $\pm \alpha$, then the filaments of one layer rotate relative to those of the other layer during the deformation. This relative rotation of two crossing fibers has no direct effect on the matrix material in the interior of the filament layers (that is, in the region away from the skins of layers), but it introduces a severe shearing strain $\gamma_{r\phi}$ in the thin and small

matrix region between two crossing fibers near the point of crossing, where r is the thickness coordinate and ϕ is associated with the circumferential direction of a polar coordinate system (ρ, ϕ) with the origin at the point of crossing. This scissoring effect at the crossing points of fibers effectively results in a distributed couple moment action (i.e., a couple stress) from one filament layer to the adjacent layer with the opposite winding angle (Fig. 5). The effect of the couple moment action tends to reduce the relative orientation angle from 2α towards the initial value $2\alpha_o$. If we consider a rectangular element of area ΔA, taken from one filament sheet with the orientation angle $+\alpha$, which contains only one fiber crossing point and which has the edges parallel either to the global coordinate axes z and θ or to the material axes 1 and 2 (Figs. 6a and 6b, respectively), then the upper and lower faces of the element are each subjected to a clockwise couple moment $m_o\Delta A$ which tends to restore the deformed orientation angle α to the original angle α_o. The moment equilibrium of the element requires that these two moments be balanced by a counterclockwise moment of the magnitude $2m_o\Delta A$, which can only be produced by the macroscopic shearing stresses $\tau_{z\theta}$ and $\tau_{\theta z}$ in Fig. 6a or by the macroscopic shearing stresses τ_{12} and τ_{21} in Fig. 6b. It follows that the macroscopic stress tensor σ_{ij} for a filament layer cannot be symmetric, and the differences in the two in-plane components of the shearing stress are determined by the distributed couple moment m_o between the adjacent layers according to

$$\tau_{12} - \tau_{21} = \tau_{z\theta} - \tau_{\theta z} = 2m_o.$$

It is reasonable to make the constitutive assumption concerning the scissoring action that the distributed couple moment m_o depends essentially on the change in the orientation angle, $\alpha-\alpha_o$, i.e., for a given α_o, m_o is essentially a function of α. For deformations of filament-wound tubes without

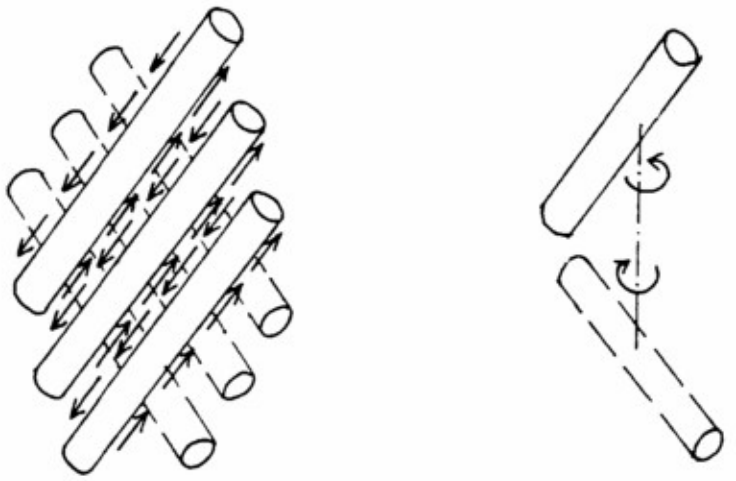

Fig. 5: Scissoring action at a filament cross-over point and the resulting distributed moment between adjacent filament layers

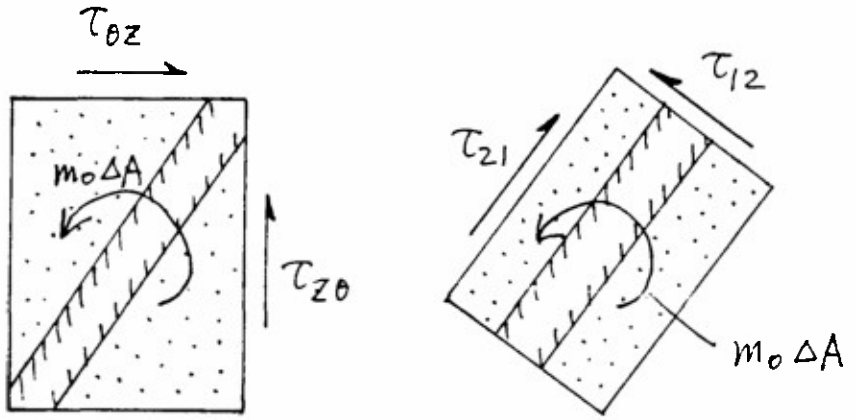

(a) (b)

Fig. 6: Moment equilibrium of a layer element under non-symmetric shearing stresses and the distributed moment

twisting, Eq. (2.4) indicates that α depends only on the shearing strain γ_{12}. Consequently, the non-symmetry of the in-plane shearing stresses, $\tau_{12} - \tau_{21}$, depends essentially on γ_{12} only (the functional relationship is determined by the initial winding angle α_o). This conclusion implies that, in formulating the gross constitutive equation of a filament layer, no additional kinematical variable need be included. The three intrinsic stress components σ_1, σ_2 and τ_{12} are determined constitutively by the histories of the three strain parameters ϵ_1, ϵ_2 and γ_{12}. The stress tensor is generally not symmetric and the difference in the in-plane stress, $\tau_{12} - \tau_{21}$, depends essentially on γ_{12}.

Although the consideration of the scissoring effect around the fiber cross-over point does not introduce additional kinematical variable in the (nonlinear) constitutive equation of a filament layer, the severe shear deformation of the resin material in the cross-over region may constitute an important dissipative mechanism with significant effects on the inelastic behavior of the layer.

2.4 Infinitesimal and incremental deformation

The characterization of special axisymmetric deformations of a tube (i.e., axisymmetric deformations that are also independent of the axial coordinate z) given in Sec. 2.2 reduces, in the case of infinitesimal deformation, to the following expression for the infinitesimal displacement functions along the axial, circumferential and radial directions

$$u_z = z\,\epsilon_z\,, \qquad u_\theta = D\,r\,z\,, \qquad w = w(r)\,. \tag{2.12}$$

Naturally, rigid-body displacements may be superposed without affecting the stress in the tube.

A finite deformation may be decomposed into a series of incremental deformations. The displacement functions in each incremental step have the form given in Eq. (2.12). The components of the incremental strain are $\Delta\epsilon_z$, $\Delta\epsilon_\theta$ =

$\Delta w(r)/r$ and $\Delta\gamma_{\theta z} = \Delta D\ r$, where Δw is the incremental radial displacement.

Let $\Delta\epsilon_1$ and $\Delta\alpha$ denote small changes in the filament strain and in the deformed winding angle resulting from an increment in the load. Then, by differentiating Eq. (2.3), we obtain the following relation for infinitesimal increments

$$\Delta\epsilon_2 = (\sin 2\alpha / \sin 2\alpha_o)\ \{\Delta\epsilon_1 + 2(1+\epsilon_1)\ \text{ctn}\ 2\alpha\ \Delta\alpha\}\ . \qquad (2.13)$$

In an advanced stage of deformation of a tube with relatively stiff filaments, the filament strain increment $\Delta\epsilon_1$ is usually small compared to the angle increment $\Delta\alpha$. Then the algebraic sign of $(\cos 2\alpha / \sin 2\alpha_o)\Delta\alpha$ determines the algebraic sign of $\Delta\epsilon_2$. The sign of $\Delta\epsilon_2$ determines whether the spacing between the neighboring filaments increases or decreases in continued loading, and has a significant effect on the failure mode of the tube.

2.5 Linearized or incremental constitutive relation

At each step in the loading process, the stress and strain increments in each layer are related by the incremental constitutive relation:

$$\begin{Bmatrix} \Delta\epsilon_z \\ \Delta\epsilon_\theta \\ \Delta\epsilon_r \\ -\Delta\gamma_{\theta z} \end{Bmatrix} = \begin{bmatrix} a_{11} & a_{12} & a_{13} & a_{16} \\ a_{12} & a_{22} & a_{23} & a_{26} \\ a_{13} & a_{23} & a_{33} & a_{36} \\ a_{16} & a_{26} & a_{36} & a_{66} \end{bmatrix} \begin{Bmatrix} \Delta\sigma_z \\ \Delta\sigma_\theta \\ \Delta\sigma_r \\ -\Delta\tau_{\theta z} \end{Bmatrix} \qquad (2.14)$$

where $[a_{ij}]$ is the incremental compliance matrix of the particular layer. Since the layers are very thin, the dependence of a_{ij} upon the radial coordinate r within each thin layer due to slight variation of the stress history in the layer may be neglected. Consequently, at each stage of loading, we regard the incremental compliance matrix as a constant matrix within each layer. The matrix may vary from layer to layer due to different stress and strain histories of the layers.

Equation (2.14) may be partially inverted to yield expressions of $\Delta\epsilon_\theta$, $\Delta\epsilon_r$, $\Delta\sigma_z$ and $\Delta\tau_{\theta z}$ in terms of $\Delta\sigma_\theta$, $\Delta\sigma_r$, $\Delta\epsilon_z$ and $\Delta\gamma_{\theta z} = \Delta D\ r$. We adopt the notation of Lekhnitskii

$$\beta_{ij} = a_{ij} - a_{i1}\, a_{j1}/a_{11} \qquad \text{for } i,j \neq 1. \tag{2.15}$$

From the first row of Eq. (2.14) we obtain

$$\Delta\sigma_z = (\Delta\epsilon_z - a_{12}\,\Delta\sigma_\theta - a_{13}\,\Delta\sigma_r + a_{16}\,\Delta\tau_{\theta z})/a_{11}.$$

Substitution into the last three rows of Eq. (2.14) yields

$$\Delta\epsilon_\theta = (a_{12}/a_{11})\Delta\epsilon_z + \beta_{22}\,\Delta\sigma_\theta + \beta_{23}\,\Delta\sigma_r - \beta_{26}\,\Delta\tau_{\theta z},$$

$$\Delta\epsilon_r = (a_{13}/a_{11})\Delta\epsilon_z + \beta_{23}\,\Delta\sigma_\theta + \beta_{33}\,\Delta\sigma_r - \beta_{36}\,\Delta\tau_{\theta z},$$

$$-\Delta\gamma_{\theta z} = (a_{16}/a_{11})\Delta\epsilon_z + \beta_{26}\,\Delta\sigma_\theta + \beta_{36}\,\Delta\sigma_r - \beta_{66}\,\Delta\tau_{\theta z}.$$

By eliminating $\Delta\tau_{\theta z}$ from the last three equations we obtain the expressions of $\Delta\epsilon_\theta$ and $\Delta\epsilon_r$ in terms of $\Delta\epsilon_z$, $\Delta\sigma_\theta$, $\Delta\sigma_r$ and $\Delta\gamma_{\theta z} = \Delta D\ r$. Corresponding expressions can be subsequently obtained for $\Delta\tau_{\theta z}$ and $\Delta\sigma_z$. The results are

$$\Delta w/r = \Delta\epsilon_\theta = (\Gamma_2\,\Delta\epsilon_z + \Psi\,\Delta\sigma_\theta)/\Gamma_1 - \Phi\,\Delta\sigma_r/\Gamma_1 - \Delta D\,(\beta_{26}/\beta_{66})r, \tag{2.16}$$

$$d(\Delta w)/dr = \Delta\epsilon_r = (a_{13}\,a_{66} - a_{16}\,a_{36})\,\Delta\epsilon_z/\Gamma_1 + (\beta_{23}\,\beta_{66} - \beta_{26}\,\beta_{36})\,\Delta\sigma_\theta/\beta_{66}$$
$$+ (\beta_{33}\,\beta_{66} - \beta_{36}^2)\,\Delta\sigma_r/\beta_{66} - \Delta D\,(\beta_{36}/\beta_{66})r, \tag{2.17}$$

$$\Delta\tau_{\theta z} = (a_{16}\,\Delta\epsilon_z/a_{11} + \Delta D\ r + \beta_{26}\,\Delta\sigma_\theta + \beta_{36}\,\Delta\sigma_r)/\beta_{66}\ , \tag{2.18}$$

$$\Delta\sigma_z = (a_{66}\,\Delta\epsilon_z + a_{16}\,\Delta D\ r - \Gamma_2\,\Delta\sigma_\theta + \Gamma_3\,\Delta\sigma_r)/\Gamma_1. \tag{2.19}$$

where the symbols Γ_1, Γ_2, Γ_3, Φ and Ψ are defined by

$$\Gamma_1 = a_{11}\beta_{66} = a_{11}a_{66} - a_{16}^2,$$

$$\Gamma_2 = a_{12}\,a_{66} - a_{16}\,a_{26},$$

$$\Gamma_3 = a_{16}\,a_{36} - a_{13}\,a_{66}, \tag{2.20}$$

$$\Phi = a_{11}\,(\beta_{26}\,\beta_{36} - \beta_{23}\,\beta_{66}),$$

$$\Psi = a_{11}\,(\beta_{22}\,\beta_{66} - \beta_{26}^2)$$

Substituting Eqs. (2.16) and (2.17) into the compatibility equation

$$\Delta\epsilon_r = d(r\,\Delta\epsilon_\theta)/dr,$$

and making use of the first equilibrium equation for the incremental stress, $d(r\ \Delta\sigma_r) = \Delta\sigma_\theta$, we obtain the following differential equation

$$d^2(r\ \Delta\sigma_r)/d(\ell n\ r)^2 - \lambda^2\ r\ \Delta\sigma_r = H\ \Delta D\ r^2 - K\ \Delta\epsilon_z\ r, \tag{2.21}$$

where

$$\begin{aligned} \lambda^2 &= (\beta_{33}\ \beta_{66} - \beta_{36}^2)/(\beta_{22}\ \beta_{66} - \beta_{26}^2), \\ H &= (2\ \beta_{26} - \beta_{36})/(\beta_{22}\ \beta_{66} - \beta_{26}^2)\ , \\ K &= (\Gamma_2 + \Gamma_3)/\Psi\ . \end{aligned} \tag{2.22}$$

In the i-th layer, the general solution of the differential equation is

$$r\ \Delta\sigma_r = A_i\ (r/R^*)^\lambda + B_i\ (r/R^*)^{-\lambda} + H\ \Delta D\ r^2/(4-\lambda^2) - K\ \Delta\epsilon_z\ r/(1-\lambda^2), \tag{2.23}$$

$$r\ \Delta\sigma_\theta = \lambda A_i(r/R^*)^\lambda - \lambda B_i(r/R^*)^{-\lambda} + 2H\ \Delta D\ r^2/(4-\lambda^2) - K\ \Delta\epsilon_z\ r/(1-\lambda^2), \tag{2.24}$$

where the constants A_i may be determined, in terms of the deformation parameters ΔD and $\Delta\epsilon_z$, from the boundary conditions (on the interior and exterior surfaces of the tube) of $\Delta\sigma_r$ and the continuity conditions of $\Delta\sigma_r$ and $\Delta\epsilon_\theta$ across all interfaces. The solutions for the radial and circumferential stress increments, given by Eqs. (2.23) and (2.24), may be substituted into Eqs. (2.18) and (2.19). The resulting expressions for $\Delta\tau_{\theta z}$ and $\Delta\sigma_z$ are then substituted into the following equations for the increments in the axial force and the twisting moment

$$\Delta F_z = \sum \iint \Delta\sigma_z\ r\ dr\ d\theta = \begin{cases} 0, & \text{(open end tube)} \\ \pi(R^* - t/2)^2\ \Delta p, & \text{(closed-end tube)} \end{cases} \tag{2.25}$$

$$\Delta M_z = \sum \iint \Delta\tau_{\theta z}\ r^2\ dr\ d\theta = 0, \tag{2.26}$$

where Δp is the uniform pressure increment and where the summations are taken over all layers. The last two equations determine the deformation parameters ΔD and $\Delta\epsilon_z$.

3. Solution of a multi-layer tube in infinitesimal or incremental deformation

An analysis of infinitesimal axisymmetric deformation of filament-wound tubes (assuming the deformation is also independent of the axial coordinates z) has been presented by Sherrer (Sherrer, R.E., "Filament-wound cylinders with axial-symmetric loads," J. Composite Mat., Vol. 1, pp. 344-355, 1967). Additional studies have been performed by Pagano (Pagano, N.J., "Stress gradients in laminated composite cylinders," J. Composite Mat., Vol. 5, pp. 260-265, 1971) and others. The following analysis and its results provide explicit relations involving the material parameters and the solutions. These relations provide the basis for the determination of certain material parameters from the experimental data of filament-wound tubes under internal pressure load. The present analysis also suggests a simpler solution algorithm for a filament-wound tube with alternating layers.

3.1 Linearized and incremental problems for a filament-wound tube

For the linearized problem concerned with small deformations of the tube, the elastic compliance coefficients a_{ij} and β_{ij} are material constants. For the incremental problems associated with large deformation, these coefficients change with the local deformation history. In each particular thin filament sheet, the coefficients change as deformation progresses. At any stage in the deformation of the tube, the compliance coefficients are functions of the radial coordinate because the deformation history depends on the radial coordinate. However, in the case of a thin tube subjected to a negligible twisting deformation (t/R small and $D \approx 0$), the intrinsic extensional strains ϵ_1 and ϵ_2 are nearly identical for all filament sheets and, with the exception of the sign change from $+\alpha$ layers to $-\alpha$ layers, the intrinsic shear deformation γ_{12} are also nearly identical in

magnitude. As the deformation continues under an increasing load, the compliance coefficients of all $+\alpha$ layers evolve in nearly the same way and they either remain equal to or differ only in algebraic sign from the corresponding coefficients of the $-\alpha$ layers. The coefficients belonging to the latter type are a_{16}, a_{26}, a_{36}, β_{26} and β_{36}. In the $-\alpha$ layers their values are replaced by $-a_{16}$, $-a_{26}$, $-a_{36}$, $-\beta_{26}$ and $-\beta_{36}$. It follows that, in each step of increment, the parameters λ and K in the differential equations for the incremental problem, Eq. (2.21), are the same in all layers, whereas the parameter H of a $+\alpha$ layer is replaced by $-H$ in a $-\alpha$ layer.

If the twisting parameter D is not small, then the preceding remarks concerning the relation between the compliance coefficients and the parameters λ, K and H of the $+\alpha$ and $-\alpha$ layers are only approximately valid in the case of infinitesimal deformation but not for incremental deformations in the range of large shear strain, because the deformation evolves in such a way that the state of strain in a $-\alpha$ layer ceases to be related to that of a $+\alpha$ layer by a mirror reflection.

3.2 Solution of the linearized or incremental problem

Instead of solving directly for the unknown coefficients A_i and B_i, it is convenient to consider A_1, B_1 and the jumps of A_i and B_i across the interfaces of the layers. Let $[\phi]_i$ denote the jump of ϕ across the i-th interface, i.e., the interface between the i-th layer and the (i+1)-th layer. Then, using Eq. (2.16) and the interfacial continuity of $\Delta\sigma_r$ and Δw, we obtain

$$[r\ \Delta\sigma_r]_i = 0\ , \qquad [r\ \Delta\sigma_\theta]_i = \Delta D\ r^2\ [\beta_{26}]_i a_{11}/\Psi\ . \tag{3.1}$$

Substituting Eqs. (2.23) and (2.24) into the preceding equations, we obtain a system of equations which yield the following solutions for the jumps $[A]_i = A_{i+1} - A_i$ and $[B]_i = B_{i+1} - B_i$:

$$[A]_i = \Delta D(r/R^*)^{-\lambda}(r^2/2\lambda)\{-[H]_i(\lambda+2)/(4-\lambda^2) + [\beta_{26}]_i a_{11}/\Psi\} ,$$

$$[B]_i = \Delta D(r/R^*)^{\lambda}(r^2/2\lambda)\{[H]_i(2-\lambda)/(4-\lambda^2) - [\beta_{26}]_i a_{11}/\Psi\} . \qquad (3.2)$$

These recurrence relations determine all subsequent coefficients A_i and B_i from the first two coefficients A_1 and B_1 and the parameters ΔD and $\Delta\epsilon_z$. The last four unknowns are solved from the boundary conditions of $\Delta\sigma_r$ on the interior and exterior surfaces of the tube, and the equations for the axial force and twisting moment, Eqs. (2.25) and (2.26).

A FORTRAN program has been written to implement the linear or incremental analysis of a filament-wound tube with the open-end or closed-end conditions subjected to a uniform pressure load. Using the elastic moduli of glass/epoxy layers suggested in Hull, et al. (Hull, D., Legg, M.J., and B. Spencer, "Failure of glass/polyester filament wound pipe," Composites, Vol. 9, pp. 17-24, 1978), we obtain, for a four-layer tube with R^*/t = 25.75mm/1.5mm and vanishing M_z, the results for the circumferential strain ϵ_θ and the shearing strain $\gamma_{\theta z}$ = D R^* on the middle surface of the tube as shown in Table 1.

	Closed-end tube		Open-end tube	
α	$(E_1t/pR^*)\epsilon_\theta$	$(E_1t/pR^*)\gamma_{\theta z}$	$(E_1t/pR^*)\epsilon_\theta$	$(E_1t/pR^*)\gamma_{\theta z}$
35°	2.642	3.66×10^{-3}	3.283	-7.924×10^{-3}
45°	2.031	8.37×10^{-3}	2.781	-3.681×10^{-3}
55°	1.388	14.94×10^{-3}	2.030	6.382×10^{-3}
65°	1.005	16.42×10^{-3}	1.437	16.77×10^{-3}
75°	0.853	6.73×10^{-3}	1.120	12.70×10^{-3}

Table 1: Comparison of the magnitudes of the circumferential and twisting strains in tubes subjected to internal pressure load only

These results indicate that, with a vanishing twisting moment, the shearing strain $\gamma_{\theta z}$ resulting from the twisting parameter D varies from about 0.1% to less than 2% of the value of circumferential strain on the middle surface. The effect of the twisting deformation should decrease as the number of alternating layers increases and the thickness of each layer decreases. Furthermore, comparison has been made between the stress fields in the preceding solutions associated with $M_z = 0$, and the corresponding solutions with the condition $M_z = 0$ replaced by $D = 0$. The differences in the solutions are, typically, only of the order 0.1%.

The preceding results indicate that, if a filament-wound tube consists of equal number of alternating layers with $+\alpha$ and $-\alpha$ winding angles, then the twisting deformation remains exceeding small provided that the tube is subjected to a vanishing twisting moment. When the parameter ΔD is set equal to zero, Eq. (3.2) yields zero jumps of the coefficients A_i and B_i across each interface. Hence the coefficients are the same in all layers. Furthermore, Eq. (3.1) shows that $\Delta\sigma_\theta$ is continuous across layer interfaces. Indeed, as far as the solutions for the radial and circumferential stress increments $\Delta\sigma_r$ and $\Delta\sigma_\theta$ are concerned, the present problem for a balanced filament-wound tube with zero twisting deformation ($D = 0$) is exactly the same as that for an equivalent homogeneous orthotropic tube. When these stresses are determined, the remaining non-vanishing stress increments $\Delta\sigma_z$ and $\Delta\tau_{\theta z}$ are given by Eqs. (2.18) and (2.19), with $\Delta D = 0$. The resulting axial stress increment $\Delta\sigma_z$ is continuous across each interface, while the shearing stress increment $\Delta\tau_{\theta z}$ is discontinuous because of the jumps of a_{16}, β_{26} and β_{36} across the interfaces.

4. Determination of the constitutive equations of a filament layer from the experimental results of a pressure-loaded tube

The solutions of a thin filament-wound tube described in the preceding section are extremely useful for the experimental determination of certain constitutive properties of a filament layer by direct tests on filament-wound tubes. Due to the limited type and range of deformations experienced by the filament layers in the tube test, the experimental results and the theoretical solutions cannot provide a complete description of the constitutive behavior of a filament layer. However, they do provide a great deal of information concerning linear and incremental constitutive properties, particularly those aspects relevant to similar but more general applications such as axisymmetric deformations of a thick tube.

4.1 Two approximate equalities for a thin filament-wound tube

If experiments under pressure loading are performed on a balanced filament-wound tube with a large radius-to-thickness ratio, R/t, then the axial and circumferential stresses may be considered constant in the tube. They are approximated by the well known formulae

$$\Delta\sigma_\theta = \Delta p(R/t) , \qquad \Delta\sigma_z = q\ \Delta p(R/2t) , \tag{4.1}$$

where Δp is the internal pressure increment and q has the values 0 and 1, respectively, for open-end and closed-end tubes. Since $\Delta\sigma_\theta$ and the radial coordinate r vary only slightly across the thickness of the tube, the equilibrium equation $d(r\ \Delta\sigma_r) = \Delta\sigma_\theta$ implies that $\Delta\sigma_r$ depends almost linearly on r. Using the boundary conditions of $\Delta\sigma_r$ on the interior and exterior surfaces ($-\Delta p$ and 0, respectively), we have

$$\iint \Delta\sigma_r\ dA = -\ \pi R t\ \Delta p,$$

where the area integral extends over the cross-section of the tube. By

neglecting the terms involving ΔD in Eqs. (2.16) and (2.19), integrating Eq. (2.16) over the cross-section of the tube, and substituting Eq. (2.19) into (2.25), we obtain the following approximate equalities valid for a thin tube subjected to a vanishing twisting moment:

$$Z\,\Gamma_2 + \Psi = \Theta\,\Gamma_1 - (t/2R)\,\Phi, \tag{4.2a}$$

$$Z\,a_{66} - \Gamma_2 - (t/2R)\,\Gamma_3 = (q/2)\,\Gamma_1, \tag{4.2b}$$

where

$$Z = \Delta\epsilon_z\,(t/R\Delta p), \qquad \Theta = \Delta\epsilon_\theta\,(t/R\Delta p) \tag{4.3}$$

are easily evaluated in terms of experimental data.

The compliance coefficients a_{ij}, and the parameters β_{ij}, Γ_1, Γ_2, Γ_3, Φ and Ψ, which are defined in terms of a_{ij} by Eqs. (2.15) and (2.20), are determined by the orientation angle of the filament layer and the <u>intrinsic</u> linear or incremental stiffness parameters of the layer. These intrinsic stiffness parameters are the extensional moduli along and perpendicular to the filament direction, E_1 and E_2, the in-plane shear modulus G_{12}, and the Poisson ratios ν_{12} and ν_{23}. We denote

$$x^* = 1/E_1, \qquad y^* = 1/E_2, \qquad z^* = 1/G_{12},$$

$$u^* = \nu_{12}/E_1, \qquad v^* = \nu_{23}/E_2. \tag{4.4}$$

Then,

$$a_{66} = -(x^*+y^*-z^*+2u^*)(\cos 4\alpha)/2 + (x^*+y^*+z^*+2u^*)/2, \tag{4.5a}$$

$$\Gamma_1 = a_{11}\beta_{66} = \{(x^*+y^*-2u^*)z^*-4(x^*y^*-u^{*2})\}(\cos 4\alpha)/8 + (x^*-y^*)z^*(\cos 2\alpha)/2 + (3x^*+3y^*+2u^*)z^*/8 + (x^*y^*-u^{*2})/2, \tag{4.5b}$$

$$\Gamma_2 = a_{12}a_{66} - a_{16}a_{26} = \{(x^*+y^*-2u^*)z^*-4(x^*y^*-u^{*2})\}(\cos 4\alpha)/8 - (x^*+y^*+6u^*)z^*/8 + (x^*y^*-u^{*2})/2, \tag{4.5c}$$

$$\Gamma_3 = a_{16}a_{36} - a_{13}a_{66} = \{(u^*+v^*)z^*/4-(u^*y^*+v^*x^*+u^*v^*+u^{*2})/2\}(\cos 4\alpha) + (u^*-v^*)z^*(\cos 2\alpha)/2 + (u^*+v^*)z^*/4 + (u^*y^*+v^*x^*+u^*v^*+u^{*2})/2, \tag{4.5d}$$

$$\Phi = a_{11}(\beta_{26}\beta_{36} - \beta_{23}\beta_{66}) = - z^*(u^*y^*-v^*x^*+u^*v^*-u^{*2})(\cos 2\alpha)/2 + z^*(u^*y^*+v^*x^*+u^*v^*+u^{*2})/2, \quad (4.5e)$$

$$\Psi = a_{11}(\beta_{22}\beta_{66} - \beta_{26}^2) = (x^*y^* - u^{*2})z^*. \quad (4.5f)$$

4.2 Use of the data from ±45° tube -- Determination of the shear modulus G_{12}

We now consider the task of determining the material moduli E_1, E_2, G_{12}, ν_{12} and ν_{23} (or, equivalently, x^*, y^*, z^*, u^* and v^*) from the experimental results of filament-wound tubes with various winding angles $\pm\alpha$ undergoing linear elastic deformation. The tubes are assumed to be under an internal pressure load and both the open-end condition and the closed-end condition will be considered. By substituting the expressions of Eq. (4.5) into Eqs. (4.2a) and (4.2b), we obtain, for each winding angle, two equations for x^*, y^*, z^*, u^* and v^* in the case of open-end test, and two more equations in the case of closed-end test. Additional sets of equations for the five material parameters may be obtained by testing filament-wound tubes with different winding angles. These equations provide conditions for determining the material parameters.

Of particular interest is the system of equations corresponding to $\alpha = 45°$. For this winding angle Eq. (4.5) reduce to

$$a_{66} = x^*+y^*+2u^*, \quad (4.6a)$$

$$\Gamma_1 = (x^*+y^*+2u^*)z^*/4 + x^*y^* - u^{*2}, \quad (4.6b)$$

$$\Gamma_2 = - (x^*+y^*+2u^*)z^*/4 + x^*y^* - u^{*2}, \quad (4.6c)$$

$$\Gamma_3 = u^*y^*+v^*x^*+u^*v^*+u^{*2}, \quad (4.6d)$$

$$\Phi = z^*(u^*y^*+v^*x^*+u^*v^*+u^{*2})/2, \quad (4.6e)$$

$$\Psi = (x^*y^* - u^{*2})z^*. \quad (4.6f)$$

Substitution into Eq. (4.2) yields

$$4\{1+(2-\theta)/z^*\}(x^*y^*-u^{*2}) = (2+\theta)(x^*+y^*+2u^*)-(t/R)(u^*y^*+v^*x^*+u^*v^*+u^{*2}), \quad (4.7a)$$

$$(2+q)(x^*y^*-u^{*2}) = \{2Z+(2-q)*z^*/4\}(x^*+y^*+2u^*)-(t/R)(u^*y^*+v^*x^*+u^*v^*+u^{*2}). \quad (4.7b)$$

Taking the difference of the last two equations, we have

$$(Z - \theta + (2-q)z^*)\,(4(x^*y^*-u^{*2})/z^* + x^*+y^*+2u^*) = 0.$$

Using the definitions of x^*, y^* and u^*, one can show that the second factor of the left-hand side of the last equation is positive. Hence the equality requires that

$$1/G_{12} = z^* = 4(\theta-Z)/(2-q)\,\big|_{\alpha=\pi/4}. \tag{4.8}$$

Substitution into Eq. (4.7b) yields

$$(2+q)(x^*y^*-u^{*2}) = (Z+\theta)\big|_{\alpha=\pi/4}(x^*+y^*+2u^*) - (t/R)(u^*y^*+v^*x^*+u^*v^*+u^{*2}). \tag{4.9}$$

For a tube with a small thickness-to-radius ratio t/R, one may neglect the term involving the factor t/R in Eq. (4.9) in comparison with the remaining terms (to a certain extent, this approximation is implicit in Eq. (4.1)). This yields the approximate result:

$$(x^*y^*-u^{*2})/(x^*+y^*+2u^*) = \rho = (Z+\theta)/(2+q)\big|_{\alpha=\pi/4}. \tag{4.10}$$

The last equation yields an expression of u^* in terms of x^* and y^*:

$$u^* = \{(x^*-\rho)(y^*-\rho)\}^{1/2} - \rho. \tag{4.11}$$

Since the expressions of Eqs. (4.9) and (4.10) involve only the experimental data measured from a particular test specimen (with $\alpha = \pm 45°$ and with a specific fiber content) at a particular stage of the deformation process, they may be used to determine the values of z^* and $(x^*y^*-u^{*2})/(x^*+y^*+2u^*)$ at that stage of deformation. This is in contrast to the task of determining the remaining material parameters, which require, in addition, data taken under different test conditions or from other tubes with different winding angles. Those other specimens have different stress and strain histories. Hence their incremental moduli do not evolve in the same manner as the incremental moduli of the tube with $\pm 45°$ winding angles. Therefore, the incremental shear modulus G_{12} and the relation (4.11) among the incremental compliances x^*, y^* and u^*

associated with the deformation of ±45° tubes generally cannot be combined with the relations among the incremental compliances associated with the experimental results of tubes with different winding angles to yield a complete set of equations for determining all incremental compliances. A method that can be used to circumvent this difficulty, at least to a certain extent, is by first subjecting several identical tubes with the same winding angle (not equal to 45°) to the same load history, and subsequently impose incremental loads of different nature, e.g., by varying the end conditions or by superimposing different axial loads upon the pressure load.

We note that when the terms involving t/R in Eqs. (4.2) and (4.7) are neglected in comparison with the remaining terms, the material parameter v^* no longer appears in the governing equations. Thus, in the limit of vanishing t/R, the stresses in the tube (under axisymmetric deformation with zero twisting deformation) are unaffected by the Poisson's ratio ν_{23}. The latter cannot be determined by the type of experiments considered here if the thickness ratio t/R is small.

4.3 Use of the data from tubes with other winding angles

In using the test data from tubes with winding angles different from ±45° subjected to open-end or closed end conditions (where q = 0 and 1, respectively), it is convenient to refer the incremental stresses and strains to the material axes parallel and perpendicular to the fibers. The intrinsic strain increments $\Delta\epsilon_1$, $\Delta\epsilon_2$ and $\Delta\gamma_{12}$ may be calculated from the measured axial and circumferential strain increments by using the transformation rule of the strain, or, in case of large shear deformation, by using Eqs. (2.5), (2.6) and (2.4). From the definitions of Eq. (4.4) we have

$$\Delta\epsilon_1 = x^* \Delta\sigma_1 - u^* \Delta\sigma_2, \qquad \Delta\epsilon_2 = -u^* \Delta\sigma_1 + y^* \Delta\sigma_2.$$

Hence,

$$\Delta\sigma_1 = (y^*/(x^*y^*-u^{*2}))\ \Delta\epsilon_1 + (u^*/(x^*y^*-u^{*2}))\ \Delta\epsilon_2,$$

$$\Delta\sigma_2 = (u^*/(x^*y^*-u^{*2}))\ \Delta\epsilon_1 + (x^*/(x^*y^*-u^{*2}))\ \Delta\epsilon_2.$$

Summing the last two expressions and making use of the equality

$$\Delta\sigma_1 + \Delta\sigma_2 = \Delta\sigma_z + \Delta\sigma_\theta = (1+q/2)\ \Delta\sigma_\theta = (1+q/2)\ R\Delta p/t,$$

we obtain

$$\Xi_1\ (y^*+u^*)/(x^*y^*-u^{*2}) + \Xi_2\ (x^*+u^*)/(x^*y^*-u^{*2}) = 1 + q/2, \qquad (4.12)$$

where

$$\Xi_1 = \Delta\epsilon_1\ (t/R\Delta p), \qquad \Xi_2 = \Delta\epsilon_2\ (t/R\Delta p), \qquad (4.13a,b)$$

and, for subsequent use,

$$\Xi_{12} = \gamma_{12}\ (t/R\Delta p). \qquad (4.13c)$$

Now, using the transformation rule of the incremental stress, we obtain

$$\Delta\tau_{12} \csc 2\beta \cos 2(\alpha+\beta) = (\Delta\sigma_z - \Delta\sigma_\theta)/2 = -(2-q)R\Delta p/(4t),$$

and, consequently,

$$\csc 2\beta \cos 2(\alpha+\beta) = -(2-q)z^*/(4\Xi_{12}), \qquad (4.14a)$$

where 2β satisfies

$$2 \operatorname{ctn} 2\beta = (\Delta\sigma_1 - \Delta\sigma_2)/\Delta\tau_{12}$$

$$= (\Delta\epsilon_1/\Delta\gamma_{12})(y^*-u^*)z^*/(x^*y^*-u^{*2}) - (\Delta\epsilon_2/\Delta\gamma_{12})(x^*-u^*)z^*/(x^*y^*-u^{*2}). \qquad (4.14b)$$

We note that 2β is the angle between the horizontal axis of the $\Delta\sigma$-$\Delta\tau$ plane and the radial line through the point $(\Delta\sigma_1,\ \Delta\tau_{12})$ in the Mohr's circle for the incremental stress.

Expressing 2Δ in terms of the right hand side of Eq. (4.14b), and substituting the result into Eq. (14.a), one obtains, in addition to Eq. (4.12) another algebraic relation among x^*, y^*, z^* and u^*, with Ξ_1, Ξ_2, Ξ_{12} and q as parameters. The two equations reduce to Eqs. (4.8) and (4.10) in the case $\alpha = 45°$.

The parameter q may be changed at any stage of the loading process by changing the end conditions. Consider two identical test specimens under the same end conditions and subjected to identical pressure loads until the present state. Subsequently, the tubes are subjected to an incremental pressure load, with one tube under the open-end condition (q = 0) and the other tube under the closed-end condition. Then each set of data for Ξ_1, Ξ_2 and Ξ_{12} (calculated from the experimental data by using Eqs. (2.4), (2.5), (2.6) and (4.13)) with the corresponding value of q yield two relations among the incremental compliances according to Eqs. (4.12) and (4.14). The solution of the four resulting relations yield x^*, y^*, z^* and u^*.

4.4 Determination of the initial elastic moduli in the range of small strain

For the determination of the initial elastic moduli in the range of small strain, relations based on experimental results of tubes with different winding angles may be combined to yield a complete system of equations for calculating the moduli. First, the test data of the ±45° tubes are used to obtain z^* from Eq. (4.8) and a relation (Eq.(4.10) or (4.11)) among x^*, y^* and u^*. Substituting the relation into Eq. (4.12), we obtain

$$y^*+u^* = \{(1+q/2)\rho/(\Xi_1-\Xi_2) - \Xi_2/(\Xi_1-\Xi_2)\}\ (x^*+y^*+2u^*), \qquad (4.15)$$

or,

$$x^*+u^* = \{-(1+q/2)\rho/(\Xi_1-\Xi_2) + \Xi_1/(\Xi_1-\Xi_2)\}\ (x^*+y^*+2u^*).$$

The test data of a tube with $\alpha \neq 45°$ is then used to solve for 2β from Eq. (4.14a). The solution is substituted into Eq. (4.14b) to yield

$$(\Xi_1/\Xi_{12})(y^*-u^*) - (\Xi_2/\Xi_{12})(x^*-u^*) = 2\ (\mathrm{ctn}\ 2\beta)\ (\rho/z^*)\ (x^*+y^*+2u^*). \qquad (4.16)$$

Equations (4.15) and (4.16) are two linear relations among the unknowns x^*, y^* and u^* which may be used to express x^* and y^* as products of u^* with factors involving known quantities. Substituting the expressions into Eq. (4.10), we

obtain a quadratic equation for u^*, which is readily solved. The only nontrivial step in the process of computation is solving 2β from Eq. (4.14a). This may be done by the Newton-Raphson iterative scheme.

Hence, the experimental results for two tubes, one with the winding angle $\pm 45°$ and another with a different angle, suffice to determine the four compliance coefficients z^*, x^*, y^* and u^* associated with the linear elastic behavior at small strain. The two filament-wound tubes must be identical in material and geometry except for the winding angle. In particular, the fiber volume content must be the same.

Hull and coworkers have presented a comprehensive set of test results on glass/polyester filament wound tubes under both the open-end and the closed-end conditions, for $\alpha = 54°44'$ (the "ideal winding angle" for a closed-end tube, see Hull, D., Legg, M.J. and Spencer, B., "Failure of glass/polyester filament wound pipe", Composites, Vol. 9, pp. 17-24, 1978) as well as for tubes with other winding angles (Spencer, B and Hull, D., "Effect of winding angle on the failure of filament wound pipe," Composites, Vol. 9, pp. 263-271 (1978). Twisting deformation was apparently not noticeable at least in the initial stages of the experiments and therefore were not reported. The fiber volume fractions in different specimens were measured by using ASTM method D2584, and were found to vary in the range from 0.39 to 0.56. Since the fiber content affects the composite property, only the relations based on specimens with nearly identical fiber contents should be combined to determine the initial compliance parameters. For the six specimens with $\alpha = \pm 45°$ (including two specimens under the open-end conditions and four under the closed-end conditions), the reported fiber volume fraction V_f, the measured initial stiffnesses $1/\Theta = \sigma_\theta/\epsilon_\theta$ and $1/Z = \sigma_\theta/\epsilon_z$ (taken from Table 1 and 2 in Spencer and Hull, 1978) and the value of $G_{12} = z^*$ and $1/\rho$

$= (x^*+y^*+2u^*)/(x^*y^*-u^{*2})$ calculated from Eqs. (4.8) and (4.10) are shown in Table 2, where all numbers except V_f have the unit of GPa. Notice that

$$1/\rho = \{(1+\nu_{21})E_1+(1+\nu_{12})E_2\}/(1-\nu_{12}\nu_{21}). \tag{4.17}$$

	V_f	$1/\theta$ (GPa)	$1/Z$ (GPa)	G_{12} (GPa)	$1/\rho$ (GPa)
Open-end	0.43	17.7	-30.7	5.61	83.6
Open-end	0.46	15.3	-23.2	4.61	89.9
Closed-end	0.46	20.8	large	5.20	62.4
Closed-end	0.45	22.8	large	5.70	68.4
Closed-end	0.39	17.8	large	4.45	53.4
Closed-end	0.43	20.4	large	5.10	61.2

Table 2: Response of $\pm 45^\circ$ tubes in the initial small-strain range (Base on the experimental data of Spencer and Hull, 1978)

There are significant differences in the results (especially in $1/\rho$, between open-end and closed-end tubes) which cannot be attributed primarily to the differences in the fiber volume fraction. The very large difference in the measured data for $1/Z = pR/(t\epsilon_z)$ of the two open-end tubes and the near 10% difference in the measured data of $1/\theta$ from the two closed-end tubes with similar fiber contents ($V_f = 0.46$ and 0.45) suggest that the specimen properties are not consistent, due perhaps to unevenness in fiber property and variations in the winding process (with the resulting misalignment and waviness of fibers).

The significant differences in the elastic compliance coefficients as

determined by testing of different tube specimens suggest that, for a particular material system and winding process, a sufficiently large number of specimens should be tested to provide information concerning the average values and the range of variation of the parameters characterizing the behavior of the composite. It is risky to rely on empirical formulas of the composite elastic moduli or on analytical predictions of the composite behavior (based on micromechanical analysis using the fiber and matrix properties as supplied by manufacturers) as the sole basis for the design and analysis of filament-wound structures.

Spencer and Hull also presented test results for open-end and closed-end tubes with other winding angles. These results supply additional relations among the compliance coefficients. The values of z^* and $1/\rho$ are based on the test results of the tube with ±45° winding angle, after excluding the data for the tube with the exceptionally small fiber content (the one with $V_f = 0.39$). Thus $G_{12} = 1/z^* = 5.24$ GPa is obtained by averaging the results of the remaining five tubes, while two values of $1/\rho$, 86.8 GPa and 64.0 GPa, respectively, will be used for the open-end and closed-end cases, because of the significant differences in the respective results from the ±45° tubes. Using the experimental data of open- and closed-end tubes with winding angles 35°, 55°, 65° and 75°, and Eqs. (4.15), (4.16) and (4.10), we obtain for the open-end tubes the elastic moduli as shown in Table 3. The results for the closed-end case shown considerable discrepancies among the tubes with different winding angles and, therefore, are not presented. These discrepancies are possibly due to the inconsistency of the specimen material and fiber content so that the values of z^* and $1/\rho$ as determined from the average experimental results of ±45° tubes are significantly different from their true values for the tubes with other winding angles.

α	θ	Z	Ξ_1	Ξ_2	Ξ_{12}	E_1	E_2	ν_{12}
	MPa^{-1}	MPa^{-1}	MPa^{-1}	MPa^{-1}	MPa^{-1}	GPa	GPa	
35°	67	-27	3.9	36.2	88.3	62.3	20.0	.11
55°	44	-27	20.6	-3.6	66.7	50.7	26.3	.16
65°	33	-19.5	23.6	-10.1	40.2	45.8	19.9	.39
75°	26	-8.3	23.7	-6.0	17.2	43.9	28.0	.22

Table 3: Linear elastic moduli determined from the experimental results of the open-end, ±45° tube ($G_{12} = 1/z^* = 5.24$ GPa and $1/\rho = 86.8$ GPa) and another open-end tube with a different winding angle.

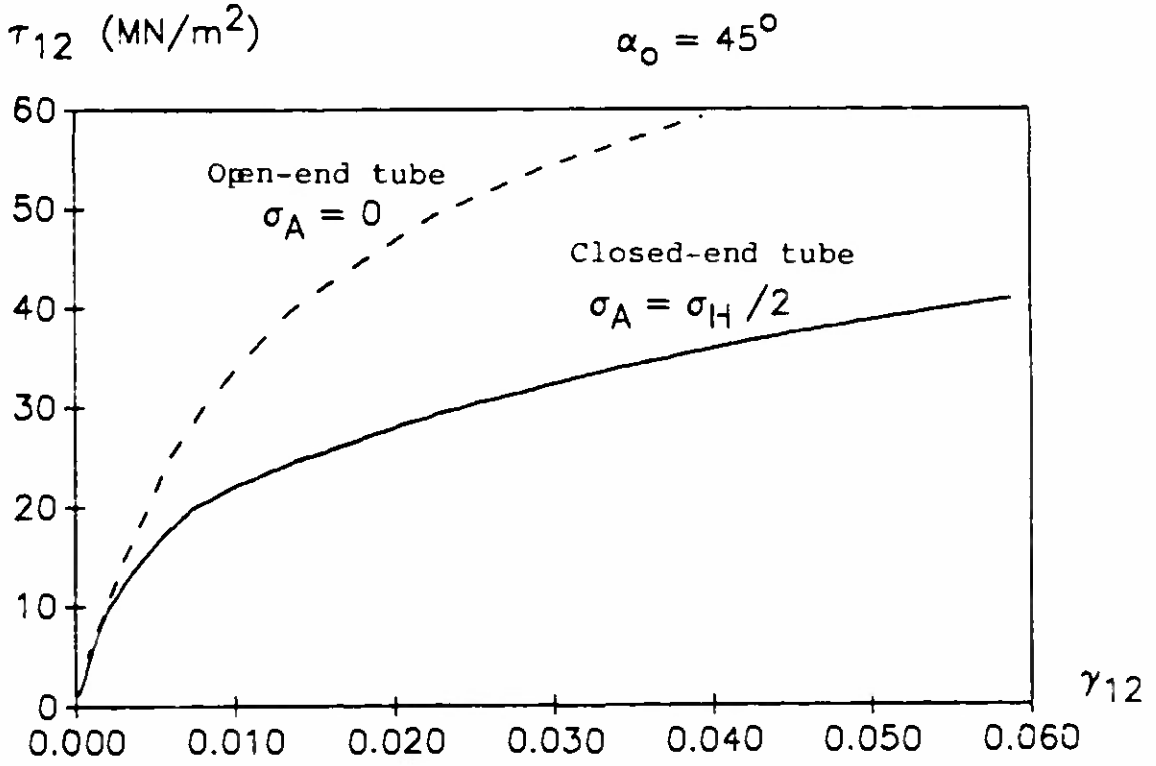

Fig. 7: Shear stress vs. shear strain in 45° tubes under increasing internal pressure

4.5 Comparison of the nonlinear shear responses associated with the open-end and closed-end conditions

Figures 5 and 8 of Spencer and Hull (1978) show the data of the axial and circumferential strains versus the pressure load for open and closed-end tubes of various winding angles when the pressure increases from zero to the level at final failure. The data corresponding to $\alpha = \pm 45°$ are used here to obtain the incremental moduli G_{12} and $1/\rho$ at the successive stages of deformation. Since the incremental stiffness of the composite is dependent on the entire history of deformation, the dependence of G_{12} and $1/\rho$ upon γ_{12} is affected by the present and past values of ϵ_1 and ϵ_2. For the sake of illustrating the dependence of the incremental moduli on the history, the values of all three strain components at the successive stages of deformation are shown in the following two tables (Table 4 and 5, respectively, for the open-end case and the closed-end case) with the corresponding values of the incremental moduli and the pressure. Notice that in the open-end experiments of $\pm 45°$ tubes, the shearing strain is greater than the extensional strains by an order of magnitude. In the closed-end experiments, γ_{12} varies from two to four times the magnitude of ϵ_1 or ϵ_2. Therefore, the relation between τ_{12} and γ_{12} as suggested by the incremental moduli G_{12} in the first table is more representative of the shear response in the absence of significant accompanying normal stresses, while the effect of the normal stresses is certainly important in the relation described by Table 5. For $\pm 45°$ tubes we have $\tau_{12} = (\sigma_\theta - \sigma_z)/2 \approx (1-q)pR/(2t)$. Therefore, τ_{12} may be directly associated with the corresponding value of γ_{12} in the successive stages of deformation. In Fig. 7, the results are plotted for both the open-end and closed-end cases. The two curves are tangential at the origin, because the common slope equals the initial shear modulus. The relation for the close-end tube deviates significantly from

linearity at a very early stage of deformation, because of the relatively larger values of ϵ_1 and ϵ_2 in the deformation of the closed-end tubes.

pR/t (MPa)	ϵ_1 (10^{-3})	ϵ_2 (10^{-3})	γ_{12} (10^{-3})	G_{12} (GPa)	$1/\rho$ (GPa)
10	.05	.05	.94	5.3	150.
20	.10	.10	1.97	4.85	117.
30	.23	.22	3.11	4.39	70.
40	.39	.38	4.56	3.45	59.
50	.61	.60	5.88	3.2	51.
60	.79	.76	8.0	2.5	69.
70	.85	.79	10.5	2.0	95.
80	.97	.88	13.4	1.61	80.
90	1.15	.99	17.8	1.27	61.
100	1.51	1.26	22.4	1.03	23.
110	2.33	1.90	29.3	0.73	13.
120	4.35	3.57	39.5	0.48	5.2

Table 4: Incremental moduli G_{12} and $1/\rho$ calculate from the large-deformation experimental results of a ±45°, open-end tube

pR/t (MPa)	ϵ_1 (10^{-3})	ϵ_2 (10^{-3})	γ_{12} (10^{-3})	G_{12} (GPa)	$1/\rho$ (GPa)
10	.23	.23	.53	5.3	70.
20	.46	.46	1.08	4.7	64.
30	.70	.70	1.66	3.9	57.
40	.96	.96	2.30	2.9	55.
50	1.30	1.29	3.17	2.0	51.
60	1.63	1.62	4.33	2.5	45.
70	1.99	1.98	5.69	1.9	51.
80	2.43	2.40	7.32	1.13	27.
90	2.99	2.94	10.2	0.77	27.
100	3,69	3.60	13.7	0.63	21.
110	4.37	4.21	17.9	0.58	19.2
120	5.17	4.92	22.5	0.49	19.9
130	6.10	5.70	28.3	0.43	16.9
140	7.04	6.45	34.0	0.37	16.9
150	8.01	7.17	41.0	0.33	16.8
180	8.92	7.71	49.1	0.28	13.4
190	10.3	8.58	58.7	0.24	12.4

Table 5: Incremental moduli G_{12} and $1/\rho$ calculated from the large-deformation experimental results of a ±45°, closed-end tube

The preceding two tables indicate that, for both the open-end and closed-end conditions, the incremental shear modulus G_{12} decreases monotonically as the pressure load increases. Since the factor $(1-\nu_{12}\nu_{21})$ is close to 1 for strongly anisotropic fiber-reinforced composites, the incremental stiffness $1/\rho$ as given by Eq. (4.17) is approximately equal to the sum of the incremental stiffnesses along the fiber and the transverse directions, characterized respectively by $(1+\nu_{21})E_1$ and $(1+\nu_{12})E_2$. Since glass and carbon fibers show linearly elastic axial response before tensile failure, and since the stiffness of the filament layer in the fiber direction is largely contributed by the elasticity of the fiber, $(1+\nu_{21})E_1$ remains almost constant throughout the process of deformation. Hence the significant decrease in the stiffness $1/\rho$, as indicated in the preceding two tables, may imply that the incremental stiffness in the transverse direction eventually becomes negative. A negative incremental stiffness in the transverse direction is not physically unreasonable. It simply means that, at a certain stage of deformation, additional positive strain increments $\Delta\epsilon_1$ and $\Delta\epsilon_2$ may be produced by increasing the tensile stress σ_1 along the fiber direction while partially relieving the tensile stress σ_2 in the transverse direction.

4.6 A constitutive model for large deformation of a filament layer

The experimental results of Hull and coworkers for glass/polyester filament-wound tubes show significant deviation from linear stress-strain relation at even a low level of pressure. Similar nonlinearity at moderate or large pressure loads were also observed in experiments on filament-wound tubes with carbon fibers (see, for example, Uemura, M. and Fukunaga, H., "Probabilistic Burst Strength of Filament-Wound Cylinders Under Internal Pressure," J. Composite Materials, Vol. 15, pp. 462-480. A large body of experimental results on tubes with glass and carbon filaments have been obtained at Redstone Arsenal, Alabama,

including Technical Report RL-84-11, "Mechanical Property Characterization of the Sentry Initial Propulsion Test Vehicle (IPTV) Composite Motorcase Materials," by Terry L. Vandiver, Technical Report RL-80-13, "Evaluation of Filament-Wound Composites with Kevlar 49 Filament and Two Resins, HBRF 55A and HBRF 241, By Hydrostatic Testing," and Tech. Report RL-75-8, "Development of the filament-wound composite launch tubes for the SMAWT program," both by G.A. Clodfelter, U.S. Army Missile Command, Redstone Arsenal, March 1975).

The nonlinearity in response and the inelastic behavior of a filament layer are primarily due to the severe shear deformation in the resin material. Constitutive equations that adequately describe these effects may be given in the incremental form, and the preceding analysis is an initial step in that direction from a purely empirical viewpoint, with very little regard to the underlying physical basis such as the plasticity behavior of the resin material and the effects of microcracking or interface debonding. In general, the incremental compliance coefficients are dependent on the history of strain. A purely empirical formulation of the incremental constitutive relations over the entire range of strain space would require a very complex set of expressions, not to mention an impossibly large amount of experimental data to be used to obtain such expressions. However, if the results of tube experiments are intended only for the purpose of formulating constitutive relations with a limited range of applicability, i.e., limited only to applications in which the geometrical configurations and loading histories are similar to those involved in the tube experiments (e.g., monotone loading or proportional loading), then the amount of the required experimental data may be significantly reduced and relatively simple empirical constitutive relations may be sought. Such constitutive equations with a limited range of applicability need not be in the incremental form. A

functional relationship between the stresses σ_1, σ_2 and τ_{12} and the strains ϵ_1, ϵ_2 and γ_{12} is convenient because of the simplicity of formulation and the ease of determining the material functions from the experimental results.

We note that, as mentioned previously, γ_{12} (defined as the reduction in the angle between two material lines originally parallel and orthogonal to the fiber direction) is not a physical component of a finite strain tensor with respect to the intrinsic material directions. Indeed, under the orthogonal transformation of the coordinates from (z, θ) to the intrinsic axes, the components ϵ_z, ϵ_θ and $\gamma_{z\theta}$ transform into ϵ_1, ϵ_2 and γ_{12} only if the strain is infinitesimal. However, the most convenient and therefore the most appropriate constitutive equation for an anisotropic filament layer need not be a relation among the tensorial components of stress and strain. It is perfectly legitimate to use a functionally related set of strain variables, provided that one keeps in mind their original definitions which, in the case of γ_{12}, is given by Eq. (2.4) for a tube suffering no twisting deformation.

Since the response of a filament layer in the filament direction is dominated by the linearly elastic behavior of the filament material, it is reasonable to assume that σ_1 depends linearly on ϵ_1 and ϵ_2, provided that these strains are small, and that σ_1 is not appreciably affected by γ_{12}. The shearing stress τ_{12} depends nonlinearly on γ_{12}, and this dependence is expected to be influenced by the transverse strain ϵ_2, because a negative ϵ_2 tends to cause compression of the resin material between two parallel fibers with the effect of increasing the resistance of the resin material to shear deformation. This effect of ϵ_2 upon τ_{12} should be reciprocated by a corresponding effect of γ_{12} upon the transverse normal stress σ_2. The nature of the coupling effect is suggested by the usual assumption concerning the symmetry of the incremental stiffness

matrix. Thus, although the general nature of the material behavior is inelastic, the special constitutive equations intended only for a limited class of deformations histories with similar geometrical and loading features may still be expressed in forms suggested by nonlinear elasticity. Consequently, for a filament layer in a certain restricted range of deformation histories we postulate the following constitutive equation for σ_1, σ_2 and τ_{12} in terms of ϵ_1, ϵ_2 and γ_{12}:

$$\begin{aligned} \sigma_1 &= S_{11}\,\epsilon_1 + S_{12}\,\epsilon_2, \\ \sigma_2 &= S_{12}\,\epsilon_1 + S_{22}\,\epsilon_2 - f(\gamma_{12}), \\ \tau_{12} &= g(\gamma_{12}) - \epsilon_2\, f'(\gamma_{12}), \end{aligned} \tag{4.18}$$

where f and g are even and odd functions, respectively, of the shear strain.

There are a number of previous works dealing with the formulation of nonlinear constitutive equations of unidirectional composites and filament-wound layers. For example, Hahn and Tsai (Hahn, H. T. and Tsai, S.W., "Nonlinear elastic behavior of unidirectional composite laminae," J. Composite Materials, Vol. 7, pp. 102-118, 1973) considered nonlinear elastic behavior and introduced a complementary energy density that is a fourth-order polynomial function of σ_1, σ_2 and τ_{12}. The formulation generally leads to an expression of the strains in terms of the stresses which, except in some special cases, is difficult to invert. Elastic relations for the strain components as polynomial functions of the stress components were also proposed recently by Luo and Chou (Luo, S-Y and Chou T-W., "Finite deformation and nonlinear elastic behavior of flexible composites," J. Appl. Mech., Vol. 55, pp. 149-155, 1988). Notice that in practice it is always preferable to use a constitutive equation of the filament layer with ϵ_1, ϵ_2 and γ_{12} as independent variables, because these variables vary continuously across the interfaces of alternating layers (whereas the stresses

may suffer discontinuities) and, in the deformation of thin tubes without twisting, they do not vary appreciably across the thickness. Furthermore, the force and moment resultants occurring in the shell equations are calculate by integrating the expression of the stresses in terms of strains with respect to the thickness coordinate. While the inversion of a linear stress-strain relation is a trivial matter, a nonlinear constitutive for the strains in terms of the stresses is in most cases extremely difficult to invert.

The direct use of a polynomial strain energy density was also suggested in the work of Hahn and Tsai. However, their results did include a coupling effect between the transverse strain and shearing strain. The coupling effect was also not taken into account in a recent study by Frost (Frost, S. R., "An approximate theory for predicting the moduli of unidirectional laminates with non-linear stress/strain behavior," J. Composite Materials, Vol. 24, pp. 269-292, 1990), or in the work of Hashin et al. (Hashin,Z., Bagchi, D. and Rosen, W., "Non-linear Behavior of Fiber Composite Laminates," NASA CR-2313, April, 1974). When the coupling effect is ignored, the shearing stress is simply a function of the shearing strain alone, unrelated to and unaffected by the transverse strain ϵ_2. But the validity of this conclusion is evidently refuted by the significant differences between the τ_{12} versus θ_{12} relations of the open-end and closed-end tubes, as shown in Fig. 7.

Equation (4.18) is proposed because it is perhaps the simplest constitutive equation for a filament layer that captures the general nonlinear dependence of the shearing stress upon the shearing strain and, at the same time, includes the nonlinear coupling effect between the shearing and transverse strains in a way consistent with the usual assumption of the symmetry of the incremental stiffness matrix. The linear dependence of τ_{12} on ϵ_2 is the simplest functional relation

consistent with the assumption that the incremental shearing stiffness increases with transverse compression (therefore, decreases with the transverse extension ϵ_2), i.e., that the resistence of the material to incremental shearing deformation is analogous to the law of friction. In contrast, Luo and Chou ("Finite deformation and nonlinear elastic behavior of flexible composites," J. Appl. Mech., Vol. 55, pp. 149-155, 1988, see Eq. (9) of the paper) assumed a coupling between the transverse stress σ_2 and the shear strain γ_{12} in such a manner that the contribution of the coupling effect to the shear stiffness is an even function of σ_2. Their assumption is contrary to the reasonable expectation that the effect of coupling is dependent on the algebraic sign of σ_2.

The incremental stress-strain relation associated with Eq. (4.18) is

$$\begin{Bmatrix} \Delta\sigma_1 \\ \Delta\sigma_2 \\ \Delta\tau_{12} \end{Bmatrix} = \begin{bmatrix} S_{11} & S_{12} & 0 \\ S_{12} & S_{22} & -2f'(\gamma_{12}) \\ 0 & -f'(\gamma_{12}) & 2\{g'(\gamma_{12})-\epsilon_2 f''(\gamma_{12})\} \end{bmatrix} \begin{Bmatrix} \Delta\epsilon_1 \\ \Delta\epsilon_2 \\ \Delta\gamma_{12}/2 \end{Bmatrix} \qquad (4.19)$$

Since the incremental stiffness matrix reduces to the initial stiffness matrix when all strain components vanish, one has the following conditions for the initial derivatives of the functions f and g:

$$f'(0) = 0, \qquad g'(0) = G_{12}. \qquad (4.20a,b)$$

Furthermore, since S_{11}, S_{12} and S_{22} are the stiffness coefficients in the range of small strain, we have

$$f(0) = 0. \qquad (4.20c)$$

Otherwise, the material functions f and g and the stiffness parameters S_{11}, S_{12} and S_{22} in Eq. (4.18) must be determined for each specific type of filament layer from experimental data. The results are presented in the following section for the glass/polyester tubes studied in work of Spencer and Hull, on the basis of their experimental results for the ±45° tubes.

4.8 Determination of the constitutive functions f and g from the results of tube experiments

In testing the ±45° tubes under an internal pressure p, we have

$$\sigma_1 + \sigma_2 = \sigma_\theta + \sigma_z = (1+q/2)\ pR/t,$$

$$\tau_{12} = (\sigma_\theta - \sigma_z)/2 = (1-q/2)\ pR/(2t).$$

Hence Eq. (4.18) yields

$$f(\gamma_{12}) = (S_{11}+S_{12})\ \epsilon_1 + (S_{12}+S_{22})\ \epsilon_2 - (1+q/2)\ pR/t, \tag{4.21}$$

$$g(\gamma_{12}) = (1-q/2)\ pR/(2t) + \epsilon_2\ f'(\gamma_{12}). \tag{4.22}$$

The linear elastic moduli $S_{11}+S_{12}$ and $S_{12}+S_{22}$ are determined from the experimental results in the range of small strain, as described in Sec. 4.4. The data for ϵ_1, ϵ_2 and pR/t corresponding to each value of γ_{12} are substituted into the right-hand side of Eq. (4.21), and this determines the material function $f(\gamma_{12})$. The function so obtained may be differentiated numerically to obtain its derivative $f'(\gamma_{12})$. Then the values of $f'(\gamma_{12})$, ϵ_2 and pR/t associated with each value of γ_{12} are substitute into Eq. (4.22) to obtain the function $g(\gamma_{12})$. This procedure is applied to the experimental results of ±45° tubes with both closed-end and open-end conditions, and the validity of the constitutive equations (4.18) may be tested by comparing the functions f and g obtained in the two cases. Because of the significant differences in the calculated values of the linear elastic moduli corresponding to the closed-end and open-end cases, the stiffness coefficients $S_{11}+S_{12}$ and $S_{12}+S_{22}$ in Eq. (4.21) are evaluated separately for these two cases from the respective experimental data, instead of using a common set of values. In view of the appreciable discrepancies in the linear elastic moduli based on different specimens, the material functions f and g determined from the experimental results in the range of large deformation along different loading paths are expected only to be in approximate or qualitative agreement. The

present results for the closed-end and open-end tubes are shown in Figs. 8a and 8b for the function f and in Figs. 9a and 9b for the function g. The approximate agreement between the two sets of results present a contrast with the significant discrepancy in the relation between τ_{12} and γ_{12} as shown in Fig. 7 (see p. 39).

The relation $\tau_{12} = (\sigma_\theta - \sigma_z)/2$ and the resulting Eq. (4.22) are not valid in the case of tubes with winding angles different from ±45°. Indeed, for such tubes the values of τ_{12} at the successive stages of deformation cannot be determined from the measured data. However, Eq. (21) still holds and the data from such tubes provide independent bases for determining the material function $f(\gamma_{12})$.

4.9 Nonlinear constitutive equations of the filament-wound structure: the incremental stress-strain relation of a laminate

The transformation of the incremental stresses and strains from a local tangential coordinate system (x, y) at a point on the shell middle surface (which, for a circular cylindrical shell, may be identified with the global cylindrical coordinates z and θ) to the material axes (1, 2) in a filament layer follows the relations

$$\begin{Bmatrix} \Delta\epsilon_1 \\ \Delta\epsilon_2 \\ \Delta\gamma_{12}/2 \end{Bmatrix} = [M(\theta)] \begin{Bmatrix} \Delta\epsilon_x \\ \Delta\epsilon_y \\ \Delta\gamma_{xy}/2 \end{Bmatrix}, \qquad \begin{Bmatrix} \Delta\sigma_x \\ \Delta\sigma_y \\ \Delta\tau_{xy} \end{Bmatrix} = [M(-\theta)] \begin{Bmatrix} \Delta\sigma_1 \\ \Delta\sigma_2 \\ \Delta\tau_{12} \end{Bmatrix},$$

where the matrix $[M(\theta)]$ is defined by

$$[M(\theta)] = \begin{bmatrix} \cos^2\theta & \sin^2\theta & \sin 2\theta \\ \sin^2\theta & \cos^2\theta & -\sin 2\theta \\ -(\sin 2\theta)/2 & (\sin 2\theta)/2 & \cos 2\theta \end{bmatrix}$$

Substituting into Eq. (4.19), we obtain

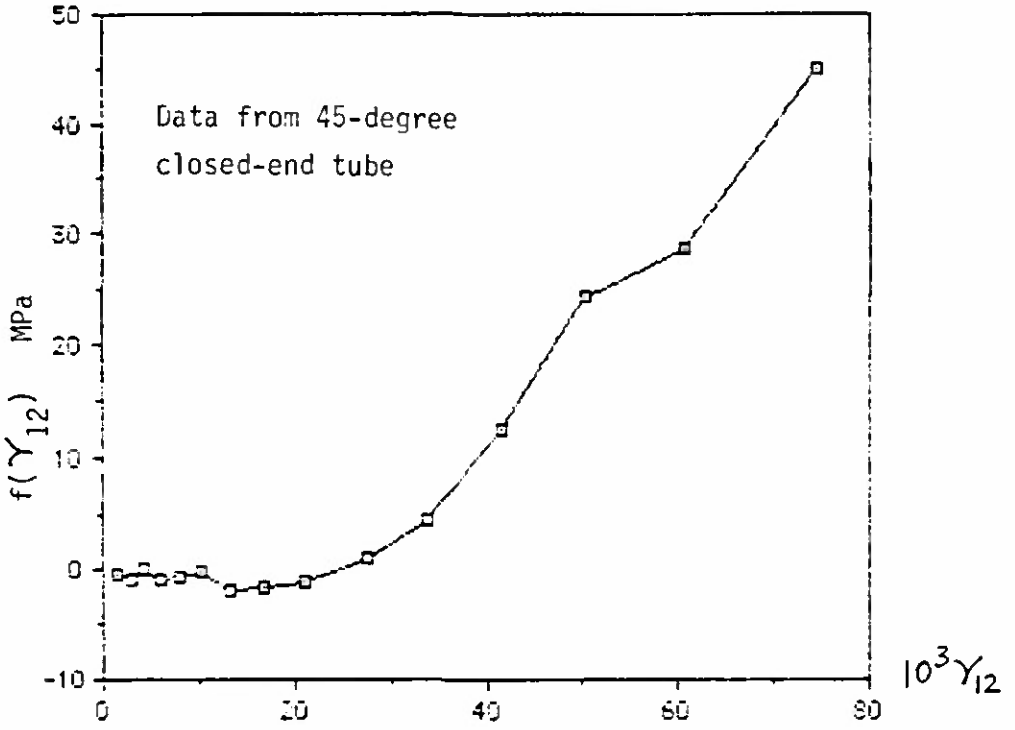

Fig. 8a: Function $f(\gamma_{12})$ based on the test results of the closed-end 45° tube

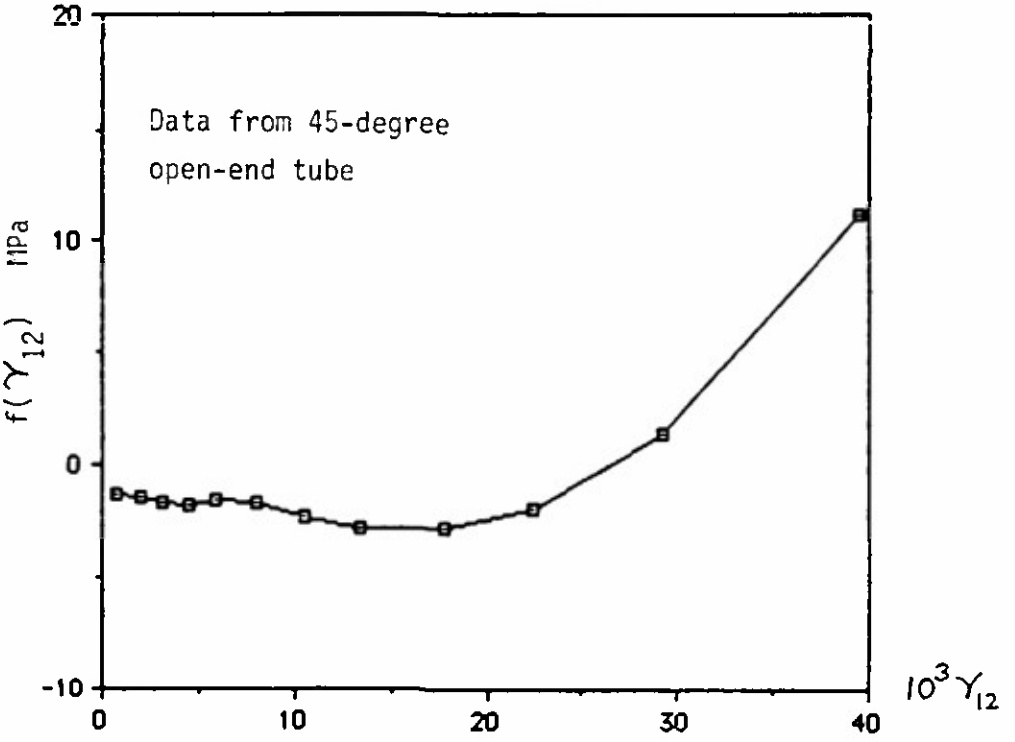

Fig. 8b: Function $f(\gamma_{12})$ based on the test results of the open-end 45° tube

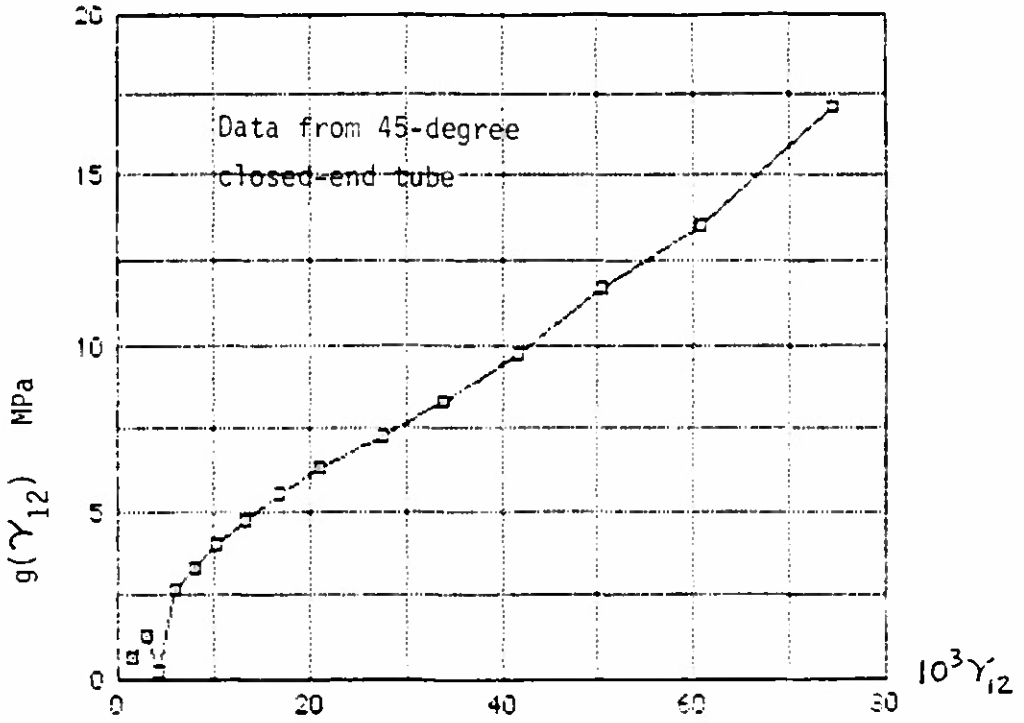

Fig. 9a: Function $g(\gamma_{12})$ based on the test results of the closed-end 45° tube

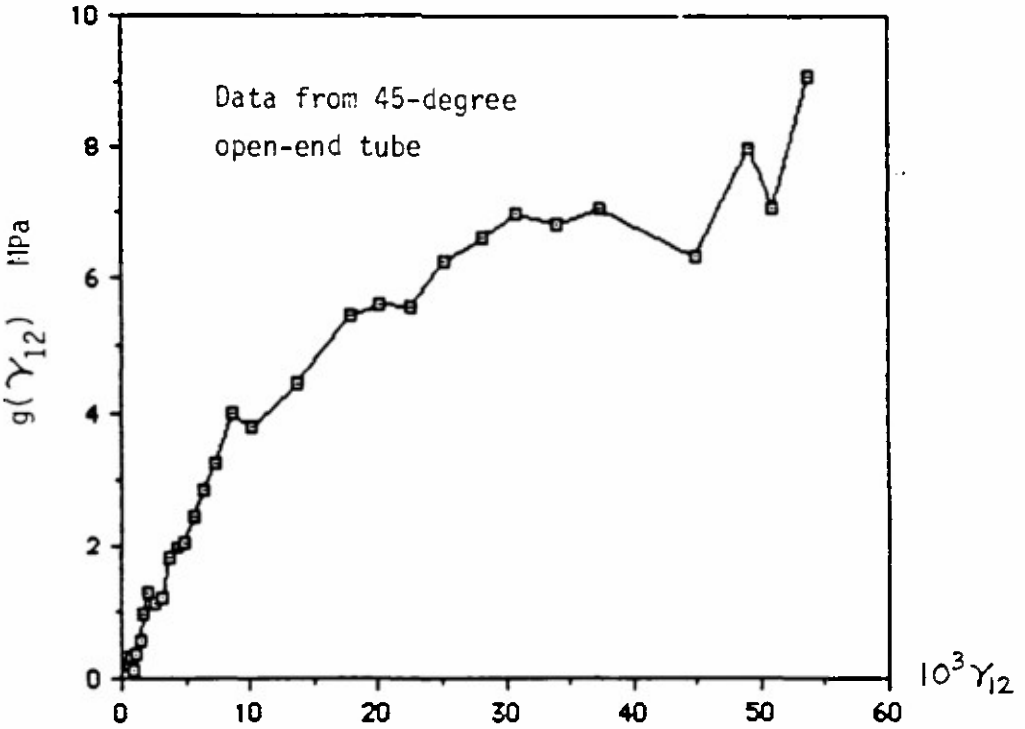

Fig. 9b: Function $g(\gamma_{12})$ based on the test results of the open-end 45° tube

$$\begin{Bmatrix} \Delta\sigma_x \\ \Delta\sigma_y \\ \Delta\tau_{xy} \end{Bmatrix} = [M(-\theta)] \begin{bmatrix} S_{11} & S_{12} & 0 \\ S_{12} & S_{22} & -2f' \\ 0 & f' & 2(g'-\epsilon_2 f) \end{bmatrix} [M(\theta)] \begin{Bmatrix} \Delta\epsilon_x \\ \Delta\epsilon_y \\ \Delta\gamma_{xy}/2 \end{Bmatrix} \tag{4.23}$$

If we adopt the Kirchhoff-Love assumption that the strain increments at a point (x,y,z) are related to the strain increments at the projected point on the middle surface (x,y,0) by the relations

$$\Delta\epsilon_x = \Delta\epsilon_x^\circ - z\,\Delta\kappa_x, \qquad \Delta\epsilon_y = \Delta\epsilon_y^\circ - z\,\Delta\kappa_y,$$

$$\Delta\gamma_{xy} = \Delta\gamma_{xy}^\circ - z\,\Delta\kappa_{xy},$$

where $\Delta\kappa_x$, $\Delta\kappa_y$ and $\Delta\kappa_{xy}$ are the increments of the curvature of the middle surface during the incremental deformation, then by integrating Eq. (4.23) across the thickness of the shell we obtain the relation between the increments of the force and moment resultants, ΔN_x, ΔN_y, ΔN_{xy}, ΔM_x, ΔM_y, ΔM_{xy}, and the increments of the middle-surface strains and curvatures. This incremental relation characterizes the response of the shell element. In each step of the solution process, the current of γ_{12} is computed and the updated values of $f'(\gamma_{12})$ and $g'(\gamma_{12})$ are substituted into Eq. (4.23) to compute the shell element stiffness matrix for the next incremental solution by integrating this equation through the thickness of the shell. Notice that, in the constitutive equation (4.18) for the filament layer, the stiffness coefficients S_{11}, S_{12} and S_{22} have constant values through the deformation process and therefore need not be updated in an incremental step.

III. Micromechanics: Calculation of the Constitutive Properties of a Filament Layer based on the Properties of the Constituents

1. Introduction

A fundamental problem in the mechanics of fiber-reinforced composite materials is the derivation of the gross (macromechanical) constitutive equations of a unidirectional composite from the properties of constituent materials. In the case of a filament-wound structure, the problem is to derive the constitutive equations of a generic filament layer from the properties of the filaments and the resin material. Since the filament layers are often subjected to large shear deformation, and since filament-wound structures show nonlinear responses under moderate external loads, one should generally consider the nonlinear behavior of the resin material in a micromechanical analysis for calculating the gross response of the filament layer. However, a nonlinear and inelastic micromechanical analysis is extremely difficult. As a first step in this direction, one should choose and develop methodology of analysis and apply it to simple cases. The methodology, when proved successful and effective, can then be further developed to investigate more general and realistic cases.

Existing micromechanical studies with the objective of formulating constitutive equations of composite materials are mostly concerned with the linearly elastic behavior. Such studies aim to calculate the gross elastic moduli of the composite on the basis of the known elastic properties of the constituents. Methods used in the previous studies include variational bound theorems, and finite-element analysis. The latter method, although more laborious, can be modified to derive gross constitutive relations including nonlinear and inelastic response. In this method, an analytical model of the

composite is used in which the parallel filaments are arranged in a rectangular or hexagonal pattern and immersed in the resin material. A representative unit cell consisting of segments of filament and matrix regions is selected and these segments of regions are divided into finite elements.

An alternative analysis method that is believed to be especially suitable for the present type of problems is the boundary element analysis. The principal advantage of this method is that it reduces the spatial dimension of the problem from three to two or from two to one, and therefore results in drastic reduction in the number of nodal points and degrees of freedom. Although the available boundary-element computer codes are mostly limited to elastic analysis, considerable theoretical progresses have been made, during the last decade, for applying the boundary element analysis to problems involving plastic deformation. These progresses have important implications for the solution of micromechanical problems related to the nonlinear constitutive equations of composites.

In the present work, we demonstrate that the problem of determining the linear elastic moduli of a unidirectional composite from the elastic properties of isotropic resin material and transversely isotropic filaments can be solved by using boundary element analysis codes for plane-strain problem of an <u>isotropic</u> elastic medium. The computational effort is considerably less than the corresponding solution by the finite-element method, and yet the results are in extremely close agreement with the previous elasticity solutions in the literature.

Further investigation should be conducted on extending the boundary element method to the determination of nonlinear constitutive equations of a composite material from the properties of the constituents. As mentioned previously, the present analysis is only a first step in that direction.

2. Boundary element analysis of the micromechanical problem for determining the gross elastic moduli of a composite

In this initial study, we assume that each constituent material of the composite material is homogeneous and linearly elastic, and that the fibers are arranged in periodic patterns. Then the calculation of the gross elastic moduli of the composite can be reduced to a small number of two-phase elasticity problems (micromechanical problems) for a unit volume cell of the composite containing one or more sectors of a single fiber and the surrounding matrix. Each elasticity problem of the unit composite cell corresponds to a particular type of loading: extension/shortening along or perpendicular to the fiber direction and longitudinal or transverse shearing. In all loading cases, the extensional strain along the fiber direction has the same constant value in the several subregions occupied by the fiber and the resin matrix. The boundary conditions over the lateral faces of the unit cell may be greatly simplified if the unit composite cell is chosen appropriately. For example, in the case of a square or hexagonal array of fibers under an extensional load along the longitudinal or transverse directions, the unit cell may be chosen in such a way that, over each lateral face, the normal displacement is a constant and the shearing stresses vanish. The constant normal displacements on the lateral faces yield constant (macroscopic) strains of the composite. The resultant normal forces over the lateral faces of the unit region, or the resultant longitudinal force over its cross-section, when divided by the respective areas, yield the gross stress components in the composite. Hence the solutions of the two-phase elasticity problems for the unit cell yield the stress-strain relation in the unidirectional composite.

In most fiber-reinforced composite materials of engineering interest the

resin matrix is an isotropic material while the fibers have transversely isotropic elastic properties. The elastic moduli of the fibers along the longitudinal and transverse directions are significantly different, in the case of graphite fibers. Therefore, if finite-element or boundary-element methods are used directly to solve general two-dimensional micromechanical problems for the unit composite cell, the computer code should have the capability to deal with a material that is not isotropic.

The boundary-element method is ideally suited for the present task. Nodal points for a boundary-element analysis are picked only on the boundary curve and on the fiber/matrix interface. No interior nodal points are required. This reduces the dimension of the problem from two to one and, consequently, provides great savings in computational effort. Evaluation of the macroscopic stresses and strains of the composite requires only the knowledge of the nodal forces and nodal displacements along the boundary of the unit cell and along the fiber-matrix interface, which are readily provided by the boundary-element analysis. Finally, the interfacial stresses between the fiber and the matrix, important for the prediction of failure initiation, are also readily available from the results of a boundary-element analysis. In contrast, conventional finite-element analysis requires a large number of internal nodes which drastically increase the size of the problem, but the computational results of the internal nodal variables may be of little or no practical use.

However, a boundary-element analysis is considerably more complicated in a case involving an anisotropic elastic medium than in problems involving only isotropic elastic media, because of the complexity of the Green's function and the resulting integral equations for an anisotropic medium. The complication may be so significant that a finite-element analysis may appear to be a better choice

in micromechanical problems involving anisotropic fiber regions.

It is shown in the present work that, in the case of an isotropic resin matrix and transversely isotropic fibers, a micromechanical problem of the unit cell associated with the determination of one or more gross elastic moduli of the unidirectional composite can be transformed mathematically into a coupled plane-strain problem for two isotropic elastic media, whose isotropic moduli are related to the true moduli of the fiber and the resin materials according to simple relations. This mathematically transformed problem requires the continuity of the tractions across the fiber-matrix interface. However, across the same interface the displacement components u' and v' of the transformed problem (along the coordinate directions x and y, which are the symmetry axes of the unit cell) are generally not continuous but may suffer jumps that are proportional to the mismatch between the Poisson's ratios of the resin matrix and the fiber (where the latter ratio is associated with longitudinal shearing). Furthermore, along the boundary curve of the unit cell, the displacement boundary conditions of the mathematically transformed problem must be modified accordingly so that, for the fiber region as well as the matrix region, the boundary displacements are consistent with the interior displacements. Since the discontinuities of u' and v' of the transformed problem are known along the interface, they are no more difficult to handle in a boundary-element analysis than, for example, the interface continuity conditions of the same displacement functions in conventional interface problems.

In summary, the present work implies that the simpler integral equations associated with the plane-strain boundary-element analysis of isotropic elastic media are applicable to, and adequate for, the micromechanical analysis of unidirectional composites consisting of an isotropic resin material and

transversely isotropic fibers, provided that the problem is appropriately transformed into a modified, plane-strain problem with suitable equivalent isotropic moduli for the fiber region and with suitable discontinuities of the in-plane displacements across the fiber-matrix interface.

3. Unit Composite Cell Subjected to a Uniform Longitudinal Strain Load

Let E_m and ν_m denote, respectively, the Young's modulus and the Poisson's ratio of the isotropic resin material. Let E_1 and E_2 be the elastic moduli of the transversely isotropic fibers in the longitudinal and the transverse directions, G_{22} and ν_{22} be the shear modulus and the Poisson's ratio associated with transverse shearing of fibers and G_{12}, ν_{12} and ν_{21} be the corresponding quantities associated with longitudinal shearing such that $\nu_{12}/E_1 = \nu_{21}/E_2$. Then $G_{22} = E_{22}/2(1+\nu_{22})$ because of the transverse isotropy of the fibers. We first consider the loading case when the unit composite cell (defined by a rectangular or square region $-a/2 < x < a/2$, $-b/2 < y < b/2$) is subjected only to a uniform extensional strain along the fiber direction, $\epsilon_z = \epsilon_o$. The boundary conditions are

$$\begin{aligned} &u = 0, \qquad \tau_{xy} = 0 \qquad \text{on } x = \pm a/2, \\ &v = 0, \qquad \tau_{xy} = 0 \qquad \text{on } y = \pm b/2, \end{aligned} \tag{1}$$

For this loading case it is obvious that in both the fiber and matrix regions one has

$$\gamma_{xz} = \gamma_{yz} = 0, \qquad \tau_{xz} = \tau_{yz} = 0. \tag{2}$$

In the fiber regions, the remaining stress components σ_x, σ_y, σ_z and τ_{xy} are related to the strains ϵ_x, ϵ_y, ϵ_o and γ_{xy} by the generalized Hooke's law:

$$\begin{aligned} &\sigma_z = \nu_{12}\,(\sigma_x + \sigma_y) + E_1\epsilon_o, \qquad \gamma_{xy} = \tau_{xy}/G_{22} \\ &\epsilon_x = (\sigma_x - \nu_{22}\sigma_y - \nu_{21}\sigma_z)/E_2 = \sigma_x(1-\nu_{12}\nu_{21})/E_2 - \sigma_y(\nu_{22}+\nu_{12}\nu_{21})/E_2 - \nu_{12}\epsilon_o, \\ &\epsilon_y = (\sigma_y - \nu_{22}\sigma_x - \nu_{21}\sigma_z)/E_2 = \sigma_y(1-\nu_{12}\nu_{21})/E_2 - \sigma_x(\nu_{22}+\nu_{12}\nu_{21})/E_2 - \nu_{12}\epsilon_o, \end{aligned} \tag{3}$$

We consider an equivalent <u>isotropic</u> material for the fiber region with the Young's modulus E_f and Poisson's ratio ν_f given by

$$E_f = (1+\nu_{22})^{-2}(1+2\nu_{22}+\nu_{12}\nu_{21})E_2, \qquad \nu_f = (\nu_{22}+\nu_{12}\nu_{21})/(1+\nu_{22}). \tag{4}$$

Then the fictitious isotropic material has a shearing modulus, G_f, equal to G_{22} of the actual fiber material:

$$G_f = E_f/2(1+\nu_f) = E_2/2(1+\nu_{22}) = G_{22}.$$

From Eqs. (3) and (4) we obtain

$$\begin{aligned}
\epsilon_x + \nu_{12}\epsilon_o &= \sigma_x(1-\nu_f^2)/E_f - \sigma_y\nu_f(1+\nu_f)/E_f, \\
\epsilon_y + \nu_{12}\epsilon_o &= -\sigma_x\nu_f(1+\nu_f)/E_f + \sigma_y(1-\nu_f^2)/E_f, \\
\gamma_{xy} &= \tau_{xy}/G_f.
\end{aligned} \tag{5}$$

In the matrix region we have

$$\begin{aligned}
\epsilon_x + \nu_m\epsilon_o &= \sigma_x(1-\nu_m^2)/E_m - \sigma_y\nu_m(1+\nu_m)/E_m, \\
\epsilon_y + \nu_m\epsilon_o &= -\sigma_x\nu_m(1+\nu_m)/E_m + \sigma_y(1-\nu_m^2)/E_m, \\
\gamma_{xy} &= \tau_{xy}/G_m.
\end{aligned} \tag{6}$$

and

$$\sigma_z = E_m\epsilon_o + \nu_m(\sigma_x + \sigma_y) \tag{7}$$

The original elasticity problem for the unit composite cell will be transformed into a <u>modified</u> micromechanical problem in which the fiber material is replaced by the fictitious isotropic material. The solutions of the original micromechanical problem and the modified problem shall have identical stress fields σ_x, σ_y and τ_{xy} in both the fiber and the matrix regions. However, the extensional strains ϵ_x' and ϵ_y' of the modified problem shall be related to those of the original problem by

$$\epsilon_x' = \epsilon_x + \nu_{12}\epsilon_o, \qquad \epsilon_y' = \epsilon_y + \nu_{12}\epsilon_o \qquad \text{in the fiber region,} \tag{8a}$$

$$\epsilon_x' = \epsilon_x + \nu_m\epsilon_o, \qquad \epsilon_y' = \epsilon_y + \nu_m\epsilon_o \qquad \text{in the matrix region.} \tag{8b}$$

Now the constitutive equations of the fictitious isotropic material and the

matrix material yield

$$\epsilon_x' = (\sigma_x - \nu_f\sigma_y - \nu_f\sigma_z')/E_f, \qquad \epsilon_y' = (\sigma_y - \nu_f\sigma_x - \nu_f\sigma_z')/E_f \quad \text{in the fiber region,}$$

$$\epsilon_x' = (\sigma_x - \nu_m\sigma_y - \nu_m\sigma_z')/E_m, \qquad \epsilon_y' = (\sigma_y - \nu_m\sigma_x - \nu_m\sigma_z')/E_m \quad \text{in the matrix region.}$$

These two set of expressions are consistent with Eqs. (5), (6) and (8) if and only if

$$\sigma_z' = \nu_f(\sigma_x + \sigma_y) \qquad \text{in the fiber region}$$

$$\sigma_z' = \nu_m(\sigma_x + \sigma_y) \qquad \text{in the matrix region.} \tag{9}$$

The two equalities of Eq. (9) imply that the solution of the modified problem satisfies the plane strain condition:

$$\epsilon_z' = 0.$$

Equations (8a) and (8b) imply that the displacement functions of the modified micromechanical problem, u' and v', must be related to the displacement solutions u and v of the original problem according to

$$u' = u + \nu_{12}\epsilon_o x, \quad v' = v + \nu_{12}\epsilon_o y \qquad \text{in the fiber region}$$

$$u' = u + \nu_m\epsilon_o x, \quad v' = v + \nu_m\epsilon_o y \qquad \text{in the matrix region} \tag{10}$$

Since the actual displacements of the original problem, u and v, are required to be continuous across the fiber-matrix interface, across the same interface the functions u' and v' of the modified problem must have the discontinuities

$$[u'] = (\nu_m - \nu_{12})\epsilon_o x, \qquad [v'] = (\nu_m - \nu_{12})\epsilon_o y, \tag{11}$$

where [u'] and [v'] denote the jumps of u' and v', respectively, across the interface from the fiber region to the matrix region. Furthermore, while any traction boundary condition of the original problem is preserved without change as a traction boundary condition of the modified problem, displacement boundary conditions for u and v transform into different conditions for u' and v' in a way consistent with Eq. (10). Hence the displacement boundary conditions of Eq. (1) become

$$u' = \pm \nu_f \epsilon_o a/2, \quad v' = \pm \nu_f \epsilon_o b/2 \quad \text{on the exterior boundary of the fiber,}$$

$$u' = \pm \nu_m \epsilon_o a/2, \quad v' = \pm \nu_m \epsilon_o b/2 \quad \text{on the exterior boundary of the matrix region.} \tag{12}$$

The solution of the modified micromechanical problem may be obtained numerically by discretizing the boundary integral equations for the matrix and fiber regions, occupied, respectively, by the isotropic resin material and the fictitious isotropic material with the elastic moduli E_f and ν_f. The numerical solution scheme must implement the continuity of the tractions and the jump conditions of the displacements, Eq. (11), across the interface of the two regions. The solution scheme must also implement the mixed boundary conditions on the exterior boundary of the fiber and matrix regions, which are provided by $\tau_{xy} = 0$ and Eq. (12).

Once the stress and displacement solutions of the modified problem, σ_x', σ_y', τ_{xy}', σ_z', u' and v' are determined (with ϵ_z' identically zero), the actual stresses and displacements of the original problem are given as follows

$$\sigma_x = \sigma_x', \quad \sigma_y = \sigma_y', \quad \tau_{xy} = \tau_{xy}' \quad \text{in the whole region}$$

$$\sigma_z = \nu_{12}(\sigma_x+\sigma_y)+E_1\epsilon_o, \quad u = u'-\nu_{12}\epsilon_o x, \quad v = v'-\nu_{12}\epsilon_o y \quad \text{in the fiber region}$$

$$\sigma_z = \nu_m(\sigma_x+\sigma_y)+E_m\epsilon_o, \quad u = u'-\nu_m\epsilon_o x, \quad v = v'-\nu_m\epsilon_o y \quad \text{in the matrix region} \tag{13}$$

4. Plane-Strain Deformations of the Unit Composite Cell

We next consider the case when the unit composite cell is subjected to a plane-strain deformation

$$u = u(x, y), \quad v = v(x,y), \quad \epsilon_z = 0. \tag{14}$$

There are two particularly important problems of this class connected with the determination of the gross elastic moduli of the composite. From the macroscopic viewpoint, the first problem is associated with a uniform strain in the composite

along the x- or y-direction, for example, $\epsilon_y = \epsilon_o$ and $\epsilon_x = 0$, and the second problem is associated with a uniform shear strain $\gamma_{xy} = \gamma_o$. From the microscopic viewpoint, the first problem is characterized by the following boundary conditions for the unit composite cell:

$$u = 0, \qquad \tau_{xy} = 0 \qquad \text{on } x = \pm a,$$
$$v = \epsilon_o y, \qquad \tau_{xy} = 0 \qquad \text{on } y = \pm b, \tag{15}$$

while the second problem is characterized by the boundary conditions

$$v = 0, \qquad \sigma_x = 0 \qquad \text{on } x = \pm a,$$
$$u = \gamma_o y, \qquad \sigma_y = 0 \qquad \text{on } y = \pm b. \tag{16}$$

These boundary conditions may be derived on the basis of symmetry considerations.

The last condition of Eq. (14) yields the following relations in the fiber region

$$\sigma_z = \nu_{12}(\sigma_x + \sigma_y), \qquad \epsilon_x = \sigma_x(1-\nu_f^2)/E_f - \sigma_y\nu_f(1+\nu_f)/E_f,$$
$$\epsilon_y = -\sigma_x\nu_f(1+\nu_f)/E_f + \sigma_y(1-\nu_f^2)/E_f, \tag{17}$$

where E_f and ν_f are as defined by Eq. (4). In the matrix region the preceding relation must be replaced by

$$\sigma_z = \nu_m(\sigma_x + \sigma_y), \qquad \epsilon_x = \sigma_x(1-\nu_m^2)/E_m - \sigma_y\nu_f(1+\nu_m)/E_m,$$
$$\epsilon_y = -\sigma_x\nu_m(1+\nu_m)/E_m + \sigma_y(1-\nu_m^2)/E_m, \tag{18}$$

Hence each original plane strain problem for the two elastic media, one isotropic and one transversely isotropic, may be reduced to a new plane strain problem for two <u>isotropic</u> media with the elastic moduli E_m, ν_m and E_f, ν_f, respectively. All the boundary conditions and interface conditions remain unchanged.

5. <u>Longitudinal Shear Deformation</u>

When the composite is subjected to a macroscopically uniform longitudinal shear deformation, the fiber and matrix regions in the unit cell are both

subjected to (nonuniform) anti-plane shear deformation. That is, in both regions the displacement functions have the from

$$u \equiv 0, \qquad v \equiv 0, \qquad w = w(x, y) \tag{19}$$

The only nonvanishing strain components are

$$\gamma_{xz} = \partial w/\partial x, \qquad \gamma_{yz} = \partial w/\partial y,$$

and the only nonvanishing stress components have the expressions

$$\tau_{xz} = G_{12}\, \partial w/\partial x, \quad \tau_{yz} = G_{12}\, \partial w/\partial y \qquad \text{in the fiber region}$$

$$\tau_{xz} = G_m\, \partial w/\partial x, \quad \tau_{yz} = G_m\, \partial w/\partial y \qquad \text{in the matrix region} \tag{20}$$

The equilibrium equations reduce to the Laplace equation for w(x,y) in both the fiber and matrix regions

$$\nabla^2 w = 0. \tag{21}$$

This equation must be solved together with the following boundary conditions

$$w = \gamma_o y \qquad \text{along } x = \pm a/2$$

$$w = \pm \gamma_o b/2 \qquad \text{along } y = \pm b/2. \tag{22}$$

and the continuity conditions of w, τ_{xz} and τ_{yz} across the fiber-matrix interface, i.e.,

$$[w] = 0, \qquad G_{12}\, \partial w/\partial x = G_m\, \partial w/\partial x, \qquad G_{12}\, \partial w/\partial y = G_m\, \partial w/\partial y \tag{23}$$

The last two conditions of Eq. (23) imply that, unless $G_{12} \neq G_m$, the gradient of the solution w is discontinuous across the interface.

Since w is governed by the Laplace equation, the boundary-element analysis of the preceding boundary-value problem for w is relatively simple.

6. The Elastic Moduli of a Unidirectional Composite

A unidirectional composite consisting of an isotropic resin material and transversely isotropic fibers has transversely isotropic gross (macroscopic) properties if the fibers are randomly distributed in the matrix. If the fibers

are periodically arranged in square or hexagonal patterns, then the mechanical behavior of the composite manifests certain symmetry properties with respect to the planes of symmetry. Strictly speaking, such a composite may be not transversely isotropic. For example, a unidirectional composite with a square array of fibers placed along the coordinate directions x and y has the same gross extensional elastic moduli in these two directions, $E_2^* = E_3^*$, and furthermore, $\nu_{23}^* = \nu_{32}^*$. However, the gross extensional modulus along other directions in the x-y plane are general different, and the gross shear modulus G_{23}^* associated with the x- and y-directions is generally not equal to $E_2^*/2(1+\nu_{23}^*)$. Whereas a material with transversely isotropic elastic properties possesses a continuous group of symmetry transformations, unidirectional composites with square or hexagonal fiber patterns possess symmetry transformations which form a discrete group. The elastic properties of such composites are generally characterized by nine independent parameters of an orthotropic material, E_1^*, E_2^*, E_3^*, ν_{12}^*, ν_{23}^*, ν_{31}^*, G_{12}^*, G_{23}^* and G_{31}^*, although certain relations among these parameters may arise as in the case of square arrays. Other frequently used elastic parameters of an orthotropic material are defined by

$$\nu_{21}^* = \nu_{12}^* E_2^*/E_1^*, \qquad \nu_{32}^* = \nu_{23}^* E_3^*/E_2^*, \qquad \nu_{13}^* = \nu_{31}^* E_1^*/E_3^*. \quad (24)$$

Notice that the fiber direction (with the associated elastic moduli E_1^*) is here identified with the z-direction while two orthogonal symmetry axes 2 and 3 are identified with the x- and y-axes, respectively.

The gross elastic moduli of a composite may be directly determined by experimental measurements under various multiaxial and shearing loads. Alternatively, they may be calculated by solving several micromechanical problems for a unit cell of the composite. Solutions to the transverse and longitudinal shear problems, described respectively in Sec. 4 and 5 of the present paper,

directly yield the gross shearing moduli G_{23}^*, G_{31}^* and G_{12}^* of the unidirectional composite. In calculating these gross moduli, the macroscopic shearing stress τ_{ij}^* is obtained by integrating the boundary shearing stress τ_{ij} of the micromechanical problem along a rectilinear boundary of the unit cell and dividing the result by the length of the boundary segment. The boundary data of the micromechanical shearing stresses τ_{ij} are directly provided by the boundary element solution of the micromechanical problem.

On the other hand, the evaluation of the gross extensional elastic moduli E_1^*, E_2^*, E_3^* and the Poisson's ratios ν_{12}^*, ν_{23}^* and ν_{31}^* of the composite requires two independent plane strain solutions of Sec. 4 and a third solution corresponding to a uniform longitudinal strain load, described earlier in Sec. 3. In the last solution, the unit cell is subjected to boundary displacements which result in an <u>average</u> strain field

$$\epsilon_x^* = \epsilon_y^* = 0, \qquad \epsilon_z^* = \epsilon^{(1)}.$$

The corresponding average stresses $\sigma_x^{*(1)}$, $\sigma_y^{*(1)}$ and $\sigma_z^{*(1)}$ are related to the preceding average strains by the gross constitutive relation of the composite, i.e.,

$$\sigma_x^{*(1)} - \sigma_y^{*(1)}\,\nu_{23}^* - \sigma_z^{*(1)}\,\nu_{21}^* = 0, \tag{25a}$$

$$\sigma_y^{*(1)} - \sigma_x^{*(1)}\,\nu_{32}^* - \sigma_z^{*(1)}\,\nu_{31}^* = 0, \tag{25b}$$

$$\sigma_z^{*(1)} - \sigma_x^{*(1)}\,\nu_{12}^* - \sigma_y^{*(1)}\,\nu_{13}^* = \epsilon^{(1)}\,E_1^*. \tag{25c}$$

In one of the two plane strain solutions, the unit cell is subjected to the average strain field

$$\epsilon_x^* = \epsilon^{(2)}, \qquad \epsilon_y^* = \epsilon_z^* = 0.$$

The corresponding macroscopic stresses $\sigma_x^{*(2)}$, $\sigma_y^{*(2)}$ and $\sigma_z^{*(2)}$ satisfy

$$\sigma_x^{*(2)} - \sigma_y^{*(2)}\,\nu_{23}^* - \sigma_z^{*(2)}\,\nu_{21}^* = \epsilon^{(2)}\,E_2^*, \tag{25d}$$

$$\sigma_y^{*(2)} - \sigma_x^{*(2)}\,\nu_{32}^* - \sigma_z^{*(2)}\,\nu_{31}^* = 0, \tag{25e}$$

$$\sigma_z^{*(2)} - \sigma_x^{*(2)}\,\nu_{12}^* - \sigma_y^{*(2)}\,\nu_{13}^* = 0. \tag{25f}$$

For the other plane strain solution, the preceding equations for the average strains and the average stresses are replaced by

$$\epsilon_y^* = \epsilon^{(3)}, \qquad \epsilon_x^* = \epsilon_z^* = 0,$$

and

$$\sigma_x^{*(3)} - \sigma_y^{*(3)}\,\nu_{23}^* - \sigma_z^{*(3)}\,\nu_{21}^* = 0, \tag{25g}$$

$$\sigma_y^{*(3)} - \sigma_x^{*(3)}\,\nu_{32}^* - \sigma_x^{*(3)}\,\nu_{31}^* = \epsilon^{(3)}\,E_3^*, \tag{25h}$$

$$\sigma_x^{*(3)} - \sigma_x^{*(3)}\,\nu_{12}^* - \sigma_y^{*(3)}\,\nu_{13}^* = 0. \tag{25i}$$

7. Calculating the average stresses σ_{ij}^* from the solutions of the modified micromechanical problem

The macroscopic stresses $\sigma_x^{*(1)}$, $\sigma_y^{*(1)}$, $\sigma_x^{*(2)}$, $\sigma_y^{*(2)}$, $\sigma_x^{*(3)}$ and $\sigma_y^{*(3)}$ may be appearing in Eq. (25) mav be calculated from the solutions of the micromechanical problems for a unit cell (Sections 3 and 4) by averaging the normal tractions over vertical and horizontal boundary segments of the unit cell. These normal tractions (σ_x or σ_y) are provided directly by the boundary-element solutions of the modified micromechanical problems, because $\sigma_x' = \sigma_x$ and $\sigma_y' = \sigma_y$ in both the fiber and matrix regions.

The average stresses $\sigma_x^{*(1)}$, $\sigma_z^{*(2)}$ and $\sigma_z^{*(3)}$, on the other hand, will be expressed in terms of the boundary and interfacial values of the displacements of the modified micromechanical problems. These boundary and interfacial values are also provided directly by the boundary-element solutions. For example, one has

$$(A_f + A_m)\,\sigma_z^{*(1)} = \iint \sigma_z \, dx\, dy, \tag{26}$$

where A_f and A_m denote the cross-sectional areas of the fiber and of the matrix material, respectively, of the unit cell, and where the integral on the right-

hand side extends over both areas. By virtue of the first equation in Eq. (3), the part of the integral over the fiber cross-section yields the contribution

$$\iint \{\nu_{12}(\sigma_x+\sigma_y) + E_1\epsilon^{(1)}\}\, dx\, dy = E_1\epsilon^{(1)}A_f + \iint \{\nu_{12}(\sigma_x'+\sigma_y')\, dx\, dy. \quad (27)$$

Since the modified micromechanical problem is a plane-strain elasticity problem for both the fiber and matrix regions, we have, in the fiber region

$$\sigma_x'+\sigma_y' = \{E_f/(1-\nu_f-2\nu_f^2)\}\ (\epsilon_x'+\epsilon_y').$$

Substitution into Eq. (27) yields the following contribution to the right hand side of Eq. (26):

$$E_1\epsilon^{(1)}A_f + \nu_{12}\{E_f/(1-2\nu_f-\nu_f^2)\} \oint u'dy - v'dx. \quad (28)$$

To this must be added a similar contribution from the matrix region:

$$\iint \{\nu_m(\sigma_x+\sigma_y) + E_m\epsilon^{(1)}\}\, dx\, dy = E_m\epsilon^{(1)}A_m + \nu_m\{E_m/(1-\nu_m-2\nu_m^2)\} \oint u'dy - v'dx. \quad (29)$$

The line integrals in the last two expressions are performed along the closed boundary curves of the fiber and matrix regions, respectively. We recall that, according to Eq. (11), the displacement solutions u' and v' of the modified problem are generally discontinuous across the interface between the fiber and matrix regions.

The preceding results show that the input data needed to compute the average stresses σ_{ij}^* in Eq. (25) are the values of boundary tractions and of the boundary and interfacial displacements associated with the micromechanical problems of the unit cell. These values are all immediately available from the boundary-element solutions of the modified micromechanical problems. There is no need to compute the stresses or displacements at any interior point of the fiber region or the matrix region. Thus the large number of interior nodes used in the finite-element analysis of micromechanical problems serve no purpose, in the present context, other than as a means to generate the finite-element solutions themselves. By eliminating the need for the internal nodes and the

associated unknown variables, the boundary-element analysis provides an exceedingly efficient method for obtaining exactly those quantities necessary for the determination of the gross elastic moduli of the composite.

After the evaluation of the average stresses, the nine gross elastic parameters E_1^*, E_2^*, E_3^*, ν_{12}^*, ν_{23}^*, ν_{31}^*, ν_{21}^*, ν_{32}^* and ν_{13}^* may be easily determined from Eq. (25). First, Eqs. (25f) and (25i) yield ν_{12}^* and ν_{13}^*, Eqs. (25b) and (25e) yield ν_{32}^* and ν_{31}^*, and Eqs. (25a) and (25g) provide ν_{23}^* and ν_{21}^*. Then Eqs. (25c), (25d) and (25h) yield E_1^*, E_2^* and E_3^*, respectively. The nine parameters thus determined should satisfy Eq. (24), because these parameter are calculated from the relations between conjugate forces and displacements in elasticity solutions.

8. Implementation of the boundary-element analysis for two-dimensional interface problems

The preceding analysis indicates that all input data needed for calculating the gross elastic moduli of a unidirectional composite with regular and periodic fiber patterns may be obtained from the boundary-element solutions of certain modified micromechanical problems. These modified micromechanical problems are plane-strain elasticity problems for two distinct isotropic elastic media, with simple types of boundary conditions for the displacements and tractions on the exterior boundary of a unit cell, and with continuous tractions and continuous or discontinuous displacements across the interfaces of the fiber and matrix regions. An existing computer program for two-dimensional, plane-strain boundary-element analysis of an isotropic medium may be applied, first to the matrix region, and subsequently to the fiber region, where the transversely isotropic fiber material is replaced by a fictitious isotropic material with the

elastic moduli E_f and ν_f defined by Eq. (4). Each node on the interface of the fiber and matrix regions will be counted twice (i.e., treated as a double node), first as a boundary node of the matrix region and later as a boundary node of the fiber region. There are four variables associated with each boundary node: the two displacement components u' and v', and the two traction components t_x and t_y (notice that, since σ_x', σ_y' and τ_{xy}' of the modified micromechanical problem are identical to σ_x, σ_y and τ_{xy} of the original problem for the unit cell, the tractions t_x' and t_y' are also identical to t_x and t_y on any segment of the exterior boundary or internal interface). For a double node associated with a point on the interface, there are eight variables, four associated with the matrix region and the other four associated with the fiber region. The computer program for boundary-element analysis generates square matrices $[A_m]$ and $[B_m]$ for the matrix region such that

$$[A_m]\ \{u_m\} + [B_m]\ \{t_m\} = \{0\}, \tag{30}$$

where $\{u_m\}$ is the column vector whose elements include <u>all</u> displacement variables u' and v' (known and unknown) associated with a boundary or interface node of the matrix region, and $\{t_m\}$ is the column vector whose elements include all traction variables t_x and t_y associated with the same nodes. For the fiber region, one has a similar equation

$$[A_f]\ \{u_f\} + [B_f]\ \{t_f\} = \{0\}, \tag{31}$$

where the column vectors $\{u_f\}$ and $\{t_f\}$ include, respectively, the displacement and traction variables associated with all boundary and interface nodes in the fiber region. Notice that, for each double node on the interface, four of the eight variables are included in Eq. (30) and the remaining four variables are included in Eq. (31).

Equations (30) and (31) may be combined into a single equation of the

following form

$$[A]\ \{u\} + [B]\ \{t\} = \{0\}, \tag{32}$$

where

$$[A] = \begin{bmatrix} [A_m] & [0] \\ [0] & [A_f] \end{bmatrix}, \qquad [B] = \begin{bmatrix} [B_m] & [0] \\ [0] & [B_f] \end{bmatrix},$$

and $\{u\}$ and $\{t\}$ are, respectively, column vectors obtained by combining $\{u_m\}$ with $\{u_f\}$ and $\{t_m\}$ with $\{t_f\}$.

Along the exterior boundary of the fiber and matrix regions, the boundary conditions are imposed according to Eqs. (1) and (10). Each boundary condition is a condition on an element of $\{u\}$ or of $\{t\}$ associated with a boundary node. Due to the geometrical symmetry of the unit cell and the symmetry of the boundary load, the displacements (tractions) at one boundary or interface node may be equal or opposite to the corresponding displacements (tractions) at another node. Furthermore, at an interface (double) node, the continuity conditions of the tractions and the continuity or jump conditions of the displacements across the fiber-matrix interface provide additional relations between two traction variables or two displacement variables associated with that node.

Every boundary condition, symmetric condition, interfacial continuity or jump condition described above has the form

$$x_i + N\, x_j - c = 0, \tag{33}$$

where x_i and x_j are two distinct elements of the column vector $\{u\}$ or $\{t\}$, c is a known number determined by the specified boundary displacement or by the specified jump of u' or v' across the interface, and the integer N may assume values 0 (in the case of a boundary condition), +1 or -1 (in case of a symmetry condition or interfacial continuity or jump conditions). There are two boundary conditions of this form at each boundary node, and four interfacial continuity

or jump conditions (two for the tractions and two for the displacements) at each double node on the interface.

Equation (33) may be used to eliminate a variable, x_j or x_i, from Eq. (32). This amounts to combining two columns of the matrix [A] or of the matrix [B], or moving a column of [A] or [B] to the right hand side of the equation after multiplication by the factor c, or doing both. In each case the operation reduces the dimension of the matrix [A] or [B]. When the operation has been repeated for each one of the boundary, interface and symmetry conditions, the total number of columns remaining in the matrices [A] and [B] is equal to the row dimension, and those variables in {u} and {t} which have not been eliminated may be solved from the reduced system of linear equations. This yield an approximate solution of the modified micromechanical problem by the boundary-element method.

The preceding method of eliminating variables suggests an algorithm for treating, in a unified and systematic way, all boundary, interface and symmetry conditions in the modified micromechanical problem involving two distinct isotropic elastic media. When these conditions are put in the form of Eq. (33), the algorithm consists of purely algebraic manipulations on the matrices [A] and [B].

9. Results

A Fortran program has been developed to implement the boundary-element analysis of the modified micromechanical problem for the unit cell composed of fiber and matrix regions (see Appendix A: Program MICROBEM). The portion of the program which generates the matrices $[A_m]$, $[B_m]$, $[A_f]$ and $[B_f]$ of Eqs. (30) and (31) are essentially taken from the two-dimensional boundary-element code for a single isotropic elastic medium give in Brebbia et al. (see Chapter 14 in

Brebbia, C. A., Telles, J.C.F. and Wrobel, L. C., Boundary Element Techniques: Theory and Applications in Engineering. Springer-Verlag, Berlin, 1984). Subroutines for combining the matrices and eliminating columns by using the boundary, interface and symmetry conditions are included in the program. The resulting system of algebraic equations are solved and the average stresses σ_{ij}^* corresponding to the three loading cases associated with Eq. (25) are computed by numerical integration of the boundary tractions along the exterior boundary and of the interfacial displacements along the interface.

In their micromechanical analysis of fiber-reinforced composites with hexagonal fiber arrangement, Chen and Cheng used the elastic moduli for the graphite fiber and the epoxy matrix given earlier by Whitney (Chen, C.H. and Shun Cheng, "Mechanical properties of anisotropic fiber-reinforced composites," J. Appl. Mech., Vol. 37, pp. 186-189, 1970; Whitney, J. M., "Elastic moduli of unidirectional composites with anisotropic filaments," J. Composite Materials, Vol. 1, p. 188, 1967). The values are

$$E_1 = 24 \text{ msi}, \qquad E_2 = 2 \text{ msi}, \qquad G_{12} = 4 \text{ msi}, \qquad \nu_{12} = 0.3, \qquad \nu_{23} = 0.15$$

for the fiber material and

$$E_m = 0.6 \text{ msi}, \qquad \nu_m = 0.3$$

for the matrix material. The composite has the fiber volume fraction $V_f = 0.5$. Chen an Cheng reduced the problem to a boundary problem for the biharmonic equation and used series expansion in polar coordinates to obtain the following results for the composite moduli:

$$E_1^* = 12.33303 \text{ msi}, \qquad \nu_{12}^* = 0.30025, \qquad \nu_{13}^* = 0.30025,$$

$$\nu_{21}^* = 0.02575, \qquad E_2^* = 1.05805 \text{ msi}, \qquad \nu_{23}^* = 0.32059,$$

$$\nu_{31}^* = 0.02567, \qquad \nu_{32}^* = 0.32265, \qquad E_3^* = 1.05389 \text{ msi},$$

In the present analysis, the micromechanical problem for the unit cell is

first transformed into a modified plane-strain problem in which the anisotropic fiber region is replaced by a suitable isotropic medium. The exterior boundary of the unit cell and the interfaces are partitioned into boundary elements as shown in Fig. 10. The boundary element equations are solved and the gross moduli of the composite are computed according to the procedure described in Sec. 8. The results are given in the following table for the preceding material system along with the results for two other material systems which have different values of ν_m but are otherwise identical.

ν_m	E_1^* (msi)	E_2^* (msi)	E_3^* (msi)	ν_{12}^*	ν_{23}^*
0.3	12.2994	1.06411	1.06406	0.3	0.31979
0.35	12.3000	1.10160	1.10150	0.32389	0.38579
0.4	12.3014	1.15481	1.15466	0.34965	0.46679

Table 6: Composite elastic moduli calculated by the boundary-element analysis of the micromechanical problem for a unit cell

For $\nu_m = 0.3$, the present results are in excellent agreement with those reported by Chen and Cheng. Notice that since for this case $\nu_m = \nu_{12}$, Eqs. (11) indicate that there are no jumps of u' and v' across the interface. It is interesting to notice that in all three cases the parameter ν_{23}^* of the composite is greater than the corresponding parameters of the fiber ($\nu_{23} = 0.15$) and the matrix ($\nu_m = 0.3$, 0.35 or 0.4).

The computed results of E_1^* and ν_{12}^* are in excellent agreement with the predictions based on the rule of mixture:

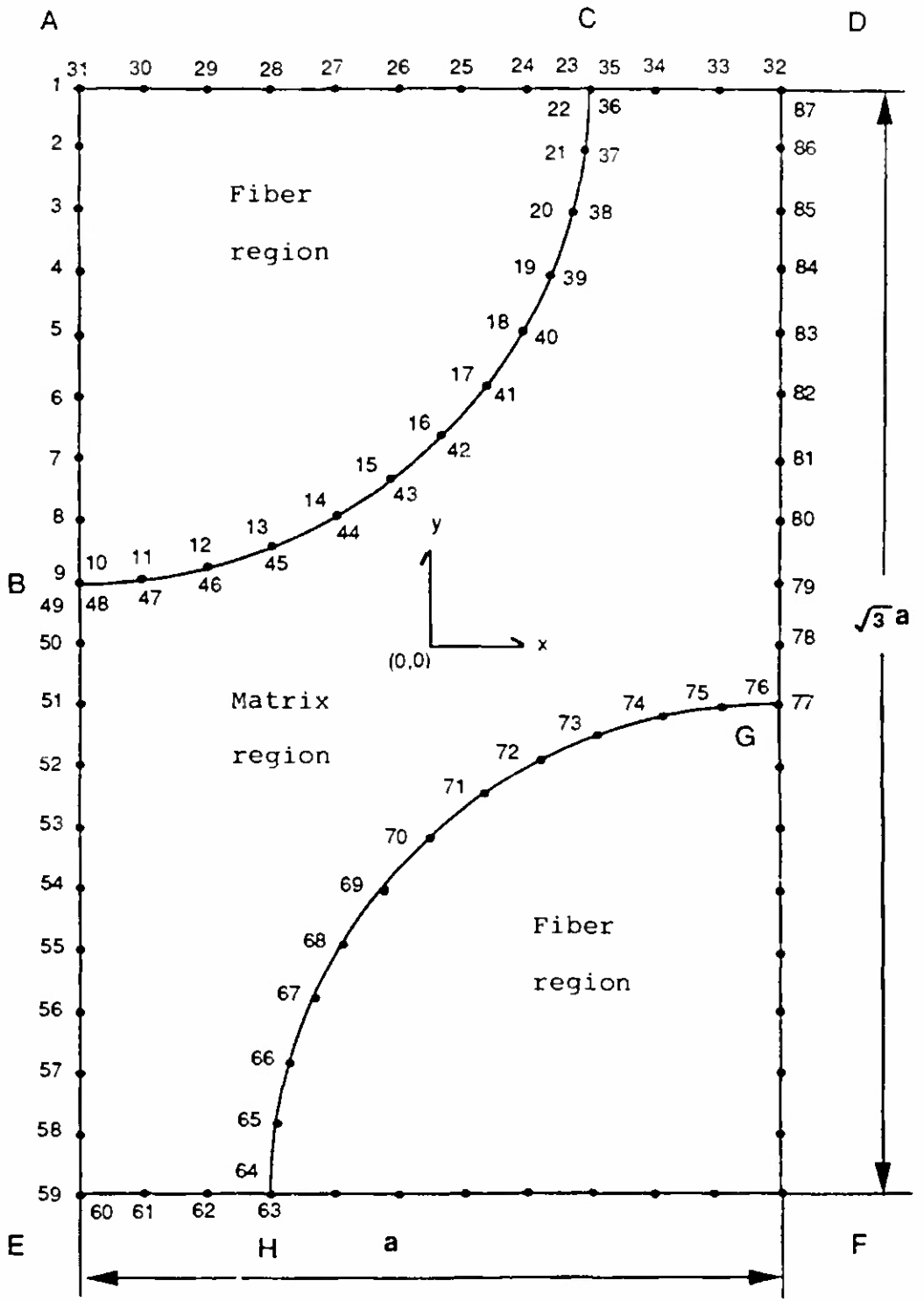

Fig. 10: Boundary-element model of the unit cell of composite with a hexagonal array of filaments

$$E_1^* \approx E_1 V_f + E_m (1 - V_f) = 12.3 \text{ msi}, \tag{34}$$

$$\nu_{12}^* \approx \nu_{12} V_f + \nu_m (1 - V_f). \tag{35}$$

Furthermore, the present results of E_2^* are also in excellent agreement with the predictions of certain empirical formulae proposed by Tsai (Tsai, S. W., Structural Behavior of Composite Materials, NASA CR-71, July, 1964) and Halpin and Tsai (Halpin, J.C. and Tsai, S.W., Effects of Environmental Factors on Composite Materials, AFML-TR 67-423, June 1969). However, the results of ν_{23}^* obtained by micromechanical solutions (including the present solution and that of Chen and Cheng, which are in close agreement) are significantly different from the empirical formulae cited above. On the other hand, the in-plane volume modulus , defined as $\sigma_2^*/(2\epsilon_2^*)$ under the isotropic plane strain condition ($\epsilon_2^* = \epsilon_3^*$ and $\epsilon_1^* = 0$) as calculate by the present analysis is in excellent agreement with the prediction of an empirical formula given in the book by Tsai and Hahn (see Eq. (3.55) in page 397 of Tsai, S.W. and Hahn, H.T., Introduction to Composite Materials, Technomic Publishing Co., Westport, Connecticut, 1980). For a composite with transversely isotropic gross elastic properties, this in-plane modulus k^* is determined by E_2^*, ν_{12}^* and ν_{23}^* according to the relation

$$k^* = E_2^*/2(1 - \nu_{23}^* - 2 \nu_{12}^* \nu_{21}^*). \tag{36}$$

For the material system considered here (with $\nu_m = 0.3$), k^* has the value 0.8005 msi from the present analysis and 0.8011 msi from the empirical formula of Tsai and Hahn. Similar agreement was found for the case $\nu_m = 0.4$, and for other values of the fiber-volume fraction. Hence the results of the present analysis confirm that an accurate prediction of ν_{23}^* can be obtained by first using the empirical formula in Tasi and Hahn to estimate the in-plane volume modulus k^*, and subsequently calculating ν_{23}^* from Eq. (36). On the other hand, direct estimation of ν_{23}^* using the Halpin-Tsai equations generally yields results that

have substantial errors.

By changing the fiber radius in the model of Fig. 10, and repeating the boundary-element analysis, we obtain the gross elastic moduli of the composite with a different fiber content. The dependence of E_2^* and ν_{23}^* upon the fiber volume fraction is shown in Figs. 11 and 12 for two values of ν_m (0.3 and 0.4).

9. Summary and a comment on future work

The determination of the gross constitutive properties of a composite material from the constitutive equations of its constituents is a fundamental problem in the mechanics of composite materials. The current literature on the subject is largely confined to linearly elastic behavior of composites. Much remains to be done in the micromechanical analysis of composites with inelastic matrix phase. The present work indicates that the boundary-element analysis provides a very efficient and accurate method for dealing with interface problems at the micromechanical level. The efficiency comes largely from reducing the dimension of the problem from three to two or from two to one. This usually results in simplified data input and modeling, and great savings in computational effort.

Significant progresses have been made in the last decade on the application of the boundary-element method to plasticity problems. Although the present analysis is restricted to elastic fibers and elastic matrices, the method can be extended to determine non-linear and inelastic gross properties of a composite composed of linearly elastic fibers and non-linear resin materials. In solving micromechanical interface problems with inelastic regions, the use of the boundary-element analysis is even more attractive, and perhaps imperative, because of the unusual complexity of the finite-element modeling and solution of

such problems. Furthermore, the nonlinear constitutive relation in an inelastic process is generally history dependent. A much greater number of solutions of different micromechanical problems (with different loading histories) must be obtained to evaluate the material parameters or material functions characterizing the inelastic response of the composite. Hence the solution procedure must be standardized and used repeatedly. Any significant saving in the modeling and computational effort for a single execution of the solution process will result in tremendous savings in the large task of calculating the nonlinear gross response of a composite material from the constituent properties.

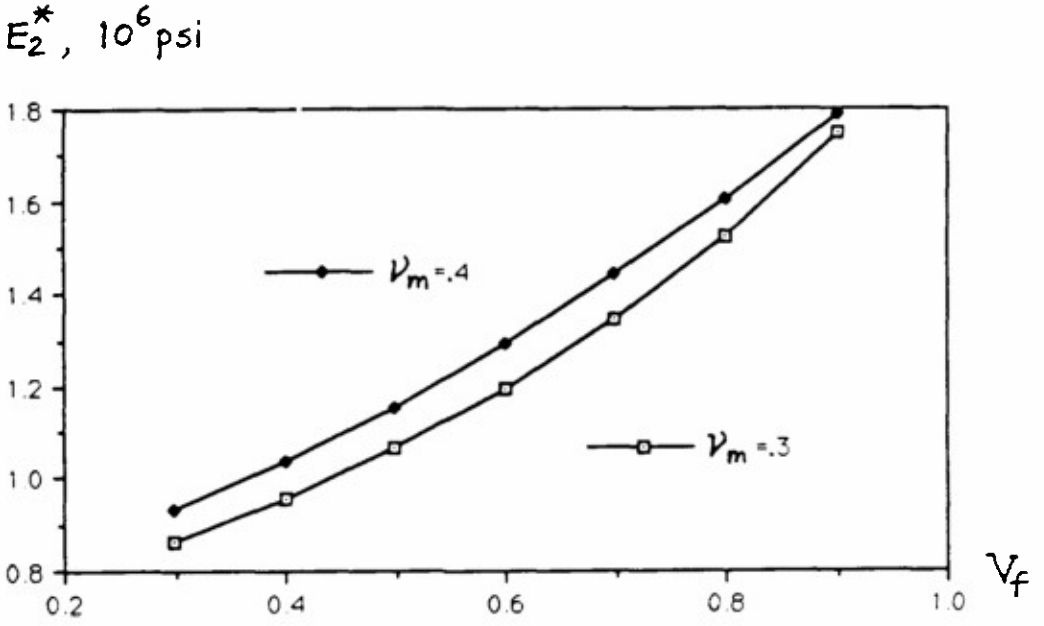

Fig. 11: Dependence of the composite transverse elastic modulus on the fiber volume fraction

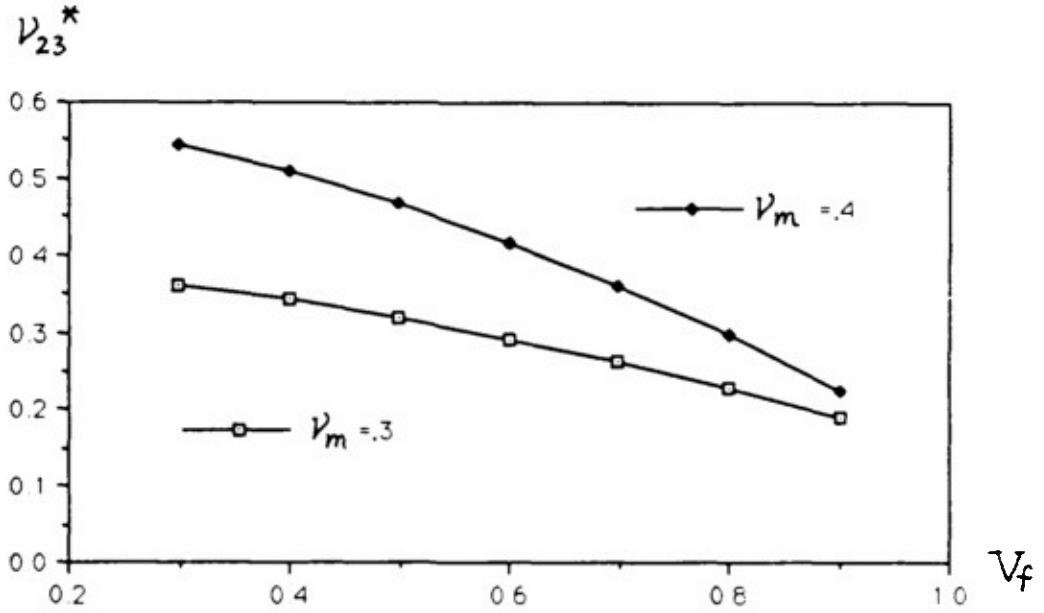

Fig. 12: Dependence of the gross Poisson's ratio, ν_{23}^*, on the fiber volume fraction

IV. Failure Modes and Analysis

1. Introduction

When a filament-wound composite structure is subjected to an internal pressure, it generates tensile membrane forces which are largely carried by two intersecting families of stiff fibers. The matrix material serves to hold the net of fibers in place, to transmit forces among unevenly stretched fibers via shear action, and to contain internal pressure. While a net of fibers alone is capable of large membrane deformation with little fiber stretching, through finite changes in the intersecting angle, such membrane deformations are opposed by the reactions from the matrix material. Thus, if the deformation of the fiber net tends to compress the matrix, the matrix material reacts to the fiber net in such a manner as to smooth out local non-uniformity in fiber tension resulting from irregularities in the fiber diameter, material defects, winding geometry, initial fiber stress and waviness. On the other hand, if the deformation of the fiber net tends to produce predominantly tensile stress in the matrix, then the composite is likely to develop matrix or interfacial cracks which propagate across the barriers of the intersecting family of fibers. This process may interact with and accelerate the breaking and debonding of fibers and the sequential failure of neighboring fibers. It is apparent that in this fracture mode of failure, the matrix and fibers behave and interact in such a manner as to enhance and accentuate, rather than smoothing out, any initial concentration of strains and defects. Thus, depending upon the nature of the deformation of the fiber net produced by the pressure loading, two fundamentally different types of failure processes can occur in a filament-wound structure, dominated respectively by intense shear deforamation in the matrix and by the expansion of

a surface element with eventual tensile fracture. While the processes of the first type may be amenable to a macromechanical analysis if one takes into consideration the distinct constitutive properties of the constituents in the various stages of the failure processes, the methodology of fracture mechanics is appropriate in modeling and analyzing the failure processes of the second type.

Since the tensile or compressive nature of the stress in the matrix material is essentially determined by the deformation of the fiber net that would occur in the absence of the matrix, and since the presence of the matrix merely modifies such deformation through shear and compression, the first step in the failure analysis is to solve the problem of finite deformation of a net of linearly elastic (or even inextensible) fibers with prescribed boundary conditions. The solution determines the character of the stress in the matrix which in turn predicts the type of the failure process that will be operative. This approach is demonstrated by the simple case of the cylindrical geometry for which the solution of the fiber net is trivial (see Secs. 3 and 4 in the following).

While the existing experimental data provide a sufficient basis for identifying the failure modes in the different specimens under different test conditions, further experimental results are need to provide a quantitative basis for determining the empirical failure criterion associated with each failure mode. The most commonly used failure criteria for composite materials, including the Tsai-Wu criteria, are represented by a failure surface in the stress space. The parameters in the criteria are evaluated by fitting the points of the failure surface with experimental data. While criteria of such nature are useful for characterizing the strength of the composite in the circumstances where the

composite is only expected to experience deformations with small strains, they are not well suited for composites which may experience significant inelastic deformation and large shear strain. Failure of filament-wound structures is generally a progressive process starting from microcracking of matrix and whitening at a relatively low level of stress. Aside from certain exceptions cases, it is not an instantaneous event reached suddenly when the stress path meets a certain fixed surface in the stress space. Hence the formal analogy of the failure criteria to the yield condition in plasticity may be inappropriate.

It appears that the failure of a filament layer should depend on the maximum values of the transverse strain ϵ_2 and of the shear strain γ_{12} experienced by an element of the layer preceding failure, as well as the filament strain ϵ_1 at the instant of failure. There are other important reasons for preferring a strain-based failure criterion over a stress-based criterion. The first is that the intrinsic components of the failure strain are easily calculated in terms of the experimental data from testing of filament-wound structures, while the stress data in the various filament layers usually cannot be obtained with certainty or cannot be obtained without an elaborate analysis. The second reason is that in the analysis of a thin filament-wound structure, the strain field is fairly smooth or uniform within the structure, and can be expressed in terms of a small number of unknowns including the middle-surface strains and curvatures, whereas the stresses may vary discontinuously from one filament band to another, because of the discontinuous change in the filament orientation and the cross-over of filament bands. Consequently, it is relatively easy to apply a strain-based failure criterion to a filament-wound structure. Recently, Feng has proposed a strain-based general failure criterion for composite materials undergoing finite deformation (Feng, W. W., "A failure

criterion for composite materials," J. Composite Materials, Vol. 25, pp. 88-100, 1991).

While empirical failure criteria are attractive from an engineering point of view because of its simplicity and ease of application, such formal criteria do not suggest the underlying failure mechanism at the micromechanical level. Although the progressive degradation of the resin matrix associated with significant transverse and shear strains, ϵ_2 and γ_{12}, is initially a spread-out, continuous process which may be characterized by a continuum theory of damage, eventually the microcracks evolve or coalesce into finite matrix cracks or fiber/matrix disbonds which ultimately determine the failure of the composite according to the failure criteria of fracture mechanics. For the filament layer in a filament-wound structure, this aspect of the failure analysis is particularly relevant to the tubes experiencing significant transverse tensile strain ϵ_2 before failure. It is less important for the prediction of failure loads governed by fiber breaking, at least in the case of axisymmetric filament-wound structures, because in such structures the position and the level of the maximum fiber tension may often be estimated by considering the global equilibrium of the structure and, consequently, an empirical failure criterion based on the average filament strength or allowable filament strain may be adequate.

In Section 5 of the present part of the report, we present boundary-element analyses of two-dimensional micromechanical models of fiber-matrix interfacial disbonds and oblique matrix cracks. For simplicity, the fiber regions are considered as rigid whereas the resin material is treated as a linearly elastic medium. The assumption of rigid fibers should yield an overestimation of the interfacial stresses (which are unbounded and oscillatory according to the exact

elasticity analysis) and therefore is on the conservative side. Analysis was conducted for two cases corresponding, respectively, to a unit transverse strain and a unit shear strain in the matrix region. It is found that the energy-release rate associated with the growth of the interfacial crack grows rapidly when the disbond length reaches a certain critical value. Subsequently, the energy release rate levels off and approaches a limiting values when the disbond length becomes sufficiently large. The case of transverse strain load is more critical because the results show that a large energy release rate can be attained when the disbond length is comparable or shorter than the spacing between two neighboring fibers.

Spencer and Hull observed the occurrence of local buckling and delamination in the failure of open-ended tubes with winding angle greater than 45°, particularly in the 65° tubes. It may appear somewhat puzzling that delamination should occur in a tube loaded under internal pressure, where the adjacent layers are pressed against each other in the radial direction, and that buckling and bending of the tube should happen under the open-end test condition, where the resultant axial load in the tube vanishes. An analysis of a possible failure mode due to the separation and growth of a helical face layer from the interior surface of the filament-wound tube is briefly mentioned in Sec. 6 and described in more detailed in the paper "Separation failure of a helical delamination in a filament-wound composite tube," Developments in Theoretical and Applied Mechanics, Vol. XV (Proceedings of the SECTAM XV, March, 1990, Atlanta, GA), pp. 440-447 (by Wan-Lee Yin, see Appendix C of this report).

Delamination is a prevalent mode of failure in composite laminates. Filament-wound structures are prone to delamination failure because the scissoring action at the cross-over point of two filaments belonging to separate

layers, mentioned in Sec. 2.3 of Part II, may produce intense local shearing deformation in the cross-over region as the fibers rotate and realign themselves to the load direction. Such scissoring action results in a system of distributed couple moment from one filament layer to the adjacent layer, which may initiate separation of the layers. After the initiation of delamination damage, catastrophic delamination growth may result from buckling and postbuckling deformation of the layer when the structure is subject to the service load. A general analysis of buckling and postbuckling growth of a thin two-dimensional delaminated layer in a composite laminate is present in a sequence of two papers: Yin, W.-L. and Jane, K.C., "Refined buckling and postbuckling analysis of two-dimensional delaminations, Part I: Analysis and Validation," and Jane, K.C. and Yin, W.-L., "Refined buckling and postbuckling analysis of two-dimensional delaminations, Part II: Results for anisotropic laminates and conclusion," Int. J. Solids & Structures, in press (see Appendix D and E).

2. Relation of the deformation a tube to the deformation of a fiber net

We consider again the deformation of the diamond-shaped region of a filament layer shown in Fig. 1 (p.12). The length of each side of the rhombus changes from L in the initial state to $L(1+\epsilon_1)$ in the deformed state. Since ϵ_1 is bounded by the fiber failure strain, it is always small. However, during the failure process the orientation angle of the fibers may deviate significantly from the initial angle α_o. This description applies not only to the actual deformation of the filament-wound tube, but also to the hypothetical deformation of a fiber net without resin matrix.

We consider an external load which causes approximately uniform axial and circumferential Cauchy stresses σ_z and σ_θ in the tube. The magnitude of the

shearing stress $\tau_{z\theta}$ is also approximately uniform but its algebraic sign changes from a $+\alpha$ filament layer to a $-\alpha$ layer. If the resin material were absent (i.e., if the filament-wound tube is replaced by a skeleton of filaments), then the orientation of the fibers under the given state of stress would be given by the angle α^* such that

$$(T \cos \alpha^*/L \sin \alpha^*)/(T \sin \alpha^*/L \cos \alpha^*) = \sigma_z/\sigma_\theta,$$

where T is the tension in each fiber. Hence,

$$\tan \alpha^* = (\sigma_\theta/\sigma_z)^{1/2}. \tag{1}$$

In the case of a closed-end tube subjected to a uniform internal pressure, one has $\sigma_\theta/\sigma_z = 2$ and $\alpha^* = 54^\circ\ 44'$. This angle is called the optimum winding angle in the literature on filament-wound structures. Its optimality is clearly dependent on the specifically assumed loading condition $\sigma_\theta/\sigma_z = 2$.

The presence of the resin material affects the deformation and prevents the fiber net from assuming the orientation angle α^*. Therefore, the actual orientation angle of the filaments corresponding to the stress state $(\sigma_z, \sigma_\theta)$ is between α_o and α^*. Under normal operating conditions, α should be close to α_o. Any significant deviation of α from α_o toward α^* would be resisted by the shearing stiffness of the resin material. In any such state of small-strain deformation (i.e., when both ϵ_1 and $\alpha - \alpha_o$ are small), an increase in the loading is accompanied by an increase in ϵ_1 and a change of α away from α_o toward α^*. Let these small increments be denoted by $\Delta\epsilon_1$ and $\Delta\alpha$, respectively. Then

$$\Delta\epsilon_1 > 0 \qquad \text{and} \qquad (\alpha^* - \alpha_o)\ \Delta\alpha > 0, \tag{2}$$

i.e., the algebraic sign of $\alpha^* - \alpha_o$ determine that of $\Delta\alpha$.

If a filament-wound tube is appropriately designed, it should deform in such a way that α remains close to α_o under a wide range of operating loads. Large deformation of the tube, i.e., significant deviation of α from α_o, should

occur only when the external load is close to the failure load. In the small-strain deformation states preceding failure, the algebraic sign of $\Delta\alpha$ is important because it generally determines the nature or mechanism of the failure process, as we shall find in the following analysis.

3. Shear failure and expansion failure

Deformation of a filament-wound tube may either increase or decrease the surface area of the rhombus shown in Fig. 1. A significant increase in the area may result in the tensile fracture of the resin material or adhesive failure between fiber and matrix. This is associated with experimentally observed progressive whitening and weepage of the tube, formation of droplets and, eventually, fiber breakage and tube rupture. The initiation of this expansion mode of failure may occur at a relatively low level of load. Large strain in the resin material and significant rotation of the fibers do not usually occur until the external load becomes close to the final failure load.

On the other hand, if the surface area decreases as the external loading continues, then the resin material eventually fails under excessive shear deformation. There is much less whitening of the tube and no slow formation of droplets. When the shear strength of the resin material is exhausted, the fiber orientation may be significantly different from the initial orientation. Consequently, large deformation of the tube may occur in the failure process, and an accurate prediction of the failure load may require the knowledge of the inelastic behavior of the matrix under large deformation. Furthermore, failure of the tube in the shear mode may be preceded by extensive delamination since the in-plane areal compression of the resin material may result in buckling of filament layers.

Let A_o and A denote, respectively, the area of the rhombus in the initial

and deformed state, and let ΔA be a small increment in A. From Eq. (2.2) of Part II (p. 11) we obtain

$$\Delta A/A_o = 2\{(\sin 2\alpha/\sin 2\alpha_o)(1+\epsilon_1)\Delta\epsilon_1 + (\cos 2\alpha/\sin 2\alpha_o)(1+\epsilon_1)^2\,\Delta\alpha\}. \qquad (3)$$

If $\alpha < 45°$, then a positive $\Delta\alpha$ contributes to a positive increment in the area. The opposite is true if $\alpha < 45°$. Consequently, there are four possible cases:

(i) $\alpha < 45°$ and $\alpha_o < \alpha^*$. In this case the area increases as α increases toward α^*. Expansion failure occurs.

(ii) $\alpha > 45°$ and $\alpha_o > \alpha^*$. In this case the area increases as α decreases toward α^*. Expansion failure also occurs.

(iii) $\alpha < 45°$ and $\alpha_o > \alpha^*$. In this case the area decreases as α decreases toward α^*. Shear failure occurs.

(iii) $\alpha > 45°$ and $\alpha_o < \alpha^*$. In this case the area decreases as α increases toward α^*. Shear failure also occurs.

At the initiation of the expansional mode of failure, α is not significantly different from the initial angle α_o. Therefore, if the angle α^* given by Eq. (1) is greater than 45°, then in order to avoid expansional failure one should choose a winding angle α_o smaller than the α^*. On the other hand, if α^* is smaller than 45°, then the winding angle should be larger than α^*. In either case, choosing a winding angle between 45° and α^* generally promotes the shear mode of failure (except when α_o is chosen to be very close to 45° or to α^*, as will be explained below). If α_o is close to α^*, then the resin material will not be subjected to excessive shear deformation in the states preceding the final failure. The final failure will be initiated by tensile failure of weak or flawed filaments.

If either $\alpha_o = \alpha^*$ or $\alpha = 45°$, then $\cos 2\alpha\,\Delta\alpha = 0$ and, consequently, there is no areal expansion due to the rotation of the fibers. However, there is some

areal expansion due to the fiber strain increment $\Delta\epsilon_1$. Thus, tubes wound at the ideal winding angle ($\alpha_o = \alpha^*$) or at 45° angle may start to fail in the expansional mode. As failure progresses in the 45° filament-wound tube under the closed-end condition, α increases toward α^* and the failure behavior may subsequently change from the expansion mode to the shear mode.

In the usual production process, a constant pitch is enforced and, as a result, the winding angle α_o is smaller toward the interior surface of the tube and larger toward the exterior surface. The deviation from the mean winding angle increases with the thickness of the tube and decreases with the mean radius. This three-dimensional effect influences the accuracy of the analysis given in Part II. It also implies that, for whatever choice of the helical pitch, a certain amount of in-plane shear deformation necessarily occurs in the resin material and this shear deformation varies in the thickness direction of the tube.

4. Experimental evidences

The preceding simple predictions are verified by various experimental results available from the existing literature. Hull et al. (Hull, D., Legg, M.J. and Spencer, B. "Failure of glass/polyester filament wound pipe" Composites, Vol 9, pp. 17-24, 1978) tested filament-wound tubes with the "ideal" winding angle (54° 44') under both closed-end and open-end conditions. Since the fiber orientation tends to stay at the "ideal" angle under the close-end test condition, the surface area expands because of fiber extensional strain rather than because of fiber rotation. Hence the tube fails under the expansion mode. In the open-end case, the fibers tend to orient toward the circumferential direction. The surface area decreases in the deformation process, and the tube fails in the shear mode. The nature of the observed failure phenomena was also

confirmed by examination of photomicrographs (Jones, M.L.C. and Hull, D. "Microscopy of failure mechanisms in filament-wound pipe," J. Material Sci., Vol. 14, pp. 165-174, 1979).

More extensive testing of pipes wound at 35, 45, 65 and 75 degree angles (Spencer, B and Hull, D., "Effect of winding angle on the failure of filament wound pipe", Composites, Vol. 9, pp. 263-271, 1978) further supports the theoretical prediction. Under both closed-end and open-end conditions, the 35° tubes failed primarily under the expansion mode, although the failure is also accompanied by significant or large shear deformation. Weepage and whitening begins at a very low level of loading. The orientation angle of the fibers increase from 35° and eventually reaches 50° in the state immediately preceding final fracture. For the tubes wound at 45° angle, the area increase due to increase in α is zero initially (because $\cos 2\alpha = 0$ in Eq. (3)). The initial failure of the closed-end tube may be associated with the expansion mode because the surface area increases with fiber elongation. However, as α increase and deviates significantly from 45°, shear deformation becomes dominant and the failure process changes into that of the shear mode. Spencer and Hull observed less extensive whitening and reduced over-all breakdown of the tube when the winding angle is 45°. Furthermore, under the open-end condition, local delamination was observed which suggested the reduction of surface area accompanying the shear mode of failure.

The 65° and 75° tubes under the closed-end condition showed very extensive whitening after weepage and generated creaking noise at the instant of failure. The phenomena are clearly associated with the expansion mode of failure as the surface area increases when the fiber orientation angle decreases toward the limiting angle $\alpha^* = 54° 44'$. On the other hand, under the open-end condition,

the same tubes (especially those wound at the 75° angle) showed much less whitening. The onset of weepage occurred suddenly with the formation of jets of liquid through the tube wall as the tube buckled before final failure. The failure process is clearly associate with the shear mode.

Spencer and Hull reported the measured data of the axial and circumferential strains as functions of the mean circumferential stress (which is related to the internal pressure) for the tubes with various winding angles under the open-end and closed-end conditions. From these data the intrinsic strains ϵ_1, ϵ_2 and γ_{12} and the areal expansion ratio $(A-A_o)/A_o$ may be calculated by using the finite-deformation kinematical relations in Part II. The results are shown in Figs. 13 to 17 for the open-end tubes and Figs. 18 to 22 for the closed-end tubes. The figures show the paths of the intrinsic strain followed by different tube specimens in the entire deformation process preceding the final failure. Large magnitudes of γ_{12}, accompanied by small or negative transverse strain ϵ_2, indicate the shear mode of failure, while a significant positive transverse strain and a large areal expansion ratio indicate the expansional failure mode (for example, the 55° and 65° tubes under the closed-end condition). Under the closed-end condition, the strain path for the 75° tube terminated prematurely at a very low level of the pressure load. Although the average intrinsic strains in the tube remained small before failure, a narrow spiral band of intense whitening was clearly observed, which suggests local failure under the expansion mode.

Experimental results of the similar kind for other composite material systems are available, e.g., the results for closed-end tubes of carbon/epoxy filament-wound cylinders reported by Uemura and Fukunaga (ibid.). Special mention should be made concerning the work of Cole and Pipes (Cole, B.W. and

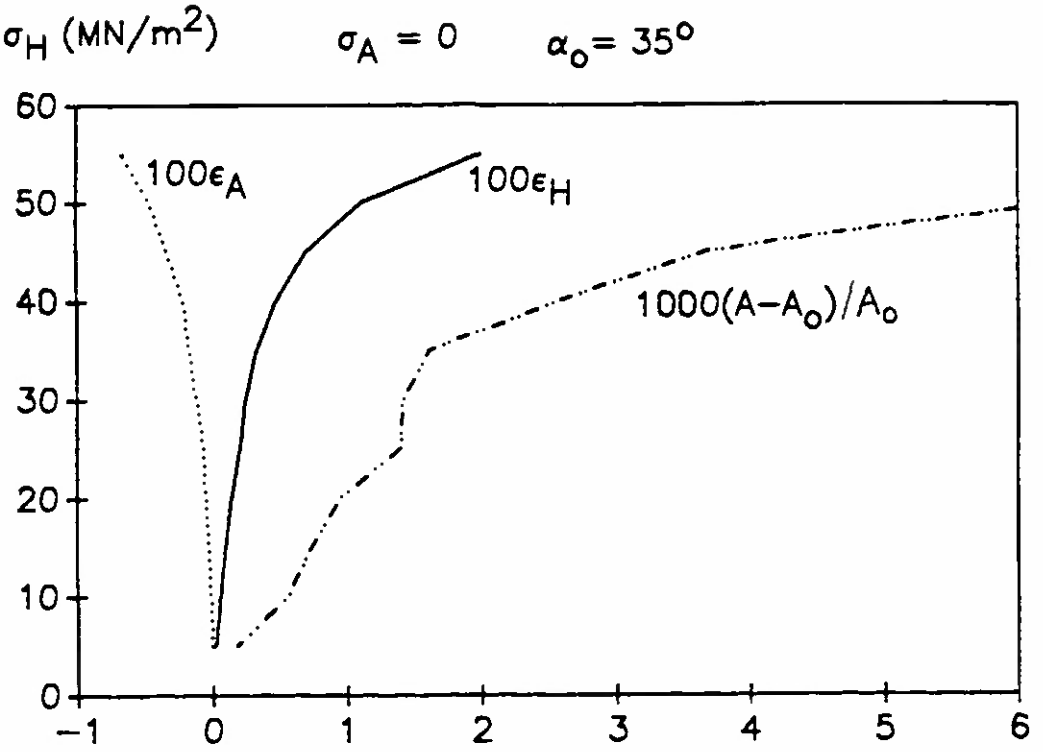

(Based on the data of Spencer and Hull)

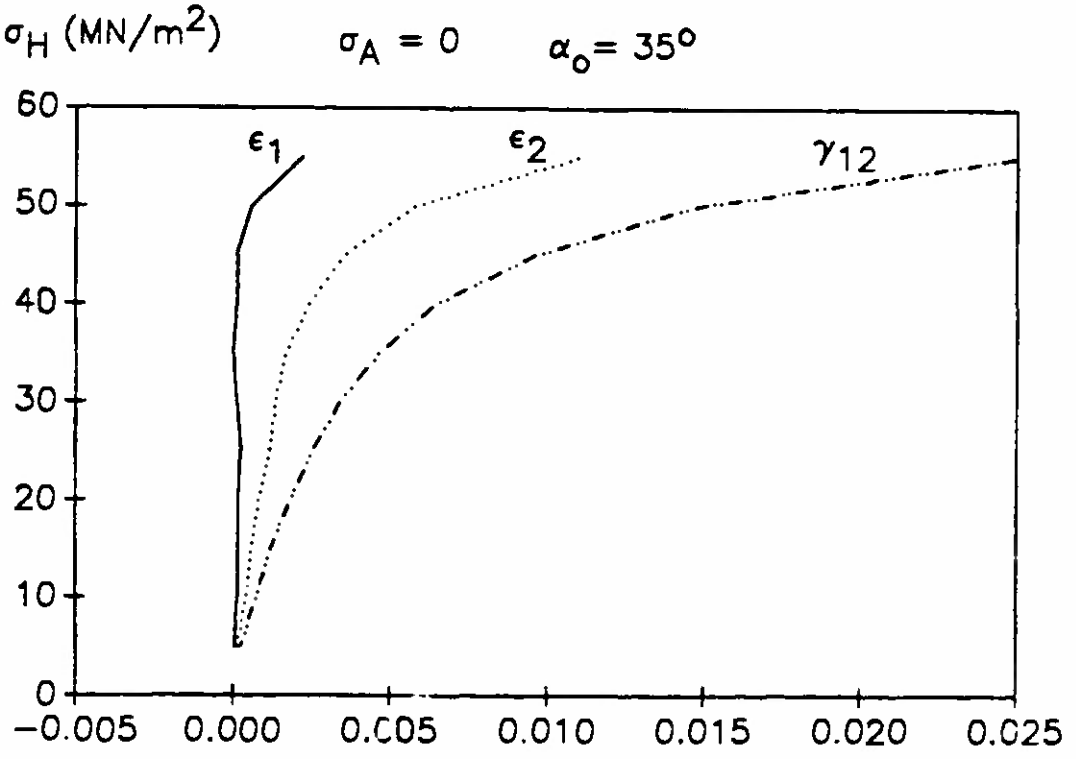

Fig. 13: Strain path to failure, 35° open-end tube

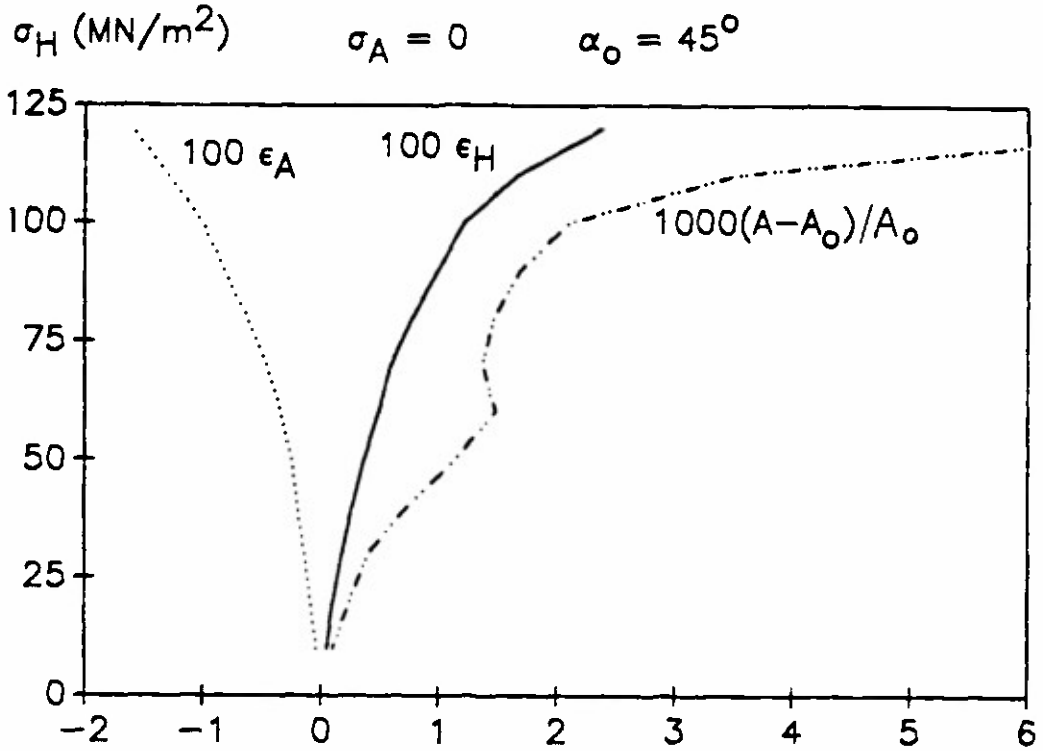

(Based on the data of Spencer and Hull)

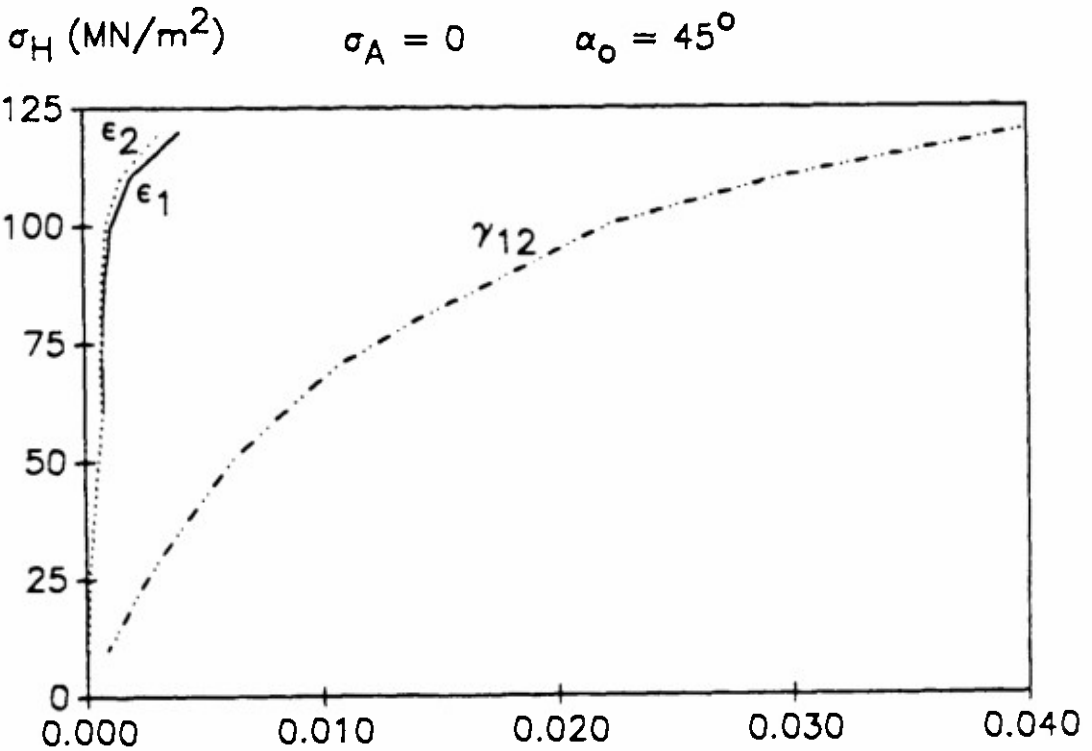

Fig. 14: Strain path to failure, 45° open-end tube

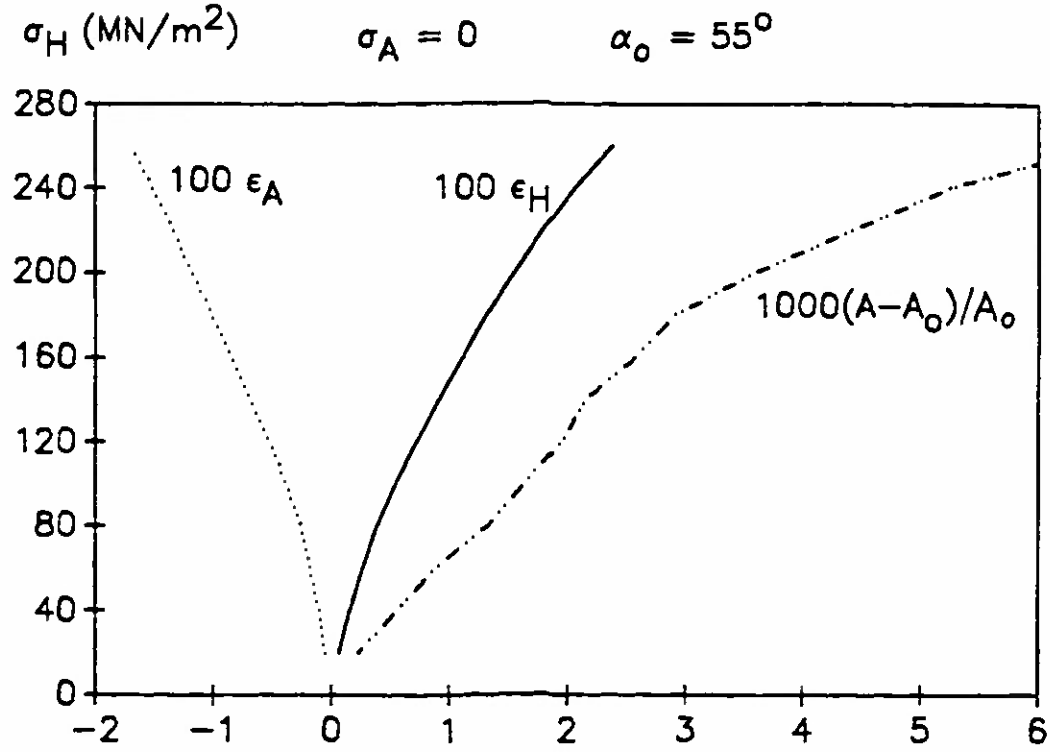

(Based on the data of Spencer and Hull)

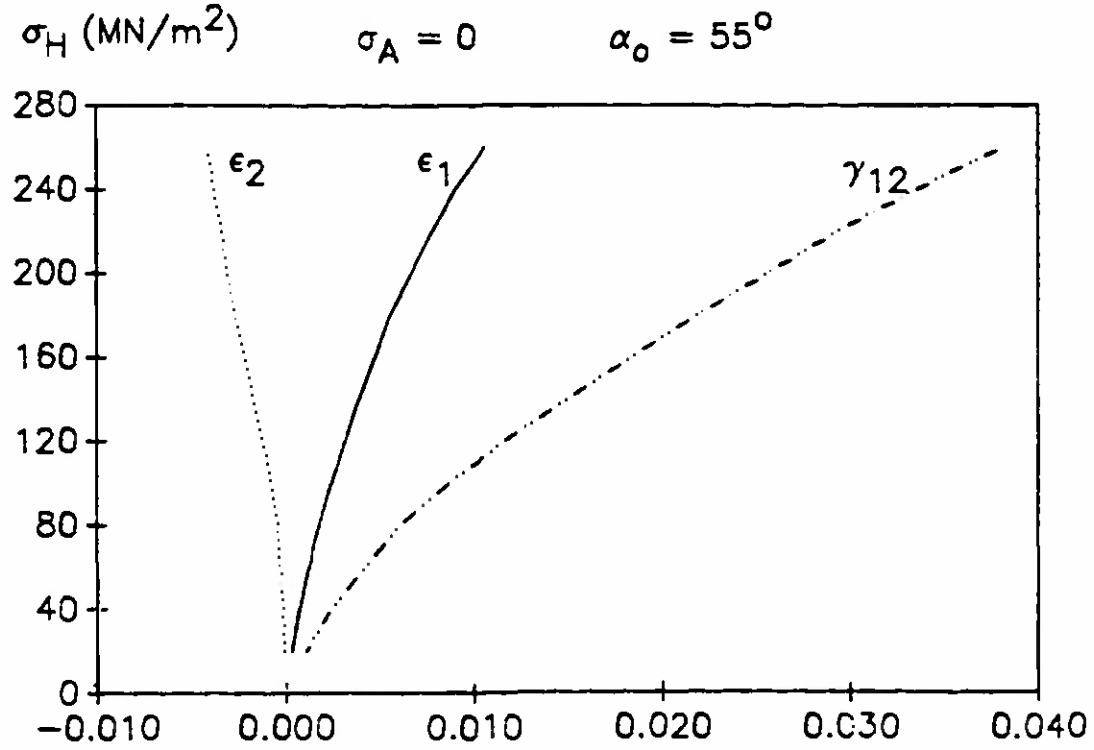

Fig. 15: Strain path to failure, 55° open tube

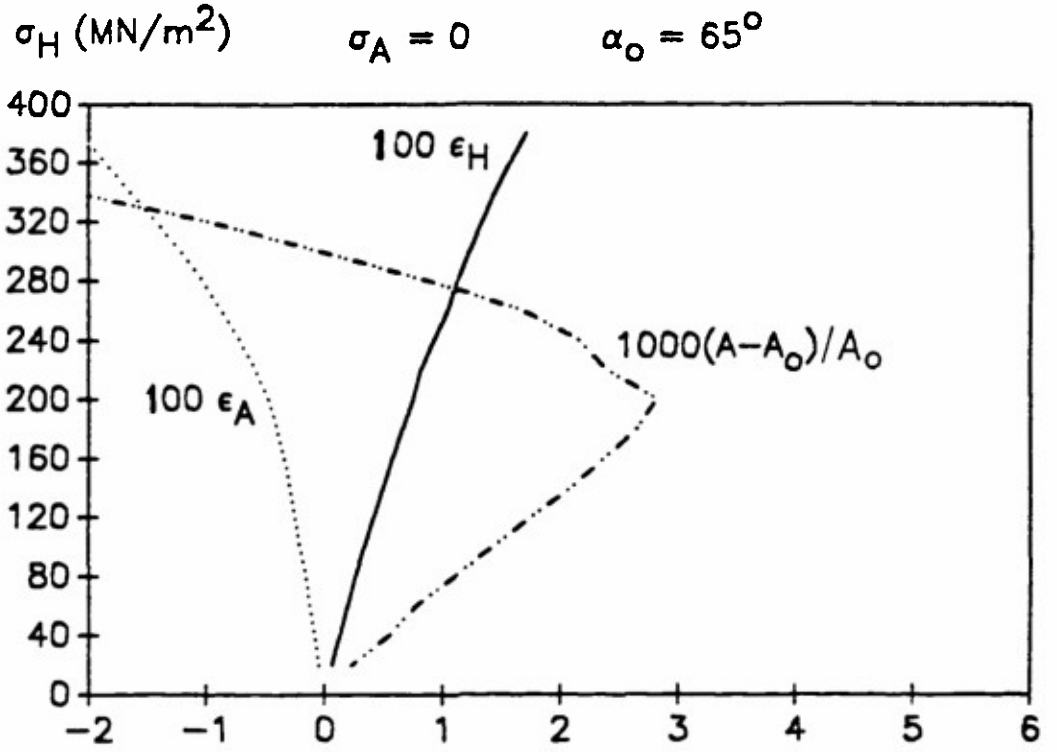

(Based on the data of Spencer and Hull)

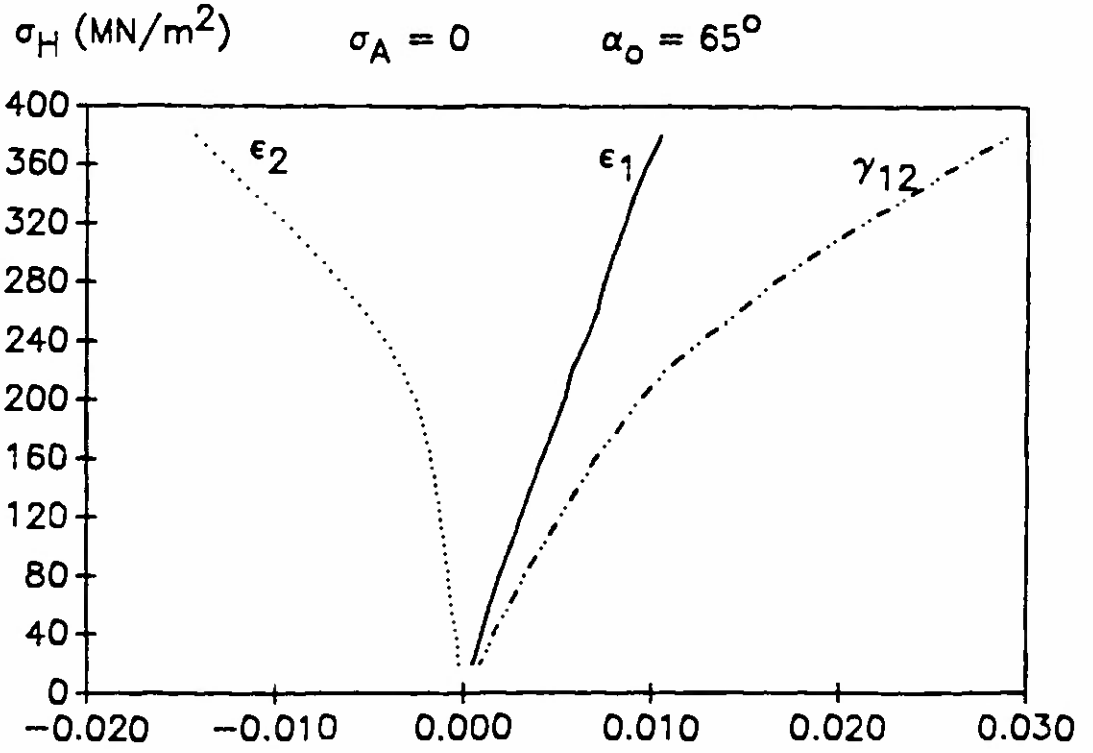

Fig. 16: Strain path to failure, 65° open-end tube

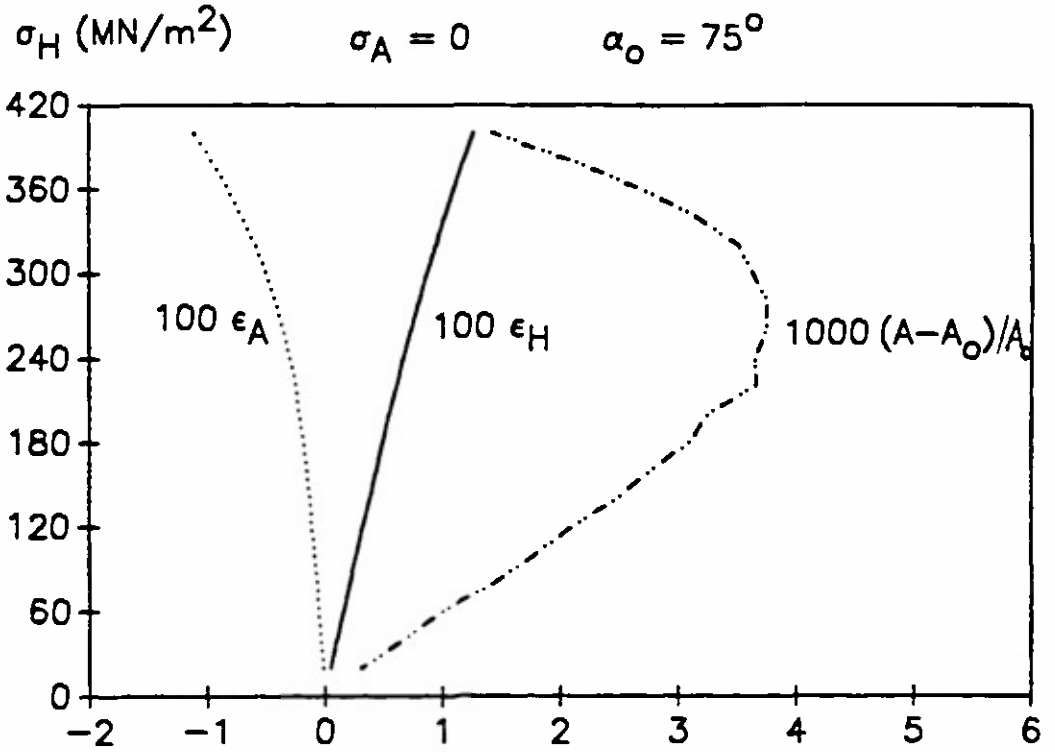

(Based on the data of Spencer and Hull)

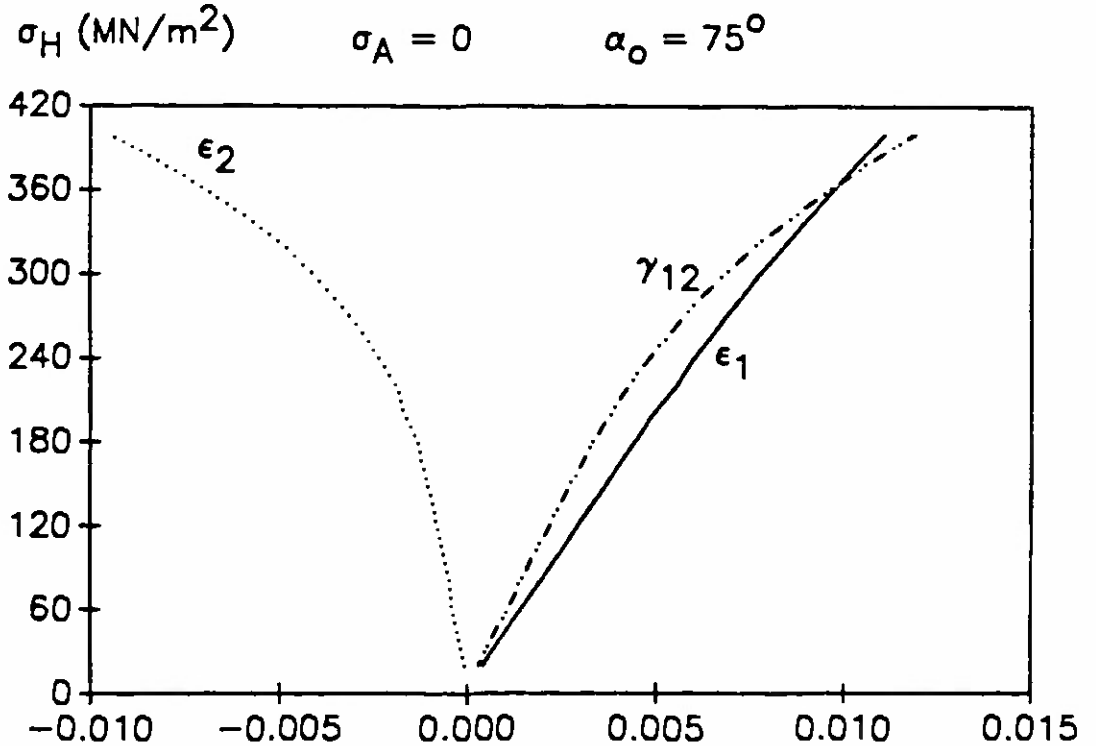

Fig. 17: Strain path to failure, 75° open-end tube

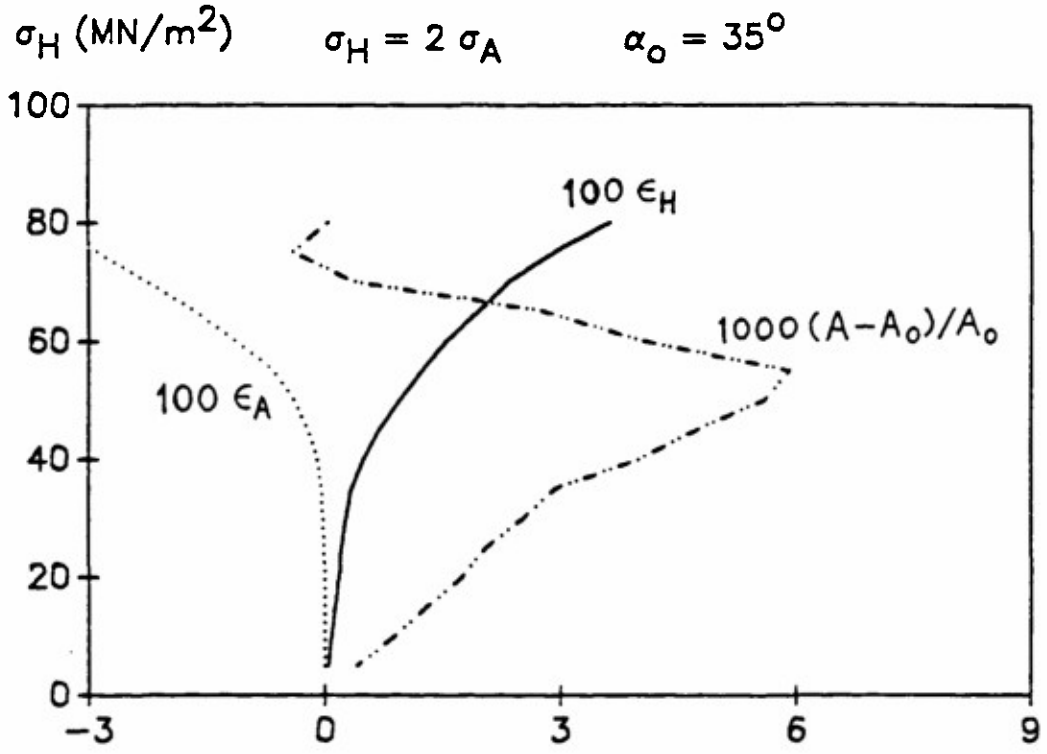

(Based on the data of Spencer and Hull)

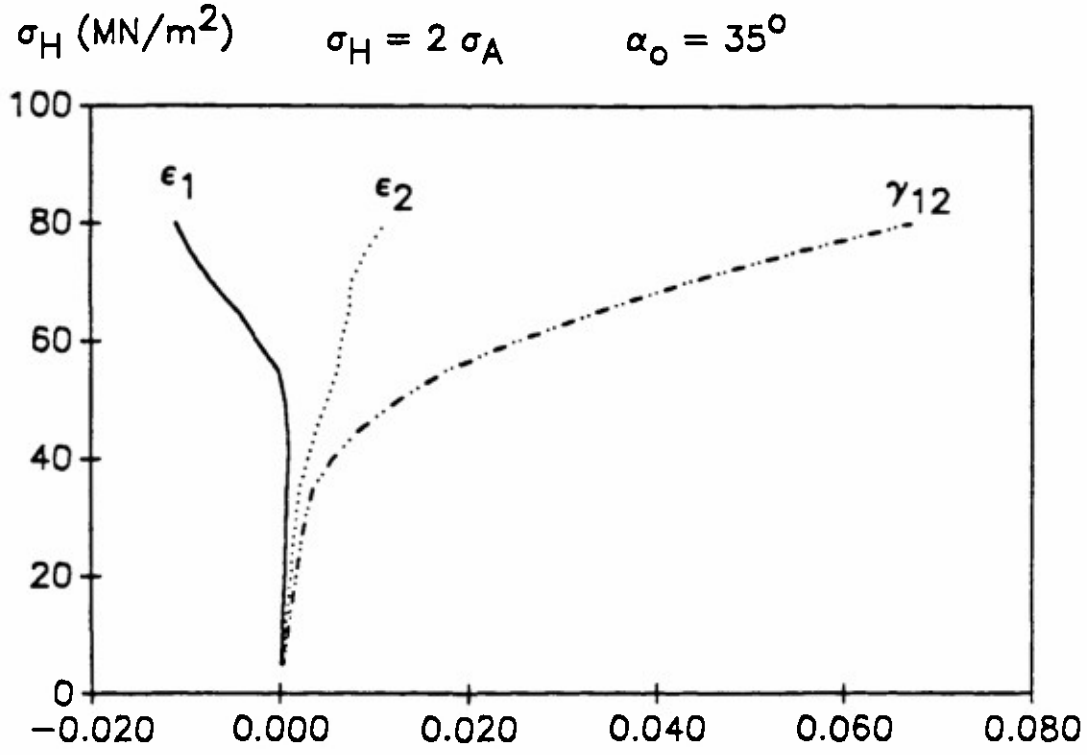

Fig. 18: Strain path to failure, 35° closed-end tube

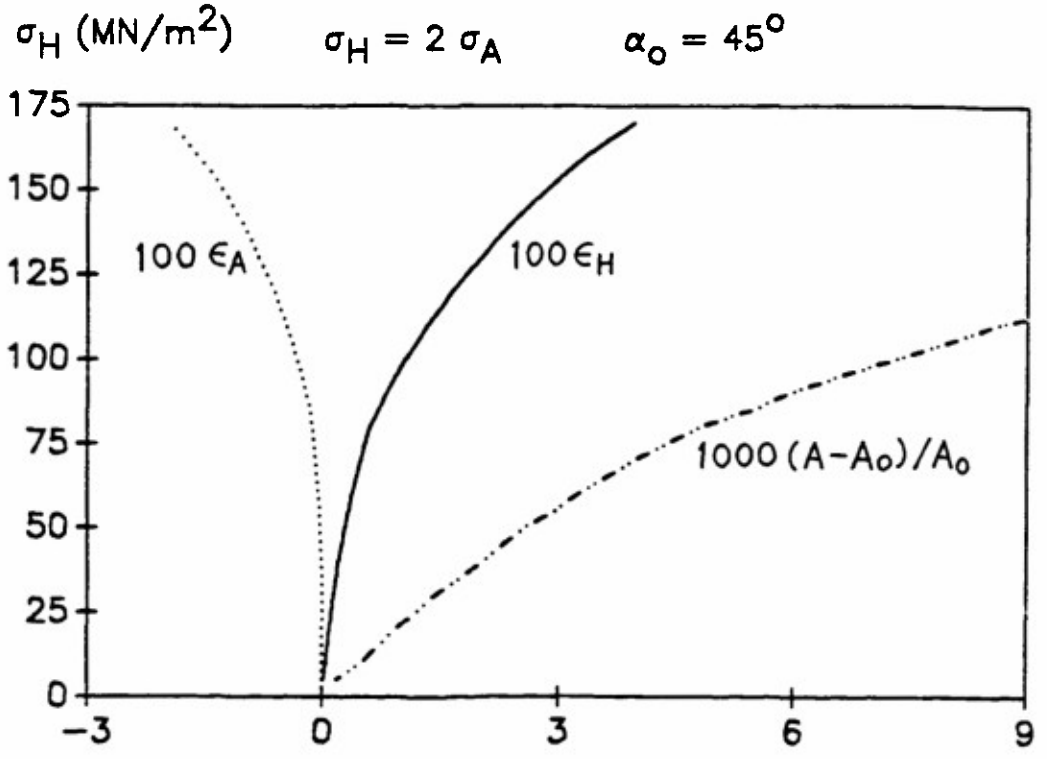

(Based on the test data of Spencer and Hull)

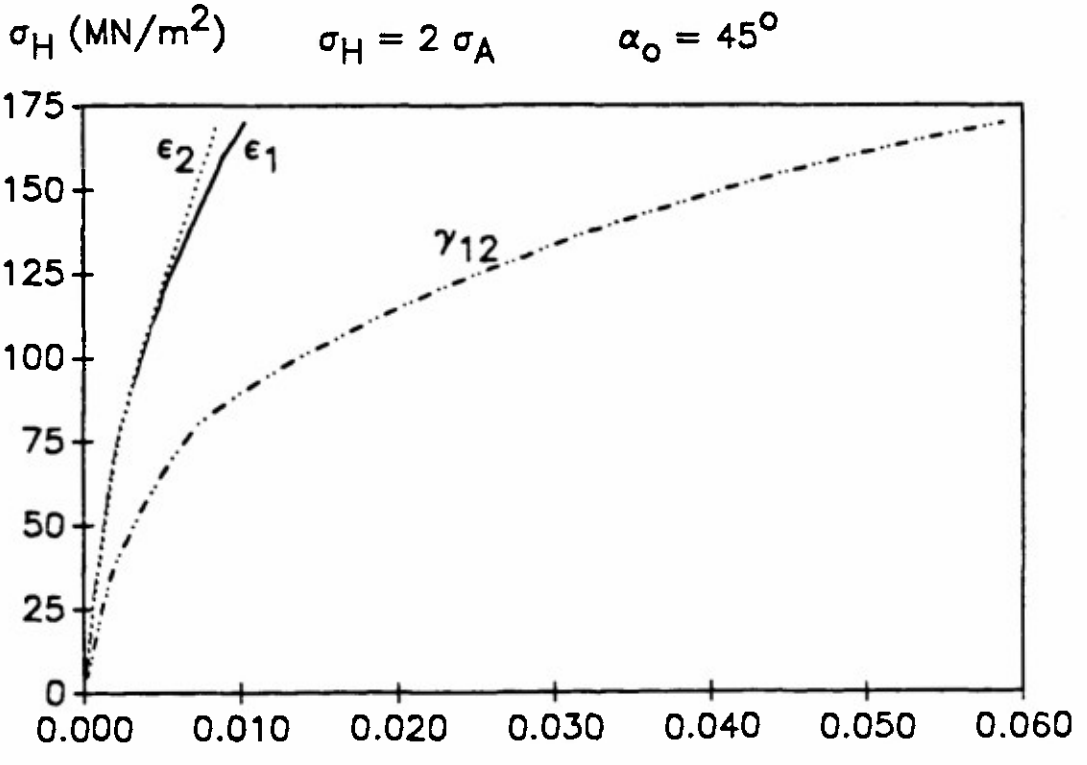

Fig. 19: Strain path to failure, 45° closed-end tube

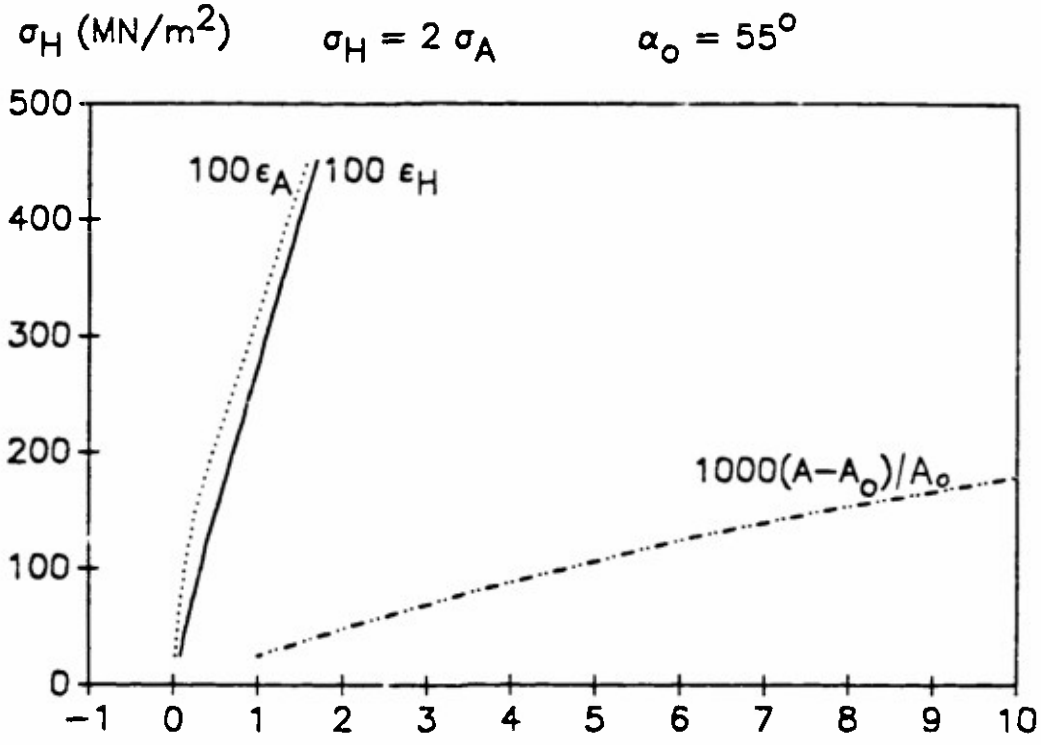

(Based on the test data of Spencer and Hull)

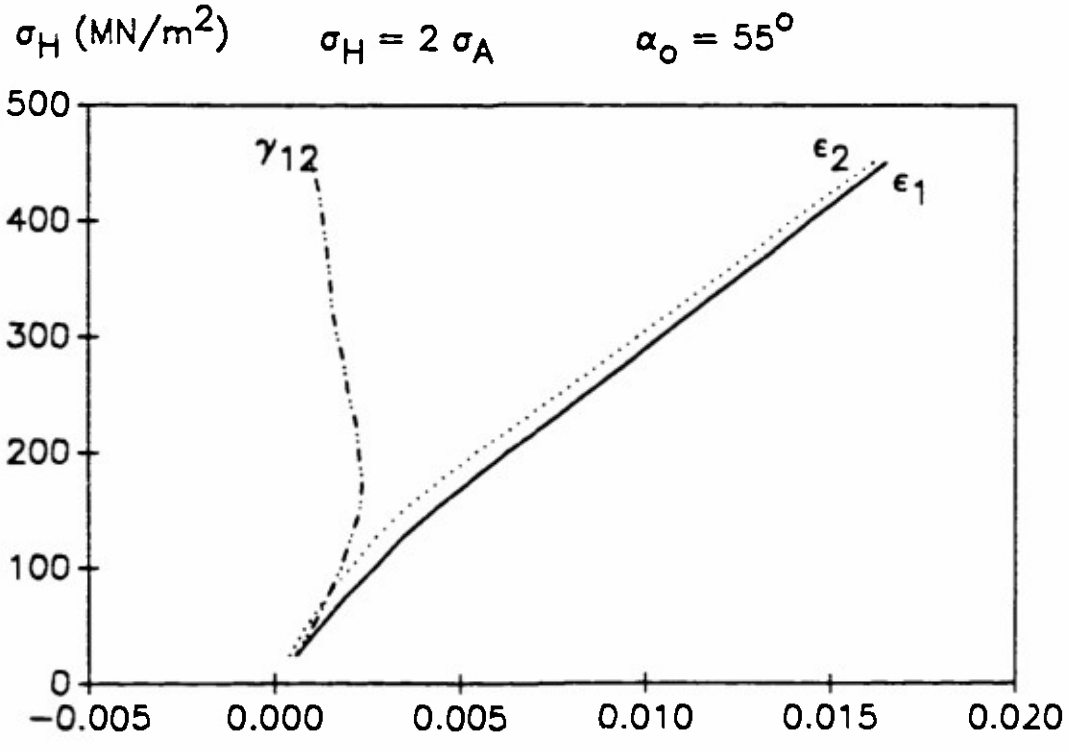

Fig. 20: Strain path to failure, 55° closed-end tube

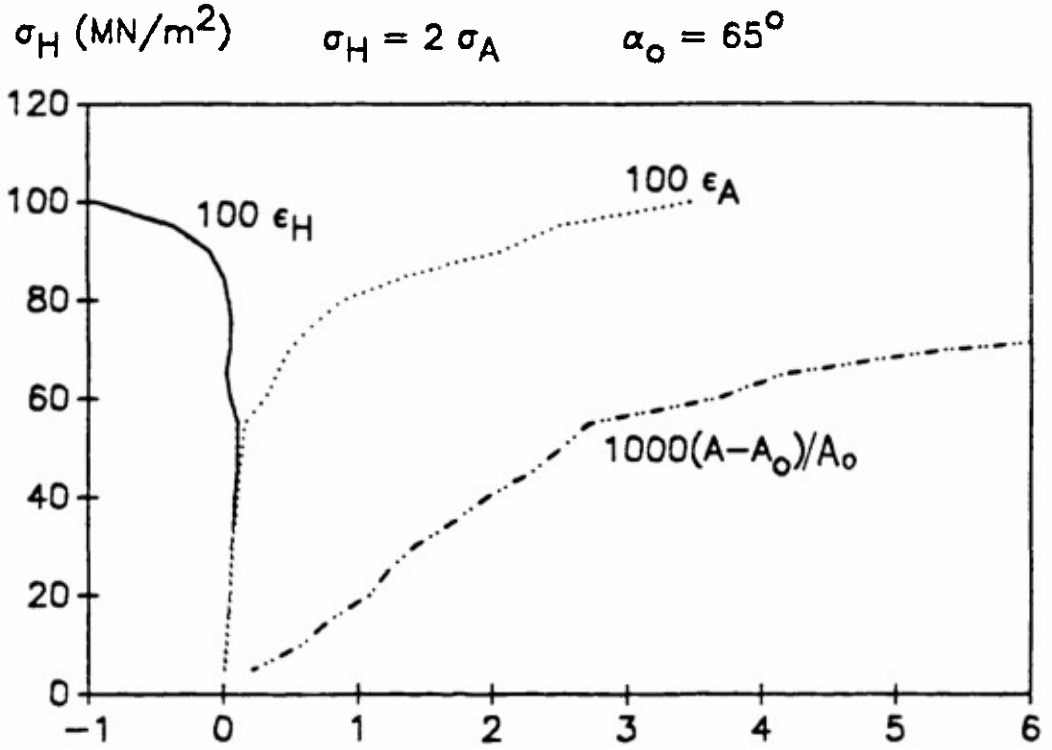

(Based on the test data of Spencer and Hull)

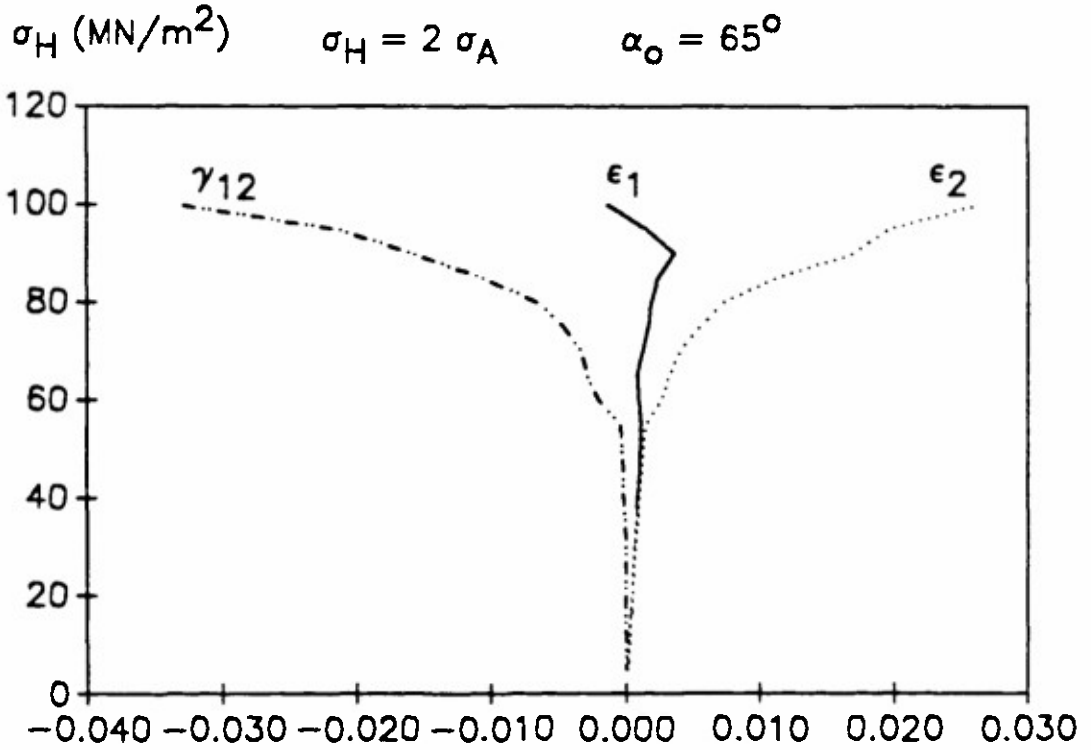

Fig. 21: Strain path to failure, 65° closed-end tube

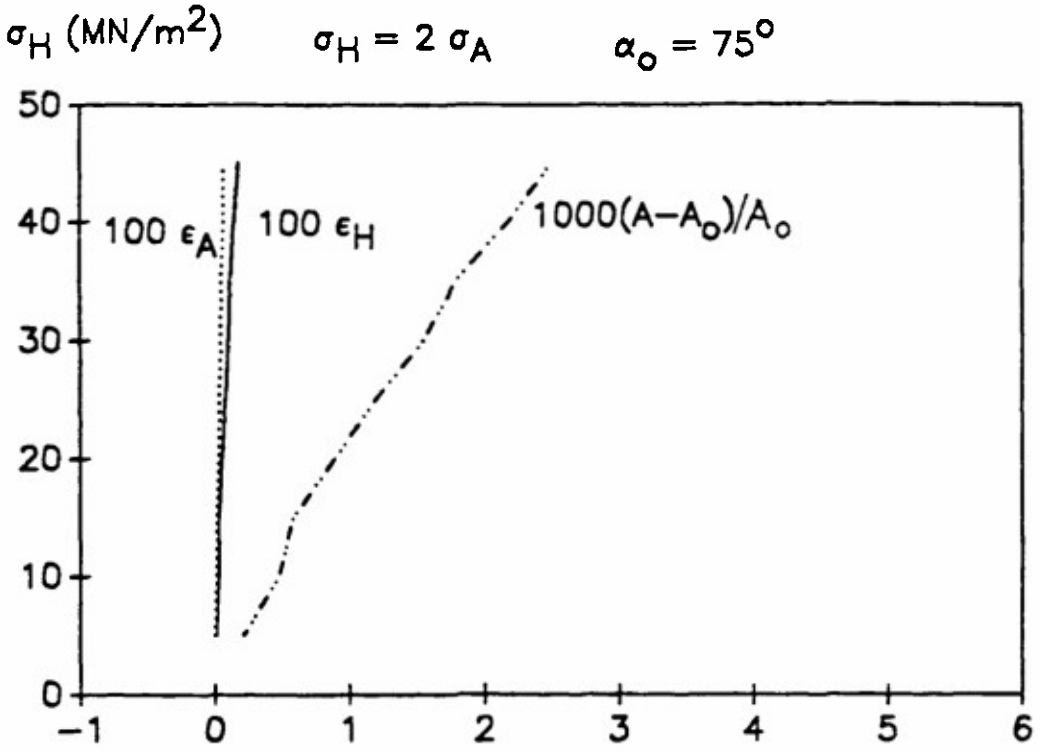

(Based on the test data of Spencer and Hull)

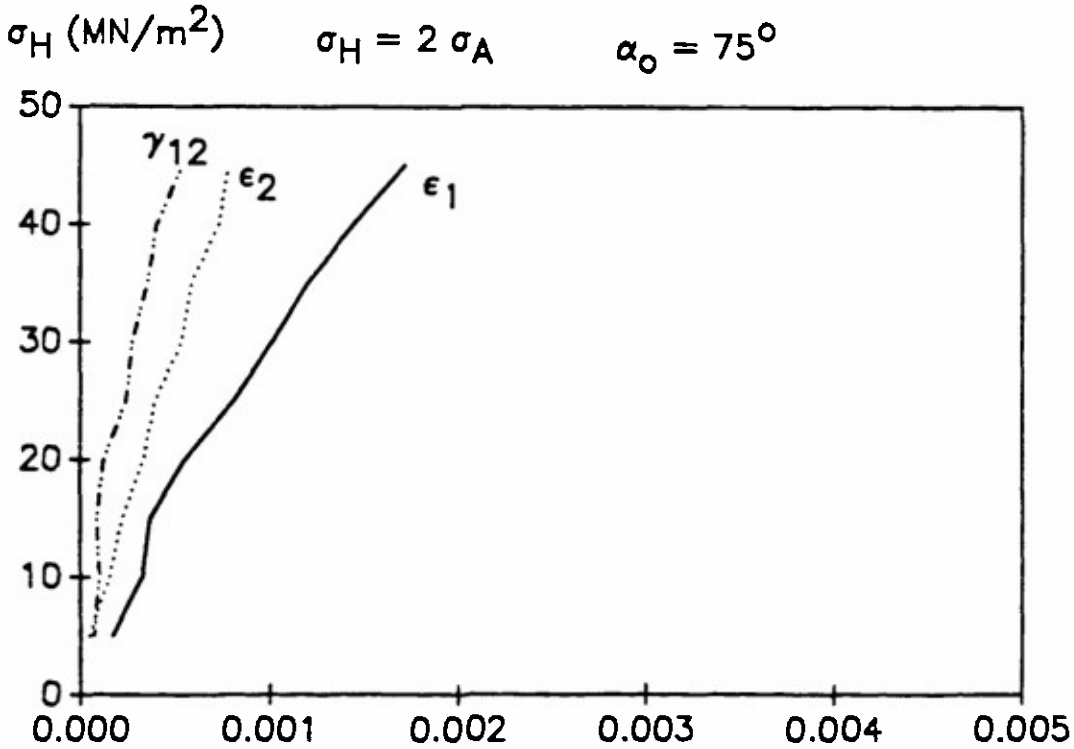

Fig. 22: Strain path to failure, 75° closed-end tube

Pipes, R.B., Filamentary Composite Laminates Subjected to Biaxial Stress Fields. IIT Research Institute Report AD-785 362, June 1974). These authors developed a testing device for tubular specimens with the capability of varying the axial to the circumferential stress ratio, so that stress paths more general than the proportional loading paths corresponding to the open-end or closed-end conditions are made feasible. Results from such tests provide valuable additional information concerning the nonlinear material behavior and the effect of the strain path on the failure mode and the ultimate strength.

5. Two-dimensional micromechanical modeling and analysis of fiber-matrix debonding

If, with a certain combination of the winding geometry and applied load, a filament-wound structure undergoes the expansion mode of failure, then whitening appears in the resin matrix at an initial stage of the failure process due to the formation of microcracks. Eventually, small cracks coalesce to form finite cracks across the resin matrix or on the filament-resin interface. As mentioned previously, the expansional mode of failure is usually associated with a transverse extensional strain in the filament layers. Under such a strain state, the resin material near the tip of a matrix crack or a fiber-matrix disbond is subjected to intense local peeling and shearing stress. This intense local stress field may result in catastrophic growth of the crack if the level of the transverse strain in the filament layer is sufficiently high, if the crack length is sufficiently large, and if an increase in the crack length under a fixed transverse strain causes an increase in the strain-energy-release rate. This possibility is investigated in the present section of the report for a fiber-matrix disbond, and in the next section for an oblique matrix crack running

across the matrix region between two adjacent fibers. At this stage, the objective of the analysis is to assess the possibility and the stability characteristics of crack growth by using simple analytical models. Specifically, we consider two-dimensional (plane strain or plane stress) micromechanical models in which the fiber regions are assumed to be rigid media. The assumption concerning the rigidity of the fiber regions is conservative because it generally yields a more severe stress state in the vicinity of the crack tip.

5.1 Boundary-element analysis

We consider a plane strain model in which an isotropic resin material of Young's modulus E and Poisson' ratio ν occupies the infinite strip, $-\infty < x < \infty$ and $0 < y < h$, between two rigid filaments. A disbond of length 2a exists between the resin and the lower filament in the interval $-a < x < a$. The upper rigid filament is then subjected to a horizontal displacement $h\gamma_o$ and a vertical displacement $h\epsilon_o$ relative to the lower filament, which result in average strains $\epsilon_y = \epsilon_o$ and $\gamma_{xy} = \gamma_o$ in the resin region. Our problem is to determine, for various ratios of a/h, the displacements of the crack surface, the interfacial stresses between the resin and the lower filament ahead of the crack, and the strain-energy-release rate associated with crack growth.

Because of the linearity of the problem, the effects of the two strain loads ϵ_o and γ_o may be considered separately. This results in two problems associated, respectively, with the vertical and horizontal displacements of the upper filament relative to the lower filament. In the first problem, the limiting stress and strain states at infinity ($x \to \pm\infty$) are given by

$$\sigma_y = \{(1-\nu)/\nu\}\lambda\epsilon_o, \qquad \sigma_x = \sigma_z = \lambda\epsilon_o, \tag{4a}$$

$$\epsilon_y = \epsilon_o, \qquad \epsilon_x = \epsilon_z = 0, \tag{4b}$$

where

$$\lambda = E/[(1-2\nu)(1+\nu)], \qquad \mu = E/[2(1+\nu)]$$

are the Lame elastic constants of the resin material. The solution to this problem may be decomposed into (i) a trivial solution characterized by uniform strains and uniform stresses which have the expressions of Eq. (4) in the entire matrix region and (ii) the solution of a complementary problem with the following boundary conditions

$$t_2 = -\sigma_y = (1-\nu)K\epsilon_o, \quad t_1 = 0 \quad \text{along the crack surface,} \tag{5a}$$

$$u = v = 0, \quad \text{along the remaining portions of the x-axis and along the entire line } y = h. \tag{5b}$$

Similarly, the solution of the second problem, associated with the horizontal displacement of the upper filament, can be decomposed into (i) a trivial uniform solution characterized by

$$\tau_{xy} = \mu\gamma_o, \qquad \gamma_{xy} = \gamma_o, \tag{6}$$

in the entire matrix region, and (ii) the solution of a complementary problem with the boundary conditions

$$t_1 = -\tau_{xy} = \mu\gamma_o, \quad t_2 = 0 \quad \text{along the crack surface,} \tag{7a}$$

$$u = v = 0, \quad \text{along the remaining portions of the x-axis and along the entire line } y = h. \tag{7b}$$

Notice that the two complementary problems defined respectively by the boundary conditions of Eqs. (5) and (7) have solutions with zero limiting displacements and stresses at infinity.

The boundary displacements u_i and the boundary tractions t_i (with i = 1 and 2 corresponding, respectively, to the x and y directions) satisfy the integral identity

$$u_j(\mathbf{x}) = \oint [G_{ij}(\boldsymbol{\xi},\mathbf{x})\ t_i(\boldsymbol{\xi}) - F_{ij}(\boldsymbol{\xi},\mathbf{x})\ u_i(\boldsymbol{\xi})]\ ds(\boldsymbol{\xi}), \tag{8}$$

where the path of the line integral encloses the matrix region and where

$$C_{ij}(\xi,x) = C_1 (C_2 \delta_{ij} \ln r - z_i z_j/r^2),$$

$$F_{ij}(\xi,x) = C_3 r^{-2} \{C_4(z_i n_j - z_j n_i) + (C_4\delta_{ij} + 2r^{-2}z_i z_j)\, z_k n_k\},$$

$$z_i = \xi_i - x_i, \qquad r^2 = z_i z_i, \qquad t_i = \sigma_{ij} n_j,$$

$$C_1 = -1/\{8\pi\mu(1-\nu)\}, \qquad C_2 = 3-4\nu,$$

$$C_3 = \cdot\ 1/\{4\pi(1-\nu)\}, \qquad C_4 = 1-2\nu.$$

In the preceding expressions, n_i is the unit outward normal vector along the boundary (Banerjee, P.K. and Butterfield, R., Boundary Element Methods in Engineering Science, 1981). The integral identity will be discretized by dividing the boundary curve into intervals (boundary elements) and by assuming that the displacements and the tractions vary linearly within each interval (which is then called a linear boundary element). In the present problems the boundary of the matrix region consists of segments of straight lines. If t_i and u_i vary linearly within each element, then the integrals on the right hand side of Eq. (8) can be evaluated exactly and numerical integration schemes are not needed. Equation (8) yields a system of linear algebraic relations for the nodal values of t_i and u_i.

At each node point, two of the four quantities u_1, u_2, t_1 and t_2 are specified while the remaining two variables are to be solved. Hence the system of linear algebraic relations obtained by discretizing Eq. (8) provides 2N linear algebraic equations for 2N unknown nodal variables, where N is the total number of boundary nodes. A double node, which stands for two boundary nodes at the same position, will be used at a boundary point of discontinuity of the traction vector t_i or of the normal vector n_i. Examples of such double nodes include the crack tip and a corner point of the matrix region. By solving the system of equations one obtains an approximate solution for the unknown nodal displacements on the crack surface and the nodal values of the interfacial tractions ahead of

the crack tip.

For the two complementary problems defined, respectively, by the boundary condition of Eqs. (5) and (7), both the displacement and the traction vectors vanish at infinity. Hence the line integrals of Eq. (6) need be performed only along the two horizontal paths and, in practice, only along a sufficiently long finite portions of the paths. Furthermore, the first problem, associated with a vertical displacement of the upper filament, is symmetric with respect to the y-axis while the second problem, associated with a horizontal displacement of the upper filament, is antisymmetric. These symmetry conditions may be used to eliminate all unknown variables associated with the boundary nodes in the region $x < 0$ by expressing them in terms of the remaining variables, according to the procedure described in Part III, Sec. 8 (pp. 71-72). Notice that this practice, which is convenient in dealing with the symmetry conditions in a boundary-element analysis, is different from the common practice in a finite-element analysis, in which one half of the region separated by the symmetry axis is removed from the finite-element model and the symmetry conditions along the symmetry axis are used as part of the boundary conditions for the reduced region. The latter practice is not used in the present boundary-element analysis because, by removing the left half region of the infinite strip $0 \leq y \leq h$, corner points would have to be introduced which generally introduce additional complication in programming the solution algorithm.

The boundary-element models used for the analysis of the first and second complementary problems are described, respectively, in Figs. 23 and 24, where only the regions $x \geq 0$ of the models are shown in the figures and the remaining portions of the models are implied by symmetry. In these models, the length scales have been normalized with respect to h so that the normalized width of the

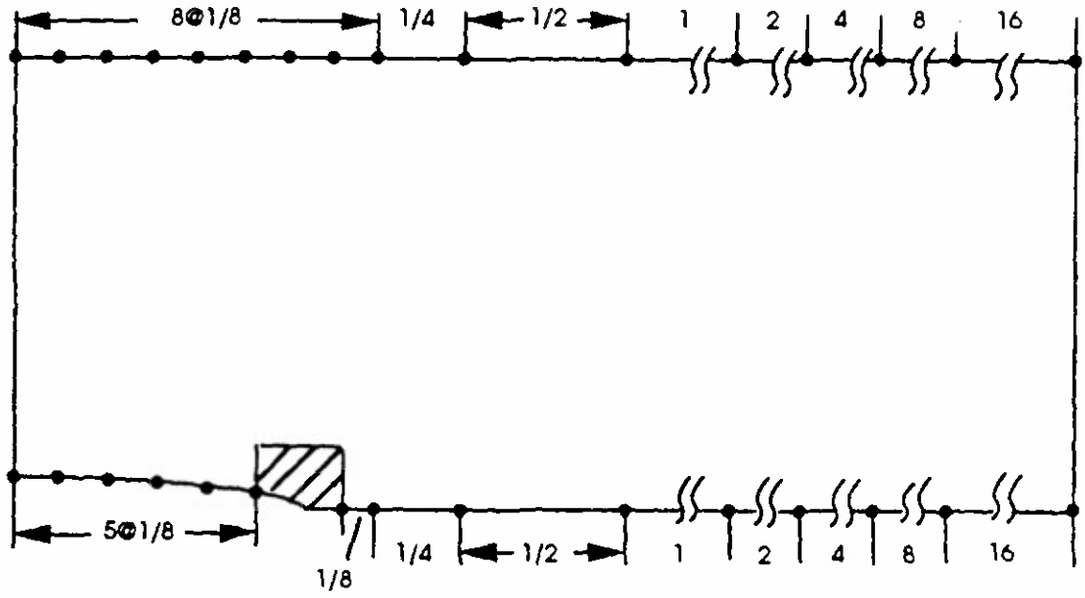

(a)

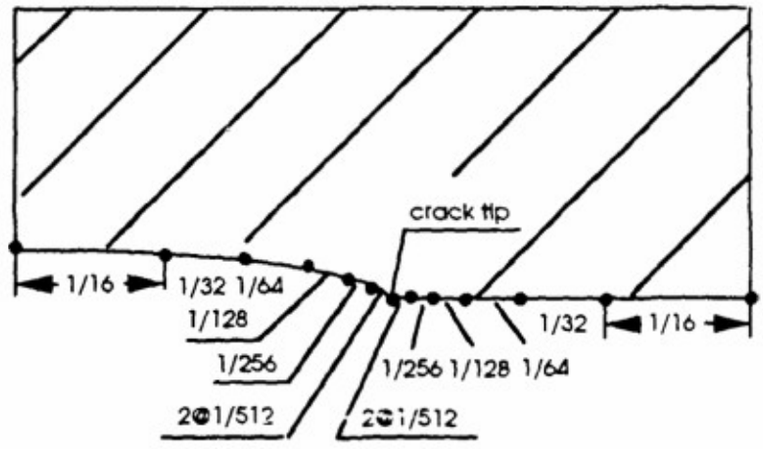

(b)

Fig. 23: Boundary-element model for a fiber-matrix disbond under a transverse strain load

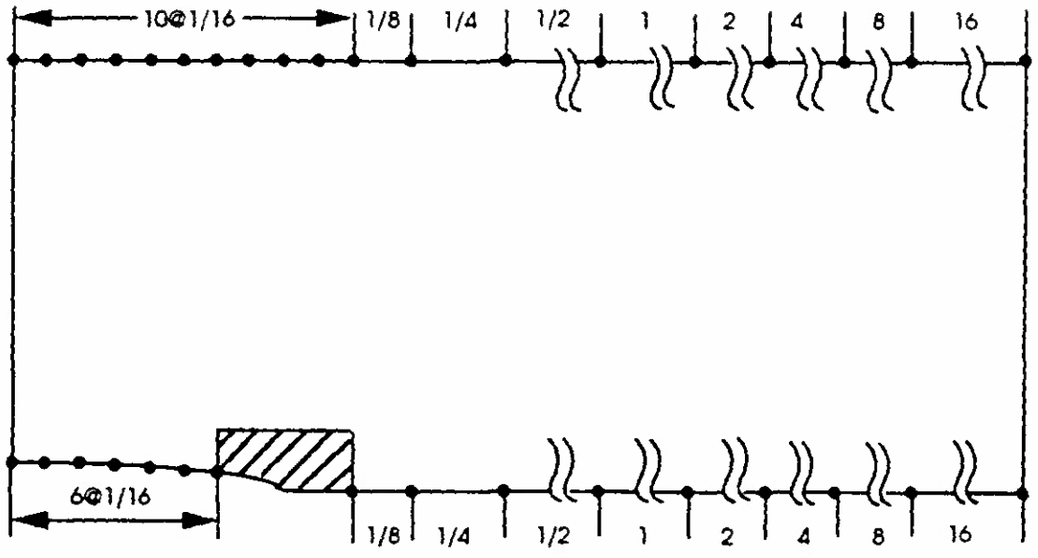

(a)

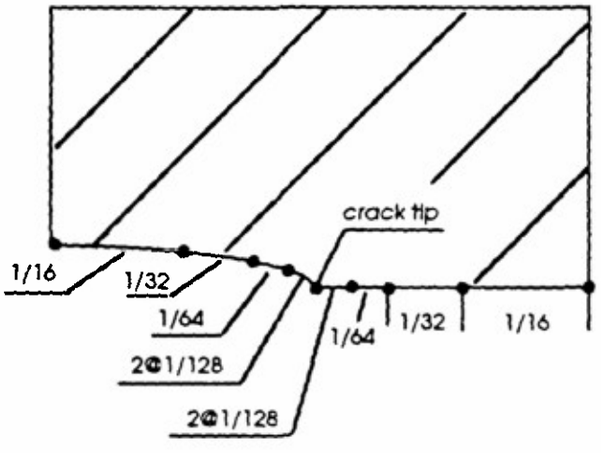

(b)

Fig. 24: Boundary- element model for a fiber-matrix disbond under a shear load

strip is unity. Figs. 23b and 24b show, in complete detail, the shaded regions around the crack tip in Figs. 23a and 24a. The mesh of boundary elements is made progressively finer as the crack tip is approached. The shortest elements have the normalized length 1/512 for the problem associated with the tension load and 1/128 for the problem associated with the shear load. Outside the shaded region, the partition of the crack face and the number of nodes may vary with the length of the crack and, therefore, may be different from those shown in the figures.

5.2 Strain energy release rates associated with crack growth

When the system of algebraic equations for the unknown nodal variables are derived by integrating Eq. (8) and the equations are solved, the energy-release rate associated with crack growth is calculated from the crack closure integral

$$G = (1/2\gamma) \int_0^{\delta} \sigma_y(x) u_2 (x-\gamma)\, dx + (1/2\gamma) \int_0^{\delta} \tau_{xy}(x) u_1 (x-\gamma)\, dx. \qquad (9)$$

In the preceding integrals the coordinate x has been shifted so that its origin is located at the crack tip, and δ is a small length parameter usually taken to be equal to the length of the boundary or finite element immediately ahead of the crack tip. The two integrals are often referred to as the mode I and mode II strain-energy-release rates and denoted by G_I and G_{II}. However, there appears to be no rigorous theoretical basis for such a partition (except for the special case of an interior crack in a single homogeneous medium) because the interfacial stresses σ_y and τ_{xy} oscillate wildly in a tiny immediate neighborhood of the crack tip, and the values of the two integrals are sensitively dependent on the length parameter δ when δ assumes values comparable to the size of the tiny immediate neighborhood. Sun and Manoharan showed that for a crack between two dissimilar orthotropic media, the two integrals eventually approach the same limiting value, G/2, when δ approaches zero (Sun, C.T. and Manoharan, M.G., "Strain energy release rates of an interfacial crack between two orthotropic

solids," J. Composite Materials, Vol. 23, pp. 460-477, 1989). The sum of the two integrals, however, is quite insensitive to the length parameter δ provided that δ is sufficiently small, i.e., insensitive to mesh refinement in the boundary-element or the finite-element model.

In spite of the lack of a rigorous theoretical justification for the partition of G into G_I and G_{II}, one may argue heuristically that the latter two quantities, as calculated by using a sufficiently small (but not excessively small) length parameter δ, provide quantitative measures of two different types of interaction (associated, respectively, with peeling and shearing) between an immediate neighborhood of the crack tip (of size comparable to δ) and the region of the matrix outside that neighborhood. While the interfacial stresses of the elasticity solution show wild oscillations and increasingly large positive and negative peak values in an immediate neighborhood of the crack tip, such an abnormal and singular stress field is invariably modified in a real material by nonlinear and inelastic effects. However, the modified (i.e., the actual) stress field in the real material in the immediate neighborhood of the crack tip may still share with the singular stress field of the elasticity solution certain common gross characteristics such as the magnitudes of energy transfer associated with the tearing and shearing action. If the redistribution of the stress within the small immediate neighborhood of the crack tip due to the nonlinear and inelastic material effects does not totally invalidate all results of the elasticity solution (this assumption must be made, because otherwise there would be no use to compute or consider the elasticity solution at all), then certain gross quantities derivable from the approximate elasticity solutions may be physically significant, provided that their values are not sensitively dependent on the mesh refinement when the mesh is not so over-refined that the wild

oscillation of the interfacial stresses is no longer limited to one element ahead of the crack tip but spreads out over several elements. In the present analysis, the two integrals have been separately evaluated. This is done by first taking δ to be the length of one element ahead of crack tip, and subsequently taking δ to be the combined length of two elements ahead of the crack tip.

5.3 Results of the analysis

The results described in the following refer to the solutions of the two complementary problems described in Sec. 5.1. The solutions to the corresponding original problems may be obtained by combining the present solutions with the respective trivial uniform solutions expressed by Eqs. (4) and (6). In the present solutions, the Poisson's ratio of the resin material is taken to be 0.3.

For two different crack lengths $2a = h$ and $2a = 4h$, the displacements of the crack face in the first complementary problem (corresponding to the average tensile load $\epsilon_y = \epsilon_o$ in the matrix material) are shown in Figs. 25 and 26. These displacements have been normalized with respect to $\epsilon_o h$. The interfacial normal and shearing stresses between the upper rigid filament and the matrix (along $y = h$) is shown in Fig. 27 for the model with a crack length $2a = 4h$. Figure 28 shows the interfacial stresses ahead of the crack tip on $y = 0$. These approximate solutions of the stresses show oscillatory behavior near the crack tip and very large peak values at the crack tip. The effects of the mesh size on the interfacial normal and shearing stresses near the crack tip are shown, respectively, in Figs. 29a and 29b, by comparing the results using the boundary element model shown in Fig. 23 (fine mesh) and a less refined model in which the smallest element size is increased from h/512 to h/256. Although the interfacial stresses near the crack tip are significantly changed, their patterns away from the crack tip are not appreciably dependent on mesh refinement.

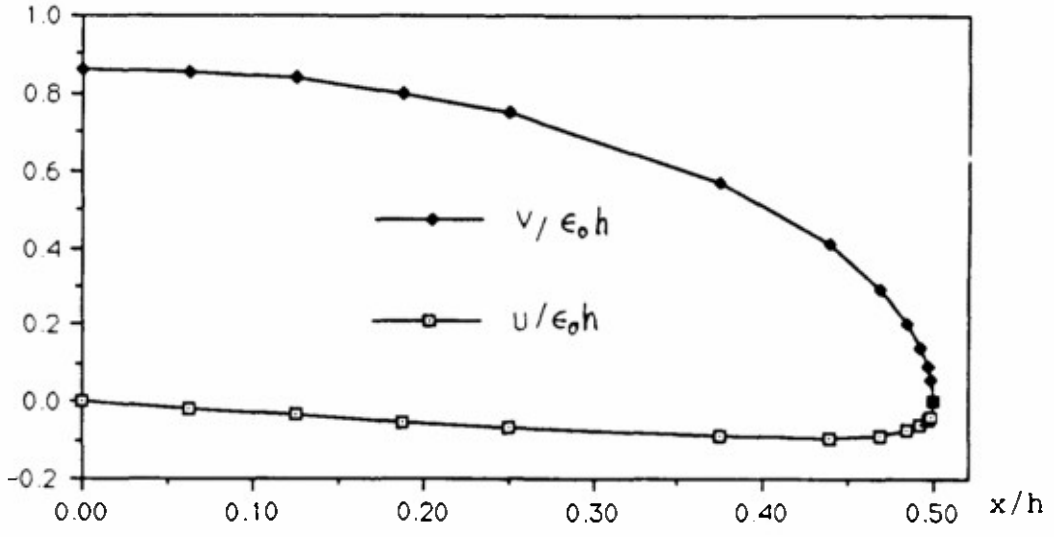

Fig. 25: Normalized crack-surface displacements under the transverse tension load (crack length 2a = h)

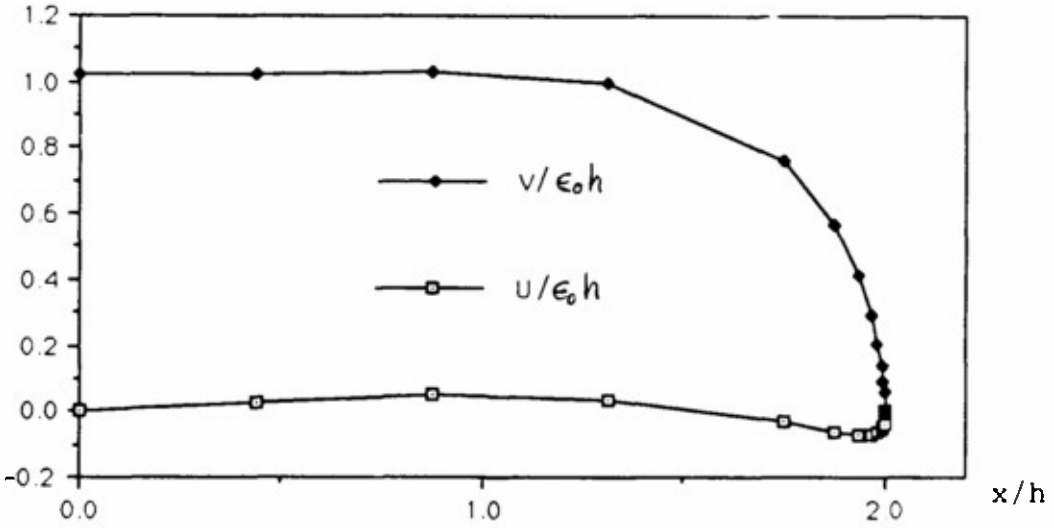

Fig. 26: Normalized crack-surface displacements under the transverse tension load (crack length 2a = 4h)

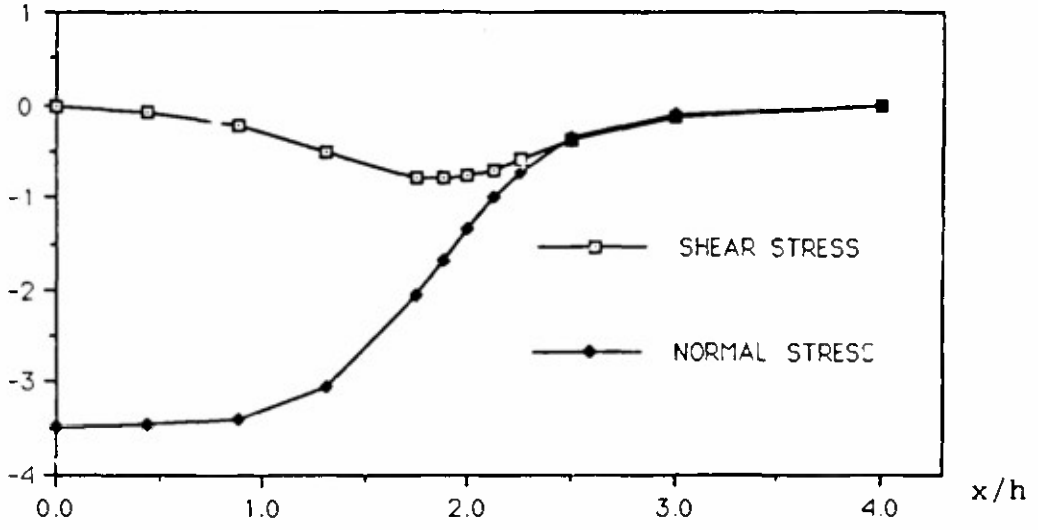

Fig. 27: Interfacial stresses on y = h
(Stresses normalized with respect to $\mu\varepsilon_0$
crack length 2a = 4h)

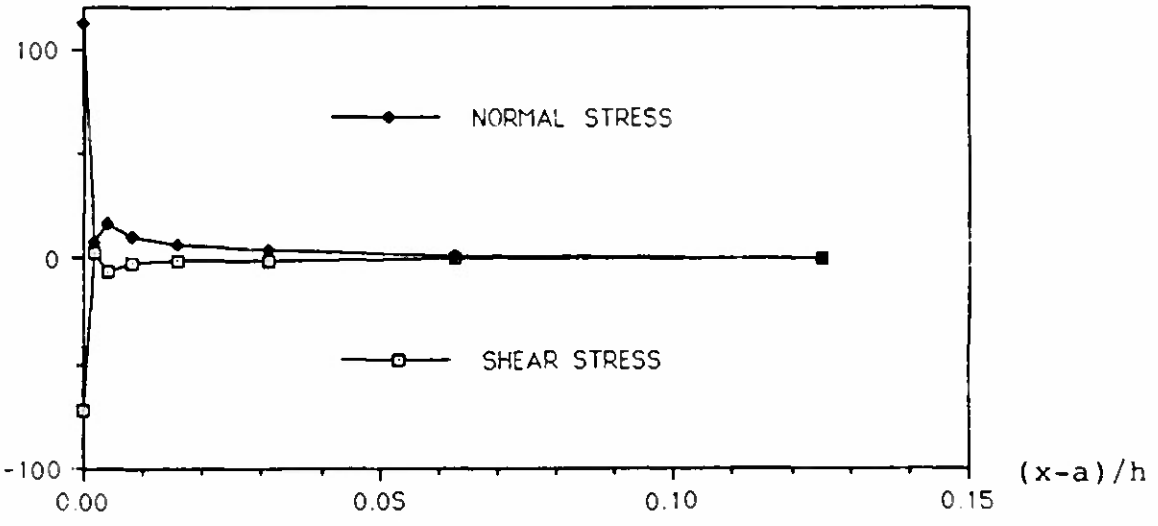

Fig. 28: Interfacial stresses ahead of the crack tip
(Stresses normalized with respect to $\mu\epsilon_0$,
crack length 2a = 4h)

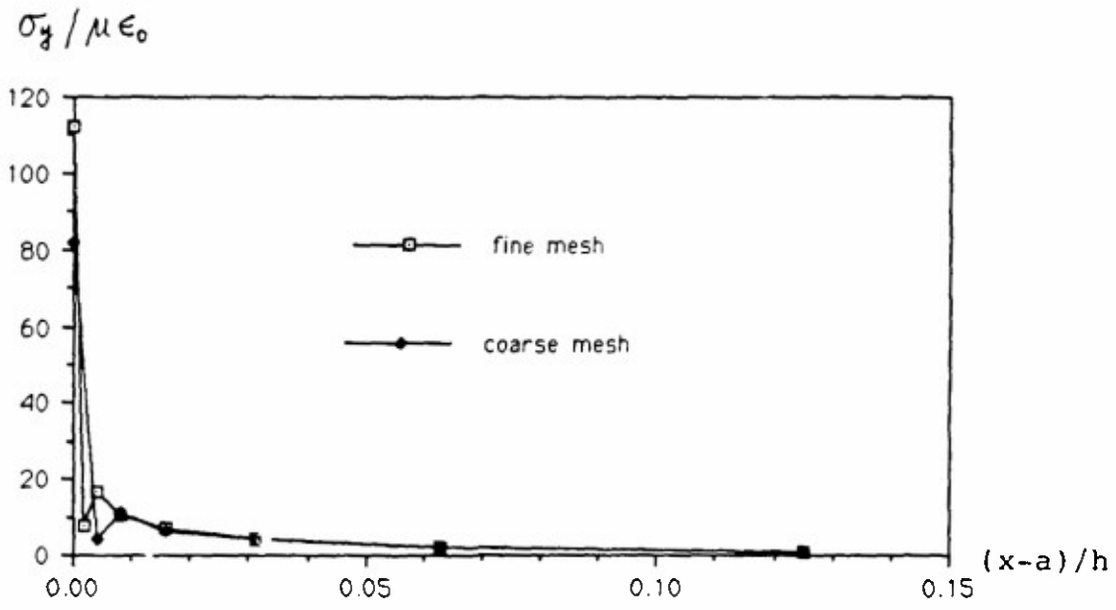

Fig. 29a: Effect of the size of crack-tip elements on the normalized interfacial normal stress (Crack length 2a = 4h, under transverse tension load)

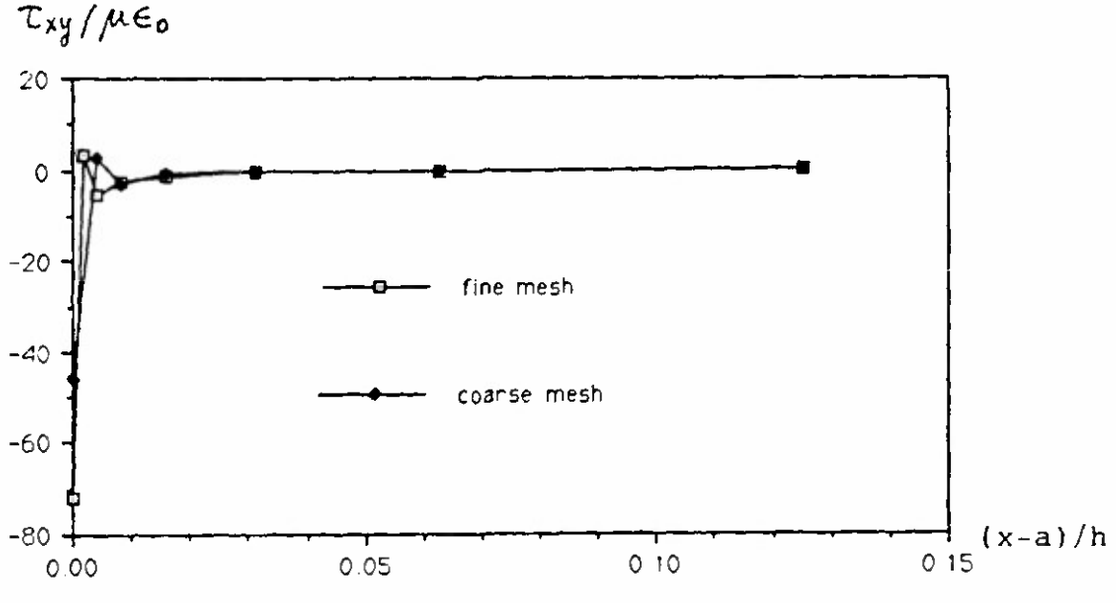

Fig. 29b: Effect of the size of crack-tip elements on the normalized interfacial shear stress (Crack length 2a = 4h, under transverse tension load)

For the second complementary problem (associated with an average shear strain load $\gamma_{xy} = \gamma_o$ in the matrix), the results of the crack surface displacements are shown in Figs. 30 and 31 for two different values of the crack length. Notice that in the case of shear load the horizontal displacement along the crack surface is an order of magnitude greater than the vertical displacement (i.e. the crack opening displacement). While the crack opening displacement is positive near the crack tip $x = a$, it is negative in an interval to the right of the origin. Since the vertical displacement is anti-symmetric with respect to the coordinate x, the opening displacement near the crack tip $x = -a$ is negative. Negative opening displacements imply that the resin material actually contacts the fiber region and the solution should be modified by the effect of partial contact. However, this effect is not investigated in the present study. The large value of the horizontal displacement in comparison with the opening displacement implies that, in case of negative opening displacement, there may be severe friction effect associated with the sliding of the crack surfaces.

The interfacial stresses on $y = h$ and $y = 0$ are shown, for the crack length $2a = 4h$ only, in Figs. 32 and 33. However, in order to provide more information concerning the various solutions, the effect of mesh refinement on the interfacial normal and shearing stresses is shown for a different crack length, $2a = h$, in Figs. 34a and 34b. In the case of shear load the fine mesh (shown by the boundary-element model of Fig. 24) has the smallest element size h/128 while the coarse mesh has the smallest element size h/64.

The integrals G_I and G_{II} associated with each of the two loading cases are shown in Figs. 35 and 36 as functions of the crack length. For the case of tension load G_I and G_{II} as shown in Fig. 35 have been normalized with respect to $\mu h \epsilon_o^2$, while for the case of shear load they have been normalized with respect

to $\mu h\gamma_o^2$. Comparison is made between the results based on the fine-mesh model and the coarse-mesh model. The differences are not significant for the larger modal contribution (G_I in the case of tension load and G_{II} in the case of shear load). As mentioned previously, the results for G_I and G_{II} are obtained by choosing the length parameter δ in Eq. (9) to be equal to the length of the crack tip element in the present model. No significant changes in values of the dominant modal contribution are found when δ changes with mesh refinement, provided the refinement is not excessive. The results are expected to vary significantly with δ when δ becomes extremely small, since G_I and G_{II} should approach a common limit G/2 when δ approaches zero.

The dependence of the total strain-energy-release rate upon the crack length is shown in Fig. 37. As in the two preceding figures, the energy-release-rate is normalized with respect to $\mu h\epsilon_o^2$ for the case of tension load and with respect to $\mu h\gamma_o^2$ for the case of shear load. The actual result corresponding to a combined strain load $\epsilon_y = \epsilon_o$ and $\gamma_{xy} = \gamma_o$ may be evaluated by superposition. The trends of the two curves in Fig. 37 have important implications on the characteristics of disbond growth. We find that G associated with the shear strain load increases monotonically with the crack length. Hence, if the growth of the disbond is governed by a critical level of the total strain-energy-release rate, G_{cr}, and if the shear strain load γ_o is raised to a sufficiently high level so that G attains the critical value, then the disbond starts to grow and subsequently G increases with the lengthening of the crack and becomes increasingly greater than G_{cr} even if the shear strain load is held fixed at the level required for the initiation of growth. The growth of the crack under the fixed shear strain load is therefore a catastrophic process.

Under the tensile strain load $\epsilon_y = \epsilon_o$, the relation of G to the crack

length increases rapidly and reaches a peak value at a crack length of approximately 1.5h. Subsequently G suffers a slight decrease and eventually it approaches a constant value as the crack length further increases. From a practical standpoint, the slight decrease in the G following the attainment of its peak value does not change the essentially catastrophic nature of disbond growth under the tension load. For a given disbond length 2a and for a resin material with a known fracture toughness G_{cr}, the level of the strain load ϵ_o and γ_o required to initiate the growth of the disbond can be found by using the curves in Fig. 37. The present analysis implies that, under the assumption of a growth criterion depending only on the total strain-energy-release rate, the disbond growth will continue catastrophically once it is initiated. Gonsequently, in a filament-wound structure, fiber-matrix debonding is a possible failure mechanism in the filament layers subjected to transverse expansion and shear deformation.

It should be reiterated that since widespread microcracking of the resin material usually precede final failure associated with disbond growth, there is a need to use a continuum theory of damage to evaluate the degradation of the elastic moduli of the resin material in the initial failure process. The elastic moduli to be used in the micromechanical fracture analysis should be the degradated values.

Supplement In order to find the dependence of the two integrals in Eq. (9) upon the length parameter δ, we added increasingly smaller elements at the crack tip, and obtained boundary-element solutions and computed closure integrals using increasingly smaller δ/h, varying from $2^{-8} = 1/256$ to $2^{-14} = 1/16384$, for a crack length $2a = 2h$ under the tension load. The results for G_I, G_{II} and G are shown in Fig. 38.

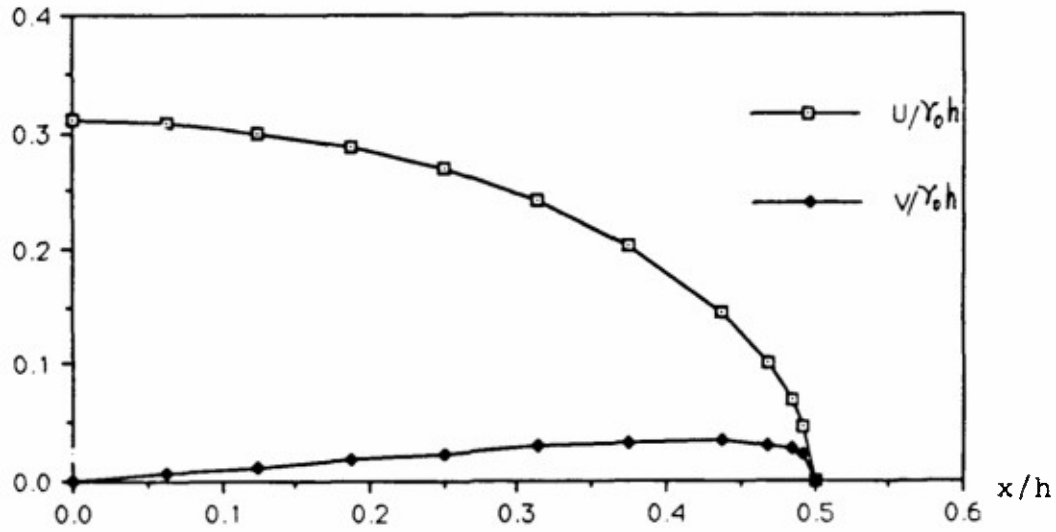

Fig. 30: Normalized crack-surface displacements under the shear load (crack length 2a = h)

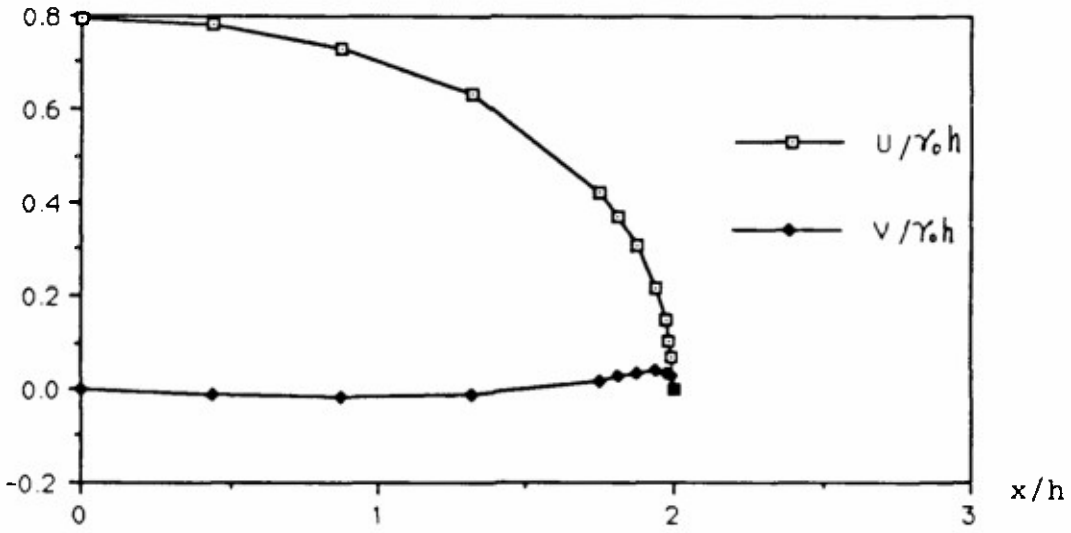

Fig. 31: Normalized crack-surface displacements under the shear load (crack length 2a = 4h)

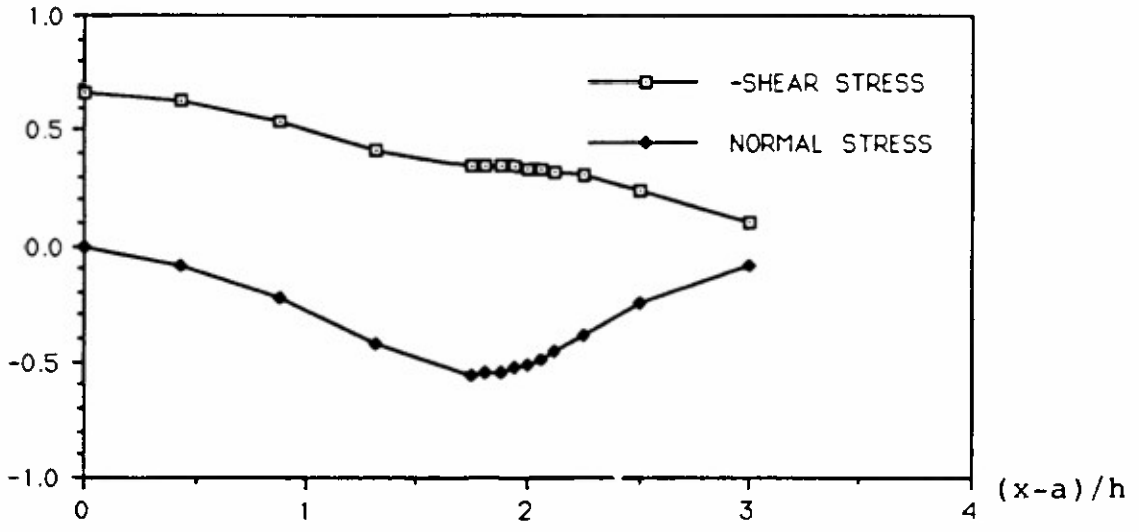

Fig. 32: Interfacial stresses on y = h (Stresses normalized with respect to $\mu\gamma_0$, 2a = 4h)

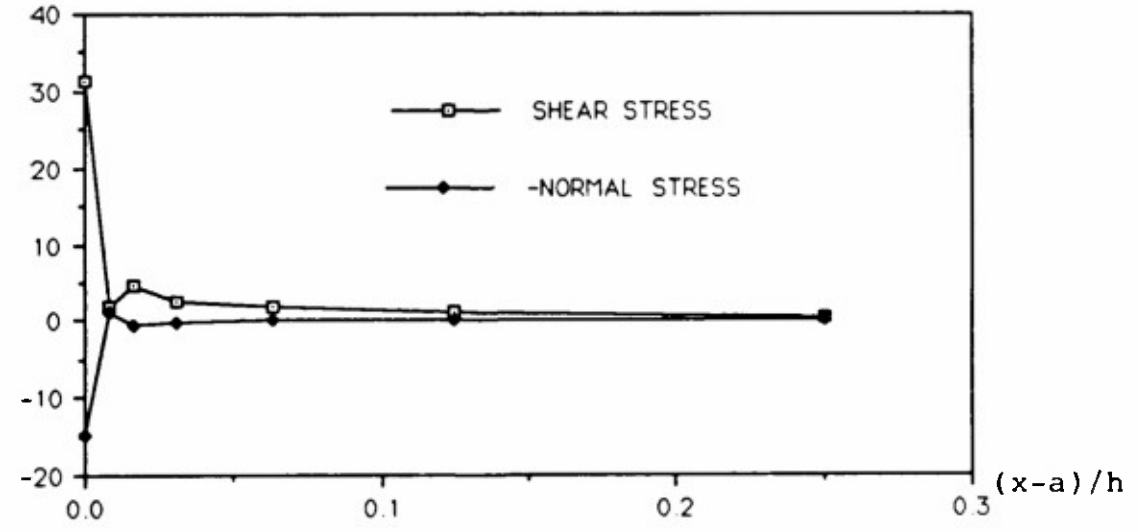

Fig. 33: Interfacial stresses ahead of the crack tip (Stresses normalized with respect to $\mu\gamma_0$, crack length 2a = 4h)

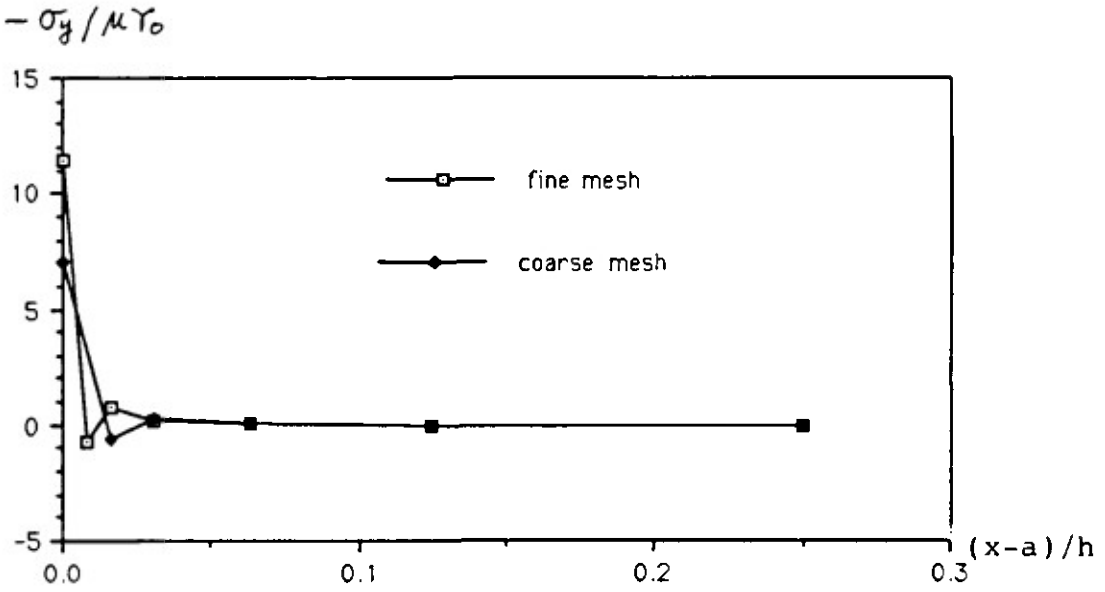

Fig. 34a: Effect of the size of crack-tip elements on the normalized interfacial normal stress (Crack length 2a = h, under shear load)

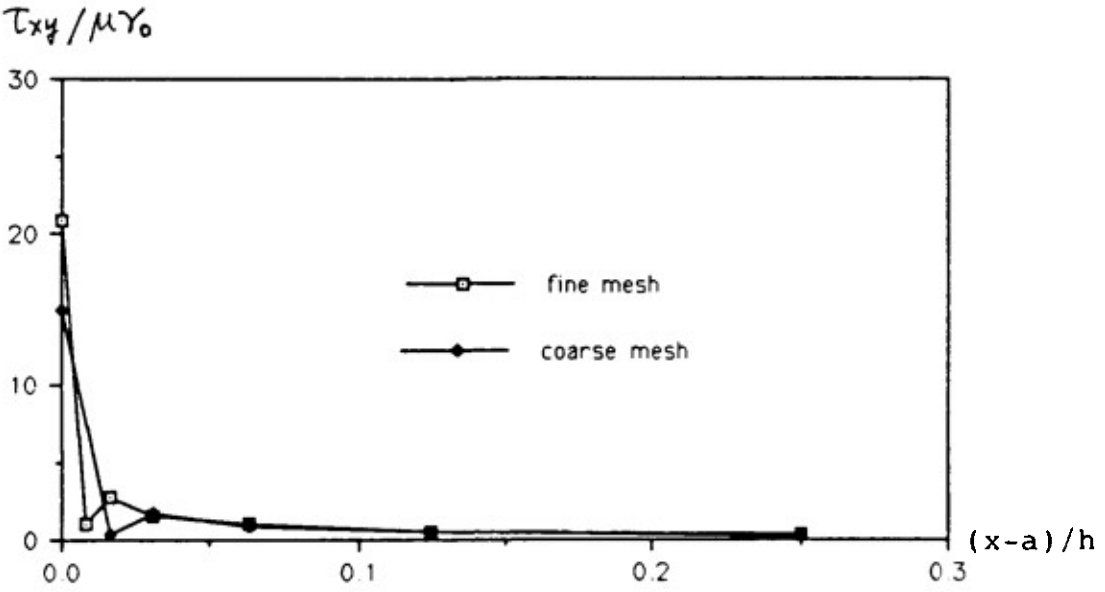

Fig. 34b: Effect of the size of crack-tip elements on the normalized interfacial shear stress (Crack length 2a = h, under shear load)

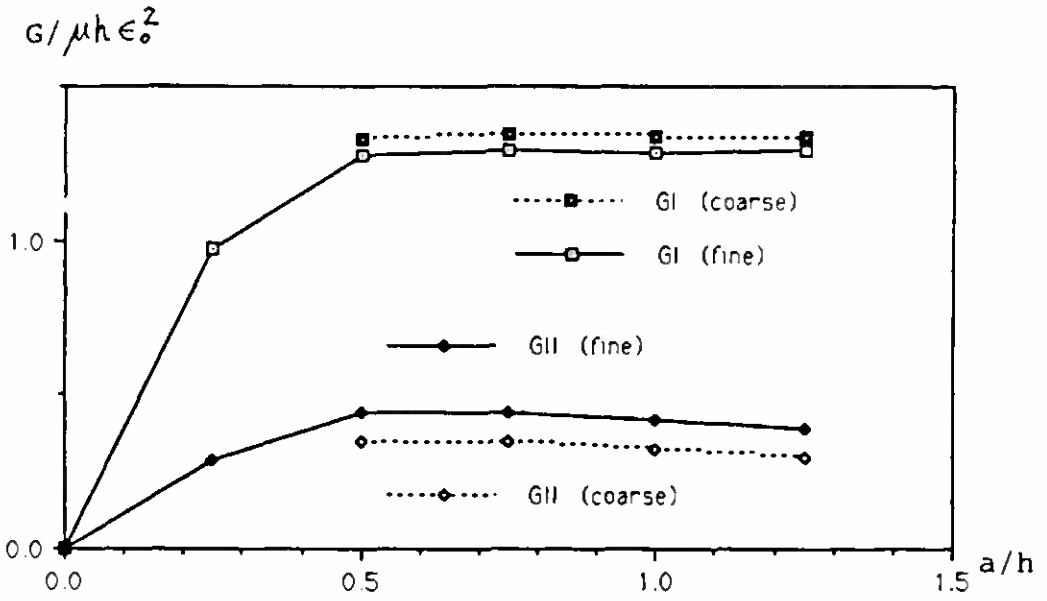

Fig. 35: Strain-energy-release rates vs. crack length, under transverse tension load

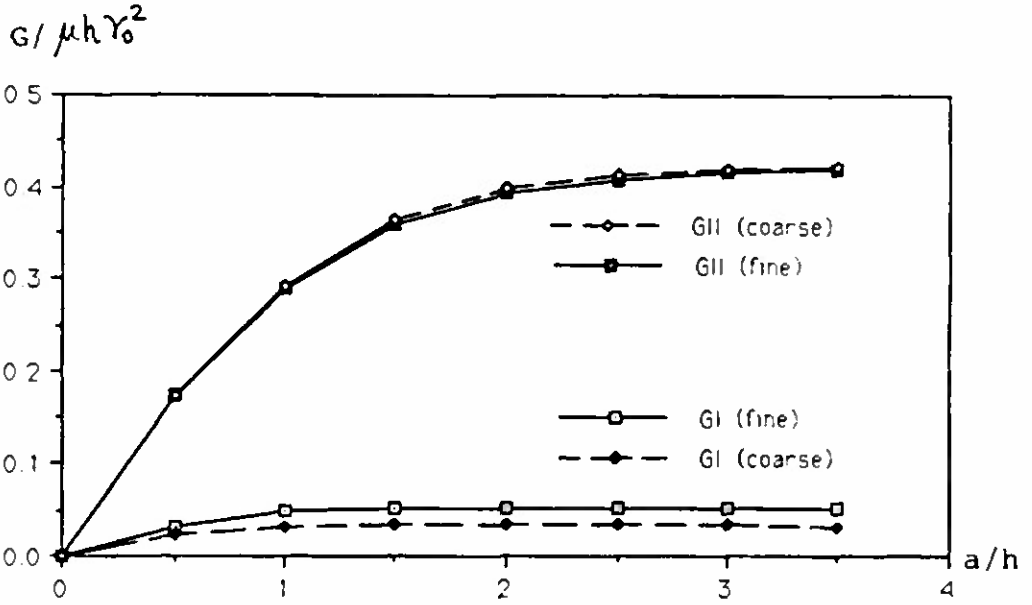

Fig. 36: Strain-energy-release rates vs. crack length, under shear load

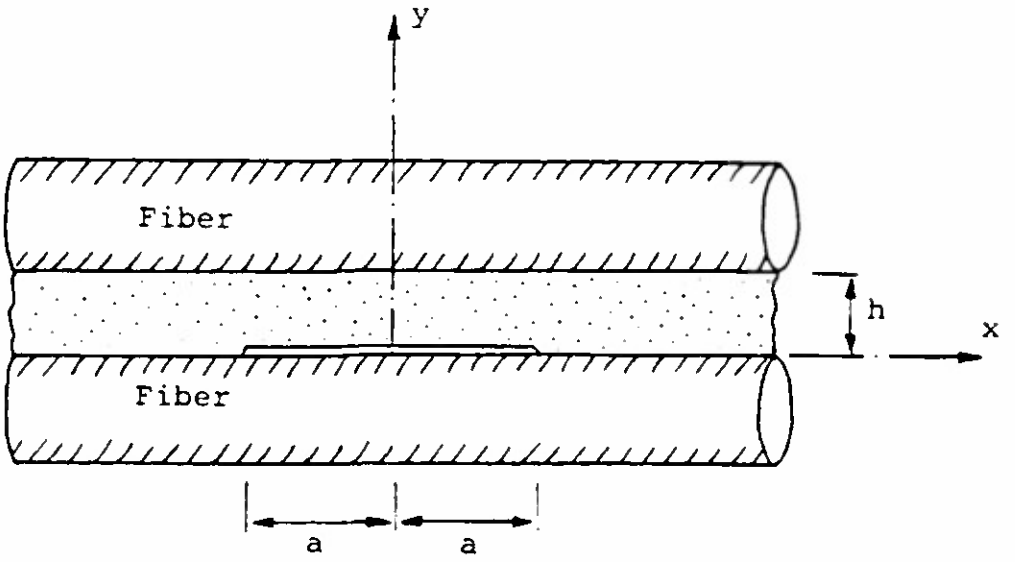

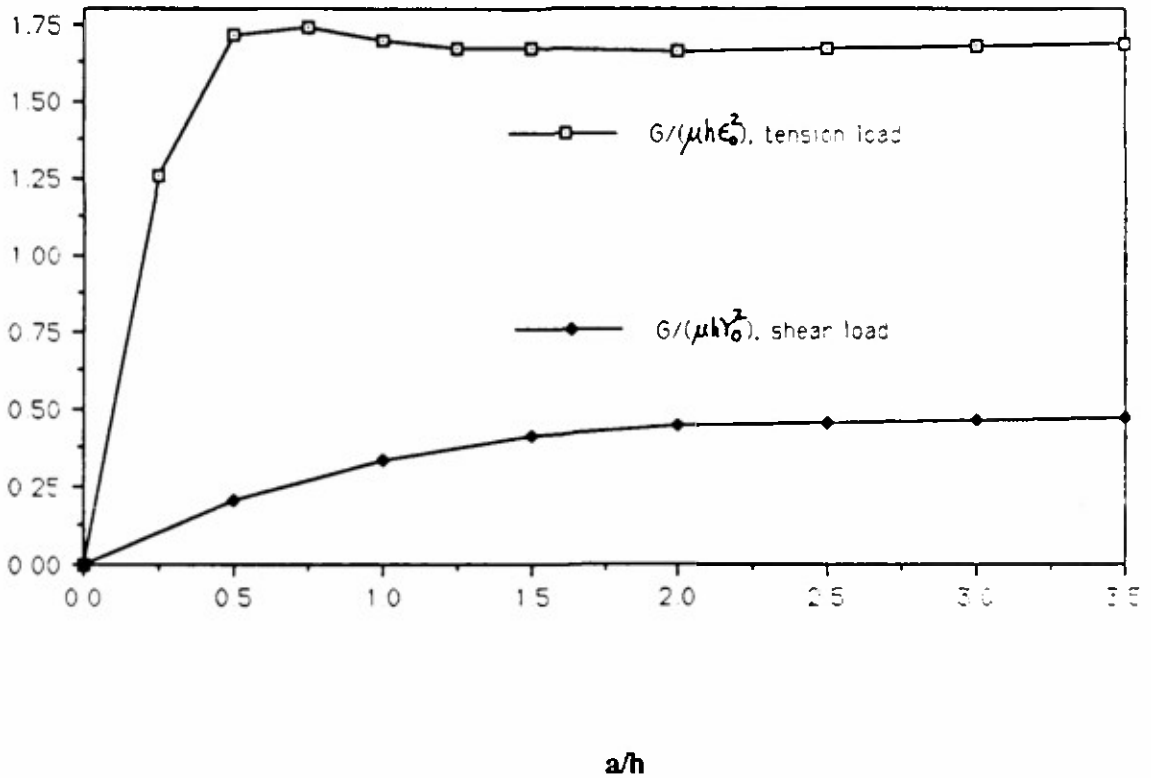

Fig. 37: Total energy-release rate vs. interfacial crack length, transverse tension load and shear load

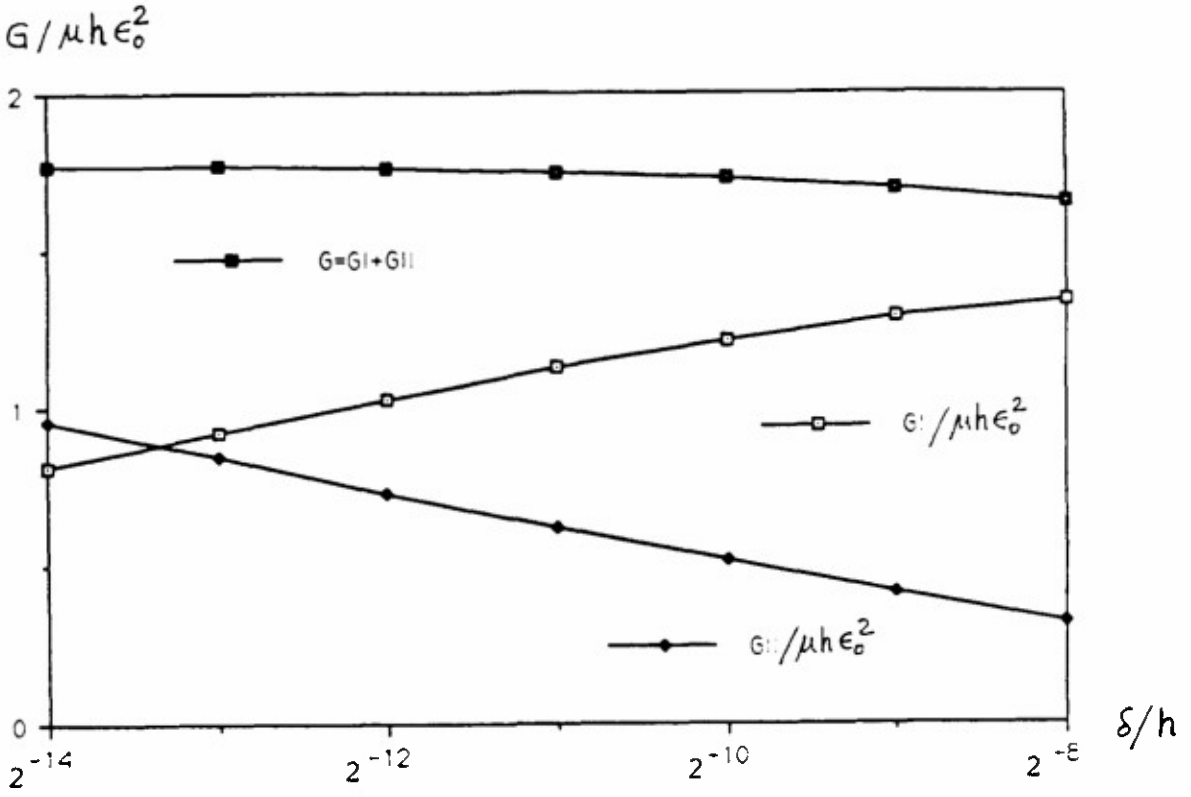

Fig. 38: Dependence of G_I and G_{II} on the length parameter δ in the crack-closure integrals, disbond length 2a = 2h, under tension load

6. Modeling and Analysis of an Oblique Matrix Crack

In this section, we consider a two-dimensional boundary-element model of an oblique matrix crack running across the matrix region (of thickness h) between two parallel filaments. As in the previous analysis of an interface disbond, the two fibers are modeled as rigid media, and the load is introduced by the translational displacements of the upper fiber relative to the lower fiber, $u_1 = h\gamma_o$ and $u_2 = h\epsilon_o$, along the x- and y-directions, respectively. Results in the following analysis are obtained for a resin material with the Poisson's ratio $\nu = 0.3$, and the resin material is assumed to be under the plane stress condition. However, any plane stress solution of a resin material with Poisson's ratio ν may be converted into a plane strain solution of a material with Poisson's ratio $\nu/(1-\nu)$.

The analytical model for the boundary element analysis is shown in Fig. 39. The upper and lower boundaries of the region in Fig. 39b are the interfaces of the resin material with the upper and lower fibers. The oblique crack surface has the inclination angle β. All length dimensions are normalized with respect to the height of the region, and the vertical boundary on the right side is chosen to be at a large distance away from the oblique crack. One segment of the lower boundary which has an unmarked length may be empty, or may be divided into several element depending on the value of the inclination angle β. A detailed sketch of the shaded region at the lower left corner is shown in Fig. 40a. Under the displacement loading, intense local stresses are expected around the reentrant corner of the region where the crack meets the upper interface. Two submodels of the shaded region at the reentrant corner are considered and shown in Figs. 40b and 40c. The second submodel has a short interfacial crack of small length h/128, which is divided into two boundary elements, while the first

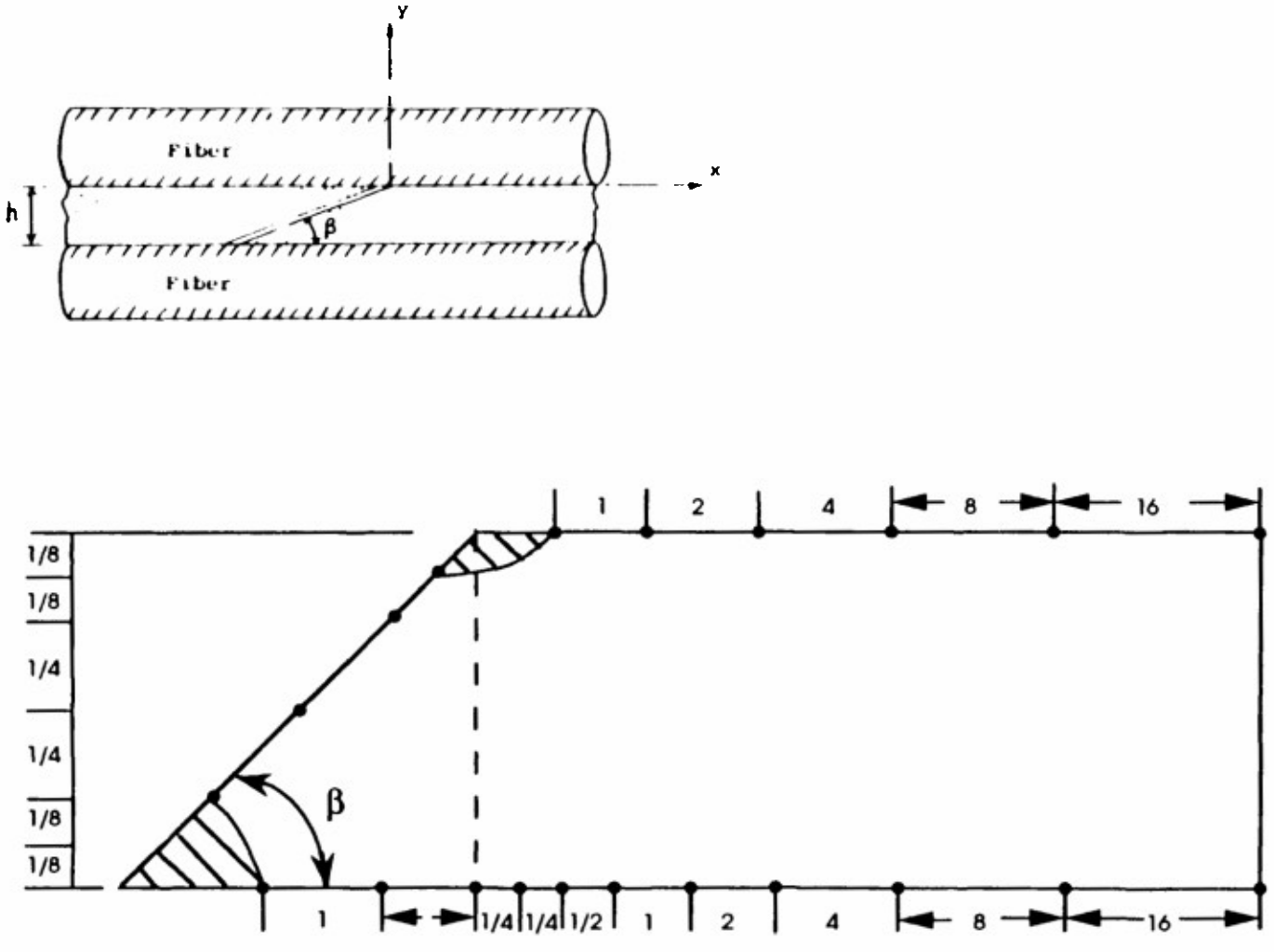

Fig. 39: Boundary-element model of an oblique matrix crack

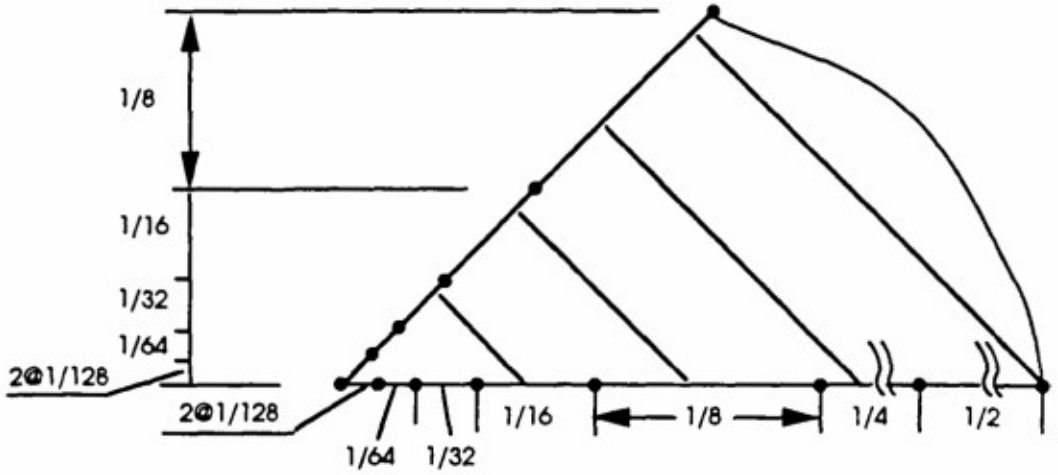

(a)

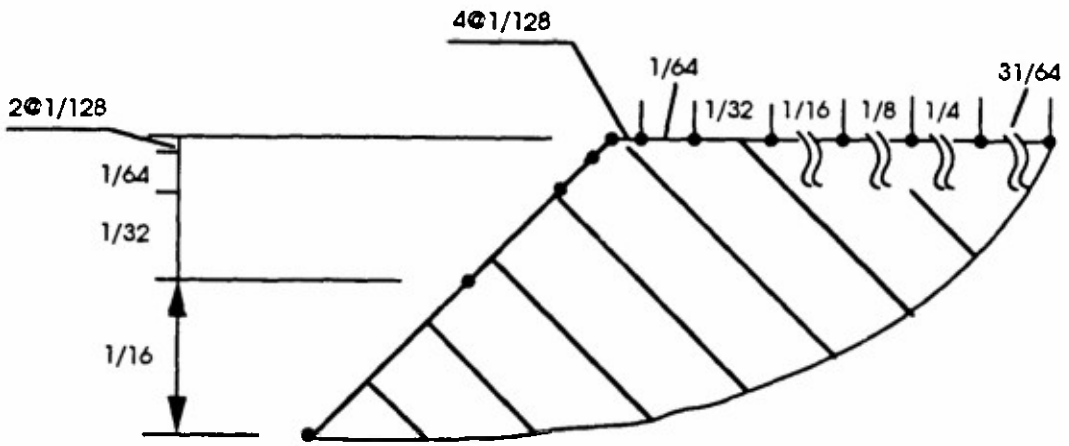

(b)

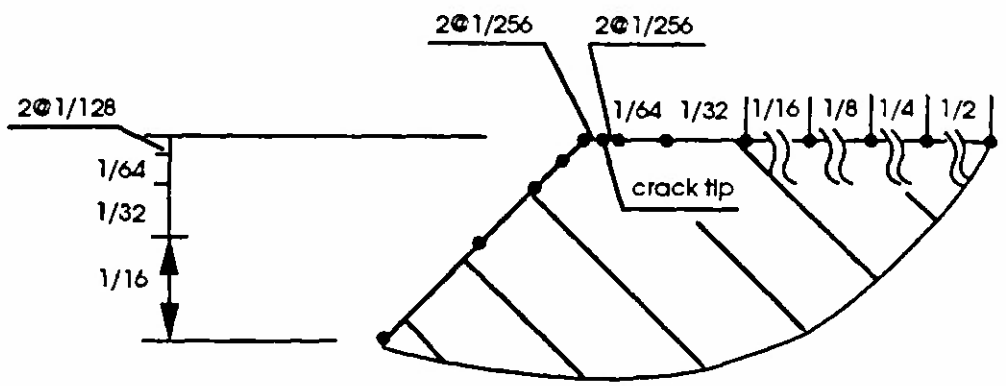

(c)

Fig. 40: Details of the corner regions in Fig. 39

submodel has no interfacial crack.

The problems associated with the transverse tension and shear loads are again decomposed into (i) trivial solutions with uniform stress and strain fields, and (ii) complementary solutions with zero displacements on the fiber-matrix interfaces and vanishing stresses and strains at infinity. For the case of transverse tension load $\epsilon_y = \epsilon_o$, the complementary problem is characterized by the following traction boundary conditions on the crack surface

$$t_1 = \nu\sigma_o \sin\beta, \qquad t_2 = -\sigma_o \cos\beta, \tag{10}$$

where

$$\sigma_o = \begin{cases} 2\mu\epsilon_o(1-\nu)/(1-2\nu) & \text{under the plane strain condition,} \\ 2\mu\epsilon_o/(1-\nu) & \text{under the plane stress condition.} \end{cases}$$

In the case of shear load, the preceding traction boundary conditions are replaced by

$$t_1 = -\mu\gamma_o \cos\beta, \qquad t_2 = \mu\gamma_o \sin\beta. \tag{11}$$

The boundary element solutions reported in the following have the angle of inclination ranging from 15° to 75° at increments of 7.5°.

Figure 41 shows the interfacial normal stress (normalized with respect to $\mu\epsilon_o$) near the reentrant corner, under the tension load, for oblique matrix cracks with various inclination angles. Figure 42 shows the corresponding results when there is a short interface crack of length h/128 at the reentrant corner. The horizontal axis in Fig. 42 has been shifted so that the origin is at the crack tip. The peak stresses in Fig. 42 are significantly greater than the corresponding values in Fig. 41, particularly in the cases of large β. The results for the interfacial shearing stresses under the tension load are shown in Figs. 43 and 44, respectively, for the cases without and with a short interfacial crack. It is found that the introduction of a short crack

drastically increases the peak interfacial shearing stress by doubling or tripling the values.

Under a positive average shear strain load $\gamma_{xy} = \gamma_o$, the region around the reentrant corner is clearly subjected to vertical compression (i.e., a peeling action should be produced by a negative shear strain load). The results for the interfacial normal stresses are shown in Figs. 45 and 46, respectively, for the cases without and with a short interfacial crack. The corresponding results for the interfacial shearing stresses are given in Figs. 47 and 48. The four figures also demonstrate the significant increases in the interfacial stresses due to the presence of a short interfacial crack at the reentrant corner.

Since the evaluation of the crack-closure integrals requires the solutions of the crack surface displacements near the crack tip, the strain-energy-release rates are computed only for the model with a short interfacial crack at the reentrant corner. The length parameter δ appearing in Eq. (9) is taken to be the length of the short crack (which is divided into two boundary elements). Results under the tension load are normalized with respect to $\mu h\epsilon_o^2$ and shown, for various winding angles, in Fig. 49a for the total G and in Fig. 49b for G_I and G_{II}. The corresponding results under the shear load are normalized with respect to $\mu h\gamma_o^2$ and shown in Figs. 50a and 50b. If the strain load is large enough to initiate the growth of the short interfacial crack, then the subsequent growth behavior is expected to be qualitatively similar to what has been found in Sec. 5 for an interfacial disbond, i.e., the strain-energy-release rate generally increases as the crack length increases and, consequently, catastrophic failure occurs.

If the inclination angle β is allowed to decrease and approach zero, then the present results, which are based on the plane stress assumption, should

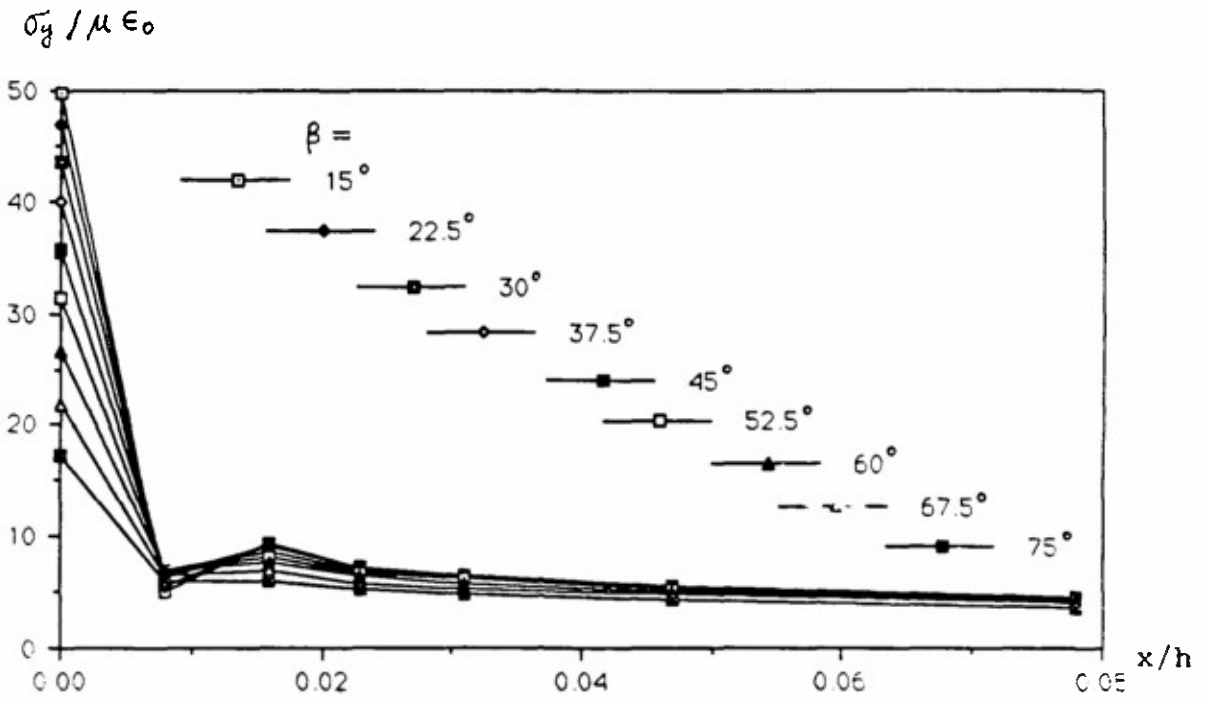

Fig. 41: Interfacial normal stress near the reentrant corner, tension load

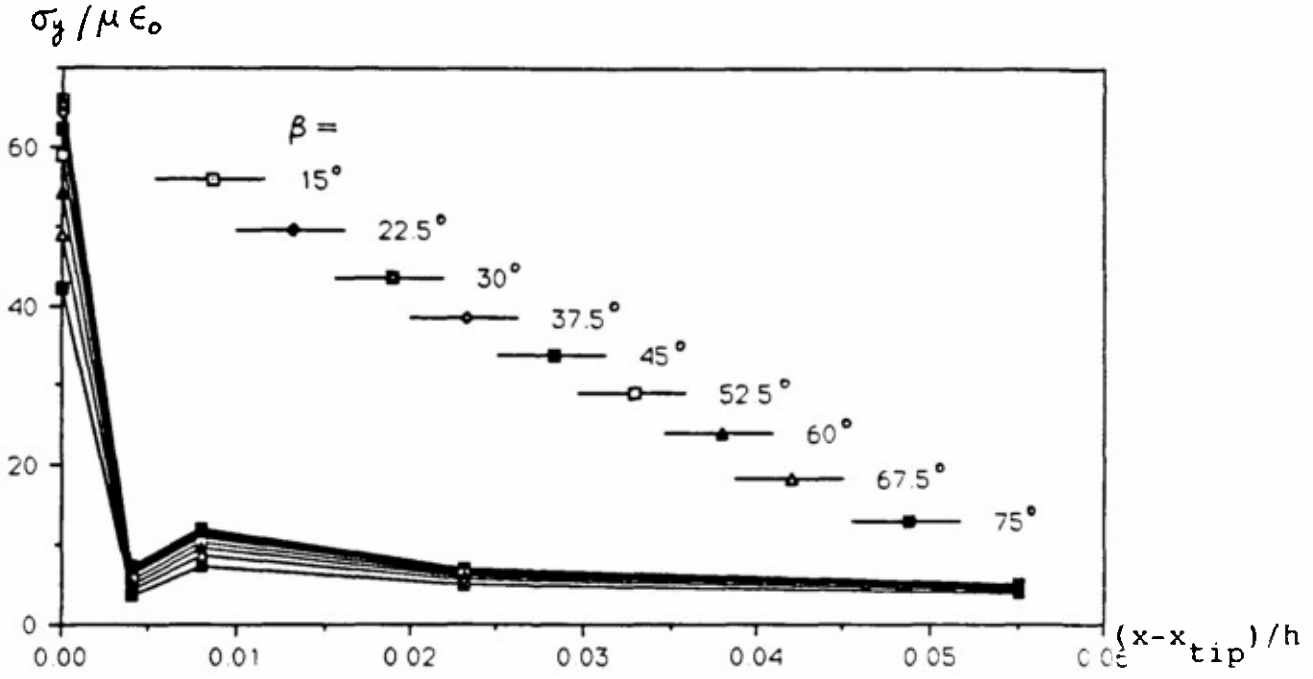

Fig. 42: Interfacial normal stress near the cracked reentrant corner (crack length = h/128)

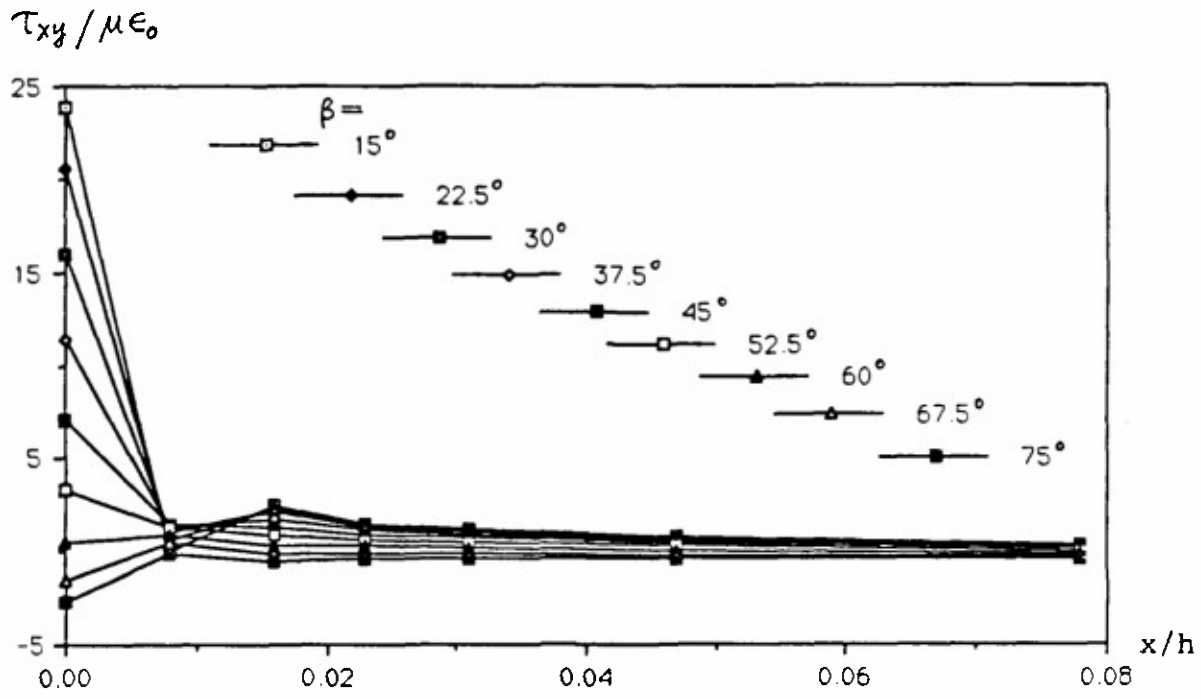

Fig. 43: Interfacial shear stress near the reentrant corner, tension load

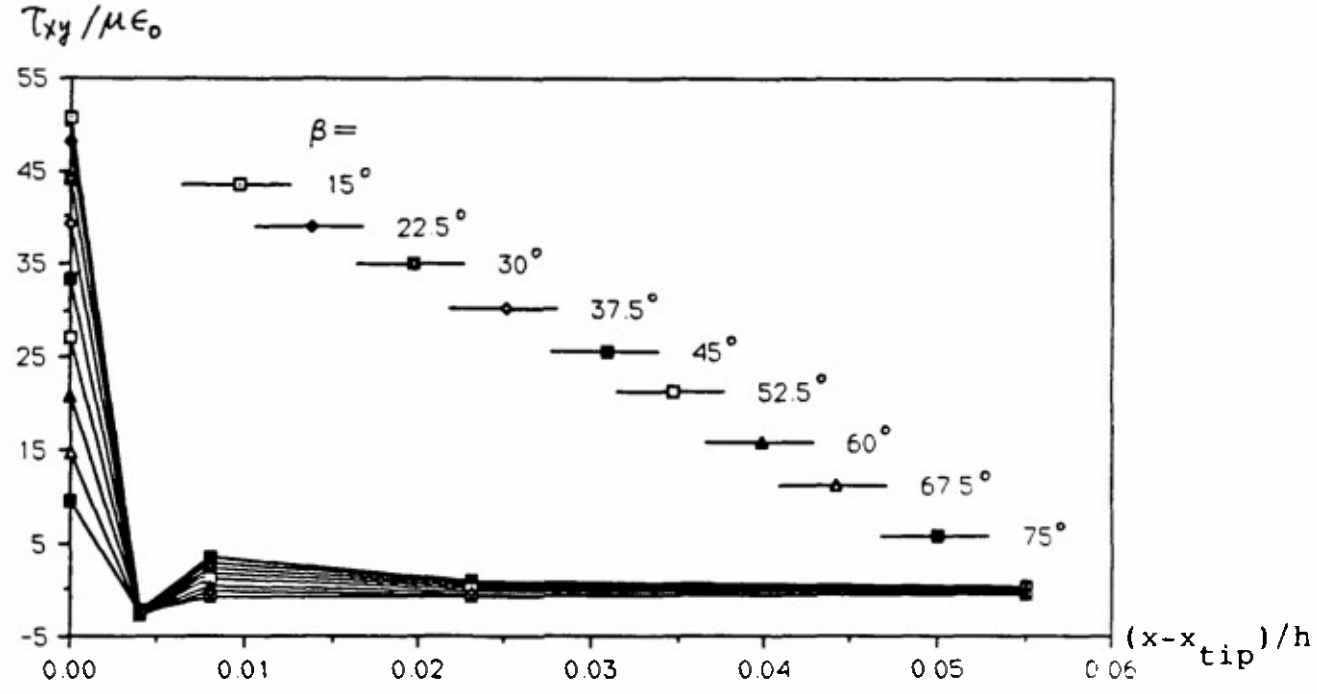

Fig. 44: Interfacial shear stress near the cracked reentrant corner (crack length = h/128)

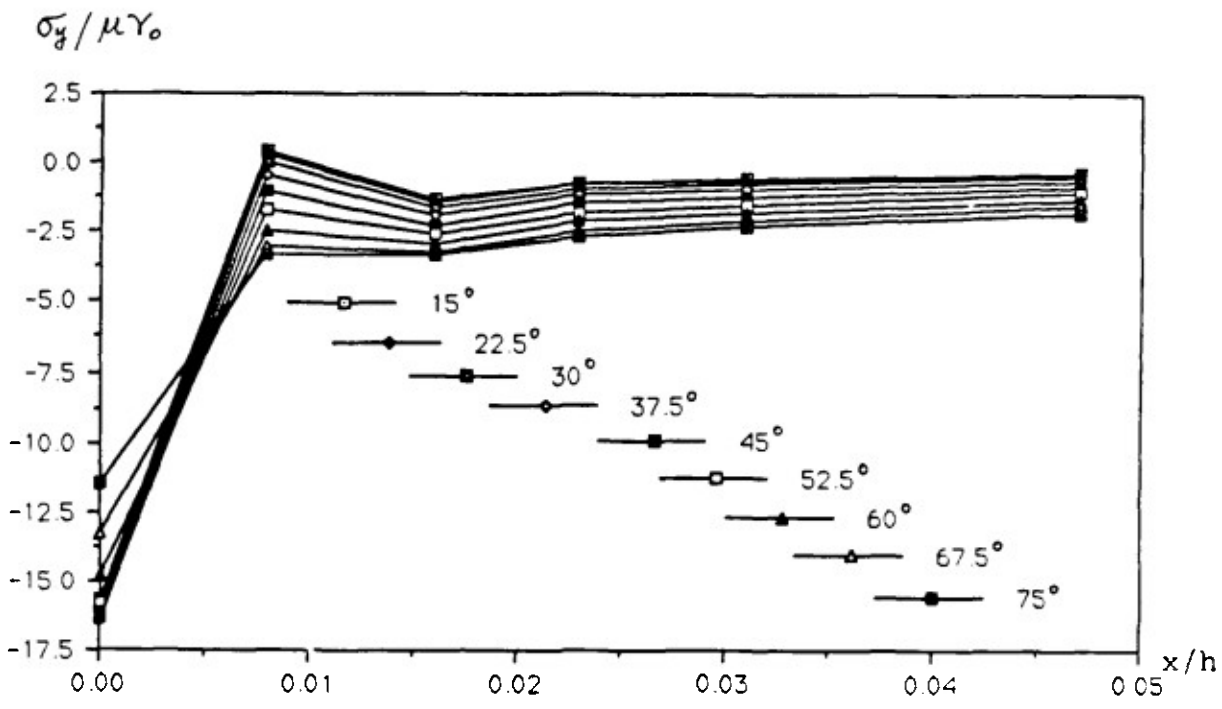

Fig. 45: Interfacial normal stress near the reentrant corner, shear load

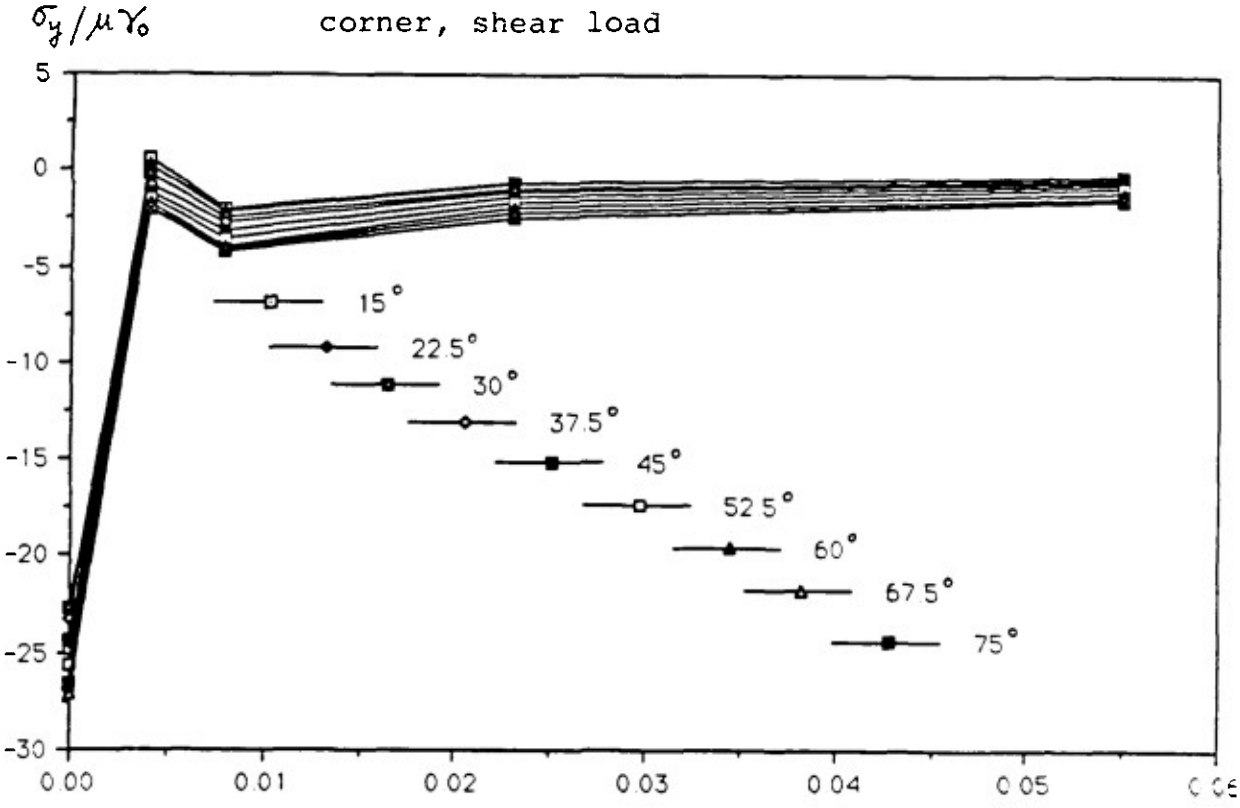

Fig. 46: Interfacial normal stress near the cracked reentrant corner (crack length = h/128), shear load

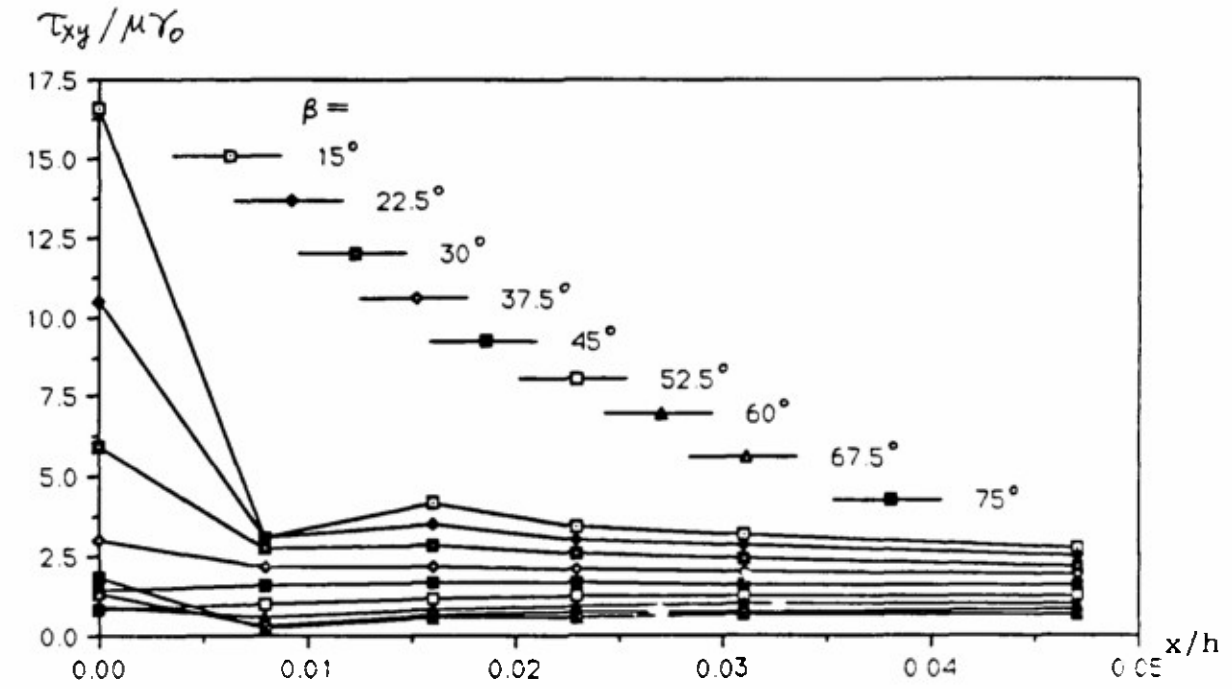

Fig. 47: Interfacial shear stress near the reentrant corner, shear load

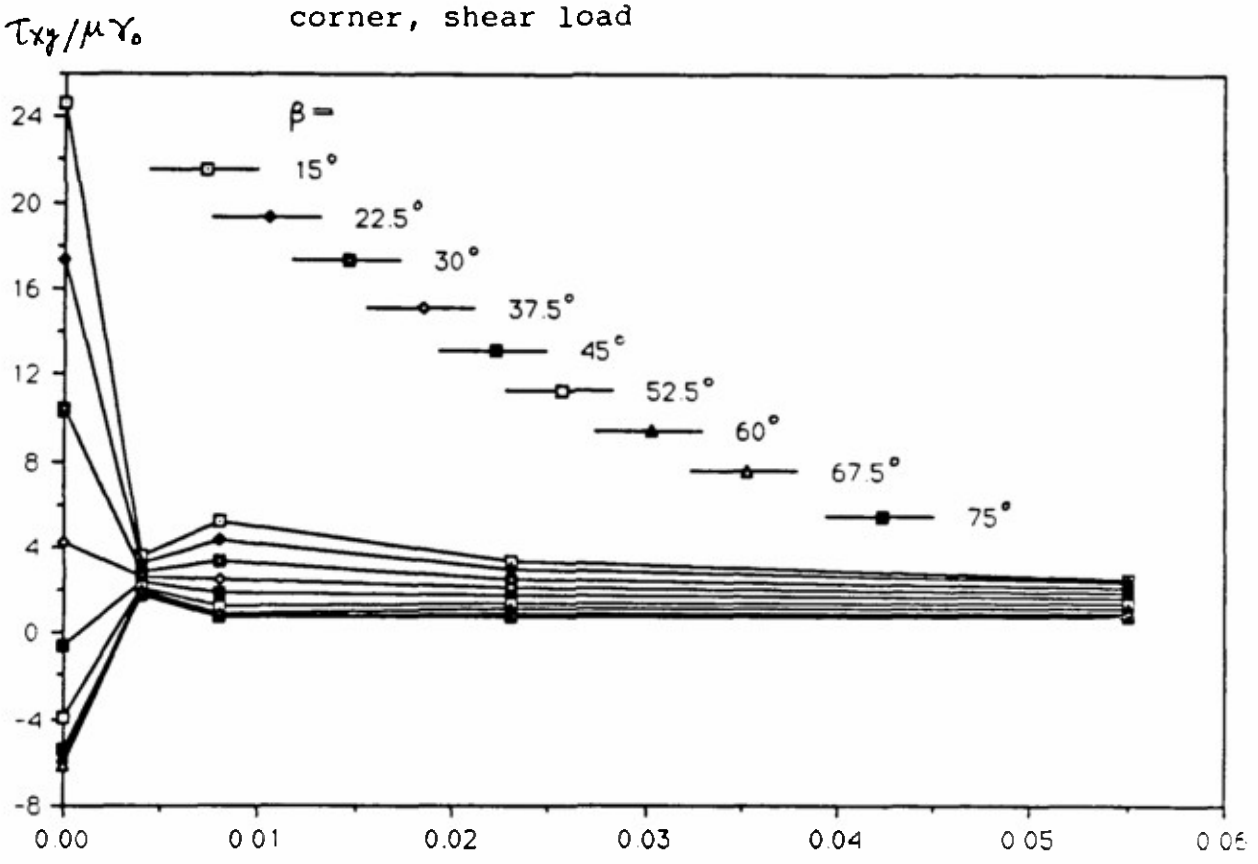

Fig. 48: Interfacial shear stress near the cracked reentrant corner (crack length = h/128), shear load

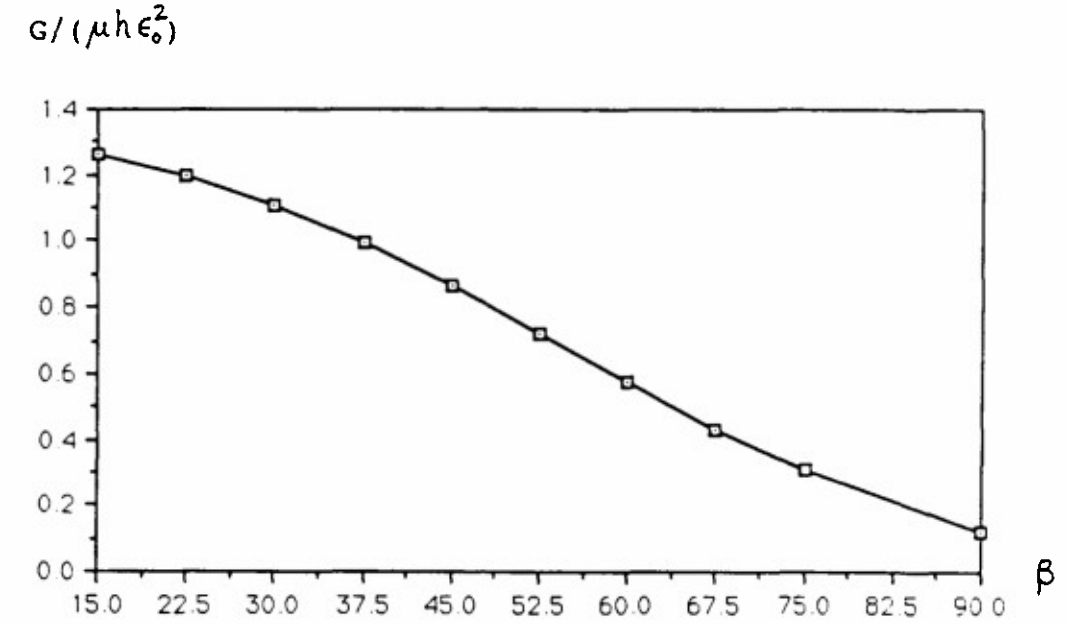

Fig. 49a: Normalized strain-energy-release rate vs. crack inclination angle, tension load

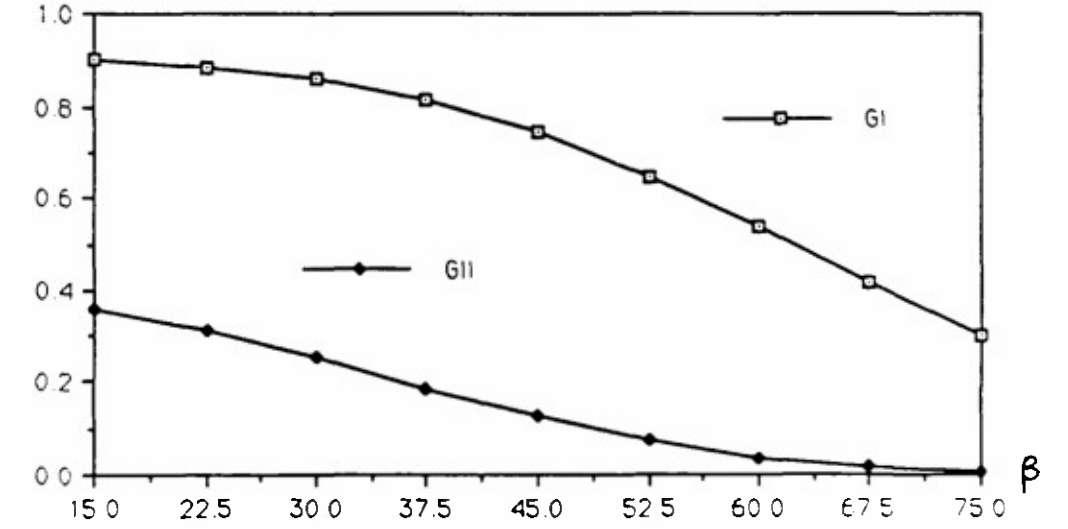

Fig. 49b: Normalized G_I and G_{II} vs. crack inclination angle, tension load

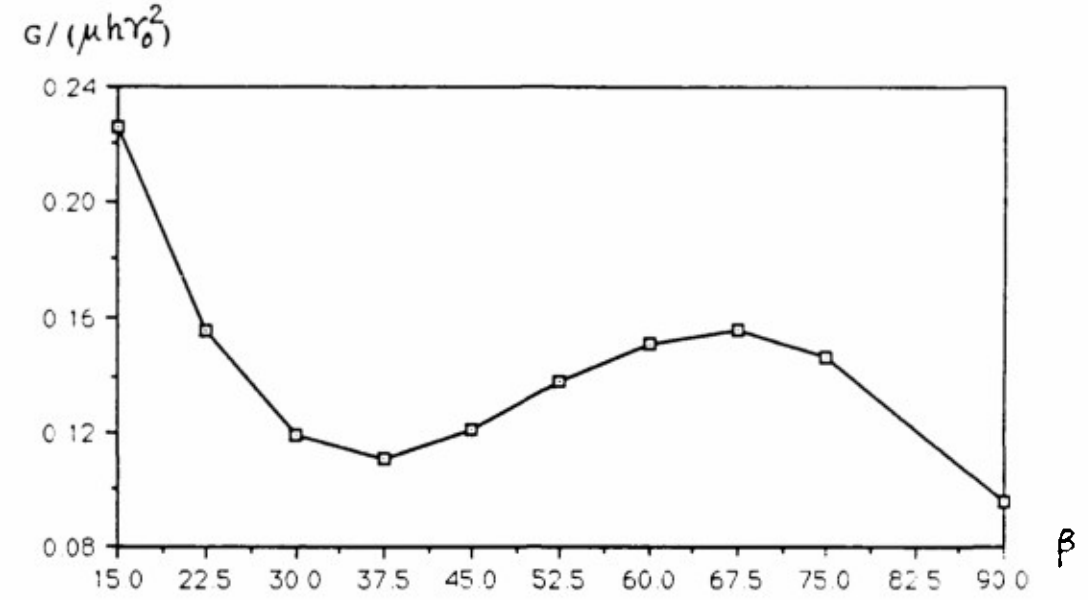

Fig. 50a: Normalized strain-energy-release rate vs. crack inclination angle, shear load

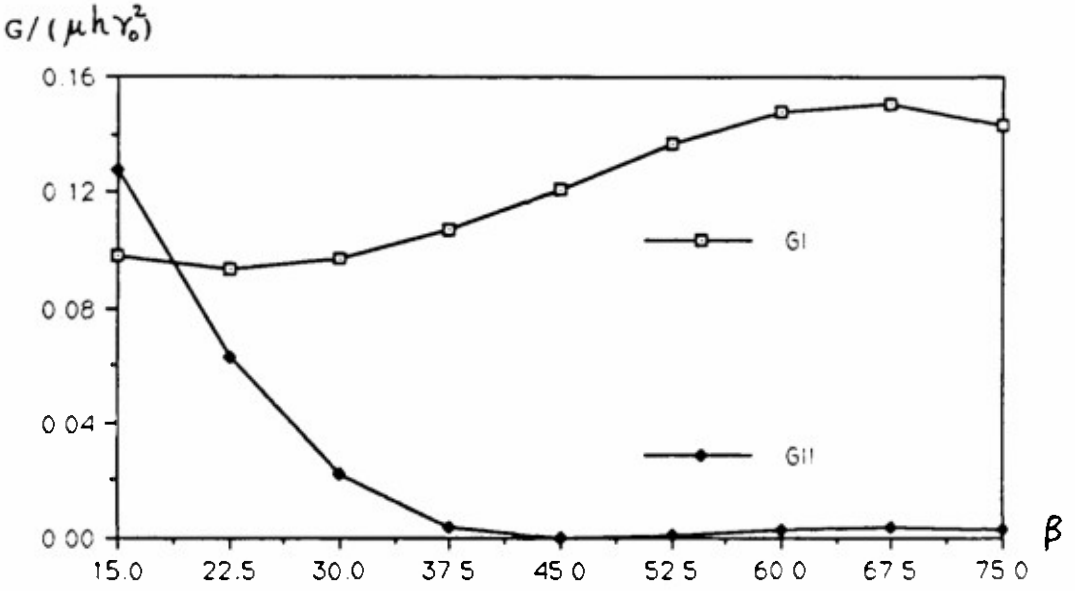

Fig. 50b: Normalized G_I and G_{II} vs. crack inclination angle, shear load

increase and approach the limiting values of the strain-energy-release rates associated with an infinitely long interfacial disbond under the plane stress condition. In the present model, deviation of β from 0 yields lower values of the strain-energy-release rates. In the model for the interfacial disbond of the previous section, smaller disbond lengths yield lower values of G. For both types of cracks, a sufficiently large combination of strain loads ϵ_0 and γ_0 may initiate crack growth and lead to catastrophic failure.

7. Delamination Failure in Filament-Wound Structures and Composite Laminates

In the pressure testing of filament-wound tubes with winding angles greater than 45° under the open-end condition, it has been observed that the final failure appears to be often preceded by bending, local buckling and delamination (see Sec. 4, Part IV). Filament-wound tubes are prone to delamination damage because the scissoring action in the fiber cross-over region introduces intense local twisting action in the resin material between adjacent filament layers as the differently oriented, relatively rigid filaments align themselves, through opposite rotations, toward the principal stress axis of the tube (see Sec. 2.3, Part II). If the filament-wound structure with an existing delamination is later subjected to a service load that results in a local compression along a certain direction, a thin delaminated layer may buckle and may grow catastrophically in the postbuckled state.

7.1 Separation failure of a helical delamination in a filament-wound tube

The observed delaminations in filament-wound tubes often have spiral or helical shapes. An analysis of the separation failure of a helical delaminated layer from the interior surface of a filament-wound tube was presented in a paper attached as Appendix C. In that paper, we considered the separation of a thin

helical delaminated sheet of width 2a, composed of a single filament layer with the winding angle ϕ, from a relatively thick tube subjected to the pressure load. Under the assumption that the separation of the thin layer does not appreciably affect the existing deformation of the main body of the tube, we calculated the amplitude of separation and the change in the boundary normal curvature of the thin layer resulting from separation, for various combinations of the delamination width and the tangential strains on the interior surface of the tube. It was remarked that the strain-energy-release rate associated with the widening of the helical delamination may be computed in terms of the boundary values of the solution (along the helical boundaries of the delamination). Since the appearence of the paper, further analysis has been made for the case of a delaminated sheet composed of two filament layers with +65° and -65° winding angle, and the strain-energy-release rates associated with the widening of one-layer and two-layer delaminated sheets have been obtained by evaluating a path-independent integral. The results are summarized in the following.

We consider a helical delaminated sheet of width 2a on the interior surface of a relatively thick filament-wound tube with the interior radius R_o (Fig. 51),

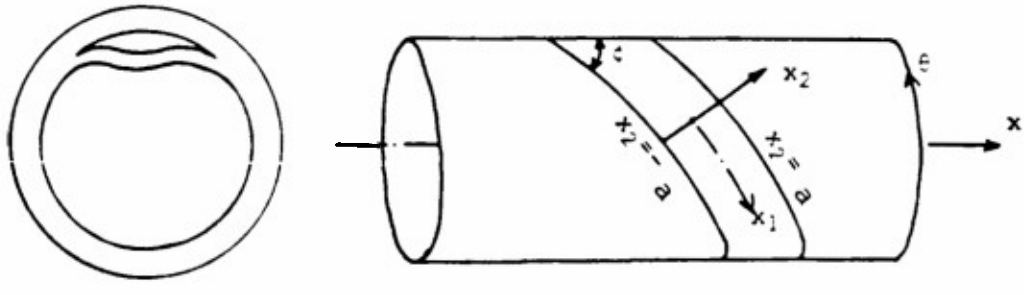

Fig. 51: A helical delamination near the interior surface of a filament-wound tube

subjected to a uniform axisymmetric load so that the interior surface suffers the axial strain ϵ_z and the circumferential strain ϵ_θ. The delaminated sheet is composed of a single filament layer with the winding angle ϕ and thickness t = h, or two filament layers wound at $+\phi$ and $-\phi$ angles with a combined thickness t = 2h (ϕ is taken to be 65° in computing the numerical solutions because Spencer and Hull observed severe delamination damage in open-ended tubes wound at ±65° angles, see Composites, Vol. 9, pp. 263-271, 1978). We define a non-dimensional delamination width b and a non-dimensional strain parameter ϵ^* by the expressions

$$b = a (\sin \phi)/\sqrt{(R_o t)},$$

$$\epsilon^* = (R_o/t) [\epsilon_\theta + \epsilon_z - (\epsilon_\theta - \epsilon_z) \cos 2\phi]/(2 \sin^2\phi).$$

The solutions for a two-layer delaminated sheet are obtained for different combinations of the non-dimensional parameters b and ϵ^* (the corresponding results for a one-layer delaminated sheet were shown in the paper attached as Appendix C). For two different values of the normalized delamination length, b = 1.0 and b = 2.5, the dependence of the amplitude of separation (normalized with respect to the total thickness t of the delaminated sheet) upon the strain load parameter ϵ^* is shown in Fig. 52. The amplitude increases monotonically with the strain load and the wider delamination has a much greater amplitude of separation. Figure 53 shows the increase in the normalized boundary normal curvature of the delaminated sheet (normalized according to the definition given in the paper in Appendix C) induced by its separation from the main body of the tube. This curvature change is a principal measure of the peeling action at the delamination front caused by separation. While the normalized curvature change also increases monotonically as the strain load increases, the two curves for the two different delamination widths are rather close. In Figs. 54 and 55, the same results for the amplitude of separation and the change of the boundary curvature

are shown as functions of the non-dimensional delamination width for three values of the strain load, $\epsilon^* = 0.1$, 0.5 and 1.0. The change in the boundary normal curvature, which increases initially with the delamination width, tends to approach a constant value as the normalized width attains a level of about 1.5.

The results for the strain-energy-release rates (normalized with respect to $A_{22}(t/R_o)^2\sin^2\phi$) associated with the growth of the two-layer delaminated sheet, are shown in Fig. 56 as functions of ϵ^* for two fixed values of b, and shown in Fig. 57 as functions of b for three fixed values of ϵ^*. The corresponding results for the one-layer delaminated sheet (which has a thickness $t = h$, i.e., one half the thickness of the two-layer sheet) show similar trends but the physical (dimensional) strain-energy release rate has a much smaller value compared to the two-layer sheet. These results are shown in Figs. 58 and 59.

Figures 57 and 59 show that, under a fixed strain load in the tube, the energy-release rate increases initially as the delamination width increases. It reaches a peak value when the nondimensional delamination width b attains a level between 1.0 and 2.0. The subsequent drop in the energy-release rate is very slight. This behavior suggests catastrophic growth of the helical delamination under a sufficiently high strain load. For a given initial delamination width, the level of strain load sufficient to initiate delamination growth can be determined by comparing the analytical result of the strain-energy-release rate with the experimentally measured fracture toughness of the material.

7.2 Postbuckling deformation and growth of a thin two-dimensional delamination in a composite laminate

Fundamental studies of this important problem have been presented for the ideal but representative case of thin elliptical delaminations in a flat laminate. See the two papers attached as Appendices D and E.

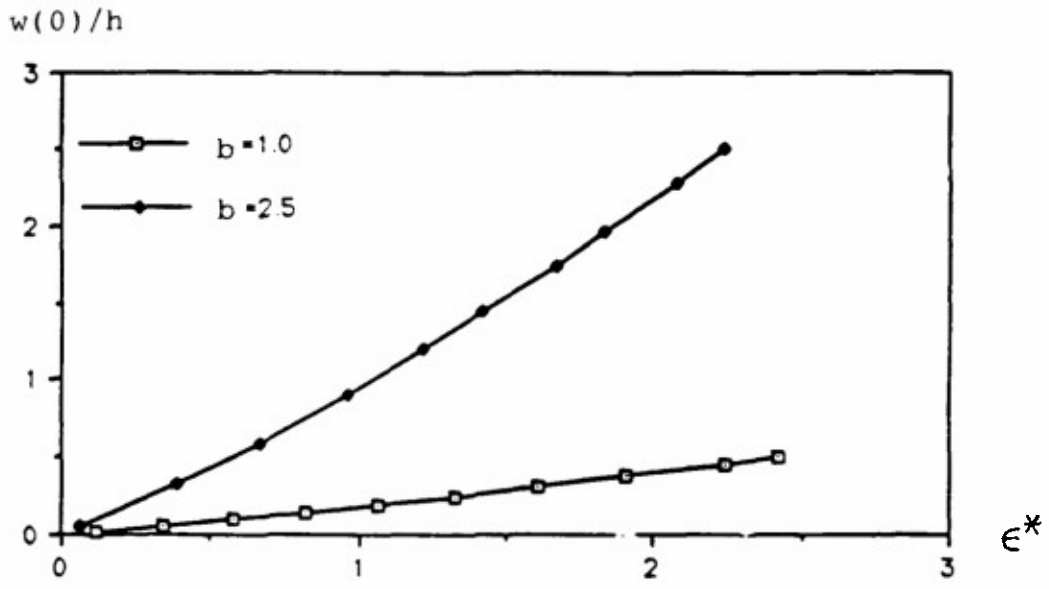

Fig. 52: Separation of a helical delaminated sheet vs. the normalized strain load (two-layer sheet)

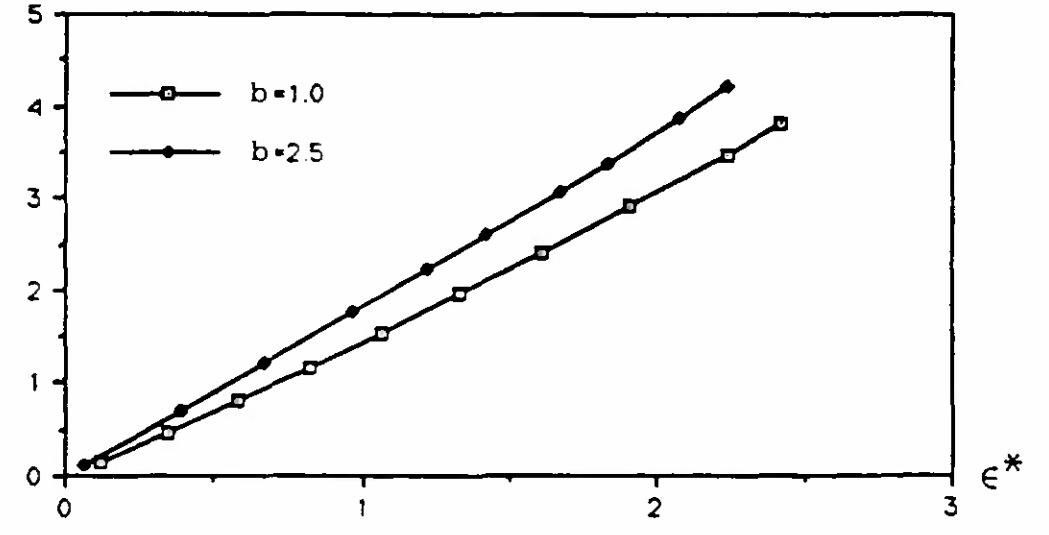

Fig. 53: Normalized boundary normal curvature vs. the normalized strain load (two-layer sheet)

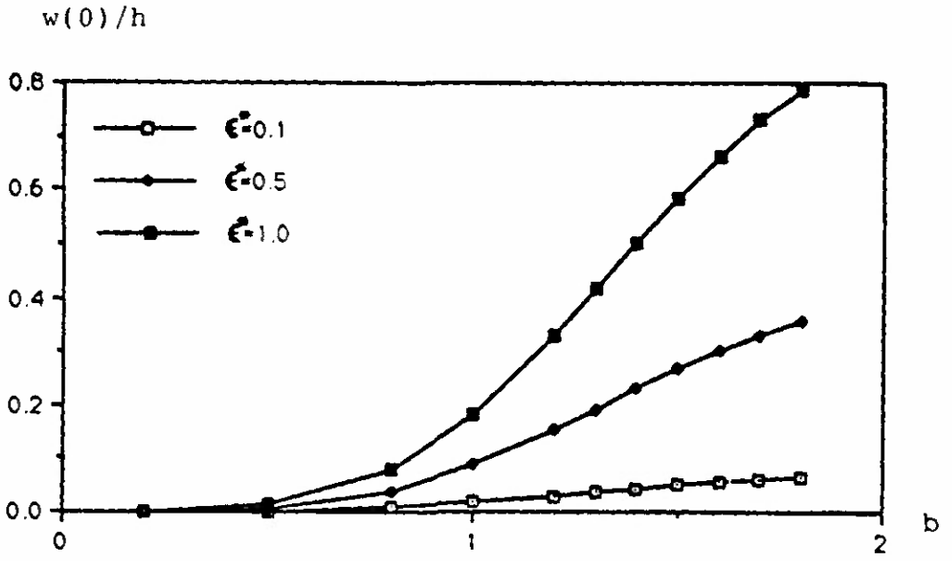

Fig. 54: Separation of a two-layer helical delaminated sheet vs. the normalized delamination width (fixed strain load)

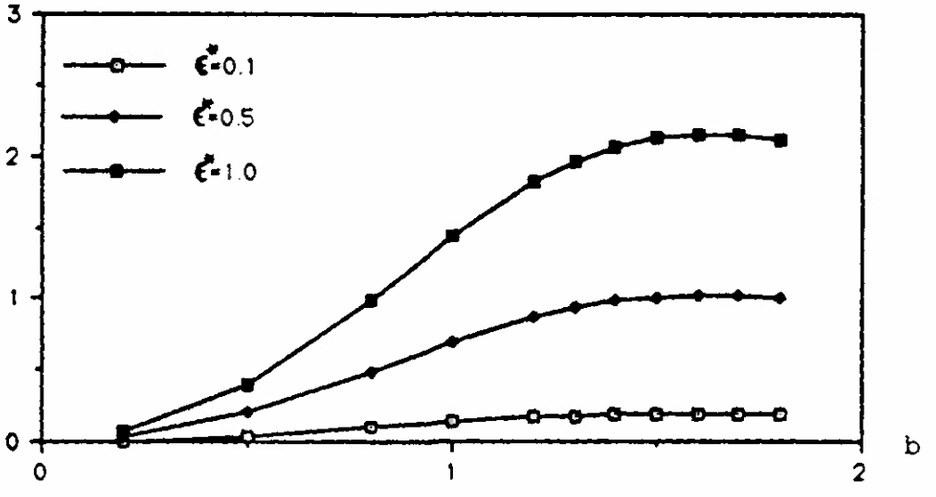

Fig. 55: Normalized boundary normal curvature vs. the normalized delamination width (fixed strain load)

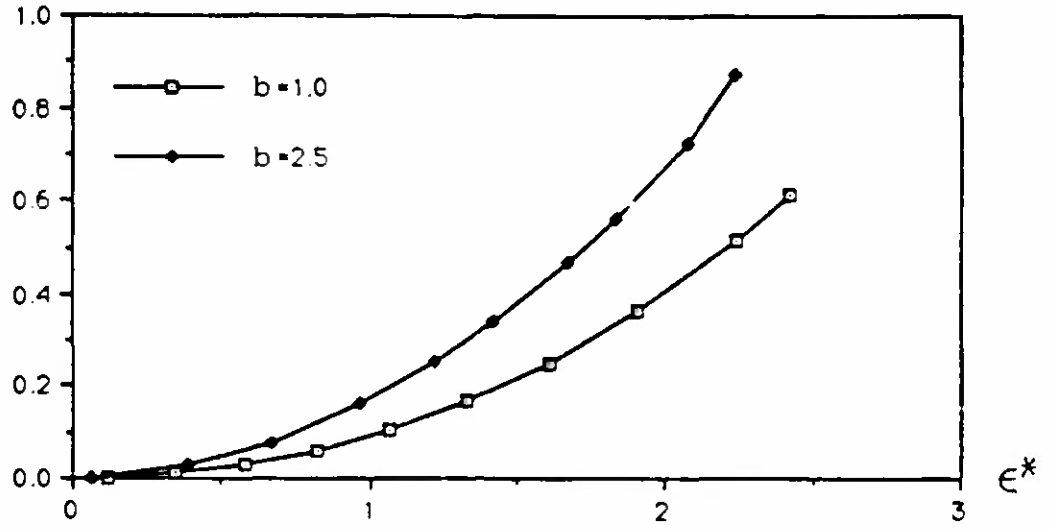

Fig. 56: Normalized energy-release rate vs. the normalized strain load (fixed delamination width, two-layer delaminated sheet)

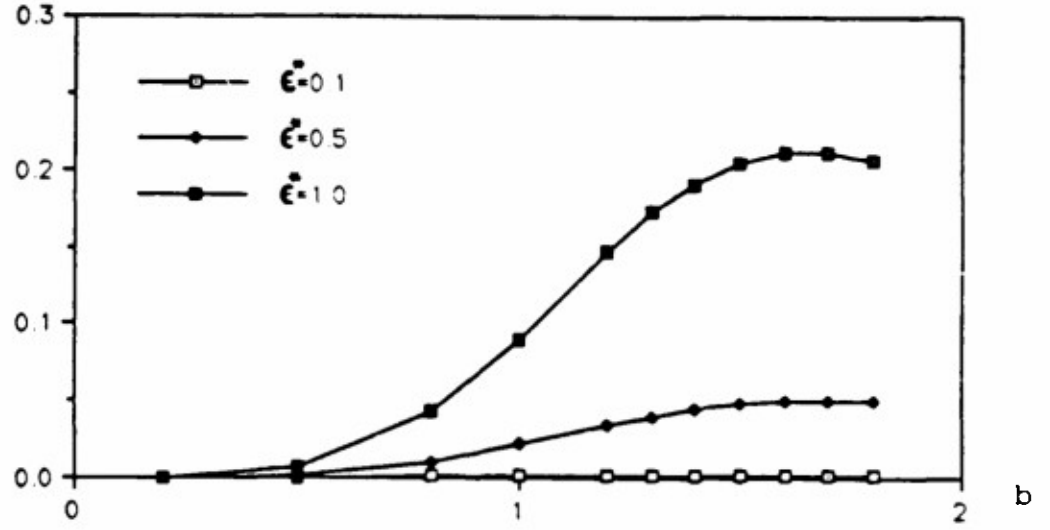

Fig. 57: Normalized energy-release rate vs. normalized delamination width (fixed strain load, two-layer delaminated sheet)

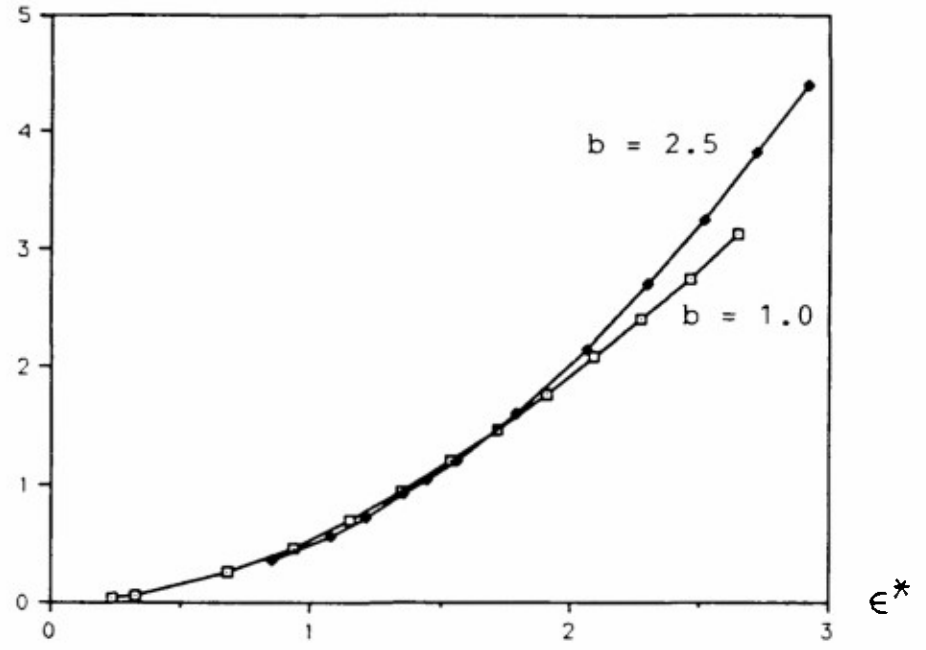

Fig. 58: Normalized energy-release rate vs. normalized strain load (fixed delamination width, one-layer delaminated sheet)

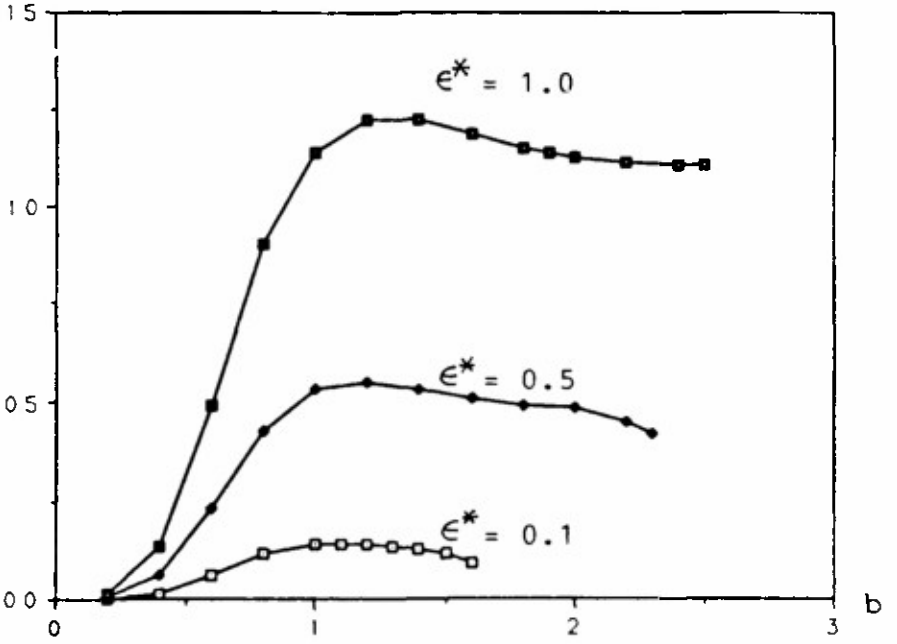

Fig. 59: Normalized energy-release rate vs. normalized delamination width (fixed strain load, one-layer delaminated sheet)

Part V. End and Edge Effects

Cylindrical filament-wound vessels are usually enclosed by axisymmetric caps at the two ends which require special winding patterns. An early but comprehensive introduction to the winding geometry and design issues involved in filament-wound structures for various applications was given in the book by Rosato, D.V. and Grove, C.S., Jr., Filament Winding: its development, manufacture, applications and design, Interscience, New York, 1964. The complex winding geometry at the closed ends results in special and inhomogeneous response behavior of the shell elements which constitute the caps. The problems of stress and deformation analysis are complex and difficult, and finite-element or other numerical modeling and analysis methods are often required to obtain approximate solutions. Special attention must be given to a region with discontinuities in the curvature, such as the junction between the cylindrical part and the end cap. Significant local stresses due to abrupt changes in the winding geometry may be developed in such regions under pressure-induced bending action.

End effects near the open ends of laminated anisotropic tubes have been studied by several authors (see, for example, Pagano, N.J. and Halpin, J.C., "Influence of end constraint in the testing of anisotropic bodies," J. Composite Materials, Vol. 1, p. 18, 1968; Rizzo, R.R., "More on the influence of end constraints on off-axis tensile tests," J. Composite Materials, Vol. 3, p. 202, 1969; Vicario, A.A. and Rizzo, R.R., "Effect of length on laminated thin tubes under combined loading," J. Composite Materials, Vol. 4, p. 273, 1970; Rizzo, R.R. and Vicario, A.A., "A finite element analysis of laminated anisotropic tubes," J. Composite Materials, Vol 4, p. 344, 1970). Although an approximate analysis of the stresses in the interior region of a filament-wound tube can be

conducted on the basis of the anisotropic shell theory, such an analysis cannot adequately account for the three-dimensional stress fields at the ends of the tube. Along the free edge or opening of a laminated structure, the mismatches in the elastic moduli and in the orientation angles of the adjacent layers of a laminate may introduce severe interlaminar peeling and shearing stresses. Although these interlaminar stresses decay rapidly away from the free edge, they may cause the initiation and growth of free-edge delamination because of the localized high intensity of the stresses. Significant free-edge interlaminar stresses may occur in a composite vessel made of a metal lining and a filament-wound exterior shell, or in a filament-wound vessel bonded to a metal fitting. Such interlaminar stresses may be caused by mechanical and thermal loads. In the latter case the interlaminar stresses are dependent also on the different thermal expansion coefficients of the adjacent layers.

Existing studies of the free-edge interlaminar stresses in layered composite plates and cylinders are usually based on finite-element or finite-difference modeling of the structure. Because the interlaminar stresses are highly localized and depend on the differences in the mechanical and thermal properties of the adjacent layers, a proper analytical modeling must include the details of the layered structure of the laminate and the anisotropic elastic and thermal parameters of the layers. In the case of a multi-layered laminate, this usually results in a very refined computational model with a large number of degrees of freedom. A substructuring approach may be used to reduce the size of the problem. However, the modeling and analysis still involve very considerable amount of effort and are, therefore, not suitable for practical purposes of design and optimization.

An efficient and accurate method for the analysis of free-edge interlaminar

stresses has been developed by using a variational method of approach on the basis of the principle of complementary virtual work. Since our objective is to obtain reasonably accurate solutions for the interlaminar stresses, it is natural to adopt a stress formulation, rather than a displacement formulation. The stress components in each layer may be represented by the derivatives of Lekhnitskii's stress functions (Lekhnitskii, S.G., Theory of Elasticity of an Anisotropic Elastic Body. English translation by P. Fern. Holden-Day, San Francisco, 1963). This ensures that the equilibrium equations are exactly satisfied by the variational solution in all regions of the layered plate, including the regions of high stress gradient near a free edge. Furthermore, traction-free boundary conditions and interfacial continuity of interlaminar stresses may be strictly enforced by imposing homogeneous boundary conditions and interfacial continuity conditions on the stress functions and their normal derivatives. The compatibility of strain and the interfacial continuity of displacements may be enforced in an averaged sense through the use of the principle of complementary virtual work.

Since each layer of the composite structure is very thin, the stress functions in each layer may be approximated by polynomial functions of the thickness coordinate, with coefficient that are functions of the coordinate along the interface. The application of the complementary virtual work principle yields a system of ordinary differential equations for the coefficient functions of the polynomial stress functions. The inhomogeneous terms (forcing terms) in the differential equations are linearly dependent on the three deformation parameters at the free edge: an axial extensional strain along the free edge, a bending curvature and a twisting curvature. The differential equations together with the homogeneous boundary conditions for the stress functions and their

derivatives define an eigenvalue problem. Solution of the eigenvalue problem yields the stresses in the individual layers and the interlaminar stresses between adjacent layers. This analysis method has been developed and presented in a recent paper (see Appendix F). The method is extremely easy to use, because of the simplicity of data input required for the analysis. The accuracy of the results was shown to be comparable to that of the existing numerical solutions base on finite-element and finite-difference methods. However, analysis using the present variational method has been implemented on personal computers and the results were generated for the classical problem of a four-layer symmetric cross-ply or angle-ply laminate in about one second on a 486 machine.

The variational method of analysis may be extended to the case of thermal loading in laminated beams and plates. The thermal stress problem for a finite beam or laminate may be decomposed into (i) a trivial problem for an infinite but otherwise identical beam or laminate under the same temperature load, and (ii) a complementary, purely mechanical problem in which the finite beam or laminate is subjected only to boundary tractions equal but opposite to the in-plane stresses of the first (trivial) problem. In this case the differential equations for the coefficient functions of the polynomial stress functions (derived by using the complementary virtual work principle) are homogeneous but the boundary conditions for the stress functions are inhomogeneous. Following a procedure similar to that in the analysis of mechanical loading, the eigenfunction analysis is performed and the stress functions and the interlaminar stresses are determined. The analysis method has been developed for the case of layered beams. The efficacy of the method and the accuracy of the results were demonstrated in two papers attached as Appendices G and H.

If a portion of the free edge has a curved geometry and if the local radius

of curvature is an order of magnitude greater than the laminate thickness (this is usually true around holes and openings of a laminated structure), then the present analysis method may still be applied to any short segment of the curved free edge, which is approximated by an treated as a straight segment. In this case, however, the system of governing differential equations and the associated boundary conditions generally vary along the curved free edge. Hence the local values of the layer stiffness matrix (referred to the local tangent and normal directions of the free edge) and the local values of the traction data should be used in each short segment of the edge. The actual three-dimensional stress distribution near the curved free edge is effectively replaced by a local two-dimensional stress field. This approximation assumes that the characteristic length of decay of the interlaminar stresses, which is usually comparable to the laminate thickness, should be small compared to the local radius of curvature of the free edge.

In the case of multi-layered beams and plates, a combined layer/sublaminate substructuring approach may be used to significantly reduce the size of the problem. In this approach, two interior layers adjacent to a particular interface are modeled as separate anisotropic homogeneous media while the remaining layers are grouped into an upper sublaminate and a lower sublaminate. The stress and moment resultants of the upper and lower sublaminate are shown to be related to the values of the stress functions on the interfaces between the sublaminates and the interior layers. After the eigenfuntion analysis is completed and the interlaminar stresses are determined on the particular interface, another interface is considered and a new layer/sublaminate model is used for the analysis of the interlaminar stresses on the latter interface.

Appendix A: Program MICROBEM

Boundary-Element Analysis of the Micromechanical Problem

Associated with Calculating the Elastic Moduli of a Composite

from the Properties of Isotropic Matrix and Transversely Isotropic Filaments

```
C PROGRAM MICROBEM
C  SOLUTION OF MICROMECHANICAL PROBLEMS BY THE BOUNDARY ELEMENT METHOD
C  FOR OETERMINING THE GROSS ELASTIC MOOULI OF A UNIDIRECTIONAL COMPOSITE
C  BASEO ON AN EXISTING 2-D BEM CODE FOR A SINGLE HOMOGENEOUS ISOTROPIC MEDIUM
       COMMON/RW/IRE,IWR
       COMMON/A/D(2,2),X1(6,3),W(6,3),IDUP(100),INC(100,2),C(100),
      *S(100,3),ISYM(100),X(100),Y(100),IFIP(108),A(108,108),P(112),
      *XM(108),A1(62,62),BB1(62,62),A2(112,112),BB2(112,112),
      *AB1(174,348),XXM(174),XP(108),XQ(62),PQ(62),XN(28),YN(28)
       COMMON/ABC/JS1(240),JS2(240),DEL(240),JS3(240),IX(240)
       DIMENSION STF(108),BBB(108),CCC(108),MEE(108),MFF(108)
           OPEN (4,FILE='DB60.DAT',STATUS='UNKNOWN')
           OPEN (6,FILE='RB60.DAT',STATUS='UNKNOWN')
C
C   INPUT ,AND COMPUTE MATRX A AND B
C
       IRE=4
       IWR=6
       READ (IRE,*) RA,CTA,POM,PO12,UO,VO,EPO
       WRITE (IWR,100) RA,CTA,UO,VO,EPO
100    FORMAT (//2X,3HRA=,F7.4,2X,4HCTA=,F4.1
      ?/2X,3HUO=,F6.3,2X,3HVO=,F6.3,2X,4HEPO=,F6.3)
       READ (IRE,*) E1,GGF,VVF,GGM,VVM
       DF=PO12*EPO
       DM=POM*EPO
       VE=DM-OF
       CTA=CTA*3.1415926535/180.
       READ (IRE,*) N1,N2
       NNN=N1+N2
       NNR=108
       CALL INPT(NE,NN,NP,IPL,PO,NN2,NT,C1,C2,
      *C3,C4,C5,C6,C7,C8,C9,C10,C11,IOSYM,XSYM,YSYM,INFB,RA,CTA,1)
       CALL MATRX(NE,NN,NN2,NT,C1,C2,C3,C4,C5,C6,C7,C8,
      *C9,C10,C11,PO,IDSYM,XSYM,YSYM,INFB,IFA,NIF)
       CALL INPTS(NE,NN,NP,IPL,PO,NN2,NT,C1,C2,
      *C3,C4,C5,C6,C7,C8,C9,C10,C11,IDSYM,XSYM,YSYM,INFB,RA,CTA,1)
       CALL MATRS(NE,NN,NN2,NT,C1,C2,C3,C4,C5,C6,C7,C8,
      *C9,C10,C11,PO,IDSYM,XSYM,YSYM,INFB,IFA,NIF)
       DO 140 I=1,28
       XN(I)=X(I)
140    YN(I)=Y(I)
       CALL CONNECT(A1,BB1,A2,BB2,N1,N2,AB1)
       READ (IRE,*) NC
           READ (IRE,*)  (JS1(I),I=1,NC)
           READ (IRE,*)  (JS2(I),I=1,NC)
       DO 205 I=1,NC
205    JS3(I)=JS2(I)
       CALL AODI(RA,CTA)
       CALL NCSBC(VE,UO,VO,OF,OM)
       DO 230 I=1,2*NNN
230    XXM(I)=0.
       CALL REDUCE(AB1,NNN,XXM,NC,JS1,JS2,DEL,JS3,IX)

       DO 260 I=95,116
       XXM(I)=XXM(I+2)
       DO 260 J=1,NNR
260    AB1(I,J)=AB1(I+2,J)

       OO 262 I=71,114
       XXM(I)=XXM(I+2)
       OO 262 J=1,NNR
262    AB1(I,J)=AB1(I+2,J)

       DO 264 I=61,113
       XXM(I)=XXM(I+1)
       DO 264 J=1,NNR
```

```
264     AB1(I,J)=AB1(I+1,J)

        DO 266 I=43,111
        XXM(I)=XXM(I+2)
        DO 266 J=1,NNR
266     AB1(I,J)=AB1(I+2,J)

        DO 268 I=19,109
        XXM(I)=XXM(I+2)
        DO 268 J=1,NNR
268     AB1(I,J)=AB1(I+2,J)

        DO 269 I=2,NNR
        XXM(I)=XXM(I+1)
        DO 269 J=1,NNR
269     AB1(I,J)=AB1(I+1,J)

        DO 250 I=1,NNR
        XM(I)=XXM(I)
        DO 250 J=1,NNR
250     A(I,J)=AB1(I,J)
C
C  SOLVE SYSTEM OF EQUATIONS
C
        EP=1.E-10
        CALL IVS(A,BBB,CCC,MEE,MFF,NNR,EP)
        CALL MUL(A,XM,STF,108,108,1)
        DO 600 I=1,108
600     XM(I)=STF(I)
        WRITE (IWR,320) (XM(I),I=1,108)
320     FORMAT (/,2X,6(F10.5,X)/,2X,6(F10.5,X)/,2X,6(F10.5,X)
       */,2X,6(F10.5,X)/,2X,6(F10.5,X)/,2X,6(F10.5,X)
       */,2X,6(F10.5,X)/,2X,6(F10.5,X)/,2X,6(F10.5,X)
       */,2X,6(F10.5,X)/,2X,6(F10.5,X)/,2X,6(F10.5,X)
       */,2X,6(F10.5,X)/,2X,6(F10.5,X)/,2X,6(F10.5,X))
        DO 400 I=1,NNR
400     XP(I)=XM(I)
        CALL OUTPT(1,1,UO,VO,RA,CTA,DF,SXF,SYF,VF,UF1,UF2)
        CALL OUTPM(1,1,UO,VO,RA,CTA,VE,DM,SXM,SYM,VM,UM1,UM2)
        AR=SQRT(3.)
        ASX=(SXF+SXM)/AR
        ASY=SYF+SYM
        AF=3.1415926535*RA*RA/4.
        AD1=E1*EPO*AF
        EF=2.*GGF*(1.+VVF)
        CN1=EF*PO12/((1.+VVF)*(1.-2.*VVF))
        ASZF=CN1*(-VF+(UF1+UF2))+AD1
        EM=2.*GGM*(1.+VVM)
        AO2=EM*EPO*(AR-2.*AF)/2.
        CN2=EM*VVM/((1.+VVM)*(1.-2.*VVM))
        ASZM=2.*(CN2*(-VM+(UM1+UM2))+AD2)
        ASZ=(2.*ASZF+ASZM)/AR
        WRITE (IWR,450) ASX,ASY,ASZ
450     FORMAT (//2X,'ASX=',F14.9,2X,'ASY=',F14.9,2X,'ASZ=',F14.9)
4       STOP
        END



        SUBROUTINE INPT(NE,NN,NP,IPL,PO,NN2,NT,C1,C2,
       *C3,C4,C5,C6,C7,C8,C9,C10,C11,IDSYM,XSYM,YSYM,INFB,RA,CTA,IND)
        COMMON /RW/ IRE,IWR
        COMMON /A/ D(2,2),XI(6,3),W(6,3),IOUP(100),INC(100,2),C(100),
       *S(100,3),ISYM(100),X(100),Y(100),IFIP(108),A(108,108),P(112),
       *XM(108),A1(62,62),BB1(62,62),A2(112,112),BB2(112,112),
```

```
     *AB1(174,348),XXM(174),XP(108),XQ(62),PQ(62),XN(28),YN(28)
      IF (IND.EQ.1) GOTO 301
      WRITE(IWR,1)
1     FORMAT(//,13X,'***FIBER REGION***',//)
C
C  GENERAL INFORMATION ABOUT THE PROBLEM
C
301   READ(IRE,*)INFB,NE,NN,NP,IPL,IDSYM,G,PO
      IF (INFB.EQ.0)GO TO 60
      WRITE(IWR,61)
61    FORMAT(//,13X,'* INFINITE BOUNDARY *')
60    IF (IND.EQ.1) GOTO 302
      WRITE(IWR,4)NE,NN,NP,IPL,IDSYM,G,PO
4     FORMAT(//,15X,'ND. ELEMENTS =',I5,//,15
     *X,'NO.    NODES =',I5,//,15X,'NO.   POINTS =',I5,//,15X,'PROBL.  T
     *YPE =',I5,//,15X,'SYMME.  TYPE =',I5,///,15X,'MATERIAL PROPERTIES'
     *,//,15X,'G        =',F10.8,
     *//,15X,'POISSON =',F10.8,///,30X,'COORDINATES OF BOUNDARY NODES',
     *//,12X,'NODE',14X,'X',15X,'Y',12X,'DOUBLE',/)
302   NN2=NN*2
      NT=NN+NP
C
C  NODES AND POINTS COORDINATES
C
      CALL ADDI(RA,CTA)
      DO 101 I=1,NN
      IDUP(I)=0
101   ISYM(I)=0
      READ (IRE,102) IDUP(1),IDUP(9),IOUP(22)
102   FORMAT (3I3)
      IDUP(31)=1
      IDUP(10)=9
      IOUP(23)=22
      DO 5 K=1,NN
      IF(IOUP(K).EQ.0)GO TO 5
      J=IDUP(K)
      IDUP(J)=K
      X(K)=X(J)
      Y(K)=Y(J)
5     CONTINUE
      IF (IND.EQ.1) GOTO 303
      DO 63 K=1,NN
      IF(IDUP(K).NE.0)GO TO 62
      WRITE(IWR,7)K,X(K),Y(K)
      GO TO 63
62    WRITE(IWR,16)K,X(K),Y(K),IDUP(K)
16    FORMAT(10X,I5,5X,F15.4,1X,F15.4,7X,I5)
63    CONTINUE
7     FORMAT(10X,I5,5X,F15.4,1X,F15.4)
303   IF(NP.EQ.0)GO TO 9
      WRITE(IWR,8)
8     FORMAT(//,30X,'COORDINATES OF INTERNAL POINTS',//,
     *11X,'POINTS',14X,'X',15X,'Y',/)
      K=NN+1
      READ(IRE,*) (X(J),Y(J),ISYM(J),J=K,NT)
      WRITE(IWR,7) (J,X(J),Y(J),J=K,NT)
C
C  NODES AND POINTS AT SYMMETRY LINES
C
9     IF(IDSYM.EQ.0)GO TO 49
      WRITE(IWR,42)
42    FORMAT(//,30X,'BOUNDARY NODES AND INTERNAL POINTS AT SYMMETRY LINE
     *(S)',//,12X,'L. X',12X,'L. Y',/)
      DO 43 K=1,NT
      IF (ISYM(K).EQ.0)GO TO 43
      IZZ=ISYM(K)
```

```
      GO TO (44,45,46),IZZ
44    YSYM=Y(K)
      WRITE(IWR,47)K
47    FORMAT(10X,I5)
      GO TO 43
45    XSYM=X(K)
      WRITE(IWR,48)K
48    FORMAT(26X,I5)
      GO TO 43
46    WRITE(IWR,50)K,K
50    FORMAT(10X,I5,11X,I5)
43    CONTINUE
C
C  ELEMENT CONNECTIVITY
C
49    IF (IND.EQ.1) GOTO 299
      WRITE(IWR,10)
10    FORMAT(//,30X,'ELEMENT CONNECTIVITY',//,13X,'EL',13X,'N. 1',12X,'N
     *. 2',14X,'L',/)
299   CALL ADD1
      DO 11 I=1,NE
      K=I
      II=INC(K,1)
      IF=INC(K,2)
11    C(K)=SQRT((X(IF)-X(II))**2+(Y(IF)-Y(II))**2)
      IF (INO.EQ.1) GOTO 310
      WRITE(IWR,13)(I,INC(I,1),INC(I,2),C(I),I=1,NE)
13    FORMAT(10X,I5,11X,I5,11X,I5,5X,F15.4)
C
C  CONSTANTS
C
310   E=G*(2.*(1.+PO))
      C11=PO
      IF(IPL-1)40,40,41
40    PO=PO/(1.+PO)
      C11=0.
41    C2=3.-4.*PO
      C3=1./((1.-PO)*12.56637062)
      C4=1.-2.*PO
      C6=2.*C3*G
      C7=1.-4.*PO
      C1=C3/(2.*G)
      C5=C1/2.
      C8=2.*G/(1.-PO)
      C9=PO/(1.-PO)
      C10=(2.-PO)/(1.-PO)
C
C  BOUNDARY VALUES PRESCRIBED
C


C
C  INTEGRATION POINTS
C
31    XI(1,3)=-0.93246951
      XI(2,3)=-0.66120939
      XI(3,3)=-0.23861919
      XI(4,3)=-XI(3,3)
      XI(5,3)=-XI(2,3)
      XI(6,3)=-XI(1,3)
      W(1,3)=0.17132449
      W(2,3)=0.36076157
      W(3,3)=0.46791393
      W(4,3)=W(3,3)
      W(5,3)=W(2,3)
      W(6,3)=W(1,3)
```

```
      X1(1,2)=-0.86113631
      X1(2,2)=-0.33998104
      X1(3,2)=-X1(2,2)
      X1(4,2)=-X1(1,2)
      W(1,2)=0.34785485
      W(2,2)=0.65214515
      W(3,2)=W(2,2)
      W(4,2)=W(1,2)
      X1(1,1)=-0.57735027
      X1(2,1)=-X1(1,1)
      W(1,1)=1.
      W(2,1)=1.
      RETURN
      END



      SUBROUTINE INPTS(NE,NN,NP,IPL,PO,NN2,NT,C1,C2,
     *C3,C4,C5,C6,C7,C8,C9,C10,C11,IDSYM,XSYM,YSYM,INFB,RA,CTA,IND)
      COMMON /RW/ IRE,IWR
      COMMON /A/ D(2,2),X1(6,3),W(6,3),IDUP(100),INC(100,2),C(100),
     *S(100,3),ISYM(100),X(100),Y(100),IFIP(108),A(108,108),P(112),
     *XM(108),A1(62,62),BB1(62,62),A2(112,112),BB2(112,112),
     *AB1(174,348),XXM(174),XP(108),XQ(62),PQ(62),XN(28),YN(28)
      IF (IND.EQ.1) GOTO 301
      WRITE(IWR,1)
1     FORMAT(//,13X,'***MATRIX REGION***',//)
C
C  GENERAL INFORMATION ABOUT THE PROBLEM
C
301   READ(IRE,*)INFB,NE,NN,NP,IPL,IDSYM,G,PO
      IF (INFB.EQ.0)GO TO 60
      WRITE(IWR,61)
61    FORMAT(//,13X,'* INFINITE BOUNDARY *')
60    IF (IND.EQ.1) GOTO 302
      WRITE(IWR,4)NE,NN,NP,IPL,IDSYM,G,PO
4     FORMAT(//,15X,'NO. ELEMENTS =',I5,//,15
     *X,'NO.    NODES =',I5,//,15X,'NO.   POINTS =',I5,//,15X,'PROBL.  T
     *YPE =',I5,//,15X,'SYMME.  TYPE =',I5,///,15X,'MATERIAL PROPERTIES'
     *,//,15X,'G        =',F10.8,
     *//,15X,'POISSON =',F10.8,///,30X,'COORDINATES OF BOUNDARY NODES',
     *//,12X,'NODE',14X,'X',15X,'Y',12X,'DOUBLE',/)
302   NN2=NN*2
      NT=NN+NP
C
C  NODES ANO POINTS COORDINATES
C
      CALL ADDJ(RA,CTA)
      DO 101 I=1,NN
      IDUP(I)=0
101   ISYM(I)=0
      READ (IRE,102) IDUP(1),IOUP(4),IDUP(17),IDUP(28),
     ?IDUP(32),IDUP(45)
102   FORMAT(6I3)
      IOUP(56)=1
      IDUP(5)=4
      IDUP(18)=17
      IDUP(29)=28
      IDUP(33)=32
      IDUP(46)=45
      DO 5 K=1,NN
      IF(IDUP(K).EQ.0)GO TO 5
      J=IOUP(K)
      IDUP(J)=K
      X(K)=X(J)
```

```
      Y(K)=Y(J)
5     CONTINUE
      IF (IND.EQ.1) GOTO 303
      DO 63 K=1,NN
      IF(IOUP(K).NE.0)GO TO 62
      WRITE(IWR,7)K,X(K),Y(K)
      GO TO 63
62    WRITE(IWR,16)K,X(K),Y(K),IDUP(K)
16    FORMAT(10X,I5,5X,F15.4,1X,F15.4,7X,I5)
63    CONTINUE
7     FORMAT(10X,I5,5X,F15.4,1X,F15.4)
303   IF(NP.EQ.0)GO TO 9
      WRITE(IWR,8)
8     FORMAT(//,30X,'COORDINATES OF INTERNAL POINTS',//,
     *11X,'POINTS',14X,'X',15X,'Y',/)
      K=NN+1
      READ(IRE,*) (X(J),Y(J),ISYM(J),J=K,NT)
      WRITE(IWR,7) (J,X(J),Y(J),J=K,NT)
C
C  NODES AND POINTS AT SYMMETRY LINES
C
9     IF(IDSYM.EQ.0)GO TO 49
      WRITE(IWR,42)
42    FORMAT(//,30X,'BOUNDARY NODES AND INTERNAL POINTS AT SYMMETRY LINE
     *(S)',//,12X,'L. X',12X,'L. Y',/)
      DO 43 K=1,NT
      IF (ISYM(K).EQ.0)GO TO 43
      IZZ=ISYM(K)
      GO TO (44,45,46),IZZ
44    YSYM=Y(K)
      WRITE(IWR,47)K
47    FORMAT(10X,I5)
      GO TO 43
45    XSYM=X(K)
      WRITE(IWR,48)K
48    FORMAT(26X,I5)
      GO TO 43
46    WRITE(IWR,50)K,K
50    FORMAT(10X,I5,11X,I5)
43    CONTINUE
C
C  ELEMENT CONNECTIVITY
C
49    IF (IND.EQ.1) GOTO 299
      WRITE(IWR,10)
10    FORMAT(//,30X,'ELEMENT CONNECTIVITY',//,13X,'EL',13X,'N. 1',12X,'N
     *. 2',14X,'L',/)
299   CALL ADD2
      DO 11 I=1,NE
      K=I
      II=INC(K,1)
      IF=INC(K,2)
11    C(K)=SQRT((X(IF)-X(II))**2+(Y(IF)-Y(II))**2)
      IF (IND.EQ.1) GOTO 310
      WRITE(IWR,13) (I,INC(I,1),INC(I,2),C(I),I=1,NE)
13    FORMAT(10X,I5,11X,I5,11X,I5,5X,F15.4)
C
C  CONSTANTS
C
310   E=G*(2.*(1.+PO))
      C11=PO
      IF(IPL-1)40,40,41
40    PO=PO/(1.+PO)
      C11=0.
41    C2=3.-4.*PO
      C3=1./((1.-PO)*12.56637062)
```

```
      C4=1.-2.*PO
      C6=2.*C3*G
      C7=1.-4.*PO
      C1=C3/(2.*G)
      C5=C1/2.
      C8=2.*G/(1.-PO)
      C9=PO/(1.-PO)
      C10=(2.-PO)/(1.-PO)
C
C  BOUNDARY VALUES PRESCRIBED
C



C
C  INTEGRATION POINTS
C
31    XI(1,3)=-0.93246951
      XI(2,3)=-0.66120939
      XI(3,3)=-0.23861919
      XI(4,3)=-XI(3,3)
      XI(5,3)=-XI(2,3)
      XI(6,3)=-XI(1,3)
      W(1,3)=0.17132449
      W(2,3)=0.36076157
      W(3,3)=0.46791393
      W(4,3)=W(3,3)
      W(5,3)=W(2,3)
      W(6,3)=W(1,3)
      XI(1,2)=-0.86113631
      XI(2,2)=-0.33998104
      XI(3,2)=-XI(2,2)
      XI(4,2)=-XI(1,2)
      W(1,2)=0.34785485
      W(2,2)=0.65214515
      W(3,2)=W(2,2)
      W(4,2)=W(1,2)
      XI(1,1)=-0.57735027
      XI(2,1)=-XI(1,1)
      W(1,1)=1.
      W(2,1)=1.
      RETURN
      END

      SUBROUTINE MATRX(NE,NN,NN2,NT,C1,C2,C3,C4,C5,C6,C7,C8,
     *C9,C10,C11,PO,IDSYM,XSYM,YSYM,INFB,IFA,NIF)
      COMMON /A/ D(2,2),XI(6,3),W(6,3),IDUP(100),INC(100,2),C(100),
     *S(100,3),ISYM(100),X(100),Y(100),IFIP(108),A(108,108),P(112),
     *XM(108),A1(62,62),BB1(62,62),A2(112,112),BB2(112,112),
     *AB1(174,348),XXM(174),XP(108),XQ(62),PQ(62),XN(28),YN(28)
      COMMON /A4/ H(3,4),G(3,4),HL(3,4),GL(3,4)
C
C  KRONECKER DELTA
C
      D(1,1)=1.
      D(2,2)=1.
      D(1,2)=0.
      D(2,1)=0.
C
C  CLEAR ARRAYS
C
      DO 1 I=1,NN2
      DO 1 J=1,NN2
      BB1(I,J)=0.
1     A1(I,J)=0.
C
C  COMPUTE PARAMETERS FOR SYMMETRY LOOP
```

```
C
      IFA=1
      NIF=1
      IF(IOSYM.EQ.1)IFA=2
      IF(IDSYM.NE.2)GO TO 60
      IFA=3
      NIF=2
60    IF(IDSYM.EQ.3)IFA=4
C
C  TEST FOR INFINITE BOUNDARY
C
      IF(INFB.EQ.0)GO TO 90
      DO 91 I=1,NN2
      IF(IFIP(I).NE.0)GO TO 92
      A1(I,I)=1.
      GO TO 91
92    XM(I)=-P(I)
91    CONTINUE
C
C  SYMMETRY LOOP
C
90    DO 2 ISY=1,IFA,NIF
C
C  COMPUTE CHANGE SIGN CONTROLLING PARAMETERS
C
      GO TO (70,71,71,73),ISY
71    IIS=4-ISY
      IFS=IIS
      GO TO 70
73    IIS=1
      IFS=2
C
C  LOOP OVER BOUNDARY NODES
C
70    DO 2 I=1,NN
      XS=X(I)
      YS=Y(I)
      IF(ISY.EQ.2.OR.ISY.EQ.4)YS=2.*YSYM-YS
      IF(ISY.GE.3)XS=2.*XSYM-XS
C
C  GENERATE MATRIX A AND B
C
      DO 10 J=1,NE
      II=INC(J,1)
      IF=INC(J,2)
      ICOD=1
      IF(ISY.NE.1.AND.ISYM(I).NE.(ISY-1))GO TO 6
      IF(I.EQ.II.OR.I.EQ.IDUP(II))ICOD=2
      IF(I.EQ.IF.OR.I.EQ.IDUP(IF))ICOD=3
6     CALL FUNC(ICOD,J,C1,C2,C3,C4,C5,C6,C7,PO,II,IF,XS,YS,ISY,
     *IIS,IFS)
      DO 10 K=1,2
      JJ=2*(I-1)+K
      M=0
      DO 10 NX=1,2
      DO 10 NV=1,2
      M=M+1
      IC=2*INC(J,NX)+NV-2
      A1(JJ,IC)=A1(JJ,IC)+H(K,M)
      BB1(JJ,IC)=BB1(JJ,IC)-G(K,M)
      GOTO (61,62,63,64),ISY
62    IF (NV-2) 61,64,61
63    IF (NV-1) 61,64,61
64    H(K,M)=-H(K,M)
61    A1(JJ,JJ+NV-K)=A1(JJ,JJ+NV-K)-H(K,M)
10    CONTINUE
```

```
2       CONTINUE
        RETURN
        END




        SUBROUTINE MATRS(NE,NN,NN2,NT,C1,C2,C3,C4,C5,C6,C7,C8,
       *C9,C10,C11,PO,IDSYM,XSYM,YSYM,INFB,IFA,NIF)
        COMMON /A/ D(2,2),X1(6,3),W(6,3),IDUP(100),INC(100,2),C(100),
       *S(100,3),ISYM(100),X(100),Y(100),IFIP(108),A(108,108),P(112),
       *XM(108),A1(62,62),BB1(62,62),A2(112,112),BB2(112,112),
       *AB1(174,348),XXM(174),XP(108),XQ(62),PQ(62),XN(28),YN(28)
        COMMON /A4/ H(3,4),G(3,4),HL(3,4),GL(3,4)
C
C  KRONECKER DELTA
C
        D(1,1)=1.
        D(2,2)=1.
        D(1,2)=0.
        D(2,1)=0.
C
C  CLEAR ARRAYS
C
        DO 1 I=1,NN2
        DO 1 J=1,NN2
        BB2(I,J)=0.
1       A2(I,J)=0.
C
C  COMPUTE PARAMETERS FOR SYMMETRY LOOP
C
        IFA=1
        NIF=1
        IF(IDSYM.EQ.1)IFA=2
        IF(IDSYM.NE.2)GO TO 60
        IFA=3
        NIF=2
60      IF(IDSYM.EQ.3)IFA=4
C
C  TEST FOR INFINITE BOUNDARY
C
        IF(INFB.EQ.0)GO TO 90
        DO 91 I=1,NN2
        IF(IFIP(I).NE.0)GO TO 92
        A2(I,I)=1.
        GO TO 91
92      XM(I)=-P(I)
91      CONTINUE
C
C  SYMMETRY LOOP
C
90      DO 2 ISY=1,IFA,NIF
C
C  COMPUTE CHANGE SIGN CONTROLLING PARAMETERS
C
        GO TO (70,71,71,73),ISY
71      IIS=4-ISY
        IFS=IIS
        GO TO 70
73      IIS=1
        IFS=2
C
C  LOOP OVER BOUNDARY NODES
C
70      DO 2 I=1,NN
        XS=X(I)
```

```
      YS=Y(I)
      IF(ISY.EQ.2.OR.ISY.EQ.4)YS=2.*YSYM-YS
      IF(ISY.GE.3)XS=2.*XSYM-XS
C
C  GENERATE MATRIX A AND B
C
      DO 10 J=1,NE
      II=INC(J,1)
      IF=INC(J,2)
      ICOO=1
      IF(ISY.NE.1.AND.ISYM(I).NE.(ISY-1))GO TO 6
      IF(I.EQ.II.OR.I.EQ.IDUP(II))ICOD=2
      IF(I.EQ.IF.OR.I.EQ.IDUP(IF))ICOD=3
6     CALL FUNC(ICOO,J,C1,C2,C3,C4,C5,C6,C7,PO,II,IF,XS,YS,ISY,
     *IIS,IFS)
      DO 10 K=1,2
      JJ=2*(I-1)+K
      M=0
      DO 10 NX=1,2
      DO 10 NV=1,2
      M=M+1
      IC=2*INC(J,NX)+NV-2
      A2(JJ,IC)=A2(JJ,IC)+H(K,M)
      BB2(JJ,IC)=BB2(JJ,IC)-G(K,M)
      GOTO (61,62,63,64),ISY
62    IF (NV-2) 61,64,61
63    IF (NV-1) 61,64,61
64    H(K,M)=-H(K,M)
61    A2(JJ,JJ+NV-K)=A2(JJ,JJ+NV-K)-H(K,M)
10    CONTINUE
2     CONTINUE
      RETURN
      END



      SUBROUTINE FUNC(ICOD,JA,C1,C2,C3,C4,C5,C6,C7,PO,II,IF,XS,
     *YS,ISY,IIS,IFS)
C
C  INTERGRALS OVER BOUNDARY ELEMENTS
C
      COMMON /A/ D(2,2),XI(6,3),W(6,3),IDUP(100),INC(100,2),C(100),
     *S(100,3),ISYM(100),X(100),Y(100),IFIP(108),A(108,108),P(112),
     *XM(108),A1(62,62),BB1(62,62),A2(112,112),BB2(112,112),
     *AB1(174,348),XXM(174),XP(108),XQ(62),PQ(62),XN(28),YN(28)
      COMMON /A4/ H(3,4),G(3,4),HL(3,4),GL(3,4)
      DIMENSION DXY(2),BN(2),B(2),DR(2),UL(2,2),PL(2,2),ULL(2,2,2),
     *PLL(2,2,2)
      DO 5 KK=1,3
      DO 5 L=1,4
      GL(KK,L)=0.
      HL(KK,L)=0.
      G(KK,L)=0.
5     H(KK,L)=0.
      DXY(1)=X(IF)-X(II)
      DXY(2)=Y(IF)-Y(II)
      GO TO (1,2,2,1),ICOD
1     BN(1)=DXY(2)/C(JA)
      BN(2)=-DXY(1)/C(JA)
C
C  SELECT NO. INTEGRATION POINTS
C
      SEL=0.5*SQRT((2.*XS-X(II)-X(IF))**2+(2.*YS-Y(II)-Y(IF))**2)/C(JA)
      NPI=4
      IF(SEL.LE.1.5)NPI=6
      IF(SEL.GT.5.5)NPI=2
```

```
      INP=NPI/2
C
C  COMPUTE MATRICES NUMERICALLY
C
      DO 50 KK=1,NPI
      XMXI=0.5*(1.+XI(KK,INP))*DXY(1)+X(II)-XS
      YMYI=0.5*(1.+XI(KK,INP))*DXY(2)+Y(II)-YS
      R=SQRT(XMXI**2+YMYI**2)
      B(1)=-0.25*(XI(KK,INP)-1.)*C(JA)
      B(2)=0.25*(XI(KK,INP)+1.)*C(JA)
      DR(1)=XMXI/R
      DR(2)=YMYI/R
      DRDN=DR(1)*BN(1)+DR(2)*BN(2)
C
C  COMPUTE MATRICES H AND G
C
      DO 6 I=1,2
      DO 6 J=1,2
      UL(I,J)=-C1*(C2*ALOG(R)*D(I,J)-DR(I)*DR(J))
6     PL(I,J)=-C3*((C4*D(I,J)+2.*DR(I)*DR(J))*DRDN+C4*(DR(J)*BN(I)-DR(I)
     **BN(J)))/R
      DO 7 LA=1,2
      IC=0
      DO 7 LL=1,2
      DO 7 JJ=1,2
      IC=IC+1
      G(LA,IC)=G(LA,IC)+UL(LA,JJ)*B(LL)*W(KK,INP)
7     H(LA,IC)=H(LA,IC)+PL(LA,JJ)*B(LL)*W(KK,INP)
      IF(ICOD.NE.4)GO TO 50
C
C  COMPUTE THE MATRICES HL AND GL (STRESSES AT INTERNAL POINTS)
C
10    DO 11 I=1,2
      DO 11 J=1,2
      DO 11 K=1,2
      ULL(I,J,K)=C3*(C4*(DR(J)*D(K,I)+DR(I)*D(K,J)-DR(K)*D(I,J))+2.*DR(I
     *)*DR(J)*DR(K))/R
      B1=2.*DRDN*(C4*DR(K)*D(I,J)+PO*(DR(J)*D(I,K)+DR(I)*D(J,K))-4.*DR(I
     *)*DR(J)*DR(K))
      B2=2.*PO*(BN(I)*DR(J)*DR(K)+BN(J)*DR(I)*DR(K))
      B3=C4*(2.*BN(K)*DR(I)*DR(J)+BN(J)*D(I,K)+BN(I)*D(J,K))
11    PLL(I,J,K)=C6*(B1+B2+B3-C7*BN(K)*D(I,J))/R**2
      IL=0
      DO 12 I=1,2
      DO 12 J=1,2
      IL=IL+1
      IC=0
      DO 12 IAA=1,2
      DO 12 JAA=1,2
      IC=IC+1
      GL(IL,IC)=GL(IL,IC)+B(IAA)*ULL(I,J,JAA)*W(KK,INP)
12    HL(IL,IC)=HL(IL,IC)+B(IAA)*PLL(I,J,JAA)*W(KK,INP)
50    CONTINUE
      GO TO 18
C
C  COMPUTE MATRICES H AND G ANALYTICALLY (BOUNDARY CONSTRAINT EQ.)
C
2     AL=C5*C2*C(JA)
      AA=AL*(0.5-ALOG(C(JA)))
      DO 15 I=1,2
      DO 15 J=1,4
      IT=(J/2)*2+2-J
      G(I,J)=C5*DXY(I)*DXY(IT)/C(JA)
      IF(IT.EQ.I)G(I,J)=G(I,J)+AA
15    CONTINUE
      IAA=-2
```

```
      IF(ICOD.EQ.3) IAA=0
      G(1,3+IAA)=G(1,3+IAA)+AL
      G(2,4+IAA)=G(2,4+IAA)+AL
      H(1,2-IAA)=C3*C4*(1.+IAA)
      H(2,1-IAA)=-H(1,2-IAA)
C
C  SYMMETRY TEST
C
18    IF(ISY.EQ.1)GO TO 8
      DO 24 I=IIS,IFS
      DO 24 J=1,4
      H(I,J)=-H(I,J)
24    G(I,J)=-G(I,J)
      IF(ICOD.NE.4.OR.ISY.EQ.4)GO TO 8
      DO 25 J=1,4
      HL(2,J)=-HL(2,J)
25    GL(2,J)=-GL(2,J)
8     RETURN
      END


      SUBROUTINE OUTPT(IFA,NIF,UO,VO,RA,CTA,DF,SXF,SYF,VF,UF1,
     ?UF2)
C
C  OUTPUT RESULTS
C
      COMMON /RW/ IRE,IWR
      COMMON /A/ D(2,2),X1(6,3),W(6,3),IDUP(100),INC(100,2),C(100),
     *S(100,3),ISYM(100),X(100),Y(100),IFIP(108),A(108,108),P(112),
     *XM(108),A1(62,62),BB1(62,62),A2(112,112),BB2(112,112),
     *AB1(174,348),XXM(174),XP(108),XQ(62),PQ(62),XN(28),YN(28)
      COMMON /A4/ H(3,4),G(3,4),HL(3,4),GL(3,4)
      DIMENSION U(2),SA(4),XG(15),FG(15)
      CALL INPT(NE,NN,NP,IPL,PO,NN2,NT,C1,C2,
     *C3,C4,C5,C6,C7,C8,C9,C10,C11,IDSYM,XSYM,YSYM,INFB,RA,CTA,2)
      WRITE (IWR,6)
6     FORMAT (///,30X,'BOUNDARY DISPLACEMENTS AND TRACTIONS',//,
     ?12X,'NODE',14X,'U',15X,'V',14X,'PX',14X,'PY',/)
C
C  BOUNDARY DISPLACEMENTS AND TRACTIONS
C
      SR2=SQRT(3.)/2.
      DO 200 I=1,62
      P(I)=0.
200   XM(I)=0.
      DO 205 I=1,9
      J=2*I-1
      K=38+I
205   P(J)=XP(K)
      P(20)=XP(48)
      DO 210 I=21,42
      J=I+28
210   P(I)=XP(J)
      P(43)=XP(71)
      DO 220 I=1,9
      J=44+2*I
      K=71+I
220   P(J)=XP(K)
      DO 230 I=1,9
      J=2*I-1
230   XM(J)=-.5*(UO+DF)
      XM(2)=SR2*(VO+DF)
      DO 235 I=1,8
      J=2+2*I
235   XM(J)=XP(I)
      XM(19)=XM(17)
```

```
      XM(20)=XM(18)
      DO 240 I=1,23
      J=I+20
      K=I+8
240   XM(J)=XP(K)
      DO 245 I=1,10
      J=42+2*I
245   XM(J)=SR2*(VO+DF)
      XM(45)=XM(43)
      DO 250 I=1,7
      J=46+2*I-1
      K=31+I
250   XM(J)=XP(K)
      XM(61)=XM(1)
      DO 260 I=1,62
      XQ(I)=XM(I)
260   PQ(I)=P(I)
      WRITE (IWR,11) (I,XM(2*I-1),XM(2*I),P(2*I-1),P(2*I),I=1,NN)
11    FORMAT (10X,I5,5X,F15.4,1X,F15.4,1X,F15.4,1X,F15.4)
C
C  DISPLACEMENTS AND STRESSES AT NODES AND INT. POINTS
C
      WRITE(IWR,12)
12    FORMAT(//,15X,'DISPLACEMENTS AND STRESSES AT NODES AND INTERNAL PO
     *INTS',//,2X,'NO/PT',9X,'U',13X,'V',12X,'SX',12X,'SXY',11X,'SY',
     *12X,'SZ',/)
C
C  COMPUTE BOUNDARY STRESSES
C
      DO 14 I=1,NN
      DO 14 J=1,3
14    S(I,J)=0.
C
C     LOOP OVER ALL BOUNDARY ELEMENTS
C
      DO 30 I=1,NE
      II=INC(I,1)
      IF=INC(I,2)
      CC1=(Y(IF)-Y(II))/C(I)
      CC2=(X(II)-X(IF))/C(I)
      CALL FENC(C8,C9,C10,CC1,CC2,I)
      DO 30 JP=1,2
      IIF=INC(I,JP)
      XFAC=2.
      IF(IDUP(IIF).NE.0.OR.ISYM(IIF).NE.0)XFAC=1.
      DO 30 IR=1,3
      M=0
      DO 30 IP=1,2
      IO=2*IIF+IP-2
      S(IIF,IR)=S(IIF,IR)+G(IR,IP)*P(IO)/XFAC
      DO 30 JR=1,2
      M=M+1
      IO=2*INC(I,IP)+JR-2
30    S(IIF,IR)=S(IIF,IR)-H(IR,M)*XM(IO)/XFAC
C
C     PRINT VALUES ON THE BOUNDARY
C
      DO 13 I=1,NN
      SA(4)=C11*(S(I,1)+S(I,3))
      IF(ISYM(I).NE.0)S(I,2)=0.
13    WRITE(IWR,15)I,XM(2*I-1),XM(2*I),S(I,1),S(I,2),S(I,3),SA(4)
15    FORMAT (2X,I4,1X,6(1X,F13.4))
      NG=8
      NG1=9
      DO 310 I=1,NG1
      J=NG1-I+1
```

```
      XG(I)=Y(J)
310   FG(I)=S(J,1)
      CALL AST(NG,NG1,SXF,XG,FG)
      DO 320 I=1,NG1
      J=32-I
      XG(I)=X(J)
320   FG(I)=S(J,3)
      CALL AST(NG,NG1,SYF,XG,FG)
      DO 330 I=1,NG1
      XG(I)=Y(I)
330   FG(I)=XM(2*I-1)
      CALL AST(NG,NG1,UF1,XG,FG)
      NG=12
      NG1=13
      DO 340 I=1,NG1
      J=I+9
      XG(I)=X(J)
340   FG(I)=XM(2*J)
      CALL AST(NG,NG1,VF,XG,FG)
      DO 350 I=1,NG1
      J=I+9
      XG(I)=Y(J)
350   FG(I)=XM(2*J-1)
      CALL AST(NG,NG1,UF2,XG,FG)
      IF(NN.EQ.NT)GO TO 5
C
C     COMPUTE INTERNAL VALUES
C
      NN1=NN+1
      ICOO=4
C
C  LOOP OVER ALL INTERNAL POINTS
C
      DO 16 I=NN1,NT
      U(1)=0.
      U(2)=0.
      DO 17 J=1,3
17    SA(J)=0.
C
C     SYMMETRY LOOP
C
      DO 20 ISY=1,IFA,NIF
      XS=X(I)
      YS=Y(I)
      IF(ISY.EQ.2.OR.ISY.EQ.4)YS=2.*YSYM-YS
      IF(ISY.GE.3)XS=2.*XSYM-XS
      GO TO (70,71,71,73),ISY
71    IIS=4-ISY
      IFS=IIS
      GO TO 70
73    IIS=1
      IFS=2
C
C     INTEGRATE OVER THE BOUNDARY
C
70    DO 20 J=1,NE
      II=INC(J,1)
      IF=INC(J,2)
      CALL FUNC(ICOD,J,C1,C2,C3,C4,C5,C6,C7,PO,II,IF,XS,YS,ISY,
     *IIS,IFS)
      DO 20 K=1,3
      M=0
      DO 20 NX=1,2
      DO 20 NV=1,2
      M=M+1
      ICA=2*INC(J,NX)+NV-2
```

```
      IF (K.LT.3) U(K)=U(K)-H(K,M)*XM(ICA)+G(K,M)*P(ICA)
20    SA(K)=SA(K)-HL(K,M)*XM(ICA)+GL(K,M)*P(ICA)
      SA(4)=C11*(SA(1)+SA(3))
16    WRITE(IWR,15) I,U(1),U(2),SA(1),SA(2),SA(3),SA(4)
5     RETURN
      END



      SUBROUTINE OUTPM(IFA,NIF,UO,VO,RA,CTA,VE,DM,SXM,SYM,VM,UM1,
     ?UM2)
C
C  OUTPUT RESULTS
C
      COMMON /RW/ IRE,IWR
      COMMON /A/ D(2,2),XI(6,3),W(6,3),IDUP(100),INC(100,2),C(100),
     *S(100,3),ISYM(100),X(100),Y(100),IFIP(108),A(108,108),P(112),
     *XM(108),A1(62,62),BB1(62,62),A2(112,112),BB2(112,112),
     *AB1(174,348),XXM(174),XP(108),XQ(62),PQ(62),XN(28),YN(28)
      COMMON /A4/ H(3,4),G(3,4),HL(3,4),GL(3,4)
      DIMENSION U(2),SA(4),XG(15),FG(15)
      CALL INPTS(NE,NN,NP,IPL,PO,NN2,NT,C1,C2,
     *C3,C4,C5,C6,C7,C8,C9,C10,C11,IDSYM,XSYM,YSYM,INFB,RA,CTA,2)
      WRITE (IWR,6)
6     FORMAT (///,30X,'BOUNDARY DISPLACEMENTS AND TRACTIONS',//,
     ?12X,'NODE',14X,'U',15X,'V',14X,'PX',14X,'PY',/)
C
C  BOUNDARY DISPLACEMENTS AND TRACTIONS
C
      SR2=SQRT(3.)/2.
      DO 200 I=1,112
      P(I)=0.
200   XM(I)=0.
      DO 205 I=1,4
      J=2*I
      K=93+I
205   P(J)=XP(K)
      DO 210 I=1,13
      J=8+2*I
      K=46-2*I
      J1=J-1
      K1=K-1
      P(J)=-PQ(K)
210   P(J1)=-PQ(K1)
      DO 215 I=1,11
      J=34+2*I-1
      K=97+I
215   P(J)=XP(K)
      DO 220 I=1,56
      J=56+I
220   P(J)=-P(I)
      DO 230 I=1,3
      J=2*I-1
      J1=J+1
      K=80+I
      XM(J)=XP(K)
230   XM(J1)=SR2*(VO+DM)
      DO 240 I=1,15
      J=6+2*I
      K=48-2*I
      J1=J-1
      K1=K-1
      L=3+I
      XM(J)=XQ(K)+VE*Y(L)
240   XM(J1)=XQ(K1)+VE*X(L)
      DO 250 I=1,10
```

```
      J=36+2*I
      J1=J-1
      K=83+I
      XM(J1)=-.5*(UO+DM)
250   XM(J)=XP(K)
      DO 260 I=1,56
      J=56+I
260   XM(J)=-XM(I)
      WRITE (IWR,11) (I,XM(2*I-1),XM(2*I),P(2*I-1),P(2*I),I=1,NN)
11    FORMAT (10X,I5,5X,F15.4,1X,F15.4,1X,F15.4,1X,F15.4)
C
C  DISPLACEMENTS AND STRESSES AT NODES AND INT. POINTS
C
      WRITE(IWR,12)
12    FORMAT(//,15X,'DISPLACEMENTS AND STRESSES AT NODES AND INTERNAL PO
     *INTS',//,2X,'NO/PT',9X,'U',13X,'V',12X,'SX',12X,'SXY',11X,'SY',
     *12X,'SZ',/)
C
C  COMPUTE BOUNDARY STRESSES
C
      DO 14 I=1,NN
      DO 14 J=1,3
14    S(I,J)=0.
C
C     LOOP OVER ALL BOUNDARY ELEMENTS
C
      DO 30 I=1,NE
      II=INC(I,1)
      IF=INC(I,2)
      CC1=(Y(IF)-Y(II))/C(I)
      CC2=(X(II)-X(IF))/C(I)
      CALL FENC(C8,C9,C10,CC1,CC2,I)
      DO 30 JP=1,2
      IIF=INC(I,JP)
      XFAC=2.
      IF(IDUP(IIF).NE.0.OR.ISYM(IIF).NE.0)XFAC=1.
      DO 30 IR=1,3
      M=0
      DO 30 IP=1,2
      IO=2*IIF+IP-2
      S(IIF,IR)=S(IIF,IR)+G(IR,IP)*P(IO)/XFAC
      DO 30 JR=1,2
      M=M+1
      IO=2*INC(I,IP)+JR-2
30    S(IIF,IR)=S(IIF,IR)-H(IR,M)*XM(IO)/XFAC
C
C     PRINT VALUES ON THE BOUNDARY
C
      DO 13 I=1,NN
      SA(4)=C11*(S(I,1)+S(I,3))
      IF(ISYM(I).NE.0)S(I,2)=0.
13    WRITE(IWR,15)I,XM(2*I-1),XM(2*I),S(I,1),S(I,2),S(I,3),SA(4)
15    FORMAT (2X,I4,1X,6(1X,F13.4))
      NG=10
      NG1=11
      DO 310 I=1,NG1
      J=29-I
      XG(I)=YN(J)
310   FG(I)=S(J,1)
      CALL AST(NG,NG1,SXM,XG,FG)
      DO 320 I=1,NG1
      J=17+I
      XG(I)=YN(J)
320   FG(I)=XM(2*J-1)
      CALL AST(NG,NG1,UM2,XG,FG)
      NG=3
```

```
      NG1=4
      DO 330 I=1,NG1
      J=5-I
      XG(I)=XN(J)
330   FG(I)=S(J,3)
      CALL AST(NG,NG1,SYM,XG,FG)
      NG=12
      NG1=13
      DO 340 I=1,NG1
      J=4+I
      XG(I)=XN(J)
340   FG(I)=XM(2*J)
      CALL AST(NG,NG1,VM,XG,FG)
      DO 350 I=1,NG1
      J=I+4
      XG(I)=YN(J)
350   FG(I)=XM(2*J-1)
      CALL AST(NG,NG1,UM1,XG,FG)
      IF(NN.EQ.NT) GO TO 5
C
C     COMPUTE INTERNAL VALUES
C
      NN1=NN+1
      ICOD=4
C
C  LOOP OVER ALL INTERNAL POINTS
C
      DO 16 I=NN1,NT
      U(1)=0.
      U(2)=0.
      DO 17 J=1,3
17    SA(J)=0.
C
C     SYMMETRY LOOP
C
      DO 20 ISY=1,IFA,NIF
      XS=X(I)
      YS=Y(I)
      IF(ISY.EQ.2.OR.ISY.EQ.4) YS=2.*YSYM-YS
      IF(ISY.GE.3) XS=2.*XSYM-XS
      GO TO (70,71,71,73),ISY
71    IIS=4-ISY
      IFS=IIS
      GO TO 70
73    IIS=1
      IFS=2
C
C     INTEGRATE OVER THE BOUNDARY
C
70    DO 20 J=1,NE
      II=INC(J,1)
      IF=INC(J,2)
      CALL FUNC(ICOD,J,C1,C2,C3,C4,C5,C6,C7,PD,II,IF,XS,YS,ISY,
     *IIS,IFS)
      DO 20 K=1,3
      M=0
      DO 20 NX=1,2
      DO 20 NV=1,2
      M=M+1
      ICA=2*INC(J,NX)+NV-2
      IF(K.LT.3) U(K)=U(K)-H(K,M)*XM(ICA)+G(K,M)*P(ICA)
20    SA(K)=SA(K)-HL(K,M)*XM(ICA)+GL(K,M)*P(ICA)
      SA(4)=C11*(SA(1)+SA(3))
16    WRITE(IWR,15) I,U(1),U(2),SA(1),SA(2),SA(3),SA(4)
5     RETURN
      END
```

```
      SUBROUTINE FENC(C8,C9,C10,CC1,CC2,I)
C
C  EXPRESSIONS FOR STRESSES AT BOUNDARY NODES
C
      COMMON /A/ D(2,2),XI(6,3),W(6,3),IDUP(100),INC(100,2),C(100),
     *S(100,3),ISYM(100),X(100),Y(100),IFIP(108),A(108,108),P(112),
     *XM(108),A1(62,62),BB1(62,62),A2(112,112),BB2(112,112),
     *AB1(174,348),XXM(174),XP(108),XQ(62),PQ(62),XN(28),YN(28)
      COMMON /A4/ H(3,4),G(3,4),HL(3,4),GL(3,4)
C
C  MATRIX H
C
      CO=-C8/C(I)
      H(1,1)=CO*CC2**3
      H(1,2)=-CO*CC1*CC2**2
      H(1,3)=-H(1,1)
      H(1,4)=-H(1,2)
      H(2,1)=H(1,2)
      H(2,2)=CO*CC2*CC1**2
      H(2,3)=-H(1,2)
      H(2,4)=-H(2,2)
      H(3,1)=H(2,2)
      H(3,2)=-CO*CC1**3
      H(3,3)=-H(2,2)
      H(3,4)=-H(3,2)
C
C  MATRIX G
C
      G(1,1)=CC1**3+C10*CC1*CC2**2
      G(1,2)=-CC2*CC1**2+C9*CC2**3
      G(2,1)=CC2**3-C9*CC2*CC1**2
      G(2,2)=CC1**3-C9*CC1*CC2**2
      G(3,1)=-CC1*CC2**2+C9*CC1**3
      G(3,2)=CC2**3+C10*CC2*CC1**2
      RETURN
      END


      SUBROUTINE AODI(RA,CTA)
C  INPUT X AND Y COORDINATES
      COMMON /A/ D(2,2),XI(6,3),W(6,3),IDUP(100),INC(100,2),C(100),
     *S(100,3),ISYM(100),X(100),Y(100),IFIP(108),A(108,108),P(112),
     *XM(108),A1(62,62),BB1(62,62),A2(112,112),BB2(112,112),
     *AB1(174,348),XXM(174),XP(108),XQ(62),PQ(62),XN(28),YN(28)
      R2=SQRT(3.)/2.
      DO 10 I=1,9
      J=I-1
      X(I)=-.5
10    Y(I)=R2-RA/8.*J
      DO 20 I=10,22
      J=I-10
      CT=CTA*J
      X(I)=-.5+RA*SIN(CT)
20    Y(I)=R2-RA*COS(CT)
      DO 30 I=23,31
      J=I-23
      X(I)=-.5+RA*(1.-J/8.)
30    Y(I)=R2
      RETURN
      END

      SUBROUTINE ADDJ(RA,CTA)
      COMMON /A/ D(2,2),XI(6,3),W(6,3),IDUP(100),INC(100,2),C(100),
     *S(100,3),ISYM(100),X(100),Y(100),IFIP(108),A(108,108),P(112),
```

```
     *XM(108),A1(62,62),BB1(62,62),A2(112,112),BB2(112,112),
     *AB1(174,348),XXM(174),XP(108),XQ(62),PQ(62),XN(28),YN(28)
      R3=SQRT(3.)
      R2=R3/2.
      DO 10 I=1,4
      J=I-1
      X(I)=.5-(1.-RA)*J/3.
10    Y(I)=R2
      DO 20 I=5,17
      J=I-5
      CT=CTA*J
      X(I)=-.5+RA*COS(CT)
20    Y(I)=R2-RA*SIN(CT)
      DO 30 I=18,28
      J=I-18
      X(I)=-.5
30    Y(I)=R2-RA-(R3-RA)*J/10.
      DO 40 I=29,32
      J=I-28
      X(I)=-X(J)
40    Y(I)=-Y(J)
      DO 50 I=33,45
      J=I-28
      X(I)=-X(J)
50    Y(I)=-Y(J)
      DO 60 I=46,56
      J=I-28
      X(I)=-X(J)
60    Y(I)=-Y(J)
      RETURN
      END


      SUBROUTINE ADD1
      COMMON /A/ D(2,2),XI(6,3),W(6,3),IDUP(100),INC(100,2),C(100),
     *S(100,3),ISYM(100),X(100),Y(100),IFIP(108),A(108,108),P(112),
     *XM(108),A1(62,62),BB1(62,62),A2(112,112),BB2(112,112),
     *AB1(174,348),XXM(174),XP(108),XQ(62),PQ(62),XN(28),YN(28)
      DO 2 I=1,8
      INC(I,1)=I
2     INC(I,2)=I+1
      DO 4 I=9,20
      INC(I,1)=I+1
4     INC(I,2)=I+2
      DO 6 I=21,28
      INC(I,1)=I+2
6     INC(I,2)=I+3
      RETURN
      END

      SUBROUTINE ADD2
      COMMON /A/ D(2,2),XI(6,3),W(6,3),IDUP(100),INC(100,2),C(100),
     *S(100,3),ISYM(100),X(100),Y(100),IFIP(108),A(108,108),P(112),
     *XM(108),A1(62,62),BB1(62,62),A2(112,112),BB2(112,112),
     *AB1(174,348),XXM(174),XP(108),XQ(62),PQ(62),XN(28),YN(28)
      DO 2 I=1,3
      INC(I,1)=I
2     INC(I,2)=I+1
      DO 4 I=4,15
      INC(I,1)=I+1
4     INC(I,2)=I+2
      DO 6 I=16,25
      INC(I,1)=I+2
6     INC(I,2)=I+3
      DO 8 I=26,28
      INC(I,1)=I+3
```

```
8       INC(I,2)=I+4
        DO 10 I=29,40
        INC(I,1)=I+4
10      INC(I,2)=I+5
        DO 12 I=41,50
        INC(I,1)=I+5
12      INC(I,2)=I+6
        RETURN
        END


        SUBROUTINE NCSBC(VE,UO,VO,DF,DM)
        COMMON /A/ D(2,2),XI(6,3),W(6,3),IDUP(100),INC(100,2),C(100),
       *S(100,3),ISYM(100),X(100),Y(100),IFIP(108),A(108,108),P(112),
       *XM(108),A1(62,62),BB1(62,62),A2(112,112),BB2(112,112),
       *AB1(174,348),XXM(174),XP(108),XQ(62),PQ(62),XN(28),YN(28)
        COMMON /ABC/ JS1(240),JS2(240),DEL(240),JS3(240),IX(240)
        SR2=SQRT(3.)/2.
        DO 10 I=1,240
10      DEL(I)=0.
        DEL(113)=VE*X(9)
        DEL(114)=VE*Y(9)
                 DEL(116)=VE*X(10)
                 DEL(117)=VE*Y(10)
                 DEL(120)=VE*X(11)
                 DEL(121)=VE*Y(11)
                 DEL(124)=VE*X(12)
                 DEL(125)=VE*Y(12)
                 DEL(128)=VE*X(13)
                 DEL(129)=VE*Y(13)
                 DEL(132)=VE*X(14)
                 DEL(133)=VE*Y(14)
                 DEL(136)=VE*X(15)
                 DEL(137)=VE*Y(15)
                 DEL(140)=VE*X(16)
                 DEL(141)=VE*Y(16)
                 DEL(144)=VE*X(17)
                 DEL(145)=VE*Y(17)
                 DEL(148)=VE*X(18)
                 DEL(149)=VE*Y(18)
                 DEL(152)=VE*X(19)
                 DEL(153)=VE*Y(19)
                 DEL(156)=VE*X(20)
                 DEL(157)=VE*Y(20)
                 DEL(160)=VE*X(21)
                 DEL(161)=VE*Y(21)
                 DEL(164)=VE*X(22)
                 DEL(165)=VE*Y(22)
                 DEL(168)=VE*X(23)
                 DEL(169)=VE*Y(23)
        DO 20 I=1,31
        J1=176+2*I-1
        IF (I.LE.9) GOTO 30
        IF (I.GT.9.AND.I.LE.18) GOTO 40
        IF (I.GT.18.AND.I.LE.21) GOTO 50
        IF (I.GT.21) GOTO 60
30      DEL(J1)=-.5*(UO+DF)
        GOTO 20
40      DEL(J1)=SR2*(VO+DF)
        GOTO 20
50      DEL(J1)=SR2*(VO+DM)
        GOTO 20
60      DEL(J1)=-.5*(UO+DM)
20      CONTINUE
        RETURN
        END
```

```
      SUBROUTINE CONNECT(A1,B1,A2,B2,N1,N2,A)
      DIMENSION A1(2*N1,2*N1),B1(2*N1,2*N1),A2(2*N2,2*N2),
     *B2(2*N2,2*N2),A(2*N1+2*N2,4*N1+4*N2)
      N=N1+N2
      DO 10 I=1,2*N
      DO 10 J=1,4*N
10    A(I,J)=0.
      DO 20 I=1,2*N1
      DO 20 J=1,2*N1
      A(I,J)=A1(I,J)
      A(I,J+2*N1)=B1(I,J)
20    CONTINUE
      DO 30 I=2*N1+1,2*(N1+N2)
      DO 30 J=4*N1+1,4*N1+2*N2
      A(I,J)=A2(I-2*N1,J-4*N1)
      A(I,J+2*N2)=B2(I-2*N1,J-4*N1)
30    CONTINUE
      RETURN
      END


      SUBROUTINE KILLCOL(A,N,F,JA,JB,DELTA)
      DIMENSION A(2*N,4*N),F(2*N)
      DO 20 I=1,2*N
      IF (JB.LT.0) GOTO 10
      F(I)=F(I)-DELTA*A(I,JB)
      IF (JA.GT.0) A(I,JA)=A(I,JA)+A(I,JB)
      A(I,JB)=0.
      GOTO 20
10    JJ=-JB
      F(I)=F(I)+DELTA*A(I,JJ)
      IF (JA.GT.0) A(I,JA)=A(I,JA)-A(I,JJ)
      A(I,JJ)=0.
20    CONTINUE
      RETURN
      END


      SUBROUTINE REDUCE(A,N,F,NC,J1,J2,DEL,J3,IX)
      COMMON/RW/IRE,IWR
      DIMENSION A(2*N,4*N),F(2*N),J1(NC),J2(NC),DEL(NC)
      DIMENSION IX(NC),J3(NC)
      DO 100 JC=1,NC
      JA=J1(JC)
      JB=J2(JC)
      DELTA=DEL(JC)
      CALL KILLCOL(A,N,F,JA,JB,DELTA)
100   CONTINUE
      DO 200 K=1,NC
      IX(K)=K
      MX=J3(K)
      DO 150 I=1,NC
      MS=J3(I)
      IF (MS**2.GT.MX**2) THEN
      IX(K)=I
      MX=MS
      ENDIF
150   CONTINUE
      ID=IX(K)
      J3(ID)=0
200   CONTINUE
      DO 300 K=1,NC
      L=IX(K)
```

```
      JB=J2(L)
      IF (JB.LT.0) JB=-JB
      IF (JB.GT.4*N-K) GOTO 300
      DO 250 I=1,2*N
      DO 240 MI=JB,4*N-K
      A(I,MI)=A(I,MI+1)
240   CONTINUE
250   CONTINUE
300   CONTINUE
      RETURN
      END


      SUBROUTINE MUL(U,V,T,M,K,N)
      DIMENSION U(M,K),V(K,N),T(M,N)
      DO 20 I=1,M
      DO 20 J=1,N
      T(I,J)=0.
      DO 20 L=1,K
      T1=U(I,L)*V(L,J)
20    T(I,J)=T(I,J)+T1
      RETURN
      ENO


      SUBROUTINE IVS(A,B,C,ME,MF,N,EP)
      DIMENSION A(N,N),B(N),C(N),ME(N),MF(N)
      DO 10 K=1,N
      Y=0.
      00 20 I=K,N
      DO 20 J=K,N
      IF (ABS(A(I,J)).LE.ABS(Y)) GO TO 20
      Y=A(I,J)
      I2=I
      J2=J
20    CONTINUE
      IF (ABS(Y).LE.EP) GO TO 32
      IF (I2.EQ.K) GO TO 33
      DO 11 J=1,N
      W=A(I2,J)
      A(I2,J)=A(K,J)
11    A(K,J)=W
33    IF (J2.EQ.K) GO TO 44
      00 22 I=1,N
      W=A(I,J2)
      A(I,J2)=A(I,K)
22    A(I,K)=W
44    ME(K)=I2
      MF(K)=J2
      DO 50 J=1,N
      IF (J-K) 2,3,2
3     B(J)=1./Y
      C(J)=1.
      GO TO 4
2     B(J)=-A(K,J)/Y
      C(J)=A(J,K)
4     A(K,J)=0.
      A(J,K)=0.
50    CONTINUE
      DO 40 I=1,N
      DO 40 J=1,N
40    A(I,J)=A(I,J)+C(I)*B(J)
10    CONTINUE
      DO 60 L=1,N
      K=N-L+1
      K1=ME(K)
```

```
      K2=MF(K)
      IF (K1.EQ.K) GO TO 70
      DO 55 I=1,N
      W=A(I,K1)
      A(I,K1)=A(I,K)
55    A(I,K)=W
70    IF (K2.EQ.K) GO TO 60
      DO 66 J=1,N
      W=A(K2,J)
      A(K2,J)=A(K,J)
66    A(K,J)=W
60    CONTINUE
      RETURN
32    EP=-EP
      RETURN
      END

      SUBROUTINE AST(N,N1,S,X,F)
      DIMENSION X(15),F(15)
      S=0.0
      DO 10 I=1,N
      J=I+1
      H=X(J)-X(I)
      T=(F(I)+F(J))*H/2.
10    S=S+T
      RETURN
      END
```

DEVELOPMENTS IN
THEORETICAL AND APPLIED MECHANICS

Volume XV

Proceedings of the
Fifteenth Southeastern Conference on
Theoretical and Applied Mechanics

Edited by

Sathya. V. Hanagud, Professor of Aerospace Engineering
Manohar. P. Kamat, Professor of Aerospace Engineering
Charles. E. Ueng, Professor of Civil Engineering

COLLEGE OF ENGINEERING
GEORGIA INSTITUTE OF TECHNOLOGY
Atlanta, Georgia, U.S.A.

Appendix B

Paper presented in the 8th International Conference

on Composite Materials

(July 1991, Honolulu, Hawaii)

"Lamina Constitutive Equations Based on

the Mechanical Behavior of a Pressurized Composite Tube"

By Wan-Lee Yin and Lin Yang

Lamina Constitutive Equations Based on the Mechanical Behavior of a Pressurized Composite Tube

Wan-Lee Yin and Lin Yang
Georgia Institute of Technology
Atlanta, Georgia 30332

ABSTRACT

The mechanical behavior of a filament-wound composite tube under an internal pressure load depends on the constitutive properties of the resin and fiber materials, the fiber volume fraction V_f, and the winding angle α. The range of variation and the relative magnitudes of the in-plane strains ϵ_1, ϵ_2 and γ_{12} in a lamina of the tube (referred to the directions parallel and perpendicular to the fibers) vary significantly with the winding angle. For tubes of various winding angles, the experimental data of the strains and the corresponding internal pressure may be used to infer the constitutive equations of a lamina within and beyond the linearly elastic regime. It is found that the mechanical responses of filament-wound tubes cannot be accurately predicted by classical engineering theories of lamina stiffness (e.g., rule of mixture, the Halpin-Tsai equations and certain estimates based on variational bounds) in terms of the properties of the fibers and the resin material. A principal reason appears to be that the fibers in a filament-wound structure are not initially straight so that, at a low or moderate level of extensional strain, these fibers manifest an apparent Young's modulus that is appreciably smaller than the documented value.

In the present work, the lamina constitutive equations are determined from the experimental results of glass/epoxy and carbon/epsxy filament-wound tubes with various winding angles. Beyond a small initial range of the pressure load, the lamina stress-strain relation deviates significantly from linearly elastic behavior due to the occurrence of a large shear strain γ_{12} (unless the winding angle is very close to the "optimum winding angle", in which case γ_{12} remains small under a large pressure load). Furthermore, the nonlinear relation between τ_{12} and γ_{12} is strongly affected by the transverse in-plane normal stress σ_2. The following relations are shown to be in good agreement with experimental results over a wide range of strain:

$$\sigma_1 = S_{11}\,\epsilon_1 + S_{12}\,\epsilon_2\,, \qquad \sigma_2 = S_{12}\,\epsilon_1 + S_{22}\,\epsilon_2 - f(\gamma_{12})\,,$$

$$\tau_{12} = -\,\epsilon_2\, f'(\gamma_{12}) + g(\gamma_{12})\,, \tag{1}$$

where f and g are, respectively, even and odd functions. In the range of small shearing strain, g is a linear function and f practically vanishes. The elastic moduli S_{11}, S_{12} and S_{22} are determined from

$$\epsilon_1\,(S_{11} + S_{12}) + \epsilon_2\,(S_{12} + S_{22}) = \sigma_1 + \sigma_2 = \sigma_x + \sigma_\theta \tag{2}$$

$$S_{12}/S_{11} = \nu_f V_f + \nu_m(1-V_f)\,, \tag{3}$$

where ν_f and ν_m are the Poisson's ratios of the fibers and the resin material. Experimental results for a tube of a specific winding angle provide a set of coefficients ϵ_1, ϵ_2 and $\sigma_x + \sigma_\theta$ of Eq. (2). As the winding angle varies, an overdetermined system of equations is generated and it is found that these equations yield consistent results for the elastic moduli S_{11}, S_{12} and S_{22}. The material functions f and g are subsequently determined from the experimental data corresponding to large shearing strain.

Appendix C

"Separation Failure of a Helical Delamination

in a Filament-Wound Composite Tube"

By Wan-Lee Yin

Developments in Theoretical and Applied Mechanics, Vol. XV

(Proceedings of the 15th Southeastern Conference on Theoretical and

Applied Mechanics, March, 1990, Atlanta, GA), pp. 440-447.

SEPARATION FAILURE OF A HELICAL DELAMINATION IN A FILAMENT-WOUND COMPOSITE TUBE

Wan-Lee Yin
School of Civil Engineering
Georgia Institute of Technology
Atlanta, GA 30332

Abstract

The failure of a filament-wound tube loaded under internal pressure may be precipitated by the separation of a delaminated layer from the inner surface of the tube. Equilibrium solutions are obtained for a separated face sheet in the shape of a helical strip. The face sheet is subjected to reduced membrane tension in its separated state (in comparison with the attached state). The amplitude of separation and the peeling moment along the boundary of the helical strip increase with the pressure load, but the peeling moment does not vary appreciable when the width of the strip increases. Hence the helical strip may grow in width under a sufficiently large pressure load.

Introduction

In their experimental study of the failure of glass/polyester filament-wound tubes under internal pressure load, Spencer and Hull [1] reported several differnt modes of failure depending on the winding angle and the loading conditlon (i.e., open-ended or close-ended). The events precipitating or accompanying failure include whitening, weepage, large in-plane shear deformation, matrix cracking, fiber breaking and delamination. Interlaminar cracking and delamination, accompanied by buckling and bending of the tube, were observed in open-ended tubes with relatively large winding angles (45 degrees or above). It may appear somewhat puzzling that delamination should occur in a tube loaded under internal pressure, where the adjacent layers are pressed against each other, and that buckling and bending of the tube should happen under the open-ended test conditon, where the axial load in the tube vanishes. However, while the tube wall taken as a whole is stressed only in circumferential tension, the individual unidirectional laminae are subjected additionally to shearing stresses $\tau_{x\theta}$ and $\tau_{\theta x}$, except in the end regions adjacent to the free edges of the tube. As the pressure load increases, the two families of fibers tend to reorient themselves toward the circumferntial direction, producing a scissoring action at the cross-over points of intersecting fibers and introducing large shear deformation in the interleaving sheet of resin material. This shear action may tend to initiate interlaminar fracture in certain regions of a laminar interface where, because of the nonuniformity and peculiarity associated with the winding process, the thickness of the interleaving resin material is particularly thin. Incidentally, since the cross-over points are densely distributed over a laminar interface, the scissoring action effectively produces a system of distributed interacting couple moments between adjacent laminae. The presence of this distributed couple moment implies that, in each lamina, the shearing stress components $\tau_{x\theta}$ and $\tau_{\theta x}$ are generally not equal.

Because a single unidirectional layer or a group of layers has significant anisotropy, interlaminar fracture may tend to form or propagate along the general direction of one family of filaments. Hence a helical strip of delaminated face sheet, consisting of one or several filament-wound layers, may be formed in the inner surface of the tube. This delaminated face sheet is subjected to the same

lsrge membrane tenaion as that which appliea to the lntact portlon of the face sheet, so long aa the delaminated portion maintalns contact wlth the main body of the tube wall. Although there is a tendency for the delaminated sheet to deflect inward and aepaate from the tube wall, ao as to reduce the membrane tansion and the str_in energy, this tendency is balanced by the outward action of the lnternal pressure. However, lf the membrane tension and shear deformatlon in the delaminated face sheet are sufficientiy large, scattered resin cracka may be formed ao that the face sheet may fail to contain the pressure. Eventually, the fluid pressure on both sides of the delamlnated face sheet may become equalized and separation of the face sheet from the tube wall may occur spontaneously to relleve the membrane tenalon.

In the present work, equiilibrium solutions of a helical strip of the aeparated face sheet are determined for a specific combinatlon of geometrical and material parameters. The amplitude of separatlon and the peeling bending moment along the boundary of the strip increase approximately in proportlon to the internal pressure load. However, the boundary peeling moment do not vary slgnificantly with the increase of the strip wldth. The magnltude of this moment is indicative of the peeling action which tends to cause delamination growth. Thua, under a sufficientiy large pressure load a delaminated strip may separate from the tube wall snd may subaequently grow to reach a signifIcant width. This causes local atiffness degradation and rediatribution of the stresaes in the main body of the tube and may precipitste further cracking, bending, buckling and eventual catastrophic faiiure.

While the present analysis is motivated by the consideratlon of delamlnation failure in a pressurized fllament-wound tube, it yields a class of closed-form snalytical solutions of thin anisotropic shells with a nontrivlal type of geometry. Hence the reaults may have some intrinsic interest. The solutions sre rsther similar to postbuckling solutions slthough the physical process is not characterized by a bifurcation state. The problems of snap buckiing and peeling of a thin cylindrical isotropic layer from the inner surface of a thick cylinder aubjected to rsdialiy inward dispiacement load have been studied by several authors [2-5]. The layer buckles because it waa under large membrane compression in the prebuckiing state and because buckiing substantiaiiy relieves the compression. The present analysis suggests that delamination failure may also occur in tubes loaded under internal pressure where the tube wall is subjected to membrane tension, and that the formation and growth of deiamination in a filament-wound tube may assume the shape of a helicai strip rather than a sector of the cylindrical aurface.

Forsulation of the Equlllbrlum Solution of a Separated Helical Deiamlnation

We aasume that a heiicsl strip of deiaminstion exists close to the inner surface of the tube as a result of the acissoring action between sdjmcent filament-wound layers due to a sufficientiy large preasure load. The boundaries of the heiical strip are parallei to one families of filaments (say, with the winding angle φ; the fiiaments of the other family are wound at the angle $-\varphi$). The thickness of the deiamlnated face sheet, h, is assumed to be small compared to the totai thickness of the tube, t, so that when the face sheet deflects inward and separates from the tube wall, the existing deformation of the latter is not appreciabiy affected. This existing deformation is characterized by uniform axial snd circumferentiai strains ϵ_x° and ϵ_θ°. So long as the helical strip of the delsminated face sheet remains attached to the tube wall, it is subjected to the same mebrane strains ϵ_x° and ϵ_θ°. Let a system of orthogonsl geodeaic coordinstes (x_1, x_2) be defined so thst $x_2 = \pm s^\circ$ along the boundaries of the helical strip (Fig. 1). Referred to the new coordinate axes, the components of the membrane strain are

$$\epsilon_1^\circ = \frac{1}{2}(\epsilon_\theta^\circ + \epsilon_x^\circ) - \frac{1}{2}(\epsilon_\theta^\circ - \epsilon_x^\circ)\cos 2\varphi\,, \qquad \gamma_{12}^\circ = \frac{1}{2}(\epsilon_\theta^\circ - \epsilon_x^\circ)\sin 2\varphi\,, \quad (1a,b)$$

$$\epsilon_2^\circ = \tfrac{1}{2}(\epsilon_\theta^\circ + \epsilon_x^\circ) + \tfrac{1}{2}(\epsilon_\theta^\circ - \epsilon_x^\circ)\cos 2\varphi. \tag{1c}$$

When the face sheet separates from the tube wall and deflects inward, the tangential displacement components u and v (along the x_1- and x_2-directions, respectively) and the <u>inward</u> radial displacement w of the middle surface of the face sheet are constant in the x_1-direction, i.e., they depend only on the coordinate x_2. The following nonlinear strain-displacement relations may be established

$$\begin{aligned} \epsilon_1 &= \epsilon_1^\circ - w/R_1, \quad \gamma_{12} = \gamma_{12}^\circ + v', \\ \epsilon_2 &= \hat{\epsilon}_2 + z w'' = \epsilon_2^\circ - w/R_2 + u' + \tfrac{1}{2}(w')^2 + z w'', \end{aligned} \tag{2}$$

where the primes indicate differentiation with respect to x_2. In the preceding expression,

$$R_1 = R/\sin^2\varphi, \quad R_2 = R/\cos^2\varphi.$$

R is the radius of curvature of the middle surface of the undeformed face sheet and z is the coordinate in the thickness direction measured <u>radially outward</u> from the middle surface. The membrane force resultants and the moment resultants in the face sheet (Fig. 2) are related to the curvature increment $w''(x_2)$ and the middle-plane strains ϵ_1, $\hat{\epsilon}_2$ and γ_{12} through the relations

$$\begin{Bmatrix} N_1 \\ N_2 \\ N_{12} \\ M_2 \end{Bmatrix} = \begin{bmatrix} A_{11} & A_{12} & A_{16} & B_{12} \\ A_{12} & A_{22} & A_{26} & B_{22} \\ A_{16} & A_{26} & A_{66} & B_{26} \\ B_{12} & B_{22} & B_{26} & D_{22} \end{bmatrix} \begin{Bmatrix} \epsilon_1 \\ \hat{\epsilon}_2 \\ \gamma_{12} \\ w'' \end{Bmatrix}. \tag{3}$$

If the thickness h of the face sheet is very small compared to the initial mean radius R, then the stiffness matrices $[A_{ij}]$, $[B_{ij}]$ and $[D_{ij}]$ may be approximated by

$$[A_{ij}] = \Sigma \int [Q_{ij}]\, dz, \quad [B_{ij}] = \Sigma \int [Q_{ij}]\, z\, dz, \quad [D_{ij}] = \Sigma \int [Q_{ij}]\, z^2 dz, \tag{4}$$

where $[Q_{ij}]$ is the matrix of anisotropic elastic moduli of a filament-wound layer referred to the local geodesic coordinate directions and where the summations extend over all layers in the face sheet. We note that while Eq. (4) is exactly valid in the case of a flat face sheet, it is only approximately valid for an initially curved sheet. A segment of the face sheet with unit length in the x_1-direction has the strain energy

$$U = \tfrac{1}{2}\int_{-s^*}^{s^*} (N_1 \epsilon_1 + N_2 \hat{\epsilon}_2 + N_{12}\gamma_{12} + M_2 w'')\, dx_2 \tag{5}$$

It is further assumed that, due to significant membrane tension caused by the pressure load, the face sheet has developed scattered matrix cracks which allow equalization of the fluid pressure on the two sides of the sheet but which do not significantly degradate the stiffness properties of the face sheet. Then the fluid pressure performs no work as the sheet deflects inward. The work of the boundary forces and moments is also negligible if the main body of the tube wall does not undergo appreciable additional deformation when the face sheet separates. Hence the potential energy of the face sheet is equal to the strain energy. Setting the first variation of the potential energy to zero and making use of the boundary conditions along $x_2 = \pm s^*$

$$u = 0, \quad v = 0, \tag{6a}$$
$$w = 0, \quad w' = 0, \tag{6b}$$

one obtains the following equilibrium equations for the membrane forces and moments

$$N_{12}' = 0, \quad N_2' = 0, \tag{7a}$$

$$N_1/R_1 + N_2/R_2 - M_2'' + (N_2 w')' = 0. \tag{7b}$$

Except for the presence of the term N_1/R_1 in the third equation, the last two equilibrium equations are identical to those of a shallow arch.

Substituting the strain-displacement relations into the first two equilibrium equations, one obtains

$$\Psi' + \tfrac{1}{2}(w')^2 = -\frac{1}{\Delta}\begin{vmatrix} A_{26} & N_2 - A_{12}\epsilon_1^0 - A_{22}\epsilon_2^0 - A_{26}\gamma_{12}^0 + \left(\frac{A_{12}}{R_1} + \frac{A_{22}}{R_2}\right)w - B_{22}w'' \\ A_{66} & N_{12} - A_{16}\epsilon_1^0 - A_{26}\epsilon_2^0 - A_{66}\gamma_{12}^0 + \left(\frac{A_{16}}{R_1} + \frac{A_{26}}{R_2}\right)w - B_{26}w'' \end{vmatrix}, \tag{8a}$$

$$\mathfrak{K}' = \frac{1}{\Delta}\begin{vmatrix} A_{22} & N_2 - A_{12}\epsilon_1^0 - A_{22}\epsilon_2^0 - A_{26}\gamma_{12}^0 + \left(\frac{A_{12}}{R_1} + \frac{A_{22}}{R_2}\right)w - B_{22}w'' \\ A_{26} & N_{12} - A_{16}\epsilon_1^0 - A_{26}\epsilon_2^0 - A_{66}\gamma_{12}^0 + \left(\frac{A_{16}}{R_1} + \frac{A_{26}}{R_2}\right)w - B_{26}w'' \end{vmatrix}, \tag{8b}$$

where

$$\Delta = \begin{vmatrix} A_{22} & A_{26} \\ A_{26} & A_{66} \end{vmatrix}.$$

Then the third equation of (7) becomes

$$\begin{vmatrix} D_{22} & B_{22} & B_{26} \\ B_{22} & A_{22} & A_{26} \\ B_{26} & A_{26} & A_{66} \end{vmatrix} R_1 w'''' + 2\begin{vmatrix} B_{12} - R_1 N_2/2 & A_{12} & A_{16} \\ B_{22} & A_{22} & A_{26} \\ B_{26} & A_{26} & A_{66} \end{vmatrix} w'' + \begin{vmatrix} A_{11} & A_{12} & A_{16} \\ A_{12} & A_{22} & A_{26} \\ A_{16} & A_{26} & A_{66} \end{vmatrix} \frac{w}{R_1}$$
$$= \begin{vmatrix} A_{11} & A_{12} & A_{16} \\ A_{12} & A_{22} & A_{26} \\ A_{16} & A_{26} & A_{66} \end{vmatrix} \epsilon_1^0 + \begin{vmatrix} N_2 R_1/R_2 & A_{12} & A_{16} \\ -N_2 & A_{22} & A_{26} \\ -N_{12} & A_{26} & A_{66} \end{vmatrix}. \tag{9}$$

This fourth-order linear differential equation for $w(x_2)$ contains two undetermined parameters N_2 and N_{12}. Additional equations for the determination of the parameters may be obtained by integrating Eqs. (8a) and (8b) across the width of the strip and making use of the boundary conditions of Eq (6). This yields

$$\frac{\Delta}{2}\int_{-s^*}^{s^*}(w')^2 dx_2 = -2s^*\begin{vmatrix} A_{26} & N_2 - A_{12}\epsilon_1^0 - A_{22}\epsilon_2^0 \\ A_{66} & N_{12} - A_{16}\epsilon_1^0 - A_{26}\epsilon_2^0 \end{vmatrix} - \begin{vmatrix} A_{26} & \frac{A_{12}}{R_1} + \frac{A_{22}}{R_2} \\ A_{66} & \frac{A_{16}}{R_1} + \frac{A_{26}}{R_2} \end{vmatrix}\int_{-s^*}^{s^*} w\, dx_2, \tag{10a}$$

$$0 = 2s^*\begin{vmatrix} A_{22} & N_2 - A_{12}\epsilon_1^0 - A_{26}\gamma_{12}^0 \\ A_{26} & N_{12} - A_{16}\epsilon_1^0 - A_{66}\gamma_{12}^0 \end{vmatrix} + \begin{vmatrix} A_{22} & A_{12}/R_1 \\ A_{26} & A_{16}/R_1 \end{vmatrix}\int_{-s^*}^{s^*} w\, dx_2. \tag{10b}$$

The differential equation (9), the boundary conditions (6b) and Eq. (10) completely determine the deflection function $w(x_2)$ and the constants N_2 and N_{12}.

The procedure of solution may proceed as follows. Under a given pressure load, the membrane strain components in the (x, θ) coordinates may be calculated using the stiffness properties of the whole tube. The strain components in the geodesic coordinates (x_1, x_2) are calculated from Eq. (1). Estimates of the values of N_2 and N_{12} are tentatively made, and the boundary value problem of Eqs. (9) and (6b) are solved. The resulting closed form solution for $w(x_2)$ involves products of exponential and sinusoidal functions. This solution is substituted into Eq. (10) to see whether the two equalities are satisfied. If they are not satisfied, then the estimated values of N_2 and N_{12} are modified and the process is repeated until Eq. (10) is satisfied to within certain permissible margin of error. The solution is physical possible only if $w(x_2)$ is never negative, otherwise it should be discarded.

Solution for a Unidirectional Face Sheet

For the sake of simplicity we consider the case of a unidirectionally wound face sheet. For such a sheet the bending-stretching coupling matrix $[B_{ij}]$ vanishes as do the shearing-extension coupling A_{16} and A_{26}. Furthermore,

$$D_{22} = (1/12)h^2 A_{22} .$$

Hence the governing differential equation (9) reduces to

$$\frac{1}{12}(R_1 h)^2 w'''' - \frac{N_2 R_1^2}{A_{22}} w'' + (A_{22})^{-2}\begin{vmatrix} A_{11} & A_{12} \\ A_{12} & A_{22} \end{vmatrix} w = (A_{22})^{-2}\begin{vmatrix} A_{11} & A_{12} \\ A_{12} & A_{22} \end{vmatrix} \frac{R_1 \epsilon_1^o}{h} + \frac{R_1 N_2}{h A_{22}}\left(\frac{R_1}{R_2} + \frac{A_{12}}{A_{22}}\right).$$

The second condition of Eq. (10) is identically satisfied and the first condition yields

$$\frac{1}{2}\int_{-s^*}^{s^*} (w')^2 dx_2 = 2s^*\left(\frac{N_2}{A_{22}} - \frac{A_{12}}{A_{22}}\epsilon_1^o - \epsilon_2^o\right) + \left(\frac{A_{12}}{A_{22}}\frac{1}{R_1} + \frac{1}{R_2}\right)\int_{-s^*}^{s^*} w\, dx_2 .$$

We introduce dimensionless variables ξ and $W(\xi)$ and dimensionless parameters a, T, ϵ^*, α and β as follows

$$W(\xi) = w(x_2)/h , \qquad \xi = x_2/\sqrt{R_1 h} , \qquad a = s^*/\sqrt{R_1 h} ,$$

$$T = \frac{N_2 R_1}{h A_{22}} , \qquad \epsilon^* = \frac{R_1 \epsilon_1^o}{h} , \qquad \alpha = (A_{22})^{-2}\begin{vmatrix} A_{11} & A_{12} \\ A_{12} & A_{22} \end{vmatrix} , \qquad \beta = \frac{R_1}{R_2} + \frac{A_{12}}{A_{22}} . \tag{11}$$

Then the two preceeding equations become

$$\frac{1}{12}\frac{d^4 W}{d\xi^4} - T\frac{d^2 W}{d\xi^2} + \alpha W = \alpha\epsilon^* + \beta T , \tag{12}$$

$$\frac{1}{2}\int_{-a}^{a}\left(\frac{dW}{d\xi}\right)^2 d\xi - \beta\int_{-a}^{a} W\, d\xi + 2a\left\{\left(\frac{A_{12}}{A_{22}} + \frac{\epsilon_2^o}{\epsilon_1^o}\right)\epsilon^* - T\right\} = 0 . \tag{13}$$

The solution of Eq. (12) satisfying the boundary conditions of Eq. (6b) is

$$W(\xi) = (\epsilon^* + T\beta/\alpha)(1 + C_1 \cosh\lambda\xi \cos\mu\xi + C_2 \sinh\lambda\xi \sin\mu\xi), \tag{14}$$

where,

$$\lambda = \left\{(3\alpha)^{1/2} + 3T\right\}^{1/2} , \qquad \mu = \left\{(3\alpha)^{1/2} - 3T\right\}^{1/2} , \tag{15}$$

$$C_1 = -(2/H)(\lambda a \cosh \lambda a \sin \mu a + \mu a \sinh \lambda a \cos \mu a),$$
$$C_2 = -(2/H)(\mu a \cosh \lambda a \sin \mu a - \lambda a \sinh \lambda a \cos \mu a), \qquad (16)$$
$$H = \mu a \sinh 2\lambda a + \lambda a \sin 2\mu a.$$

The solution given by Eq. (14) contains an undetermined parameter T. The parameter may be determined by the following condition which is obtained by substituting (14) into Eq. (13):

$$2C_3(\epsilon^* + T\beta/\alpha)^2 + C_4(\epsilon^* + T\beta/\alpha) - \left\{1 + \frac{\beta}{\alpha}\left(\frac{\epsilon_2^\circ}{\epsilon_1^\circ} + \frac{A_{12}}{A_{22}}\right)\right\} T = 0, \qquad (17)$$

where,

$$C_3 = \frac{\lambda^2+\mu^2}{8H^2}\left[\left\{\frac{(\mu a)^2}{2\lambda a}\sinh 2\lambda a - \frac{(\lambda a)^2}{2\mu a}\sin 2\mu a\right\}(\cosh 2\lambda a - \cos 2\mu a)\right.$$
$$\left. - \left\{(\lambda a)^2 + (\mu a)^2\right\}(1 - \cosh 2\lambda a \cos 2\mu a)\right], \qquad (18)$$
$$C_4 = \frac{A_{12}}{A_{22}} + \frac{\epsilon_2^\circ}{\epsilon_1^\circ} + \beta\left\{\frac{2\lambda\mu}{(\lambda^2+\mu^2)H}(\cosh 2\lambda a - \cos 2\mu a) - 1\right\}.$$

The left hand alde of Eq. (17) is a complicated function of T because the parametera λ and μ are dependent on T (see Eq. (15)). However, for any given vaiue of T, Eq. (17) provides a quadratic equation for $\epsilon^* + T\beta/\alpha$ which may be readily aolved. We note that the membrane strain ratio $\epsilon_2^\circ/\epsilon_1^\circ$ in the main body of the tube wall ia independent of the pressure load so long as the response of the tube remains linearly elaatic. Hence, if for any specified delamination geometry we are interested in a <u>family</u> of separation solutions corresponding to *increasing values of* the membrane strain parameter ϵ^*(i.e., corresponding to a certain range of the pressure load in the tube), then Eq. (17) may be easily solved for $\epsilon^* + T\beta/\alpha$ corresponding to a aeries of values of T. No iteration process need be conducted for thia purpose. The results of the computation yield the dependence of the various properties of the aeparation aolution upon the strain parameter ϵ^*. For a helical delamination atrip with unidirectional winding at the angle $\varphi = 65°$, the dependence of the nondimenaional center-line deflection, w(0)/h, and of the nondimensional boundary peeling moment, $M_z R/(D_{zz}\sin^2 65°) = d^2W/dz^2$, upon the membrane atrain parameter $\epsilon^*$are shown, respectively, in Figs. 3 and 4 for two diatinct values of the normailzed delamination width (2α = 2 and 5). The relations are approximately linear. Here the anisotropic elastic properties of the unidirectional face sheet are taken from or computed according to Ref. [1]. Specifically,

$$E_1 = 42.0 \text{ GPa}, \quad E_2 = 11.05 \text{ GPa}, \quad G_{12} = 4.73 \text{ GPa}, \quad \nu_{12} = 0.278, \quad \nu_{21} = 0.073,$$
$$\alpha = 3.72, \quad \beta = 0.495, \quad A_{12}/A_{22} = 0.277.$$

Assuming that the tube is composed of equal number of layers wound at $\pm\varphi$ angles, and uaing the open-end condition, the following membrane strain ratios are found:

$$\epsilon_x^\circ/\epsilon_\theta^\circ = -0.360, \quad \epsilon_2^\circ/\epsilon_1^\circ = -0.155.$$

Figurea 5 and 6 show, respectively, the variation of the center line deflection and of the boundary peeling moment with the increase in the delamination width for three fixed valuea of the membrane strain parameter, $\epsilon^* = 0.5, 1.0, 1.5$. The

center-line deflection at first increases and later shows slight decrease as the delamination width increases, while the boundary peeling moment remains approximately constant in the entire range of delamination width for which the solutions of Eq. (17) can be obtained. It should be noted that, as a quadratic equation for $\epsilon^* + T\beta/\alpha$, Eq. (17) always has real solutions if T is nonnegative. When N_2 changes from tension to compression and when its magnitude becomes sufficiently large, the roots of Eq. (17) change from real into complex. Along each curve in Figs. 5 and 6, the value of T associated with a data point decreases in the direction of increasing delamination width. The curves terminate at right end points where the roots $\epsilon^* + T\beta/\alpha$ of Eq. (17) become complex.

The strain energy release rate associated with delamination growth may be evaluated by using the J-integral method [8,7]. The result is an algebraic expression in terms of the boundary peeling moment, the constant force N_2 and the membrane strains in the main body of the tube wall. If the membrane strain parameter ϵ^* is sufficiently large, the energy-release rate at the delamination boundary may exceed the fracture toughness and the width of the delamination may increase spontaneously.

A fundamental assumption used in the present analysis is that the delaminated face sheet is thin compared to the wall thickness of the tube so that the separation of the face sheet does not appreciably affect the existing deformation in the main body of tube wall. A more elaborate analysis without using this assumption may indicate the effect of delamination separation on the deformation of the main tube and provide better insight into the failure process initiated by delamination separation.

Acknowledgment The work reported here is made possible by a grant from the U. S. Army Research Office to Georgia Institute of Technology. The author gratefully acknowledges the financial support.

References

1. Spencer, B. and Hull, D., "Effect of Winding Angle on the Failure of Filament Wound Pipe," Composites, Vol. 9, pp. 263-271, 1978.

2. Zagustin, E. A. and Herrmann, G., "Stability of an Elastic Ring in a Rigid Cavity," Journal of Applied Mechanics, Vol. 34, pp. 263-270, 1967.

3. Kerr, A. D. and Soifer, M. T., "The Linearization of the Prebuckling State and Its Effect on the Determined Instability Loads," Journal of Applied Mechanics, Vol. 38, pp. 775-783, 1969.

4. El-Bayoumy, L., "Buckling of a Circular Elastic Ring Confined to a Uniformly Contracting Circular Boundary," Journal of Applied Mechanics, Vol. 39, pp. 758-766, 1972.

5. Bottega, W. J., "On Thin Film Delamination Growth in a Contracting Cylinder," International Journal of Solids and Structures, Vol. 24, pp.13-26, 1988.

6. Yin, W.-L. and Wang, J. S. T., "The Energy-Release Rate in the Growth of a One-Dimensional Delamination," Journal of Applied Mechanics, Vol. 51, pp.939-941, 1984.

7. Yin, W.-L., "The Effects of Laminated Structure on Delamination Buckling and Growth," Journal of Composite Materials, Vol. 22, pp. 502-517, 1988.

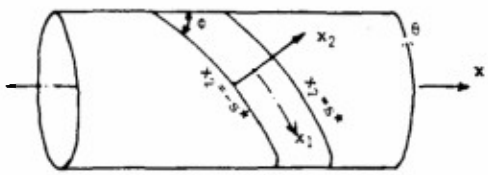

Figure 1

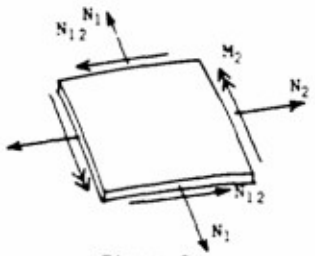

Figure 2

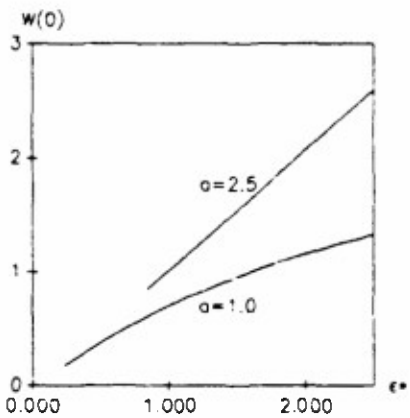

Figure 3

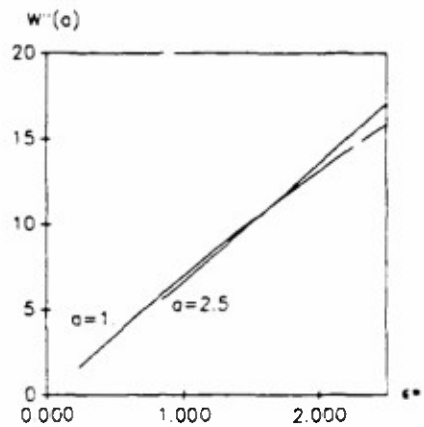

Figure 4

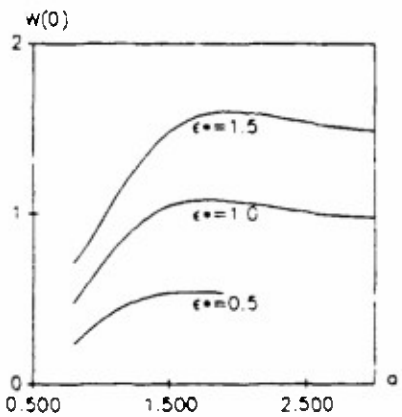

Figure 5

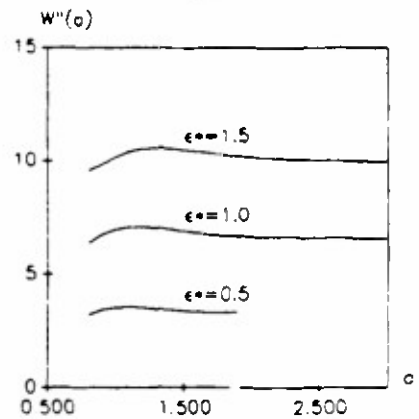

Figure 6

Appendix D

"Refined Buckling and Postbuckling Analysis of Two-Dimensional Delaminations: Part I -- Analysis and Validation"

By Wan-Lee Yin and K. C. Jane

International Journal of Solids and Structures, In Press

Int. J. Solids Structures Vol. 00, No. 00, pp. 0000–0000, 1991
Printed in Great Britain.

0020–7683/91 $3.00 + .00

REFINED BUCKLING AND POSTBUCKLING ANALYSIS OF TWO-DIMENSIONAL DELAMINATIONS PART I—ANALYSIS AND VALIDATION†

W.-L. YIN
School of Civil Engineering, Georgia Institute of Technology, Atlanta, Georgia 30332, U.S.A.

and

K. C. JANE
BMT International, Inc., Columbia, Maryland 21044, U.S.A.

(*Received* 4 *October* 1990; *in revised form* 16 *June* 1991)

Abstract—An analytical procedure, based on the Rayleigh–Ritz method and von Karman's nonlinear theory of plates, is developed for computing the buckling loads and the postbuckling solutions of laminated anisotropic elliptical plates. Lengthy algebraic equations governing the expansion coefficients of the displacement functions are generated by a symbolic algorithm. Using polynomial displacement expansions of different orders, postbuckling solutions with increasing accuracy are systematically computed for isotropic and laminated elliptical plates. The deflections, the force and moment resultants and the energy release rates associated with the solutions of various orders are compared to assess the trend of convergence. The comparison suggests the lowest order polynomial expansion needed to obtain reasonably accurate results for the force and moment resultants and the energy release rates. Previous Rayleigh–Ritz postbuckling solutions based on lower-order polynomial expansions of the displacements are found to yield results with significant errors.

1. INTRODUCTION

The problems of sublaminate buckling and crack growth in a homogeneous plate or a composite laminate containing an interior delamination have been the subject of extensive analytical and numerical studies in the past decade.‡ For thin strip or elliptical delamination models the bifurcation loads obtained by two- or three-dimensional finite element analysis [see, for example, Shivakumar and Whitcomb (1985) and Yin *et al.* (1986a)] are not appreciably different from the corresponding results of the homogeneous or laminated plate analysis. In the case of strip delamination models, closed-form analytical solutions of the postbuckling deformation may be obtained in the context of the classical laminated plate theory (Chai *et al.*, 1981; Yin *et al.*, 1986b). The energy release rates associated with delamination growth may be evaluated, by using the path-independent J-integral, in terms of the membrane forces and the bending moments in the cracked and intact parts of the laminate at the crack tip (Yin and Wang, 1984). The results also agree well with the energy release rates calculated by finite element analysis and the closure integral method (Yin *et al.*, 1986a). These findings suggest that accurate postbuckling analysis based on a homogeneous or laminated plate theory (preferably with the inclusion of the effect of the thickness–shear deformation) may be used, in place of expensive three-dimensional analysis, to obtain reliable results for the buckling and growth behavior a delamination with a general shape.

For a two-dimensional thin-film delamination with an arbitrary shape, the local membrane forces and the bending and twisting moments at a point of the delamination front determine the pointwise value of the energy release rate (Bottega, 1983; Storakers and Anderson, 1988). If one assumes a delamination growth criterion depending only on the local energy release rate, without discriminating among its separate components associated

† A preliminary version of this paper was presented in the ASME Winter Annual Meeting, San Francisco, CA, December 1989.

‡ For general reviews of the subject, see the recent articles by Garg (1988) and Storakers (1989). Additional information may be found in Kapania and Raciti (1989), Simitses (1989) and Yin (1989).

with the three fracture modes, then the principal task involved in the analysis of two-dimensional delaminations is that of obtaining accurate bifurcation loads and postbuckling solutions from the von Karman equations. This task is formidable if one wishes to take into account the postbuckling deformations of both the cracked and intact parts of the plate. It is difficult even if one completely ignores the bending deformation and the non-uniformity of the membrane deformation in the base laminate as induced by local buckling of a thin delaminated layer, i.e. if one adopts the "thin-film" approximation for the delaminated layer by imposing the conditions of vanishing deflection and slope along the crack boundary.

The difficulties arise from the geometrical non-linearity and the strong coupling, between the in-plane and transverse displacements, that are intrinsic to the von Karman equations of plates. Postbuckling solutions which ignore or inadequately account for such effects cannot yield reliable results for the membrane forces, the bending and twisting moments, or the energy release rates. Many existing solution schemes for the bending and buckling of plates use the calculated results of the central deflection as the principal test of accuracy. The criterion is inadequate and misleading because, as shown in this paper, relatively crude postbuckling solutions may yield sufficiently accurate results for the central deflection and, at the same time, very poor results for the membrane forces and the energy release rates.

In their analysis of transversely loaded and postbuckled *rectangular* plates, Chia (1980) and co-workers obtained solutions by the Rayleigh–Ritz method, using beam eigenfunctions to approximate the displacements. As the number of terms in the displacement functions increases, the results for the transverse deflection converge reasonably fast. However, accurate results for the membrane forces and the bending moments are considerably more difficult to obtain. Following Chia's method, Feng (1983) presented a computerized analysis of the postbuckling behavior of laminated anisotropic rectangular plates. His analysis used a much larger set of beam eigenfunctions to represent the displacements of the middle surface. He did not provide information concerning the rate or trend of convergence of the solutions.

In a postbuckling analysis of a simply-supported circular plate under axisymmetric compression, Friedrichs and Stoker (1941, 1942) noticed significant non-uniform membrane deformation in an advanced stage of postbuckling. As the boundary compression increases, the membrane forces in a central portion of the plate eventually become tensile. Bodner (1973) found a similar behavior in the axisymmetric postbuckling of a clamped circular plate. Due to the coupling in the von Karman equations, the non-uniformity of the in-plane deformation has important implications for the bending deformation. This results in large curvature of the deformed middle surface around the boundary of the plate. Although the perturbation method used by these authors is applicable only to within a certain range of the strain load, the general validity of their conclusions beyond this range has been confirmed by an analysis based on direct integration of the von Karman equations (Yin, 1985).

As suggested by Chai and Babcock (1985), the buckling and growth behavior associated with general two-dimensional delaminations may be studied by an analysis of elliptical delaminations. However, the displacement functions used by Chai and Babcock contain an insufficient number of terms to reflect significant non-uniform membrane deformation and the boundary effect. In the present work, power series expansions of the displacements are systematically enlarged to obtain higher order approximate solutions of postbuckled, clamped elliptical plates by means of the Rayleigh–Ritz method. In the special case of axisymmetric postbuckling of circular plates, Rayleigh–Ritz solutions of the various orders are compared with the solutions obtained by direct integration of the von Karman equations (Yin, 1985). The comparison indicates convergence of the Rayleigh–Ritz solutions, and suggests the lowest order approximate solution needed to obtain reasonably accurate results for the membrane forces, the bending moments and the energy release rates. The solutions of the required order are then computed for elliptical delaminations with various aspect ratios. It is found that these postbuckling solutions also show significant boundary effect, although in a manner more complex and fascinating than in the case of axisymmetric postbuckling of circular plates.

A Rayleigh–Ritz procedure involving a relatively large number of coefficients for the non-linear analysis of anisotropic plates requires the use of symbolic algebra. A symbolic computational program is written in the Fortran code to generate the total potential energy function in terms of the geometrical, material and loading parameters, as well as the undetermined expansion coefficients (Jane, 1989). The program also yields the non-linear algebraic equations governing the undetermined coefficients. Solutions of the equations are computed for isotropic circular and elliptical plates (in Part I of this paper) and for cross-ply and angle-ply elliptical laminates (in Part II).

Non-dimensionalization of the postbuckling problem shows that the total potential energy function depends on the geometrical and stiffness parameters through certain specific combinations. Consequently, *all postbuckling solutions of anisotropic elliptical (or rectangular) laminates may be generated from appropriate solutions of anisotropic circular (or square) laminates by rescaling of variables*. This important conclusion, shown in Section 2.3 of the present paper, allows a significant saving of computational effort in a parametric study of the postbuckling behavior of various types of elliptical laminates.

2. RAYLEIGH–RITZ SOLUTIONS

We consider an elliptical delamination with semi-axial lengths a and b along the X- and Y-coordinate axes, respectively. Let the base plate be subjected to uniform in-plane normal and shearing strains E_{XX}, E_{YY} and E_{XY}. If the strains are predominantly compressive and if they are sufficiently large, then the elliptical delaminated layer buckles and becomes completely or partially detached from the base plate. We assume that the thickness of the delaminated layer, h, is small compared to the thickness of the base plate, so that, within the base plate, the bending deformation and the non-uniformity of the in-plane deformation caused by the buckling of the delaminated layer are both negligibly small. Then the delaminated layer is subjected to displacement boundary conditions along the entire elliptical boundary. The total potential energy of the layer is identical to its total strain energy.

2.1. *The total potential energy*

In the buckled states, the membrane strains and the curvatures of the middle surface of the delaminated layer may be approximated by

$$\varepsilon_1 = \frac{\partial U}{\partial X} + \frac{1}{2}\left(\frac{\partial W}{\partial X}\right)^2, \quad \varepsilon_2 = \frac{\partial V}{\partial Y} + \frac{1}{2}\left(\frac{\partial W}{\partial Y}\right)^2, \quad \varepsilon_6 = \frac{\partial U}{\partial Y} + \frac{\partial V}{\partial X} + \frac{\partial W}{\partial X}\frac{\partial W}{\partial Y}$$

$$\kappa_1 = \frac{\partial^2 W}{\partial X^2}, \quad \kappa_2 = \frac{\partial^2 W}{\partial Y^2}, \quad \kappa_6 = 2\frac{\partial^2 W}{\partial X\,\partial Y} \tag{1}$$

where U and V are the in-plane displacements on the middle surface and where W is the transverse deflection. The force and moment resultants of the delaminated layer are related to the strains and the curvatures according to the equation

$$\begin{Bmatrix} N_1 \\ N_2 \\ N_6 \\ M_1 \\ M_2 \\ M_6 \end{Bmatrix} = \begin{bmatrix} A_{11} & A_{12} & A_{16} & B_{11} & B_{12} & B_{16} \\ A_{12} & A_{22} & A_{26} & B_{12} & B_{22} & B_{26} \\ A_{16} & A_{26} & A_{66} & B_{16} & B_{26} & B_{66} \\ B_{11} & B_{12} & B_{16} & D_{11} & D_{12} & D_{16} \\ B_{12} & B_{22} & B_{26} & D_{12} & D_{22} & D_{26} \\ B_{16} & B_{26} & B_{66} & D_{16} & D_{26} & D_{66} \end{bmatrix} \begin{Bmatrix} \varepsilon_1 \\ \varepsilon_2 \\ \varepsilon_6 \\ \kappa_1 \\ \kappa_2 \\ \kappa_6 \end{Bmatrix}.$$

The stiffness coefficients in the last equation are those defined in the classical laminated plate theory. If we abbreviate the preceding equation in the form

$$N_i = A_{ij}\varepsilon_j + B_{ij}\kappa_j, \quad M_i = B_{ij}\varepsilon_j + D_{ij}\kappa_j \tag{2}$$

then the total potential energy of the delaminated layer may be expressed as

$$\Pi = \frac{1}{2}\int\int \sum_i (N_i\varepsilon_i + M_i\kappa_i)\, dX\, dY \tag{3}$$

where the integration is carried over the region of the plate and the index i is summed over 1, 2 and 6.

2.2. *Non-dimensianalization and palynamial approximatian*

We introduce the following non-dimensional variables and constants:

$$\begin{aligned} x &\equiv X/a, \quad u \equiv Ua/h^2, \quad w \equiv W/h, \\ y &\equiv Y/b, \quad v \equiv Vb/h^2, \quad \lambda \equiv a/b, \end{aligned} \qquad \bar{\Pi} \equiv \frac{2(a/h)^4}{A_{11}ab}\Pi$$

$$\varepsilon_{xx} \equiv (a/h)^2 E_{XX}, \quad \varepsilon_{xy} \equiv (ab/h^2)E_{XY}, \quad \varepsilon_{yy} = (b/h)^2 E_{YY}$$

$$\bar{\varepsilon}_1 = (a/h)^2\varepsilon_1, \quad \bar{\varepsilon}_2 = (b/h)^2\varepsilon_2, \quad \bar{\varepsilon}_6 = (ab/h^2)\varepsilon_6$$

$$\bar{\kappa}_1 = (a^2/h)\kappa_1, \quad \bar{\kappa}_2 = (b^2/h)\kappa_2, \quad \bar{\kappa}_6 = (ab/h)\kappa_6. \tag{4}$$

Let the displacement functions be approximated by the polynomial expansions

$$\begin{aligned} U &= axE_{XX} + byE_{XY} + (1-x^2-y^2)P(x,y)h^2/a \\ V &= axE_{XY} + byE_{YY} + (1-x^2-y^2)Q(x,y)h^2/b \\ W &= h(1-x^2-y^2)^2 R(x,y) \end{aligned}$$

where P, Q and R are polynomial functions of the normalized coordinate variables. All boundary conditions along $(X/a)^2 + (Y/b)^2 = 1$ are satisfied by these displacement functions. Now the non-dimensional displacement components u, v and w have the following expressions:

$$\begin{aligned} u &= x\varepsilon_{xx} + y\varepsilon_{xy} + Z_0 P(x,y) \\ v &= x\varepsilon_{xy} + y\varepsilon_{yy} + Z_0 Q(x,y) \\ w &= Z_0^2 R(x,y) \end{aligned} \tag{5}$$

where,

$$Z_0 \equiv 1 - x^2 - y^2.$$

From eqn (1) we obtain the following expressions for the normalized membrane strain components and the normalized curvatures

$$\begin{aligned} \bar{\varepsilon}_1 &= \varepsilon_{xx} + (Z_0 P)_{,x} + (1/2)[(Z_0^2 R)_{,x}]^2 \\ \bar{\varepsilon}_2 &= \varepsilon_{yy} + (Z_0 Q)_{,y} + (1/2)[(Z_0^2 R)_{,y}]^2 \\ \bar{\varepsilon}_6 &= 2\varepsilon_{xy} + (Z_0 P)_{,y} + (Z_0 Q)_{,x} + (Z_0^2 R)_{,x}(Z_0^2 R)_{,y} \\ \bar{\kappa}_1 &= (Z_0^2 R)_{,xx}, \quad \bar{\kappa}_2 = (Z_0^2 R)_{,yy}, \quad \bar{\kappa}_6 = 2(Z_0^2 R)_{,xy}. \end{aligned}$$

The polynomials P, Q and R are defined by their respective set of coefficients $\{a_i\}$, $\{b_i\}$ and $\{c_i\}$. The number of coefficients in each set depends on the degree of the polynomial. We define twenty-one functions L_{ij}, M_{ij} and N_{ij} ($i, j = 1, 2, 6$; L_{ij} and N_{ij} are symmetric

with respect to the indices while M_{ij} is not) by the following integrals over the unit disk $x^2+y^2 \leqslant 1$:

$$L_{ij} = \iint \bar{\varepsilon}_i \bar{\varepsilon}_j \, dx \, dy, \quad M_{ij} = \iint \bar{\varepsilon}_i \bar{\kappa}_j \, dx \, dy, \quad N_{ij} = \iint \bar{\kappa}_i \bar{\kappa}_j \, dx \, dy. \tag{6}$$

It is clear that L_{ij}, M_{ij} and N_{ij} depend only on the normalized strain loads ε_{xx}, ε_{yy}, ε_{xy} and the coefficients $\{a_i\}$, $\{b_i\}$, $\{c_i\}$ of the polynomials P, Q and R. Thus, once the forms of the polynomials P, Q and R are selected, all the integrals L_{ij}, M_{ij} and N_{ij} can be evaluated and expressed *explicitly* in terms of the normalized strain loads in the base plate and the coefficients of the polynomials. These explicit expressions are *independent* of the geometrical and material parameters (a, b, h, A_{ij}, B_{ij}, D_{ij}) of the anisotropic elliptical plate. They depend only on the approximation scheme used in the analysis.

Equation (3) now yields the following expression for the non-dimensional potential energy:

$$\bar{\Pi} = \frac{(a/h)^4}{A_{11}} \sum_i \sum_j \delta_i \delta_j [A_{ij} L_{ij} + (2/h) B_{ij} M_{ij} + (1/h^2) D_{ij} N_{ij}] \tag{7}$$

where i and j are again summed over 1, 2 and 6 and

$$\delta_1 = (h/a)^2, \quad \delta_2 = (h/b)^2, \quad \delta_6 = h^2/ab.$$

Once an approximating scheme involving a set of undetermined coefficients a_i, b_i and c_i is adopted and the integrals L_{ij}, M_{ij} and N_{ij} are explicitly obtained, the total potential energy for any particular geometrical and material configuration of the elliptical laminate can be obtained straightforwardly. This yields an expression for the normalized potential energy:

$$\bar{\Pi} = \bar{\Pi}(a_i, b_i, c_i, \varepsilon_{xx}, \varepsilon_{yy}, \varepsilon_{xy}; \lambda, A_{ij}/A_{11}, B_{ij}/hA_{11}, D_{ij}/h^2 A_{11}). \tag{8}$$

It is clear that the major task involved in the explicit determination of the last expression is that of evaluating the integrals of eqn (6). Each integral is a sum of integrals of the following form:

$$\begin{aligned} I(m,n,k) &= \int_{-1}^{1} \int_{-(1-x^2)^{1/2}}^{(1-x^2)^{1/2}} x^m y^n (1-x^2-y^2)^k \, dx \, dy \\ &= \int_0^1 (1-r^2)^k r^{m+n+1} \, dr \int_0^{2\pi} \cos^m \theta \sin^n \theta \, d\theta. \end{aligned}$$

One has $I(m, n, k) = 0$ if m and n are not both even. Otherwise,

$$I(m,n,k) = 2\pi \cdot \frac{1 \cdot 3 \cdot 5 \cdots (m-1) \cdot 1 \cdot 3 \cdot 5 \cdots (n-1)}{2 \cdot 4 \cdot 6 \cdots (m+n)} \cdot \sum_{p=0}^{k} \frac{(-1)^p k!}{(2+2p+m+n) p! (k-p)!}.$$

Depending on the number of coefficients involved in the polynomials P, Q and R, the final approximate expression for the potential energy may contain hundreds or even thousands of terms. The intermediate steps leading to the final expression may involve hundreds of thousands of integrals. A special purpose symbolic algorithm was developed in the Fortran code to generate the potential energy function and the algebraic equations governing the undetermined coefficients (Jane, 1989). Cyber 205 supercomputer at the University of Georgia was used to implement the symbolic algorithm and to solve the resulting system of non-linear algebraic equations. This system consists of the following equations

$$\frac{\partial \bar{\Pi}}{\partial a_i} = 0, \quad \frac{\partial \bar{\Pi}}{\partial b_i} = 0, \quad \frac{\partial \bar{\Pi}}{\partial c_i} = 0. \tag{9}$$

Furthermore, the strains in the base plate corresponding to the states of bifurcation (from membrane states to buckled states) may be calculated from the following characteristic equation

$$\begin{vmatrix} \frac{\partial^2 \bar{\Pi}}{\partial a_i \partial a_j} & \frac{\partial^2 \bar{\Pi}}{\partial a_i \partial b_j} & \frac{\partial^2 \bar{\Pi}}{\partial a_i \partial c_j} \\ \frac{\partial^2 \bar{\Pi}}{\partial b_i \partial a_j} & \frac{\partial^2 \bar{\Pi}}{\partial b_i \partial b_j} & \frac{\partial^2 \bar{\Pi}}{\partial b_i \partial c_j} \\ \frac{\partial^2 \bar{\Pi}}{\partial c_i \partial a_j} & \frac{\partial^2 \bar{\Pi}}{\partial c_i \partial b_j} & \frac{\partial^2 \bar{\Pi}}{\partial c_i \partial c_j} \end{vmatrix}_{(a_i = b_i = c_i = 0)} = 0. \tag{10}$$

Equation (9) will be solved for the coefficients $\{a_i\}$, $\{b_i\}$ and $\{c_i\}$ by using the Newton–Raphson iteration scheme. In order to have suitable initial estimates of the coefficients, it is imperative to start from a bifurcation point (corresponding to a set of coefficients satisfying eqn (10)) in the load space, and to obtain successive postbuckling solutions along a load path by imposing small load increments. The coordinates of the load space are the imposed in-plane normal and shearing strains in the base plate. Since eqn (9) consists of algebraic equations which depend linearly on the coefficients $\{a_i\}$ and $\{b_i\}$, the emphasis in each iteration step is to obtain the proper increment of $\{c_i\}$. The new iterated values of $\{a_i\}$ and $\{b_i\}$ may be obtained easily by solving a subsystem of linear equations using the current estimates of $\{c_i\}$.

2.3. *Generating all postbuckling solutions of elliptical laminates from appropriate solutions of circular laminates by rescaling*

The structure of the expression for the total potential energy, eqn (7), implies the following important conclusion: all postbuckling solutions of elliptical laminates (according to the von Karman theory) may be obtained from the postbuckling solutions of circular laminates by rescaling the coordinate variables, the thickness, the stiffness parameters and the membrane strain loads. Indeed, if one wants to obtain the postbuckling solution U, V, W of an elliptical laminate with the thickness h, semi-axial lengths a and b, stiffness matrices $[A_{ij}]$, $[B_{ij}]$ and $[D_{ij}]$, under the strain loads E_{xx}, E_{yy} and E_{xy} in the base plate, one only has to obtain the solution U_0, V_0, W_0 of a circular laminate with the thickness h_0, radius r_0 and stiffness coefficients

$$\begin{aligned} S^0_{11} &= (r_0/h_0)^4(h/a)^4 S_{11}, & S^0_{12} &= (r_0/h_0)^4(h^2/ab)^2 S_{12} \\ S^0_{22} &= (r_0/h_0)^4(h/b)^4 S_{22}, & S^0_{16} &= (r_0/h_0)^4(h^4/a^3 b) S_{16} \\ S^0_{66} &= (r_0/h_0)^4(h^2/ab)^2 S_{66}, & S^0_{26} &= (r_0/h_0)^4(h^4/ab^3) S_{26} \end{aligned}$$

(where S_{ij} stands for A_{ij}, B_{ij} and D_{ij} in succession) under the strain loads

$$E^0_{xx} = (h_0/r_0)^2(a/h)^2 E_{xx}, \quad E^0_{yy} = (h_0/r_0)^2(b/h)^2 E_{yy}, \quad E^0_{xy} = (h_0/r_0)^2(ab/h^2) E_{xy}.$$

The solution for the elliptical laminate is related to the solution of the circular laminate by

$$U = (h/h_0)^2(r_0/a) U_0, \quad V = (h/h_0)^2(r_0/b) V_0, \quad W = (h/h_0) W_0.$$

The validity of this statement follows from the fact that the two laminates have the same $\delta_i\delta_j A_{ij}$, $\delta_i\delta_j B_{ij}$ and $\delta_i\delta_j D_{ij}$, the strain loads on the respective laminates have the same normalized values ε_{xx}, ε_{yy} and ε_{xy}, and the respective solutions have the same normalized displacements u, v and w. From eqn (7) one finds that the potential energy functions of the

two laminates are identical except for a multiplicative factor. Hence the stationary condition for the respective potential energies are realized by the same normalized displacement solution u, v and w.

Since one has the freedom to choose the radius r_0 and the thickness h_0 of the circular laminate arbitrarily, there are infinitely many postbuckling solutions of circular laminates which correspond, according to the preceding relations, to the same postbuckling solution of a given elliptical laminate. Furthermore, one may introduce new rectangular coordinate axes in such a way that, for the circular laminate, these axes coincide with the principal directions of the imposed strain tensor in the base plate (whose components in the original coordinates are E^0_{XX}, E^0_{YY} and E^0_{XY}). Referred to the new coordinate system the strain load in the base plate of the circular laminate has no shearing component. Consequently, in a parametric study of the postbuckling behavior of elliptical delaminations of various geometrical and material configurations under general membrane strain loads in the base plate, it is sufficient to deal only with *circular* anisotropic delaminations under biaxial strain loads. All solutions of the elliptical delaminations may be generated from appropriate solutions of circular delaminations according to the preceding rescaling rules.

It is clear that a similar procedure may be used to generate all postbuckling solutions of rectangular anisotropic laminates from appropriate solutions of square laminates subjected to general in-plane loads.

2.4. *Symmetry conditions on the displacement functions*

For a general anisotropic elliptical delamination in a base plate under the in-plane strain loads E_{XX}, E_{YY} and E_{XY}, the postbuckling displacement functions in the delaminated sublaminate satisfy the conditions of central symmetry:

$$u(-x,-y) = -u(x,y), \quad v(-x,-y) = -v(x,y), \quad w(-x,-y) = w(x,y). \tag{11}$$

These symmetry conditions imply that the polynomials P and Q in eqn (5) contain only terms of odd degrees while the polynomial R contains only terms of even degrees. In the cases of isotropic, specially orthotropic, or cross-ply sublaminates with aligned loading and symmetry axes, additional symmetry conditions with respect to the coordinate axes apply:

$$\begin{aligned} u(x,y) &= -u(-x,y) = u(x,-y), \\ v(x,y) &= v(-x,y) = -v(x,-y). \\ w(x,y) &= w(-x,y) = w(x,-y). \end{aligned} \tag{12}$$

Equations (11) and (12) taken together imply that P, Q and R have the forms

$$P(x,y) = xP_1(x^2,y^2), \quad Q(x,y) = yQ_1(x^2,y^2), \quad R(x,y) = R_1(x^2,y^2). \tag{13}$$

If P_1 and Q_1 include only constant terms and R_1 includes, in addition, linear terms in x_2 and y_2, then the displacement functions reduce to those used by Chai and Babcock (1985) in their five-term Rayleigh–Ritz solutions. Rayleigh–Ritz solutions of higher orders $\{p, r\}$ may be considered where p and r refer, respectively, to the degrees of the polynomials P (same as that of Q) and R of eqn (5). For example, for the solution of the order $\{5, 4\}$ satisfying the full symmetry conditions of eqns (11) and (12), the polynomials P, Q and R of eqn (5) have the following forms:

$$\begin{aligned} P(x,y) &= x(a_1 + a_2x^2 + a_3y^2 + a_4x^4 + a_5x^2y^2 + a_6y^4) \\ Q(x,y) &= y(b_1 + b_2x^2 + b_3y^2 + b_4x^4 + b_5x^2y^2 + b_6y^4) \\ R(x,y) &= c_1 + c_2x^2 + c_3y^2 + c_4x^4 + c_5x^2y^2 + c_6y^4. \end{aligned} \tag{14}$$

The Rayleigh–Ritz solutions examined in the present work are of the orders $\{1, 2\}$,

$\{3,4\}$, $\{5,4\}$, $\{5,6\}$ and $\{7,6\}$. The highest degree of the polynomial and the total number of undetermined coefficients for each order of solutions are shown in Table 1.

In the remaining sections of this paper (Part I), we obtain and examine postbuckling solutions of homogeneous isotropic circular and elliptical plates. These solutions possess the full symmetry properties of eqns (11) and (12). Postbuckling solutions of anisotropic elliptical sublaminates generally satisfy eqn (11) only and their displacement expansions include a considerably larger number of terms, as indicated in Table 1. Such solutions are presented in Part II.

3. CLAMPED ISOTROPIC CIRCULAR PLATES UNDER AXISYMMETRIC COMPRESSION

In a previous work (Yin, 1985), axisymmetric postbuckling solutions of a clamped isotropic circular plate have been obtained by numerical integration of the governing differential equations. These solutions may be used as the standard of comparison for the Rayleigh–Ritz solutions of various orders. The comparison was made over a range of the strain load from the bifurcation strain to about ten times the bifurcation strain. This wide range of the strain load far exceeds the usual range considered in existing postbuckling analyses or appropriate to most practical applications. The intension is to set an extremely severe test of the validity of the lower order approximate solutions by comparing the results with the higher order solutions, and with the solutions obtained by direct integration (Yin, 1985; hereafter called the "reference solutions"), at widely different levels of the strain load. This accounts for the very significant discrepancies in the results shown in the following figures of this paper.

3.1. *Central deflection, membrane force and bending moment*

Consider a circular sublaminate of radius a and thickness h, made of a homogeneous, isotropic elastic material with Young's modulus E and Poisson's ratio ν. The sublaminate has the bending rigidity $D = Eh^3/12(1-\nu^2)$. In an axisymmetric deformation, the radial membrane force and the radial bending moment are related to the radial and transverse displacements, U_r and W, according to the formulae

$$N_r = \frac{Eh}{(1-\nu^2)}\left(\frac{\mathrm{d}U_r}{\mathrm{d}r} + \nu\frac{U_r}{r}\right), \quad M_r = D\left(\frac{\mathrm{d}^2W}{\mathrm{d}r^2} + \frac{\nu}{r}\frac{\mathrm{d}W}{\mathrm{d}r}\right).$$

The strain load in the base plate is given by

$$E_{XX} = E_{YY} = -\varepsilon_0, \quad E_{XY} = 0.$$

We define the non-dimensional compressive radial force and the non-dimensional bending moment as follows:

$$P(\xi) = -\frac{N_r a^2}{D} = 12\left(\frac{\mathrm{d}u}{\mathrm{d}\xi} + \frac{u}{\xi}\right), \quad M(\xi) = \frac{a^2}{hD}M_r = \frac{\mathrm{d}^2w}{\mathrm{d}\xi^2} + \frac{1}{\xi}\frac{\mathrm{d}w}{\mathrm{d}\xi}$$

where a is the radius of the circular plate, w is as defined in eqn (4), and

Table 1. Rayleigh–Ritz solutions of various orders

Solution label	$\{1,2\}$	$\{3,4\}$	$\{5,4\}$	$\{5,6\}$	$\{7,6\}$
Max. degree of P & Q	1	3	5	5	7
Max. degree of R	2	4	4	6	6
Number of coefficients, when eqn (12) does not apply	8	21	33	40	56
Number of coefficients, when eqn (12) applies	5	12	18	22	30

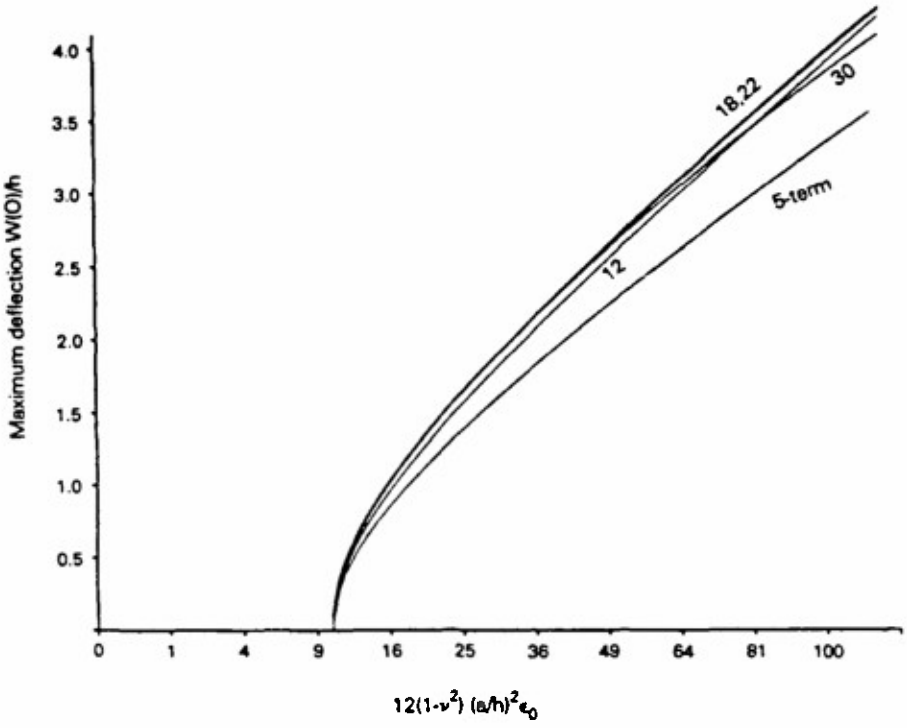

Fig. 1. Circular delamination—deflection at the center.

$$\xi = r/a, \quad u(\xi) = aU_r/h^2, \quad u(1) = -(a/h)^2\varepsilon_0.$$

It is found that, with regard to the central deflection and the radial bending moment at the boundary, Rayleigh–Ritz solutions of the order $\{5, 4\}$ or higher are in excellent agreement with the reference solutions (see Figs 1 and 2, where the solutions of the various

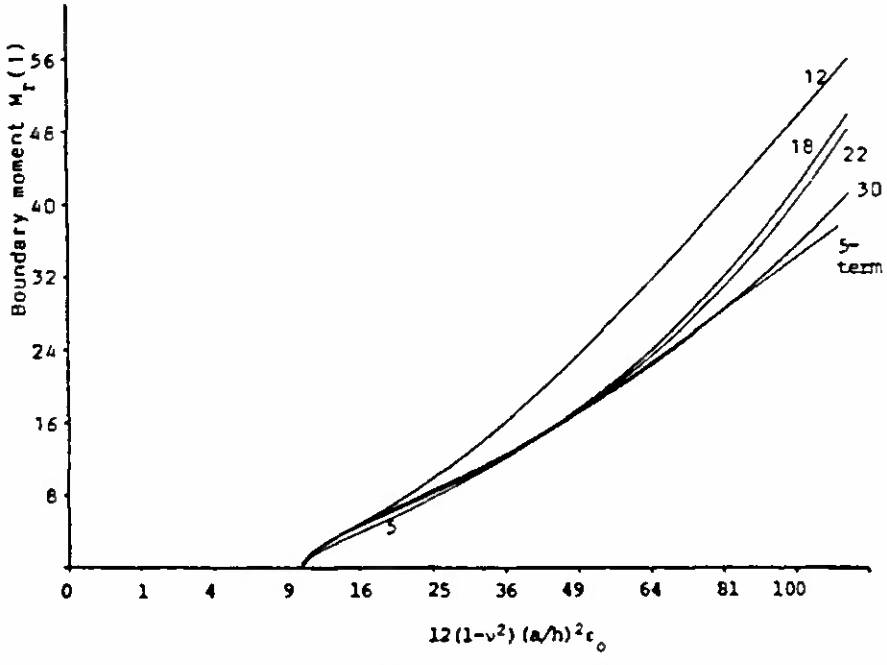

Fig. 2. Circular delamination—boundary radial moment

orders are identified by the number of coefficients given in the last row of Table 1). The curves associated with the solution of the order {7, 6}, i.e. the 30-term solution, are nearly indistinguishable from those of the reference solutions. Only the solution of the order {7, 6} includes polynomial terms of sufficiently high degree to yield very close results for the boundary radial force, and this is true only in a range of the strain load up to about two to three times the bifurcation strain (Fig. 3). The solutions of the lowest orders, {1, 3} and {3, 4}, generally show very significant errors in the membrane forces.

Strong non-uniformity of the membrane force is indicated by the difference between the radial forces at the boundary (Fig. 3) and at the center (Fig. 4). Under large postbuckling loads, all solutions except the lowest order, {1, 3}, show tensile radial force at the center. Generally speaking, the solutions of the orders {5, 4}, {5, 6} and {7, 6} yield acceptable results (i.e. with about 5% or smaller errors) for the deflections, membrane forces and boundary bending moments over a range of the radial strain load up to about three times the bifurcation strain. When the strain load exceeds this range, the deflection at the center is more than 1.5 times the thickness of the sublaminate (see Fig. 1). Compared with the solutions of the order {7, 6}, those of the orders {5, 4} and {5, 6} show significantly larger deviations from the reference solutions.

A comparison of the solutions of the orders {5, 4} and {5, 6} indicates that, by raising the degree r of the even polynomial R without at the same time also raising the degree p of the odd polynomials P and Q, one increases the number of expansion coefficients in the solution but obtains slight change or improvement in the accuracy of approximation. This is because a satisfactory representation of the non-uniformity of the membrane deformation requires polynomial functions P and Q of sufficiently high degree, and such non-uniformity significantly affects the transverse deflection through the coupling in the von Karman equations.

3.2. *Energy release rates in delamination growth*

For the particular problem at hand, let the total potential energy of the isotropic circular sublaminate be non-dimensionalized in the following manner

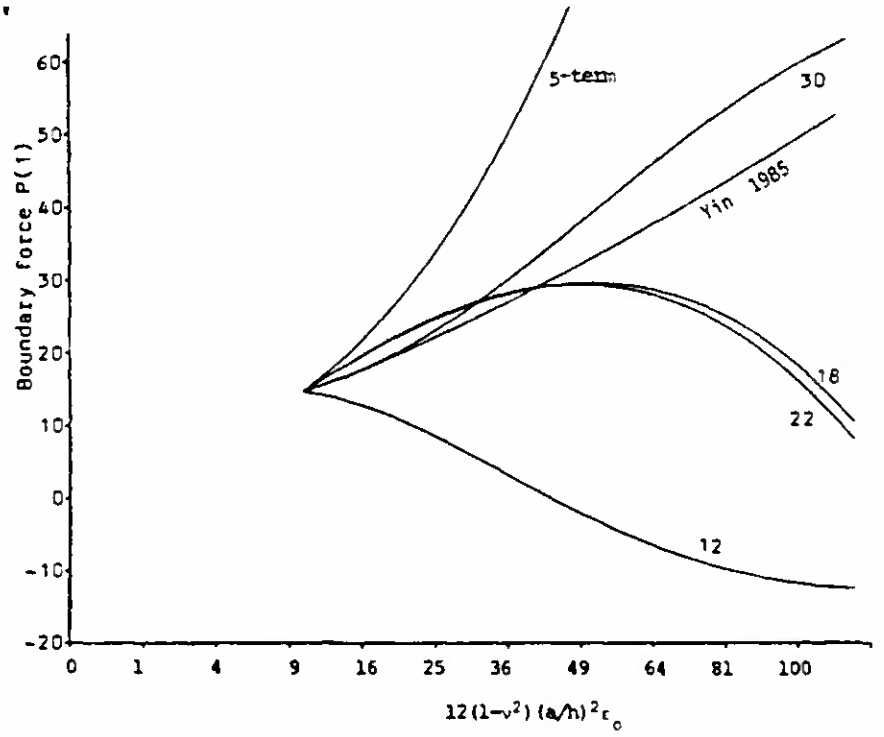

Fig. 3. Circular delamination—radial force at boundary.

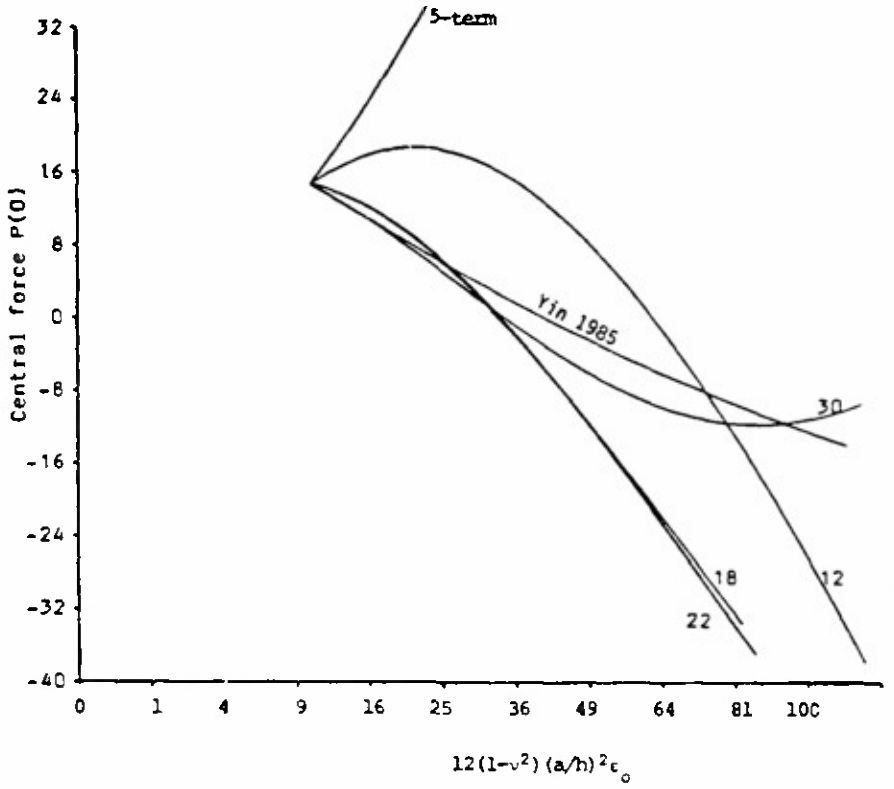

Fig. 4. Circular delamination—membrane force at the center.

$$\bar{\Pi} = (2a^2/\pi Eh^5)\Pi.$$

For the various postbuckling solutions of the sublaminate, the normalized potential energies are plotted in Fig. 5. In this and the two subsequent figures, the horizontal coordinate

$$\sqrt{12(1-\nu^2)\varepsilon_0}(a/h)$$

is interpreted as a normalized delamination radius (under a fixed radial strain load ε_0 in the base plate), rather than as a non-dimensionalized strain load (for a fixed delamination radius a). Under a fixed strain load, the potential energy for an approximate solution may be differentiated with respect to the delamination radius. The result is related to the energy-release rate in axisymmetric growth of the delamination according to the following formula

$$G = \frac{Eh\varepsilon_0^2}{1-\nu} - \frac{1}{2\pi a}\frac{d\Pi}{da}. \tag{15}$$

Comparison of the curves in Figs 5 and 6 indicate that all solutions except the lowest-order yield close results for the potential energies and the energy release rates, while the lowest order solution underestimates the energy release rate by as much as 35%.

The energy release rate may also be evaluated by means of the path-independent M-integral in terms of the boundary radial force and the boundary bending moment of the posthuckling solution (Yin, 1985). This yields the formula

$$G = \frac{1-\nu^2}{2Eh}\left\{\left(\frac{Eh\varepsilon_0}{1-\nu}+N_r(a)\right)^2+12\left(\frac{M_r(a)}{h}\right)^2\right\}. \tag{16}$$

For an exact postbuckling solution the result should agree with the previous result obtained by differentiation of the total potential energy. However, for an approximate postbuckling

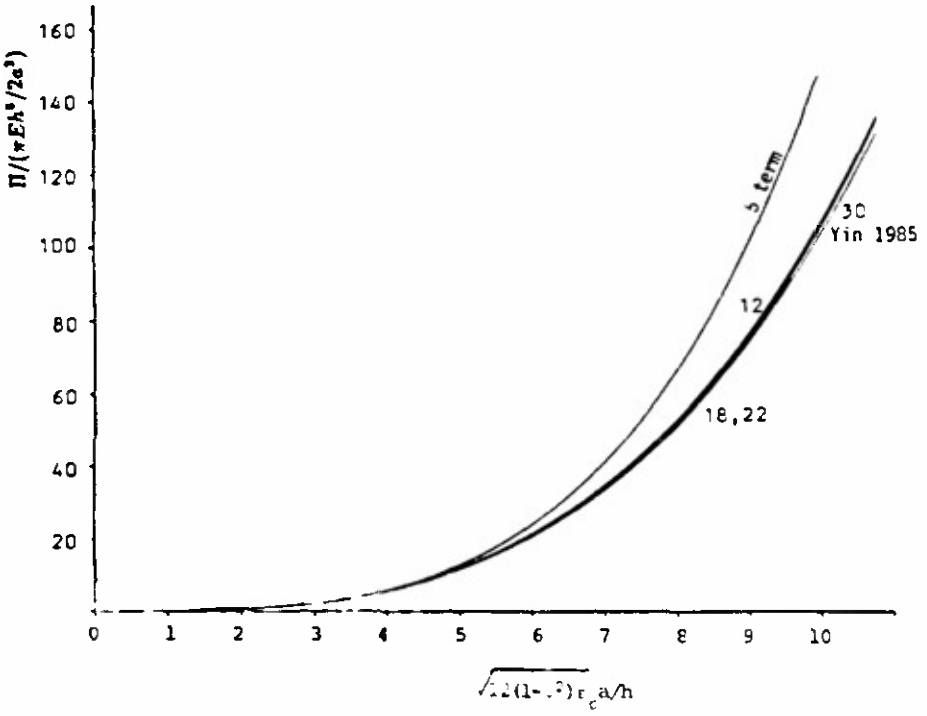

Fig. 5. Circular delamination—potential energy versus the radius

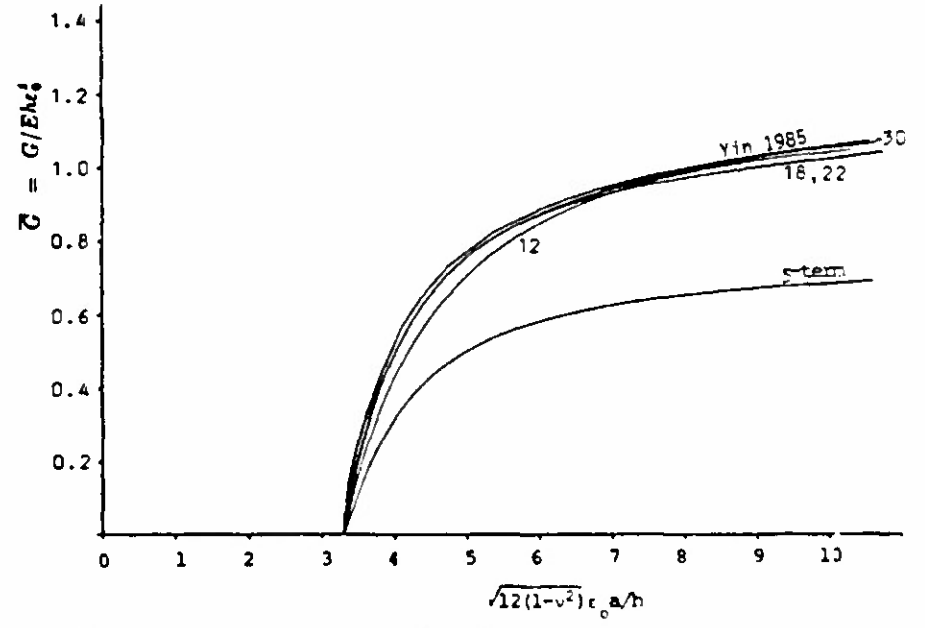

Fig. 6. Energy release rate calculated by differentiating the potential energy with respect to the radius.

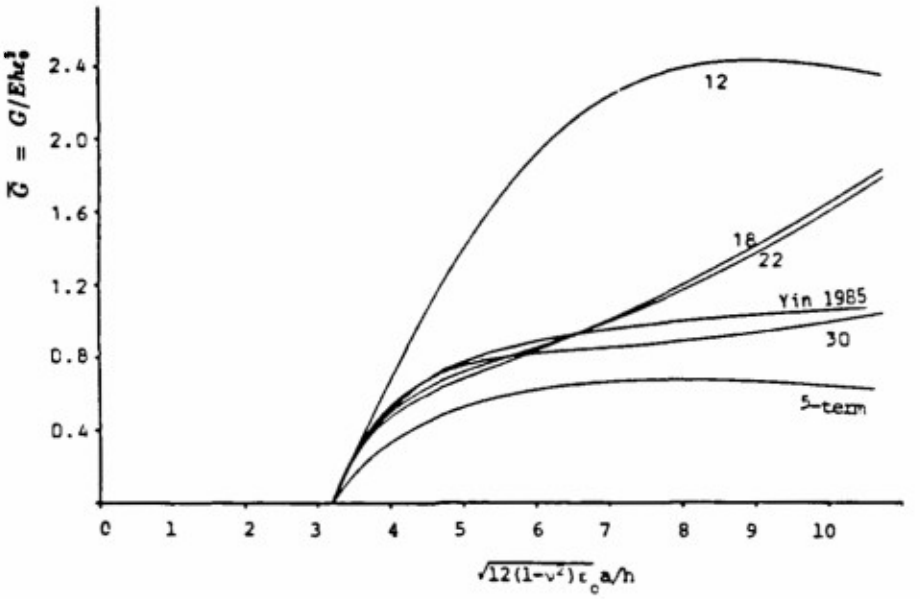

Fig. 7. Energy release rate by the J-integral method.

solution the two results may differ. For the Rayleigh–Ritz solutions of the various orders, the results from eqn (16) are normalized with respect to $Eh\varepsilon_0^2$ and shown in Fig. 7. It is seen that the solutions of the order $\{5, 4\}$ or higher yield close results over a range of strain load up to about three times the bifurcation strain.

4. ELLIPTICAL DELAMINATIONS

We next obtain the bifurcation loads and the postbuckling solutions of homogeneous isotropic elliptical plates with various aspect ratios by the Rayleigh–Ritz method.

4.1. *Bifurcation loads under equal biaxial compression*

Under equal biaxial loading along the principal axes of the ellipse (i.e. $E_{22} = E_{11} = -\varepsilon_0$), the normalized bifurcation loads have been calculated by Woinowsky-Krieger (1937) using elliptical coordinates. His results are shown in Table 2, along with two sets of Rayleigh–Ritz solutions obtained in the present analysis. One set of Rayleigh–Ritz solutions uses a polynomial $R(x, y)$ for $w(x, y)$ containing quadratic and constant terms only. In the second set of solutions, $R(x, y)$ contains quartic and lower-order terms. Since the solutions in a displacement formulation yield upper bounds of the buckling load, the present results, being smaller in value, are better estimates. Furthermore, in the case of a circular delamination ($a/b = 1$), the normalized buckling load predicted by the second set of Rayleigh–Ritz solutions is almost indistinguishable from the exact result, namely, 14.683. As the aspect ratio a/b becomes large, the present upper-bound estimates approach the limiting value $\pi^2 = 9.870$ much faster than the results of Woinowsky-Krieger (1937). Hence the bifurcation loads of elliptical plates under equal biaxial compression are accurately predicted by the Rayleigh–Ritz method involving a small number of expansion coefficients.

Table 2. Normalized buckling loads $P(b^2/D)$ for elliptical delaminations: Comparison of the results of Woinowsky-Krieger (1937) with Rayleigh–Ritz solutions

a/b	1.0	1.4	2.0	3.0	4.0	5.0
Woinowsky-Krieger (1937)	14.79	11.81	11.02	11.01	11.15	11.30
Quadratic R	14.702	11.589	10.517	10.239	10.265	10.32
Quartic R	14.683	11.562	10.436	10.002	9.929	9.955

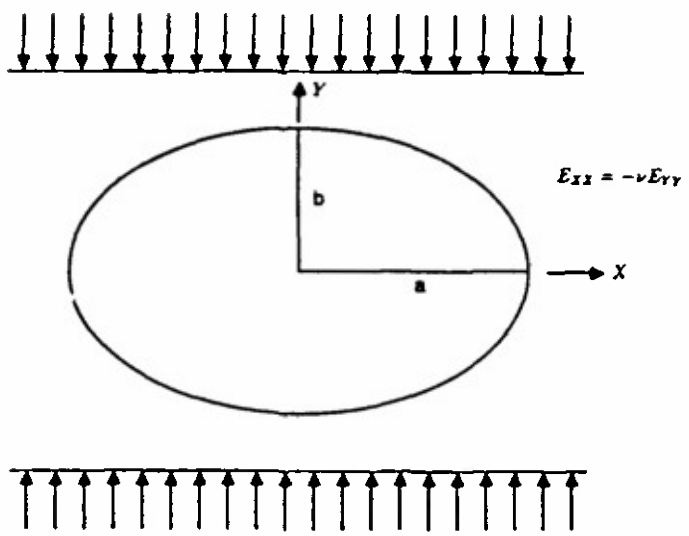

Fig. 8. Elliptical delamination—base plate under uniaxial load.

4.2. *Postbuckling solution under uniaxial compression*

For the postbuckling analyses we consider elliptical delaminations of aspect ratios $a/b = 1, 2$ and 4 in a base plate under membrane strain loads

$$E_{YY} = -\varepsilon_0, \quad E_{XX} = \nu\varepsilon_0, \quad E_{XY} = 0.$$

Such strain loads correspond to *uniaxial* compressive forces applied to the base plate along the Y-direction (Fig. 8). Under a normalized strain load $E_{YY}(b/h)^2 = 4$, and with the assumption $\nu = 0.3$, the in-plane and transverse displacements along the principal axes of the sublaminate are shown in Figs 9–12 for an elliptical sublaminate with $a/b = 2$. Additional figures for the cases $a/b = 1$ and 4 may be found in Jane (1989). Figures 9 and 10 show the deviations of the in-plane displacements in the delaminated layer from the

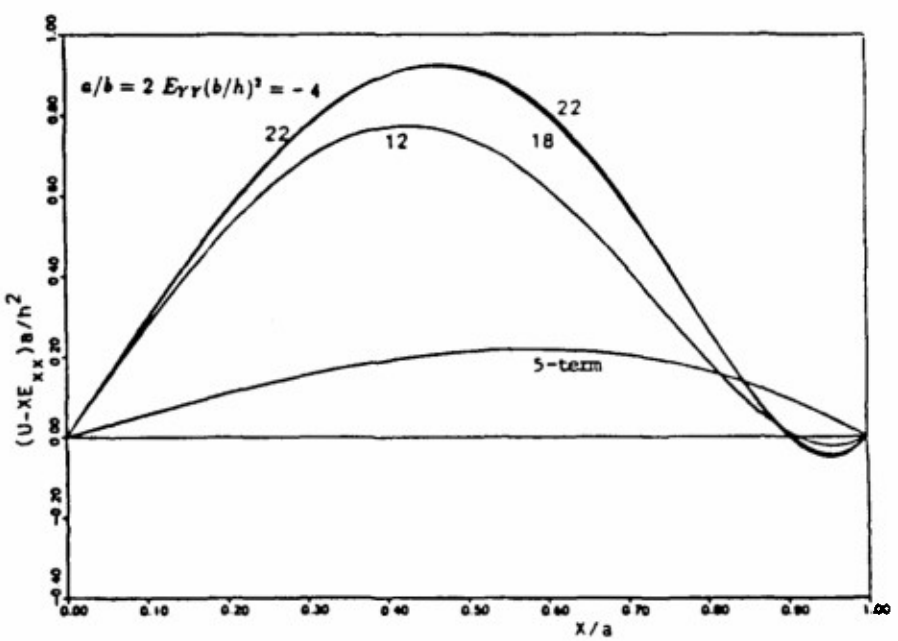

Fig. 9. Displacement U along the X-axis ($a/b = 2$)

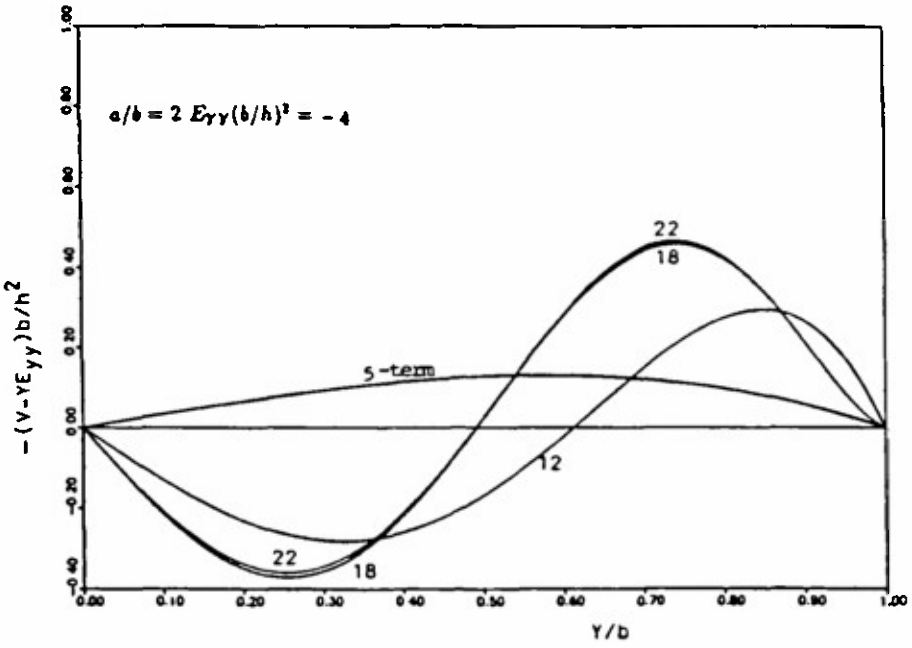

Fig. 10. Displacement V along the Y-axis ($a/b = 2$).

corresponding displacements in the base plate (where, according to the thin-film assumption, the membrane strains are uniform). The slopes of the curves in these figures indicate the deviations of the displacement gradients from the average membrane strains. The results for the solutions of orders $\{5, 4\}$ and $\{5, 6\}$, based on the same polynomial expansions for the in-plane displacements but different expansions for the deflection, are indistinguishable. The significant non-uniformity in the membrane strains shown by these higher-order Rayleigh–Ritz solutions is grossly underestimated by the lowest-order solution. Near the boundary point $(X, Y) = (a, 0)$ the results of the latter are not even qualitatively correct. The non-uniformity in the membrane strains increases with the imposed strain load and with the aspect ratio of the ellipse.

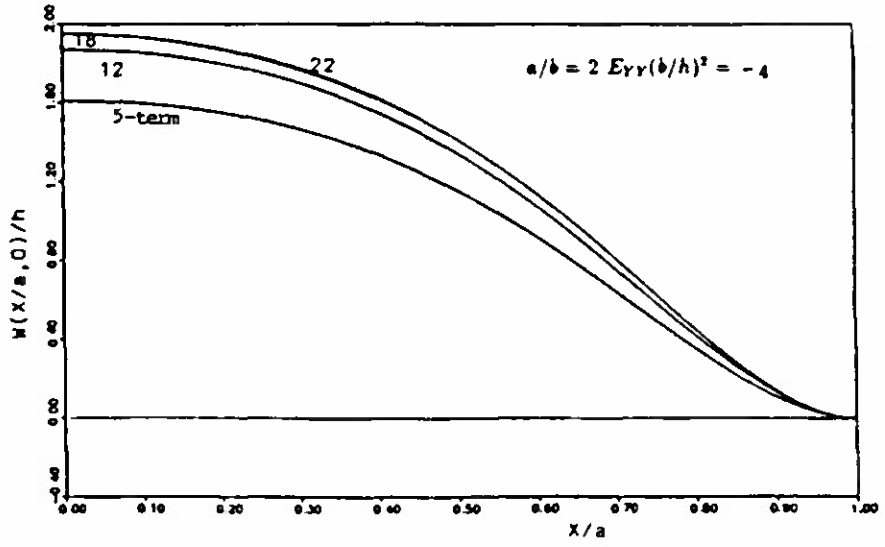

Fig. 11. Deflection profile along the X-axis ($a/b = 2$).

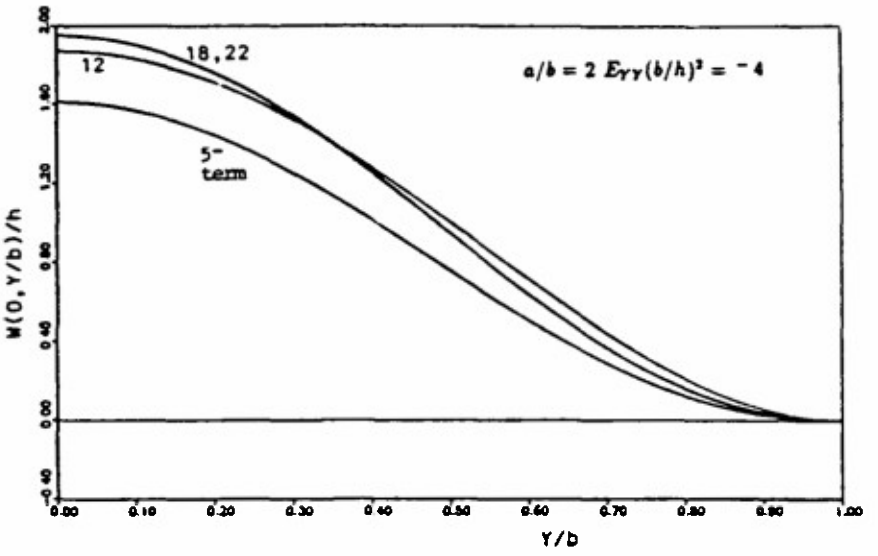

Fig. 12. Deflection profile along the Y-axis ($a/b = 2$).

Figure 11 indicates that, along the X-axis, the magnitude of the curvature of the deformed middle surface is smaller at the center of the plate and larger near the boundary points. Along the loading axis, the opposite is true (Fig. 12). Hence the normal bending moment is relatively small at the two ends of the loading axis and relatively large at the two ends of the X-axis. As the strain load increases, the concentration (attenuation) of the normal curvature and the bending moment at the end points of the X-axis (Y-axis) becomes more pronounced. This phenomenon has important implications on the postbuckling growth behavior of an elliptical delamination. Since the normal bending moment results in an opening action along the delamination boundary and contributes predominantly to the local energy release rate, delamination growth tends to initiate and continue along the X-axis until the boundary curvature and the moment at the two ends of the axis are sufficiently reduced by the lengthening of the X-axis. In addition, growth of the delamination along the X-direction exposes an interior strip around the Y-axis to states of deformation resembling those of one-dimensional delamination models, as may be seen by comparing the deflection profiles along the Y-axis for various (increasing) aspect ratios. Hence the curvature and the bending moment increase at the two ends of the Y-axis and, eventually, delamination growth may proceed simultaneously in both X- and Y-directions. The preceding reasoning provides an explanation for the initial transverse growth of a buckled two-dimensional delamination under a uniaxial in-plane compression, which has been observed experimentally (Chai *et al.*, 1983).

4.3. *Energy release rates*

The non-dimensionalized total potential energies associated with the preceding solutions are shown in Fig. 13. The results are shown as functions of the normalized strain load for elliptical delaminations with aspect ratios $a/b = 1$ and 10. At a large aspect ratio, the deviation of the results of the lowest order solution (Chai and Babcock, 1985) from the higher-order solutions becomes significant. The total potential energy may be differentiated with respect to the semi-axial length, a or b, to obtain the energy release rates associated with delamination growth along the X- or Y-directions. As the aspect ratio of the ellipse changes during the growth of the delamination, the energy release rate also varies. The results are presented in Figs 14 and 15, respectively, for delamination growth along the X- and Y-directions, and for three fixed values of the normalized strain load. It is clear that the lowest-order solution significantly underestimates the energy release rates.

The energy release rates calculated by differentiating the total potential energy with respect to the semi-axial lengths are global quantities associated with certain *assumed* modes

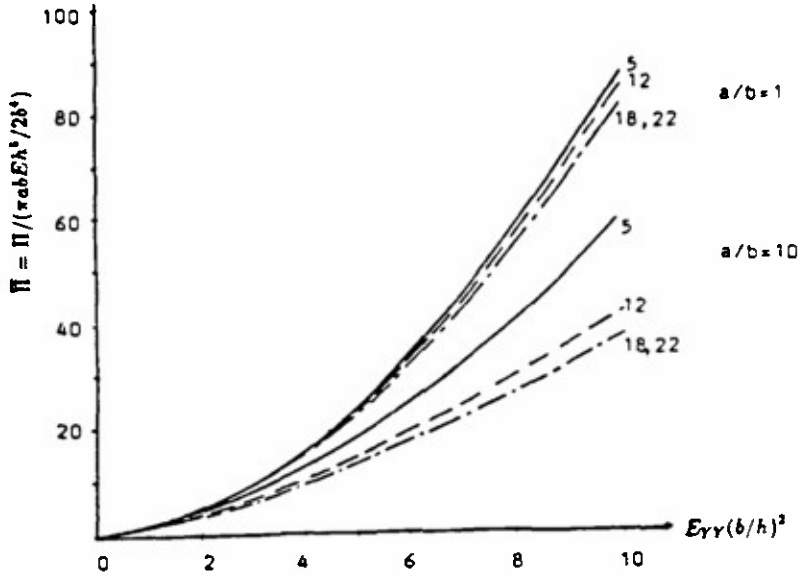

Fig. 13. Total potential energy versus the strain load.

of delamination growth. Although the shape of a two-dimensional delamination may be approximated by an ellipse in each stage of growth, the principal axes of the ellipse may rotate in the course of delamination growth if the loading axis does not coincide with the geometrical and material symmetry axes. Thus, the actual growth mode is generally not a combination of growth along two *fixed* principal directions and, strictly speaking, it can only be determined by evaluating the pointwise values of the energy release rate along the delamination boundary. Such local values of the energy release rate may be expressed in terms of the local membrane forces and bending moments. In the present case of an isotropic elliptical delaminated layer under biaxial loading, the maximum values of the energy release rate occur at the boundary points $(a, 0)$ and $(0, b)$. Figure 16 shows the normalized pointwise

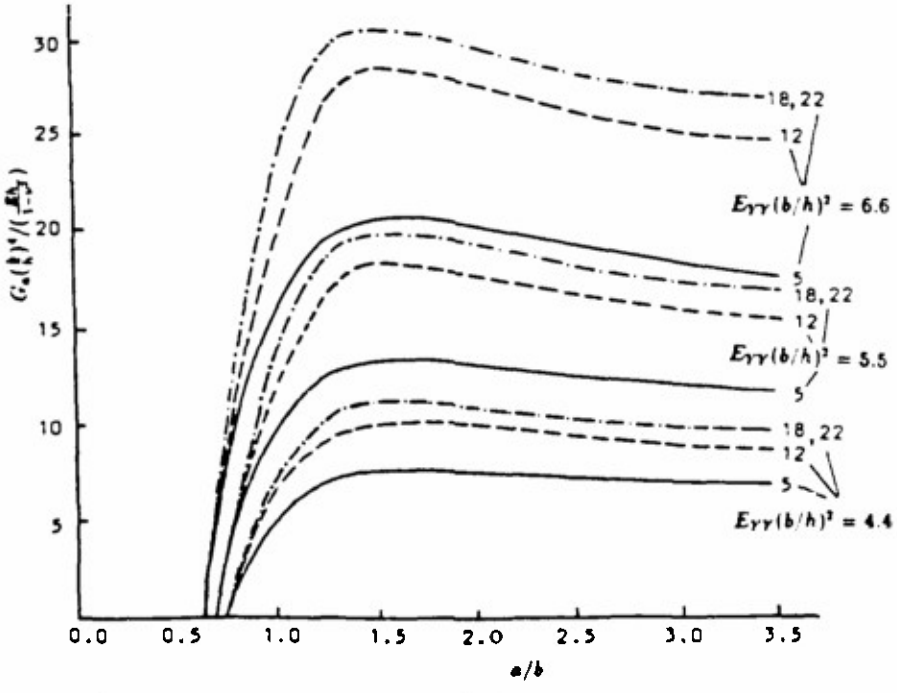

Fig. 14. Global energy release rate, delamination growth along the X-direction

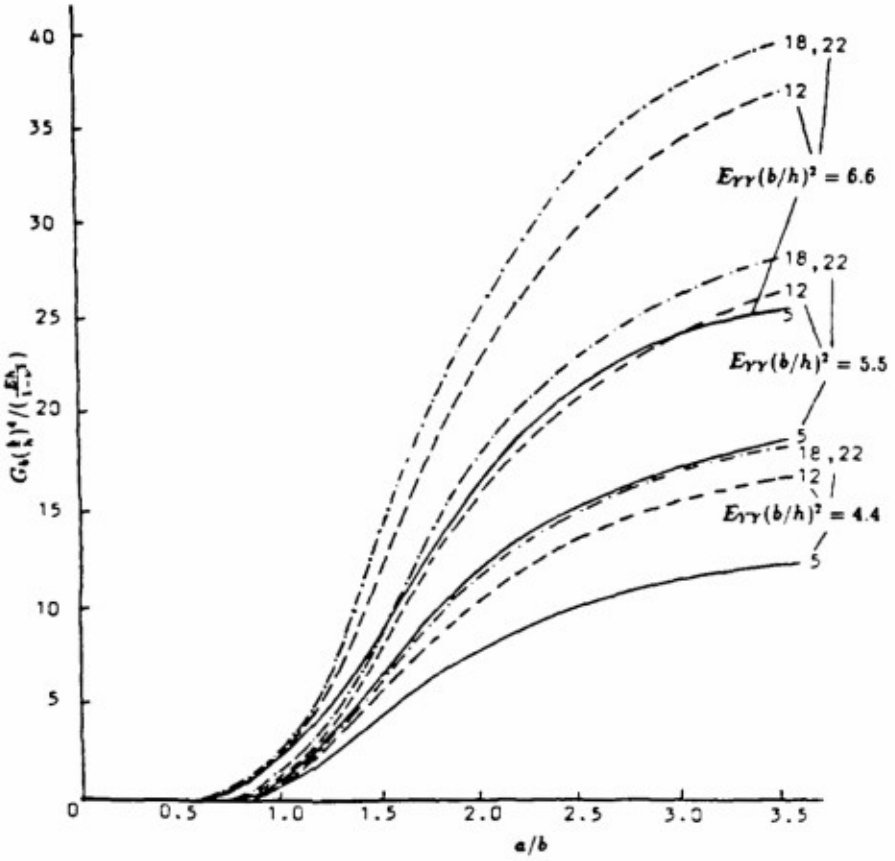

Fig. 15. Global energy release rate, delamination growth along the Y-direction.

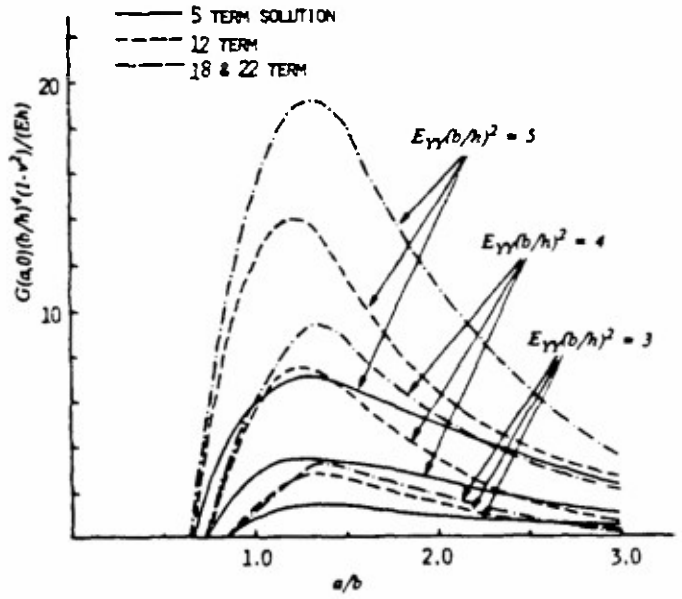

Fig. 16. Pointwise energy release rate at $(a, 0)$.

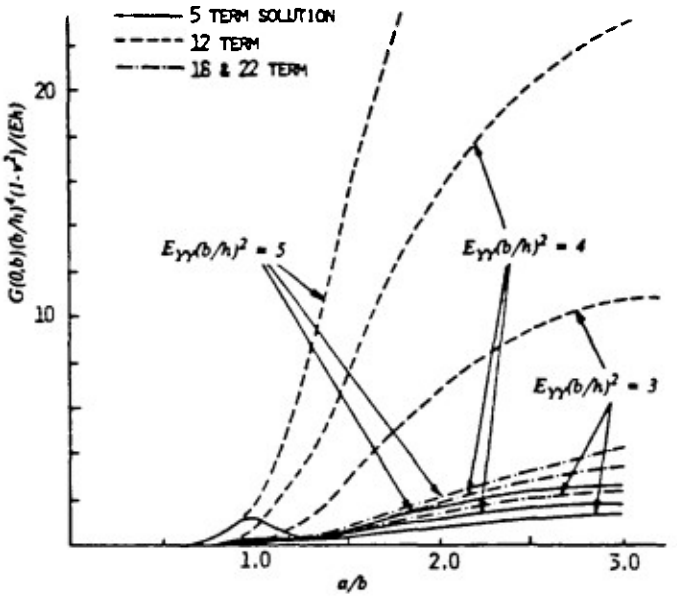

Fig. 17. Pointwise energy release rate at $(0, b)$.

energy release rate at $(a, 0)$ for three fixed levels of the strain load, and Fig. 17 shows the corresponding results at $(0, b)$. In Fig. 16, the solutions of the highest orders show the largest energy release rates, which are about twice as large are the results of the lowest-order solution. Figure 17 indicates that the solution of the order $\{3, 4\}$ greatly overestimates the pointwise energy release rate at $(0, b)$. These results suggest that solutions of the order lower than $\{5, 4\}$ cannot be used to predict the initiation and the nature of growth of a two-dimensional delamination. According to the highest-order solutions, the energy release rate at $(a, 0)$ consistently dominates over the rate at $(0, b)$ when the aspect ratio a/b is 3 or smaller. An opposite conclusion may be valid in the regime of large aspect ratios.

Some conclusions from the present buckling and postbuckling analysis of homogeneous isotropic elliptical sublaminates are summarized in Part II along with additional conclusions based on more extensive results for anisotropic cross-ply and angle-ply sublaminates.

Acknowledgements—The second author was supported by Army Research Office grant to Georgia Institute of Technology in the autumn of 1988. The computational tasks of this project were made feasible by a grant for the use of Cyber 205 supercomputer from the Advanced Computational Methods Center, University of Georgia.

REFERENCES

Bodner, S. R. (1973). The postbuckling behavior of a clamped circular plate. *Quart. J. Appl. Math* **12**, 397–401.
Bottega, W. J. (1983). A growth law for propagation of arbitrary shaped delamination in layered plates. *Int. J. Solids Structures* **19**, 1009–1017.
Chai, H. and Babcock, C. D. (1985). Two-dimensional modelling of compressive failure in delaminated laminates. *J. Composite Materials* **19**, 67–98.
Chai, H., Babcock, C. D. and Knauss, W. G. (1981). One dimensional modelling of failure in laminated plates by delamination buckling. *Int. J. Solids Structures* **17**, 1069–1083.
Chai, H., Knauss, W. G. and Babcock, C. D. (1983). Observation of damage growth in compressively loaded laminates. *Experimental Mech.* **23**, 329–337.
Chai, C. Y. (1980). *Nonlinear Analysis of Plates*. McGraw-Hill, New York.
Feng, M. (1983). An energy theory for postbuckling of composite plates under combined loading. *Comput. Struct.* **16**, 423–431.
Friedrichs, K. O. and Stoker, ●. (1941). The non-linear boundary value problem of the buckled plate. *Amer. J. Math.* **63**, 839–888.
Friedrichs, K. O. and Stoker, ●. (1942). Buckling of the circular plate beyond the critical thrust. *J. Appl. Mech.* **9**, 7–14.
Garg, A. C. (1988). Delamination—a damage mode in composite structures. *Engng Frac. Mech.* **29**, 557–584.
Jane, K. C. (1989). Buckling, Postbuckling Deformation and Vibration of a Delaminated Plate. Ph.D. Thesis, Georgia Institute of Technology, Atlanta, GA.

Kapania, R. K. and Raciti, S. (1989). Recent advances in analysis of laminated beams and plates—Part I: Shear effects and buckling. *AIAA J.* **27**, 923–934.

Shivakumar, K. N. and Whitcomb, J. D. (1985). Buckling of a sublaminate in a quasi-isotropic composite laminate. *J. Comp. Mater.* **19**, 2–18.

Simitses, G. J. (1989). Effect of delamination on buckling. In *Interlaminar Fracture in Composites* (Edited by E. A. Armanios), pp. 237–252. Trans Tech, Switzerland.

Storakers, B. (1989). Nonlinear aspects of delamination in structural members. In *Theoretical Mechanics* (Proc. XVIIth Int. Congr. Theor. Appl. Mech., Edited by P. Germain, M. Piau and D. Caillerie), pp. 315–336. Elsevier, New York.

Storakers, B. and Anderson, B. (1988). Nonlinear plate theory applied to delamination in composites. *J. Mech. Phys. Solids* **36**, 689–718.

Woinowsky-Krieger, S. (1937). The stability of a clamped elliptical plate under uniform compression. *J. Appl. Mech.* **4**, 177–178.

Yin, W.-L. (1985). Axisymmetric buckling and growth of a circular delamination in a compressed laminate. *Int. J. Solids Structures* **21**, 503–514.

Yin, W.-L. (1986). Cylindrical buckling of laminated and delaminated plates. *Proc. AIAA/ASME/ASCE/AHS 27th SDM Conference*, San Antonio, Texas, pp. 165–179.

Yin, W.-L. (1989). Recent analytical results in delamination buckling and growth. In *Interlaminar Fracture in Composites* (Edited by E. A. Armanios), pp. 253–266. Trans Tech, Switzerland.

Yin, W.-L., Reddy, A. D., Dorris, W. S. and Biggers, S. B. (1986a). Delamination Buckling and Growth in a Laminated Beam Plate with and without Stiffening. Final Report, Task 1, NAS1-17925, Lockheed-Georgia Company, Marietta, GA.

Yin, W.-L., Sallam, S. N. and Simitses, G. J. (1986b). Ultimate axial load capacity of a delaminated beam-plate. *AIAA J.* **24**, 123–128.

Yin, W.-L. and Wang, J. T. S. (1984). The energy release rate in the growth of a one-dimensional delamination. *J. Appl. Mech.* **51**, 939–941.

Appendix E

"Refined Buckling and Postbuckling Analysis of Two-Dimensional Delaminations: Part II -- Results for Anisotropic Laminates and Conclusion"

By K. C. Jane and Wan-Lee Yin

International Journal of Solids and Structures, In Press

Int. J. Solids Structures Vol. 00, No. 00, pp. 0000–0000, 1991
Printed in Great Britain

0020-7683/91 $3.00 + .00

REFINED BUCKLING AND POSTBUCKLING ANALYSIS OF TWO-DIMENSIONAL DELAMINATIONS PART II—RESULTS FOR ANISOTROPIC LAMINATES AND CONCLUSION†

K. C. JANE
BMT International, Inc., 10480 Little Papuxent Parkway, Columbia, Maryland 21044, U.S.A.

and

W.-L. YIN
School of Civil Engineering, Georgia Institute of Technology, Atlanta, Georgia 30332, U.S.A.

(*Received* 8 *October* 1990; *in revised form* 14 *June* 1991)

Abstract—The analysis scheme developed in Part I of the paper is implemented to obtain the bifurcation strains of circular delaminated layers and the postbuckling solutions of cross-ply and angle-ply elliptical sublaminates. Reasonably accurate solutions for the membrane forces, the bending and twisting moments and the pointwise energy release rates generally require 33 or more undetermined coefficients. Such refined postbuckling solutions show a variety of features including significant non-uniformity of the in-plane forces and certain boundary effects characterized by concentration of the middle-surface curvatures and the bending moments. The solutions are found to be strongly influenced by ply orientation, lay-up and the aspect ratio of the ellipse. Some implications of the analytical results on the buckling and postbuckling behavior of two-dimensional delamination models are summarized.

1. INTRODUCTION

In recent years extensive analytical and numerical studies have been made on sublaminate buckling and crack growth associated with an interior delamination in a homogeneous or laminated plate. For the simple, one-dimensional model of an across-the-width delamination, exact bifurcation loads and closed-form postbuckling solutions have been obtained, in the context of geometrically non-lionear plate theory, for delaminated homogeneous plates (Chai *et al.*, 1981; Simitses *et al.*, 1985; Yin *et al.*, 1986; Kardomateas, 1989) and for delaminated laminates with arbitrary ply configurations (Yin, 1986, 1988). The strain-energy release rate associated with delamination growth has been expressed explicitly in terms of sublaminate membrane forces and bending moments at the delamination front, and the results were found to be in agreement with the corresponding results based on non-linear finite-element analysis and the closure–integral method. Recent studies have taken into account the effects of transverse shear deformation (Kardomateas and Schmueser, 1988; Chen, 1990), which may become important in a thick or strongly anisotropic delaminated sublaminate.

The relative ease with which accurate postbuckling solutions of strip delamination models may be obtained is attributable to the fact that, in the one-dimensional case, the differential equations of von Karman's non-linear plate theory reduce to *lineor* ordinary differential equations. Hence the effect of geometrical non-linearity is present only in the boundary conditions and the crack-tip continuity conditions for the axial displacement, but not in the governing differential equations. Furthermore, in the one-dimensional case the non-linear coupling between the in-plane deformation and the transverse deflection degenerates to a particularly simple form, characterized by the presence of a *constant* axial load in the deflection equation. Accurate postbuckling solutions of general two-dimensional delamination models are considerably more difficult to obtain in view of the presence of

† A preliminary version of this paper was presented in AIAA ASME ASCE AHS 30th SDM Conference, Mobile, Alabama, April, 1989

non-linear and coupling terms in the governing equations. It may be expected that these terms will significantly affect the postbuckling behavior of the sublaminate and the nature of ensuing delamination growth.

A first step toward a better understanding of two-dimensional delamination problems is achieved through a buckling and postbuckling analysis of an isotropic circular delaminated plate subjected to a radially symmetric in-plane compression. The analysis indicates that, with proper normalization, the non-dimensional radial buckling load of the circular model depends on the normalized delamination radius and thickness according to relations extremely close to the corresponding relations for the normalized axial load of a strip delamination model in terms of the normalized delamination length and thickness (Yin and Fei, 1984). For both strip and circular models, a sharp transition from global buckling of the laminate to local buckling of the thin delaminated layer takes place when the delamination reaches a critical size. Furthermore, the postbuckling deformations of the circular and strip delamination models show the same pattern of evolution, from the initiation of buckling to final collapse, which is unique to each regime of delamination size (subcritical or supercritical) and which is fundamentally different between the two regimes (Yin *et al.*, 1986; Yin and Fei, 1988).

In spite of these similarities, there are also significant and essential differences in the buckling and postbuckling behavior of strip and circular delamination models. Axisymmetric postbuckling solutions of the circular model show pronounced boundary effects, non-uniform distribution of the in-plane forces, and generally catastrophic nature of delamination growth. As shown by the analysis of Part I, these effects are also manifest in the postbuckling response of isotropic, thin-film elliptical delamination models under uniaxialcompression in the base plate. It was also shown that an accurate assessment of these effects cannot be achieved by lower-order Rayleigh–Ritz postbuckling solutions that have been presented in the existing literature. Solutions of at least the order (5, 4), involving 33 or more undetermined coefficients in the polynomial displacement expansions for an anisotropic elliptical sublaminate, are required to provide reasonably accurate results for the membrane forces, bending and twisting moments, and the global and pointwise energy release rates.

Non-linearity and coupling in the von Karman equations, which produce the previously mentioned effects, are strongly dependent on the anisotropic elastic moduli of the plies constituting the sublaminate and on the orientation and lay-up of the plies. While the analysis of *isotropic* sublaminates in Part I has provided some general features of the buckling and postbuckling behavior of two-dimensional delamination models, an understanding of the combined effects of the various geometrical and material parameters can only be gained from a variety of solutions covering a broad range of parameter values. For example, an exact postbuckling analysis of the one-dimensional strip delamination model with a general laminated structure has indicated the significance of the destabilizing effect of bending-extensional coupling (Yin, 1986). Such effects are not present in two-dimensional symmetric sublaminates, including isotropic and orthotropic sublaminates.

In Part II of this paper, we present postbuckling solutions for anisotropic elliptical laminates with various aspect ratios, using polynomial displacement expansions of the order (5, 4). Although our computer code may handle any uniform in-plane strain loading in the base plate, in the present work we restrict the computation to the case of uniaxial compression in the base plate along the minor axis of the ellipse. This loading case was considered in previous buckling analysis of circular, unidirectional composite laminates (Shivakumar and Whitcomb, 1985) and postbuckling analysis of isotropic and specially orthotropic elliptical sublaminates (Chai and Babcock, 1985). In the present work, we obtain the solutions for cross-ply and 30° and 45° angle-ply elliptical sublaminates under postbuckling strain loads as large as four or five times the bifurcation strain. The sublaminates have symmetric or antisymmetric four-layer lay-ups and the aspect ratio of the ellipse ranges from 1.2 to 4.

Our results for the force and moment resultants and for the global and pointwise energy release rates show complex patterns of behavior, depending strongly on the orientation and the stacking sequence of the plies in the sublaminate and, to a lesser degree, on the aspect

ratio of the ellipse. These results have direct implication on the initiation and development of delamination growth. The complexity and richness of the present results suggests the need for caution in making predictions or conjectures concerning the buckling and growth behavior of two-dimensional models based either on analytical and experimental experiences with strip delaminations or on insufficiently refined approximate solutions of two-dimensional sublaminates.

2. BIFURCATION LOAD OF A CIRCULAR, UNIDIRECTIONAL SUBLAMINATE

A general and consistent scheme for polynomial representation of displacement functions associated with the buckling and postbuckling deformation of elliptical sublaminates has been developed in Part I of this paper. In the following analysis, we adopt the notations and definitions introduced in Section 2 of Part I.

We first investigate the bifurcation strain of a circular, unidirectional composite layer disbonded from an infinite base laminate, when the latter is subjected to in-plane strains $-E_0$ and $0.3\,E_0$ along the Y- and X-directions, respectively. The angle α between the material axis of fiber orientation and the compression axis is allowed to vary. This problem has been investigated by Shivakumar and Whitcomb (1985) using both finite-element and Rayleigh–Ritz methods. Their Rayleigh–Ritz solutions were based on a three-term polynomial expansion for the normalized transverse deflection w in terms of the dimensionless co-ordinates x and y:

$$w = (1 - x^2 - y^2)^2 R(x, y) \tag{1}$$

where

$$R(x, y) = c_1 + c_2 x^2 + c_3 y^2.$$

The results were found to be in close agreement with the finite-element results for small orientation angles but not for large angles (Fig. 1).

We notice that the deflection function expressed by the three-term expansion is symmetric with respect to both X- and Y-axes. Since such symmetry conditions cannot be assumed generally except for specially orthotropic sublaminates with aligned loading, material and geometrical axes, certain deflection modes are suppressed by the assumed symmetry and this has the effect of raising the calculated bifurcation load. It is clear that, at least in the initial postbuckling states the actual deflection should have central symmetry but not double symmetry with respect to both co-ordinate axes, i.e. one should *only* have

$$w(-x, -y) = w(x, y). \tag{2}$$

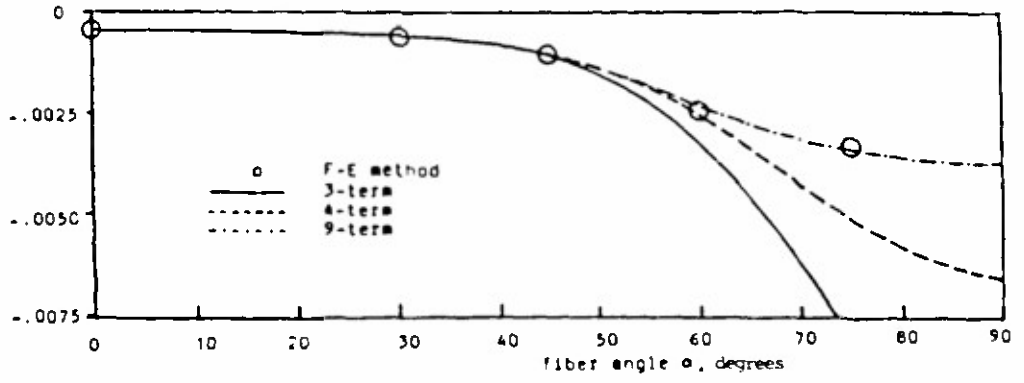

Fig. 1. Bifurcation strain of a circular unidirectional laminate versus the fiber orientation angle

This implies that, if in eqn (1) one chooses a polynomial factor $R(x, y)$ of degree two, then the factor should include an additional term c_4xy. The new deflection function yields an improved solution for the bifurcation strain (see the middle curve in Fig. 1).

Further improvement in the bifurcation strain may be obtained by including in the polynomial $R(x, y)$ all fourth degree terms that are consistent with the symmetry condition of eqn (2). This yields a nine-term deflection function:

$$w = (1-x^2-y^2)^2(c_1+c_2x^2+c_3xy+c_4y^2+c_5x^4+c_6x^3y+c_7x^2y^2+c_8xy^3+c_9y^4). \tag{3}$$

The resulting bifurcation strains are shown by the top curve in Fig. 1. The results are nearly indistinguishable from the finite-element solutions over the entire range of the orientation angle α. Thus, by including in the polynomial function $P(x, y)$ all fourth and lower degree terms that are consistent with the symmetry condition of eqn (2), the Rayleigh–Ritz analysis yields bifurcation loads that are in excellent agreement with the finite-element solutions.

3. POSTBUCKLING SOLUTIONS OF CROSS-PLY AND ANGLE-PLY ELLIPTICAL SUBLAMINATES

The number of undetermined coefficients required in the Rayleigh–Ritz solutions for the postbuckling deformation is considerably larger. For a general anisotropic elliptical delamination, the normalized postbuckling displacement functions satisfy the following symmetry conditions:

$$u(-x, -y) = -u(x, y), \quad v(-x, -y) = -v(x, y), \quad w(-x, -y) = w(x, y). \tag{4}$$

Hence P and Q (defined in eqn (5) of Part I) are odd polynomials and R is an even polynomial.

The convergence study in Part I for the Rayleigh–Ritz solutions of homogeneous isotropic sublaminates suggests that, in order to obtain reasonably accurate results for the force and moment resultants and the energy release rates, the odd polynomials P and Q must include at least terms of the fifth and lower degrees and the even polynomial R must include at least terms of the fourth and lower degrees. In this approximation, the polynomials contain a total of 33 undetermined coefficients:

$$\begin{aligned}
P(x, y) &= a_1x+a_2y+a_3x^3+a_4x^2y+a_5xy^2+a_6y^3 \\
&\quad +a_7x^5+a_8x^4y+a_9x^3y^2+a_{10}x^2y^3+a_{11}xy^4+a_{12}y^5, \\
Q(x, y) &= b_1x+b_2y+b_3x^3+b_4x^2y+b_5xy^2+b_6y^3 \\
&\quad +b_7x^5+b_8x^4y+b_9x^3y^2+b_{10}x^2y^3+b_{11}xy^4+b_{12}y^5, \\
R(x, y) &= c_1+c_2x^2+c_3xy+c_4y^2+c_5x^4+c_6x^3y+c_7x^2y^2+c_8xy^3+c_9y^4.
\end{aligned} \tag{5}$$

A further improvement in the solution may be obtained when *all* terms of the next order consistent with the symmetry conditions of eqn (4) are included in the expressions of u, v and w. This will bring the total number of coefficients to 56.

Although higher-order solutions are desirable for improved accuracy, the computer storage and time requirements for evaluating the integrals L_{ij}, M_{ij} and N_{ij} in the potential energy expression (see eqns (6) and (7) of Part I) become increasingly demanding. Besides, since the thin-film assumption itself (i.e. ignoring the effect of layer buckling on the deformation of the thick base plate) may introduce significant error in the results, as has been demonstrated in the cases of strip and circular delamination models (Chai *et al.*, 1981; Yin and Fei, 1988), there is little justification to obtain extremely elaborate postbuckling solutions based on the thin-film approximation. Consequently, the displacement expansions including 33 undetermined coefficients (eqn (14)) are used in the present analysis to obtain postbuckling solutions of four-layer cross-ply, 30° angle-ply and 45° angle-ply elliptical sublaminates with symmetric or anti-symmetric layup (denoted in the figures by S-cross,

U-cross, S30, U30, S45 and U45, respectively). The individual layers are made of T300/5208 graphite/epoxy unidirectional composite whose longitudinal elastic modulus E_1 is 17.57 times the transverse elastic modulus E_2 and for which $\nu_{12} = \nu_{21}E_1/E_2 = 0.28$. The aspect ratio of the ellipse, a/b, assumes the values 1, 2 and 4.

The results of a non-linear problem with strong coupling among the dependent variables and involving many geometrical and material parameters cannot be reduced to simple rules of thumb. In this section, an attempt is made to present the large and complex body of postbuckling solutions for various elliptical sublaminates without oversimplification and with a certain degree of consistency and comprehensiveness. As mentioned previously, we restrict the analysis to the loading case when the base plate is subjected to uniform strains $0.3\,E_{YY}$ and $-E_{YY}$ along the X- and Y-directions, respectively.

3.1. *Central deflection*

The central deflection of the delaminated layer in the buckled state is shown in Fig. 2 for the various symmetric and unsymmetric delaminations. Sublaminates with the antisymmetric lay-up buckle at lower compressive strains compared to the corresponding sublaminates with the symmetric lay-up, and the former show larger central deflections, at least in the initial postbuckling states. These results attest to the destabilizing effect caused by the bending–stretching coupling of antisymmetric sublaminates. Figure 2 indicates that, for aspect ratios 2 and 4, the results for the central deflection show similar patterns, while in the case $a/b = 1$ the deflections are generally smaller and the 30° angle-ply sublaminates have the lowest bifurcation strains and the largest postbuckling deflections. This may be explained by the constraining effect provided by the relatively-short transverse in-plane axis in the case $a/b = 1$. This constraining effect is less significant for the 30° angle-ply sublaminates because the fibers are largely aligned along the Y-axis and, consequently, the bending stiffness in the X-direction is smaller than in the case of cross-ply and 45° angle-ply sublaminates. Generally, the curves of E_{YY} versus the central deflection show nearly parabolic variations.

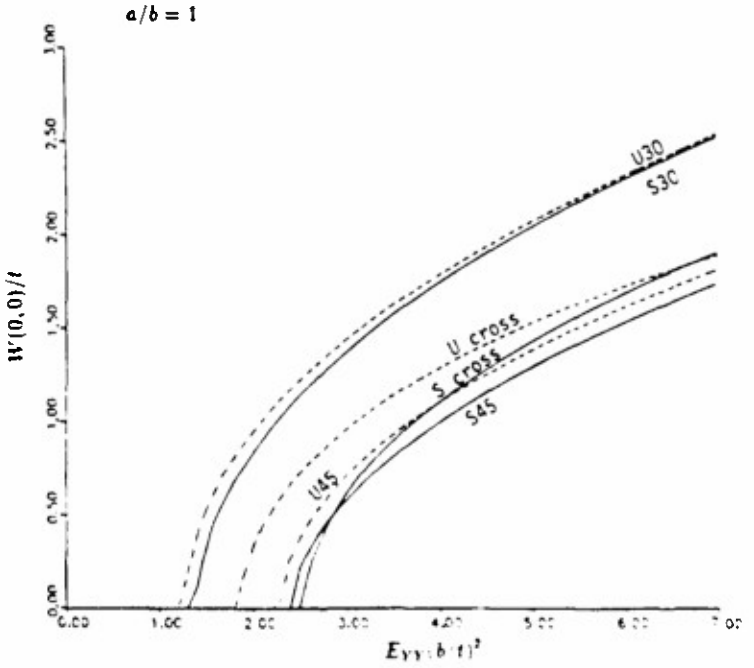

(a)

Fig. 2. Deflection at (0, 0)

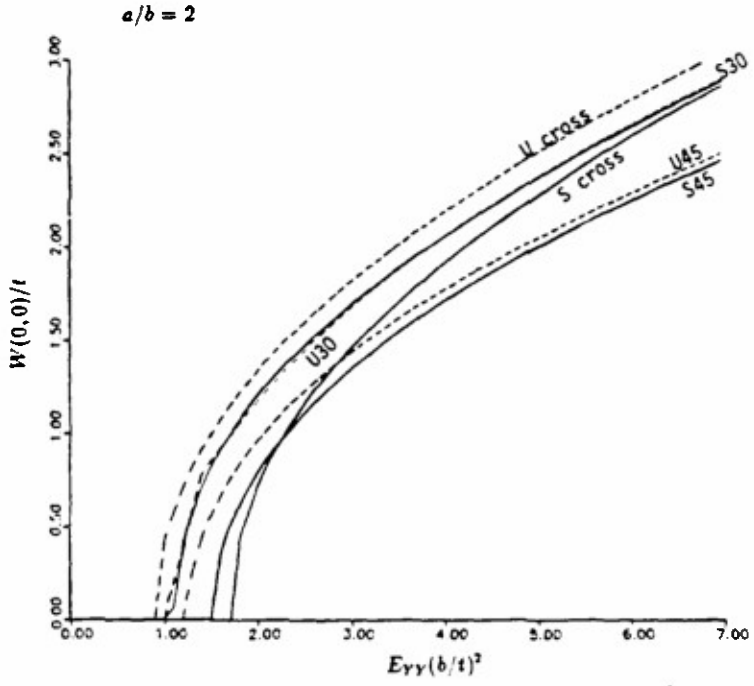

(b)

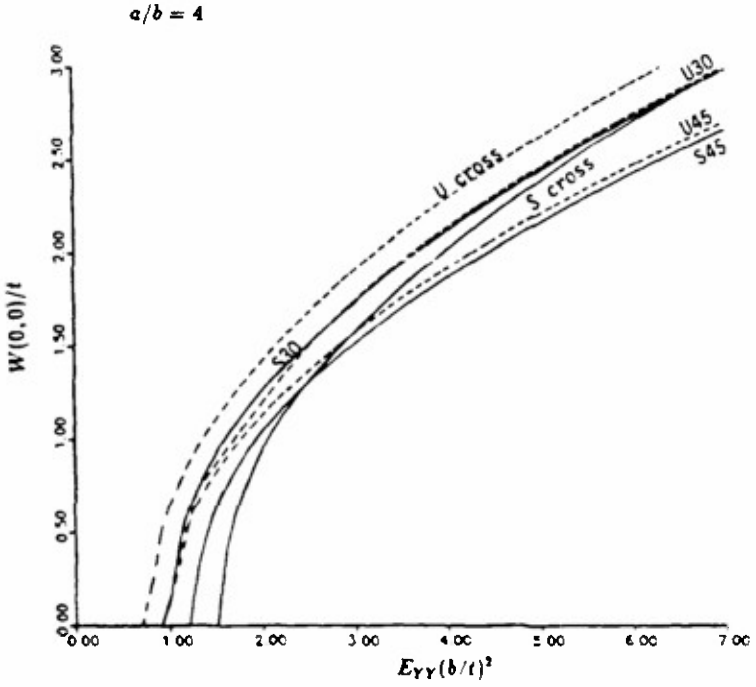

(c)

Fig. 2—*continued*

3.2. *Membrane forces*

The normal and shearing forces N_{XY} and N_{YY} at the boundary point $(X, Y) = (0, b)$ are shown in Figs 3 and 4. Before buckling, the shearing force vanishes, the normal force is proportional to the applied strain E_{YY} and the results for the sublaminates with symmetric and unsymmetric lay-ups are identical. At the bifurcation strain, the relationship between

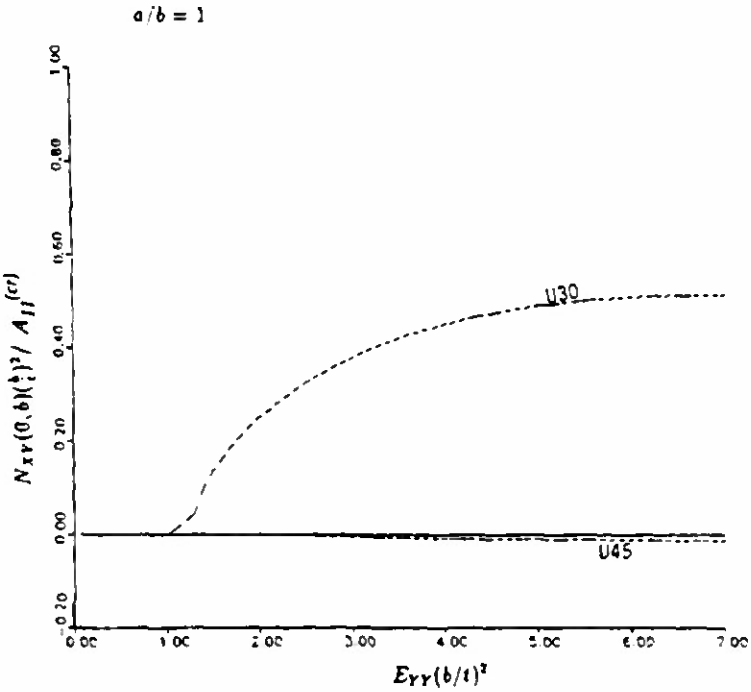

(a)

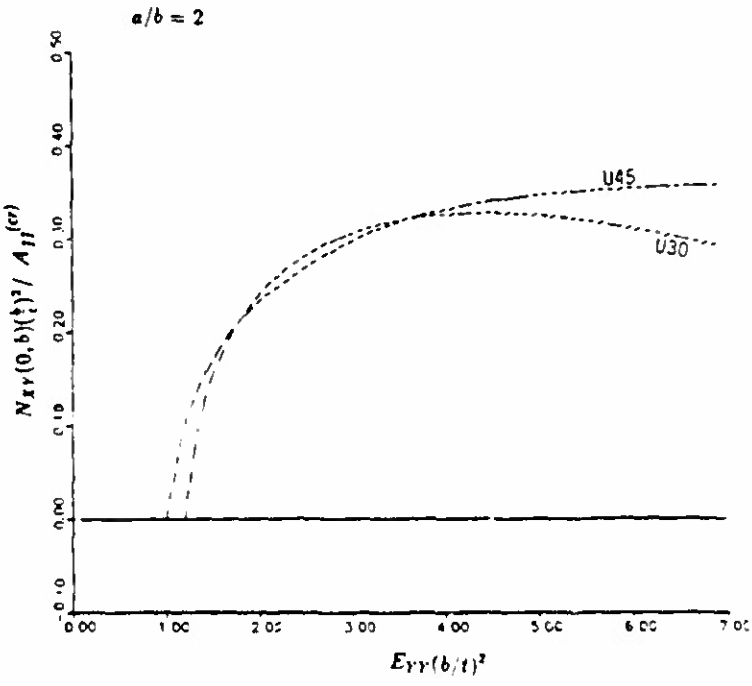

(b)

Fig. 3. N_{11} at the boundary point $(0, b)$

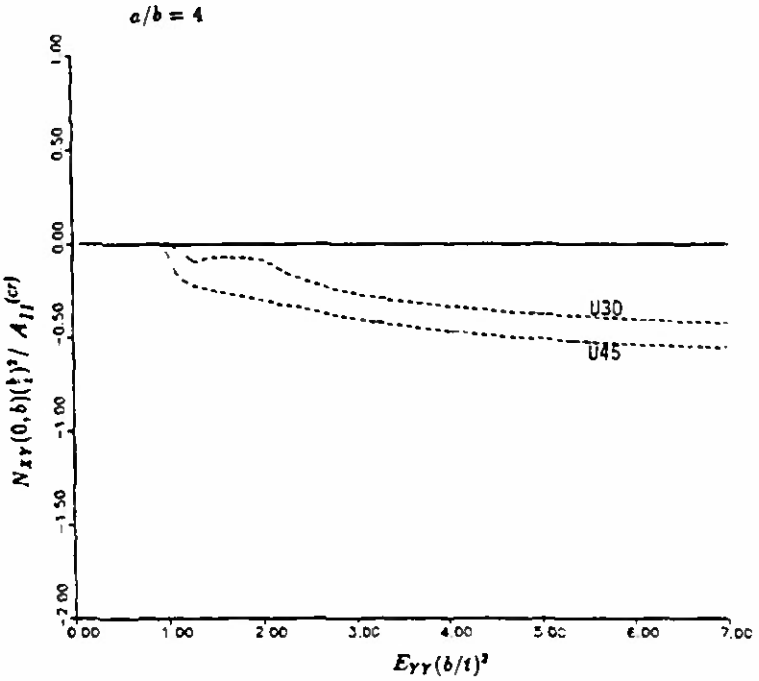

(c)

Fig. 3.—*continued.*

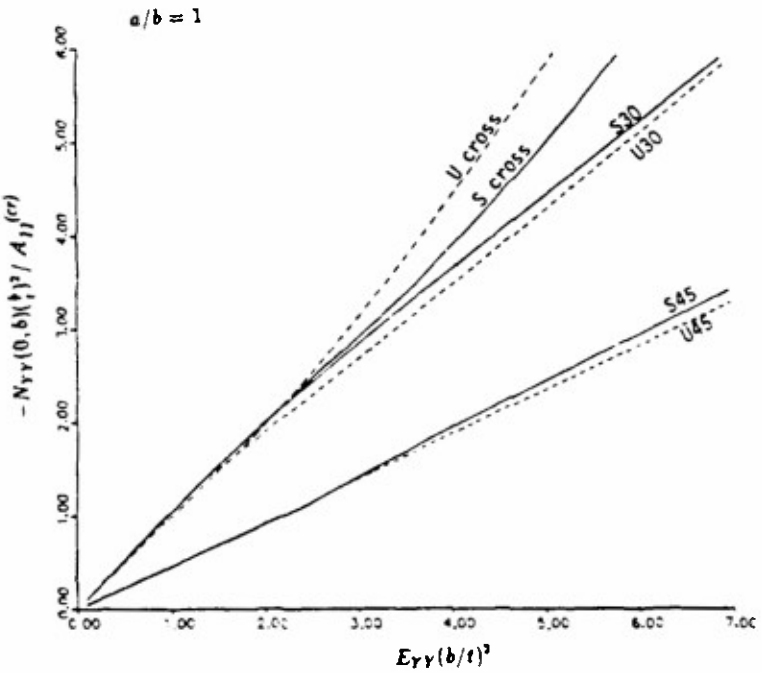

(a)

Fig. 4. N_{yy} at the boundary point $(0, b)$.

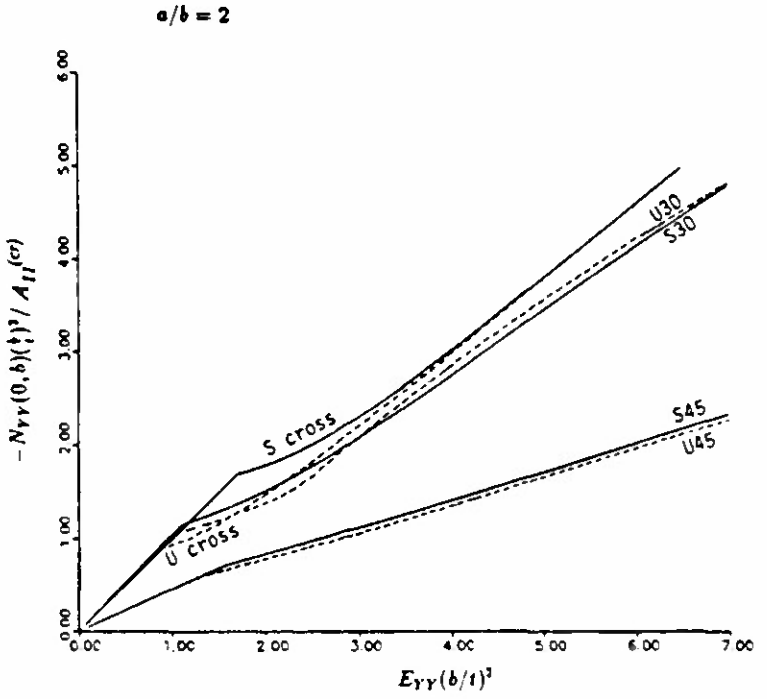

(b)

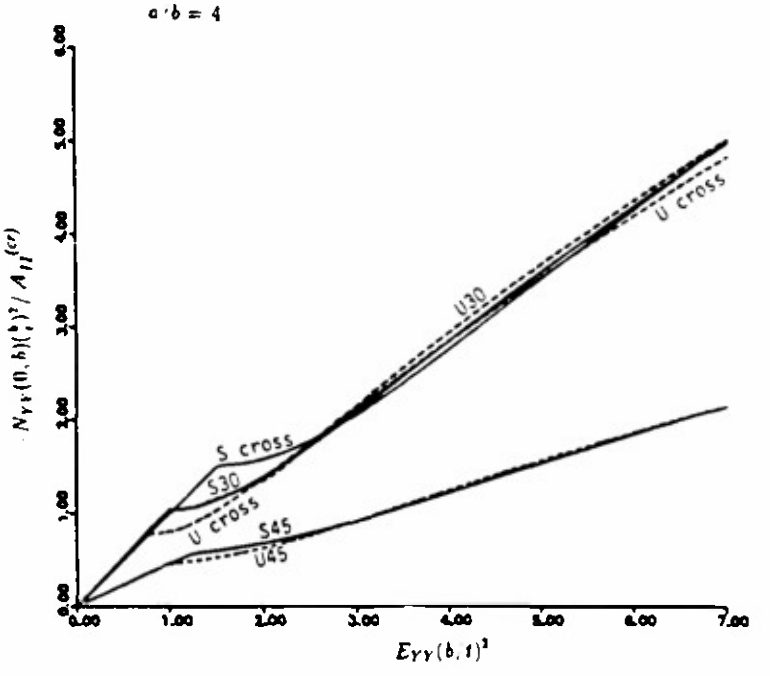

(c)

Fig. 4—*continued*.

E_{YY} and N_{YY} changes from linear to non-linear. In the cases examined, the larger the aspect ratio a/b, the greater is the deviation from linear relationship in the postbuckling stage. With the exception of the antisymmetric cross-ply circular sublaminate, the deviation of N_{YY} from linear dependence on the postbuckling load is generally on the negative side (i.e. a softening behavior). The postbuckling shearing force N_{XY} is non-zero only for unsymmetric 30° and 45° angle-ply sublaminates, and its values are small compared to the normal force N_{YY} at the same point.

It is interesting to compare the values of N_{YY} at the boundary point $(0, b)$ and at the central point $(0, 0)$. The results at $(0, 0)$, presented in Fig. 5, show much greater deviation from linear dependence on the postbuckling strain load. That is, the decompression in the Y-direction due to sublaminate buckling is greater at the center of the sublaminate and smaller at the two ends of the Y-axis. This is particularly true for the unsymmetric cross-ply sublaminates with aspect ratios 2 and 4, where N_{YY} at $(0, 0)$ changes from compression to tension at an advanced stage of postbuckling. Consequently, the normal force N_{YY} varies significantly from the boundary point $(0, b)$ to the central point $(0, 0)$. A comparison of the results in Fig. 5 yields the rather unexpected observation that the non-uniformity of the in-plane forces tends to be more prominent when the aspect ratio increases from 1 to 2 and finally to 4, i.e. when the geometry of the elliptical delamination becomes more similar to a strip delamination. Although we have not computed the results for elliptical delaminations with even larger aspect ratios, the present results indicate that, as regards the membrane force N_{YY}, there is a significant difference between the postbuckling responses of one-dimensional delaminated layers and of elliptical sublaminates with aspect ratios as large as four. In the first case the axial force is constant whereas in the second case N_{YY} is significantly non-uniform. The non-uniformity of the in-plane forces affects the bending deformation directly, through the bending–stretching coupling of unsymmetrical sublaminates, and indirectly through the strong coupling of in-plane and transverse displacements in the von Karman equations.

Comparison of the transverse in-plane force N_{XX} at the central point and the boundary

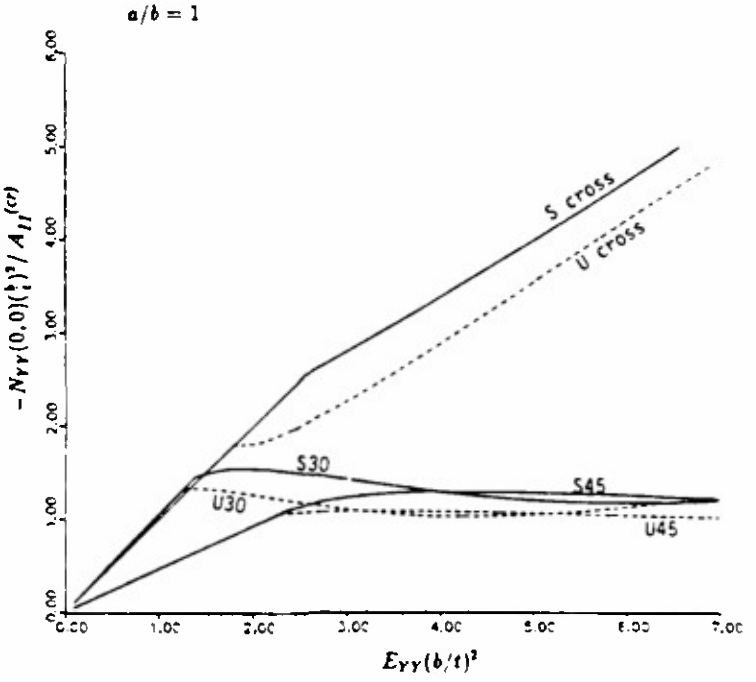

(a)

Fig. 5. N_{YY} at (0, 0).

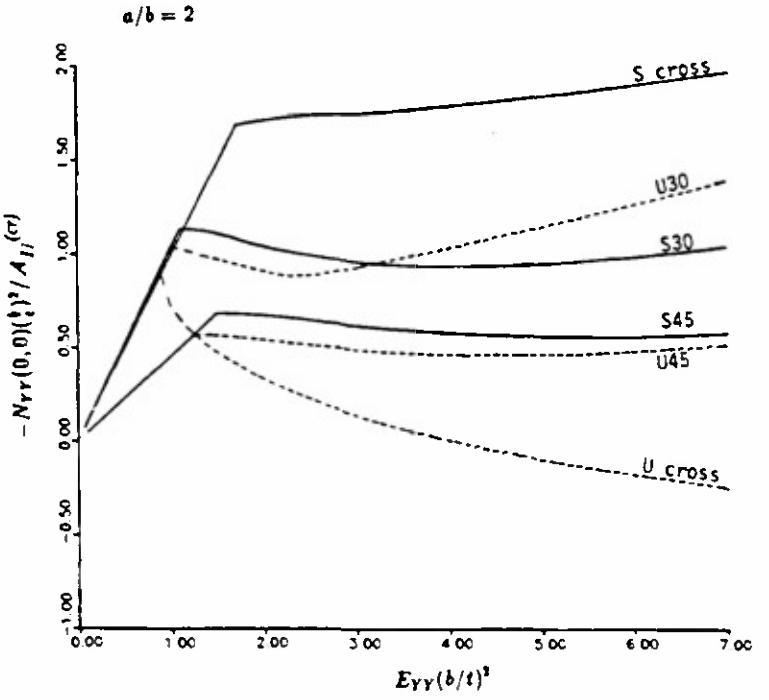

(b)

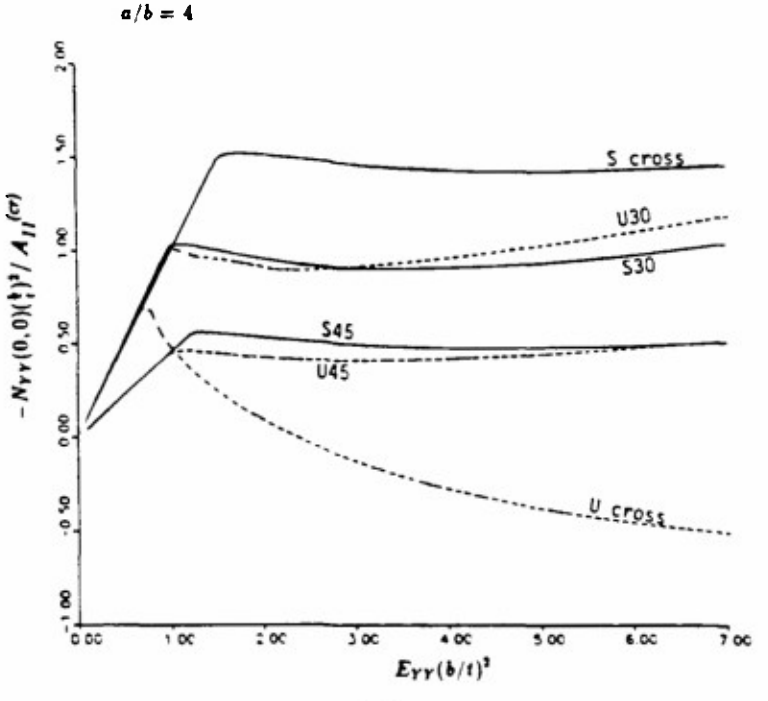

(c)

Fig. 5—*continued*.

point $(a, 0)$ (shown respectively in Figs 6 and 7) also indicates a significant non-uniformity of that force in the postbuckling stage. Due to the differences of the coupling coefficients in the extensional stiffness matrices, the membrane force N_{xx} in the prebuckling states is tensile for the cross-ply sublaminates and compressive for the 30° and 45° angle-ply sublaminates. For the angle-ply case, the deviation from the linear relationship between N_{xx} and the postbuckling strain load E_{yy} is generally on the positive side (i.e. a hardening behavior), is greater at the central point than at the boundary point $(a, 0)$, and greater for the case of smaller aspect ratio than for the case of larger aspect ratio. However, the unsymmetric cross-ply sublaminates show the almost opposite type of behavior; the postbuckling force N_{xx} in these sublaminates also shows the largest deviation from uniformity.

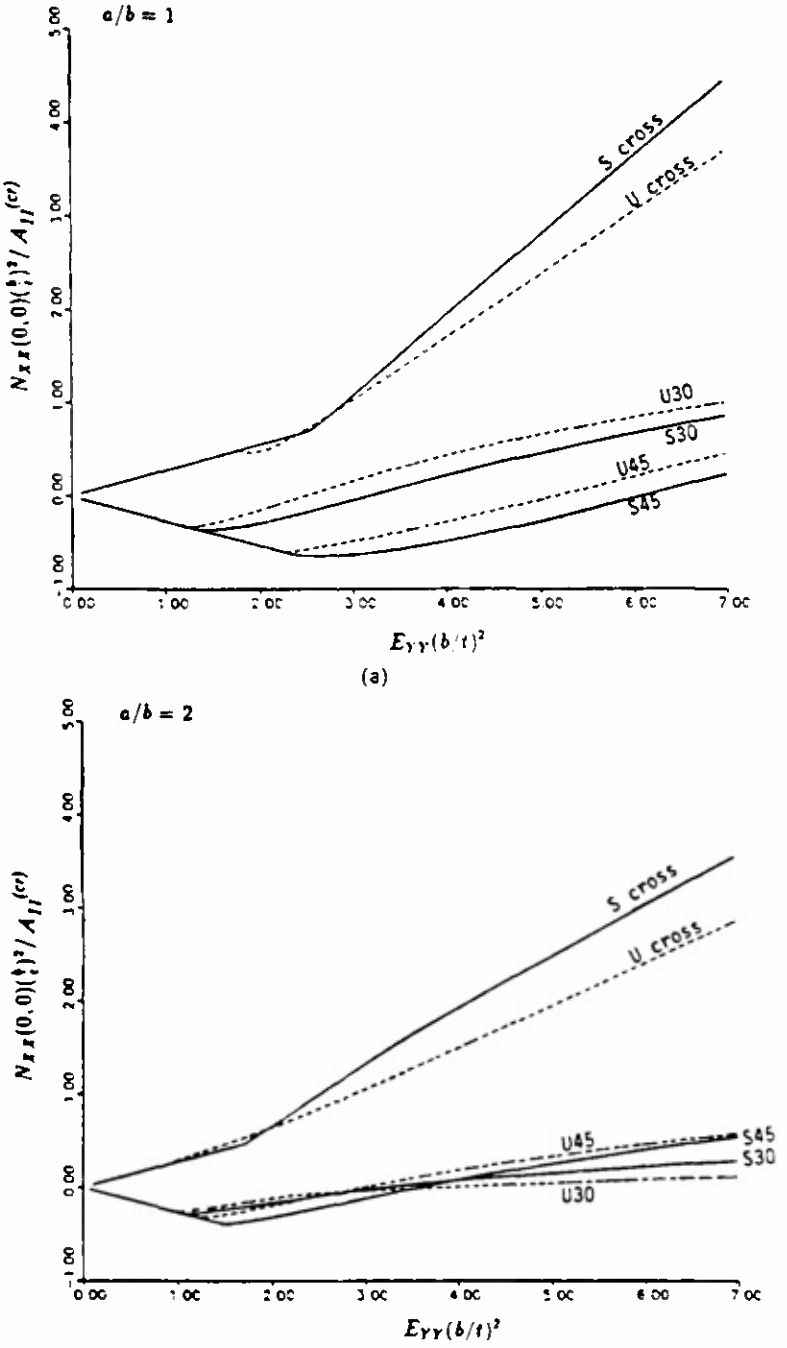

Fig. 6. N_{xx} at (0, 0)

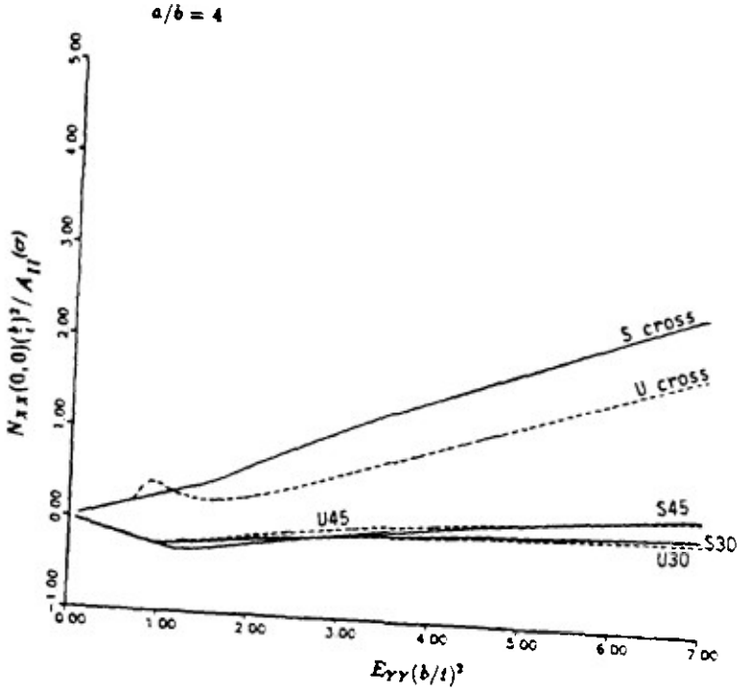

(c)

Fig. 6.—*continued.*

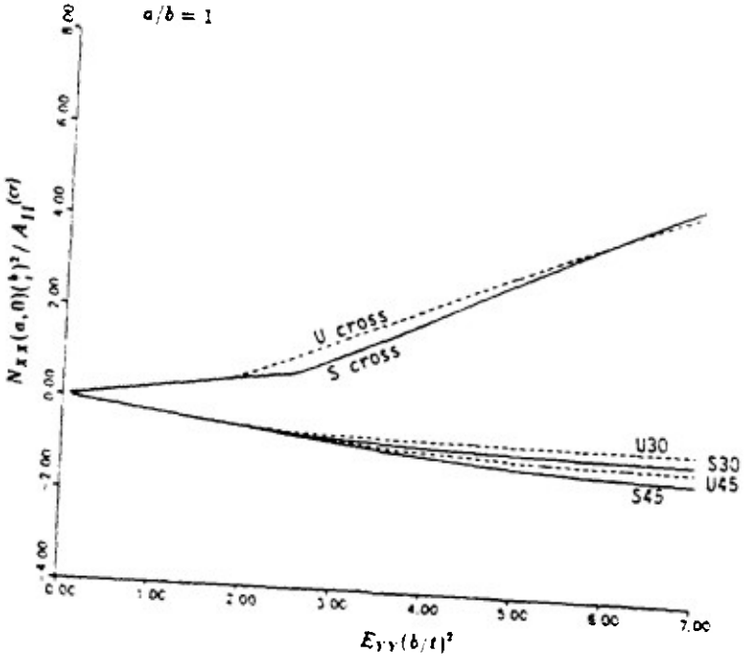

(a)

Fig. 7. N_{xx} at the boundary point $(a, 0)$

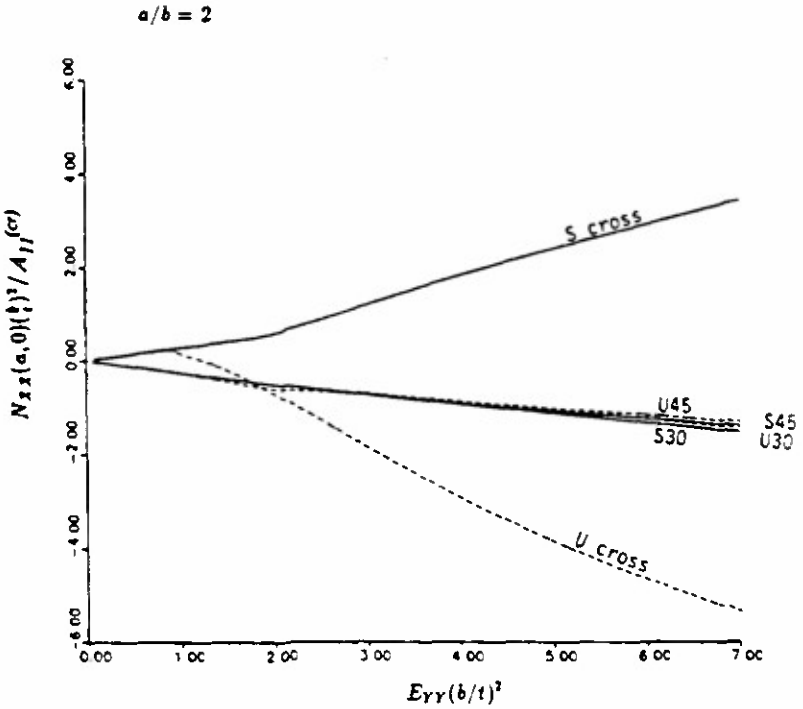

(b)

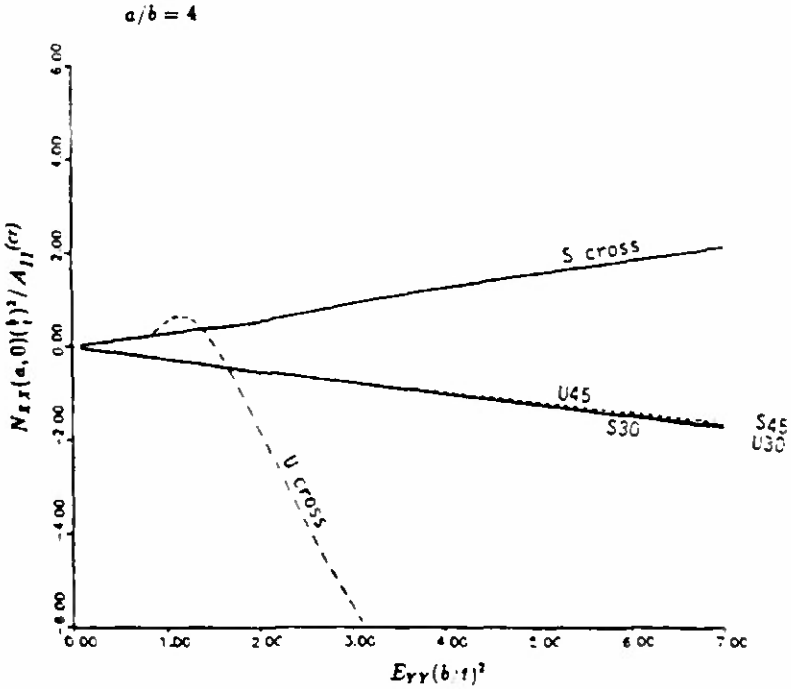

(c)

Fig. 7—*continued*

3.3. *Bending and twisting moments; deflection profile*

For all combinations of ply orientation and lay-up, the general behavior of the in-plane forces in the postbuckling stage are remarkably similar between sublaminates with aspect ratios 2 and 4, as may be seen by comparing the respective plots in Figs 2–7. The somewhat different behavior of circular sublaminates is apparently caused by the constraining effect of a relatively short X-axis, as already mentioned before. A similar conclusion holds for the bending moments M_{yy} and M_{xx}. Plots for M_{yy} at $(0, b)$ are shown in Fig. 8 while those for M_{xx} at $(a, 0)$ are shown in Fig. 9. Additional plots for the present

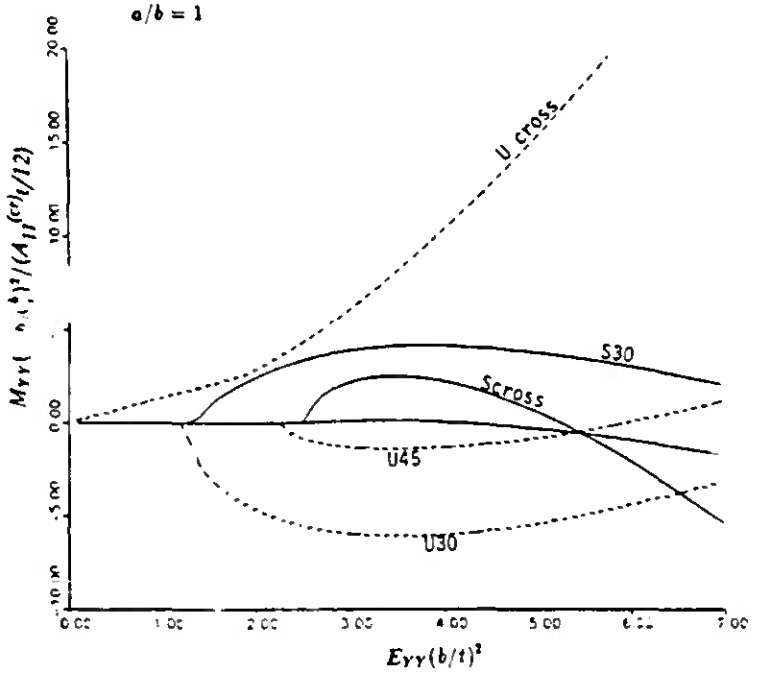

(a)

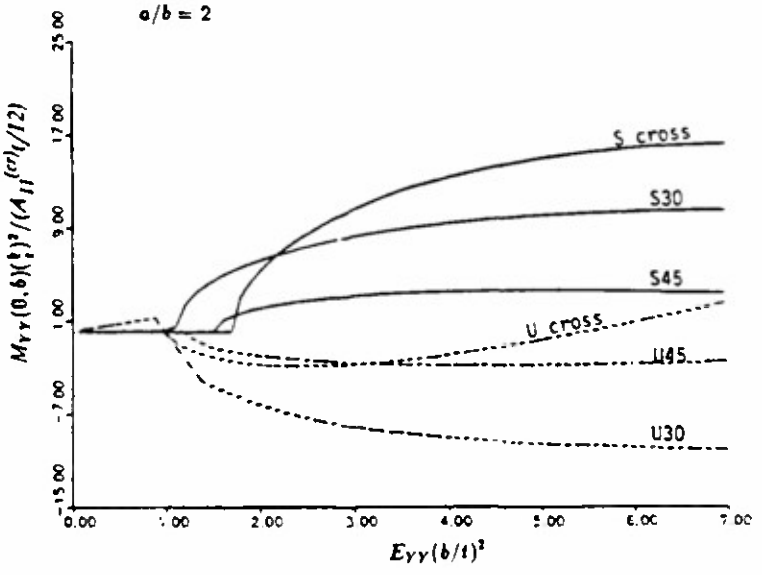

(b)

Fig. 8. Boundary moment M_{yy} at $(0, b)$

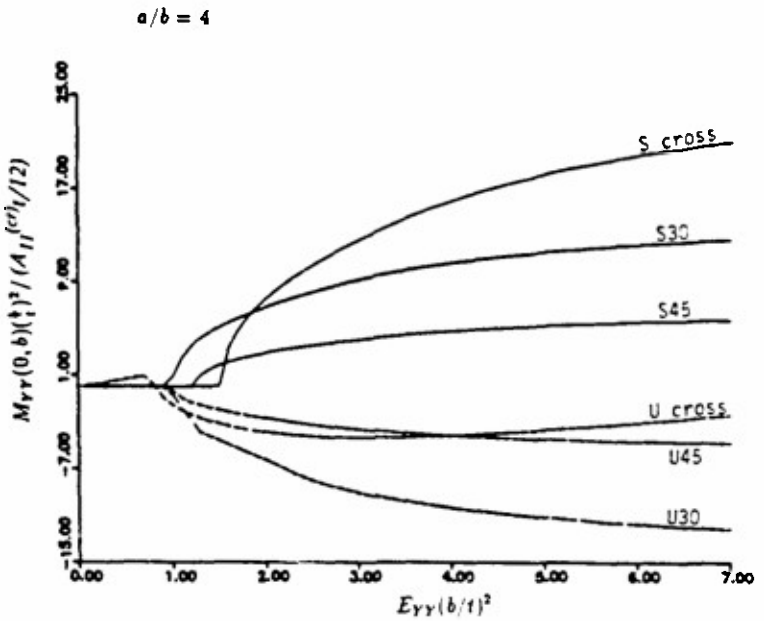

(c)

Fig. 8.—*continued.*

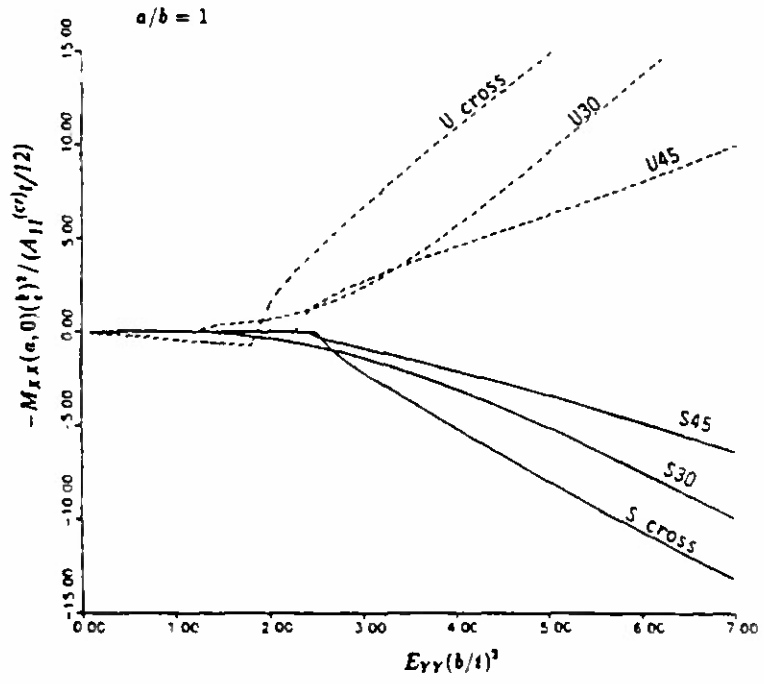

(a)

Fig. 9. Boundary moment M_{11} at $(a, 0)$

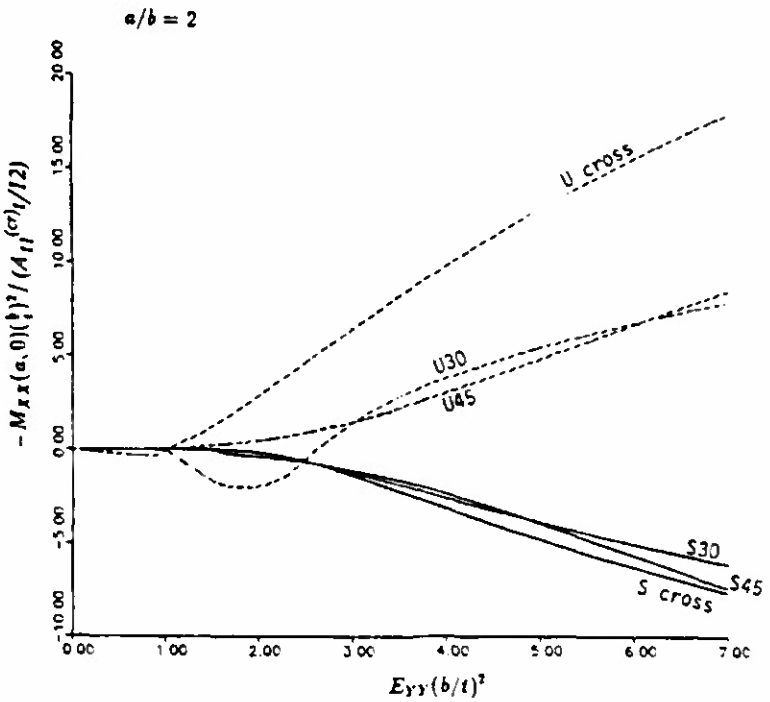

(b)

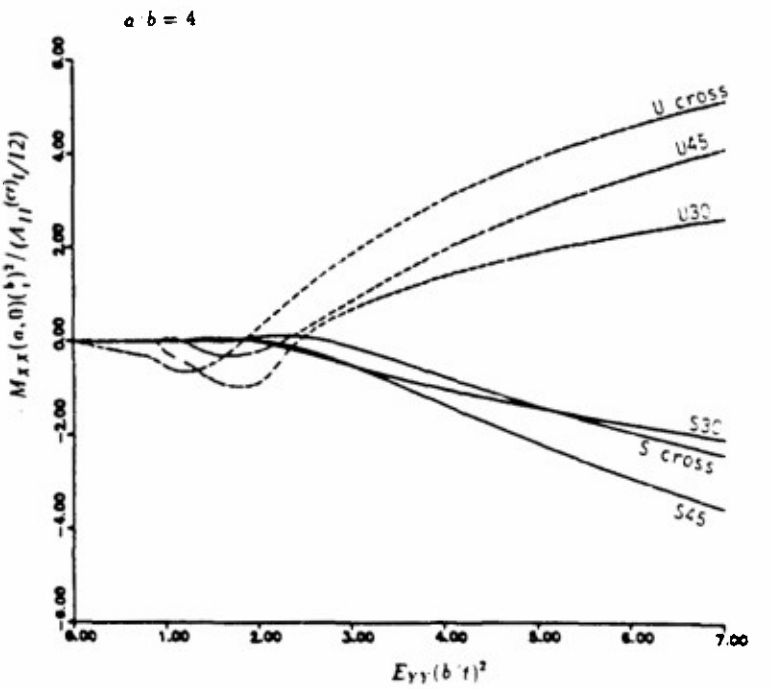

(c)

Fig. 9.—*continued.*

analysis results, including those for the bending moments at the central point (0, 0) may be found in Jane (1989).

The coupling stiffnesses B_{11}, B_{12} and B_{22} vanish in all sublaminates examined in this study except for the unsymmetric cross-ply sublaminate. Hence only the unsymmetric cross-ply sublaminate shows non-zero bending moments M_{XX} and M_{YY} in the prebuckling states. In the postbuckling stage, the relation of the bending moments to the strain load is very complex. However, for sublaminates with aspect ratios 2 and 4, the bending moment M_{YY} at the boundary point $(0, b)$ is generally much greater, in absolute value, than the corresponding moment at the central point. For sublaminates with aspect ratios 1 and 2, the bending moment M_{XX} at $(a, 0)$ is also much greater, in absolute value, than the corresponding moment at (0, 0). For $a/b = 4$, the bending moment M_{XX} at $(a, 0)$ is not large, because a relatively large curvature of the clamped boundary curve at that point provides a restraining effect on the transverse deflection in the vicinity.

In the absence of strong bending–stretching coupling, the bending moment is largely determined by the curvature of the deformed sublaminate. The profiles of the deformed middle surface are shown in Figs 10 and 11 for cross-ply and 45° angle-ply sublaminates under a normalized strain of $-E_{YY}(b/t)^2 = 3$, and in Fig. 12 for 30° angle-ply sublaminates under a normalized strain of 2.0. The left and right portions of the figures indicate the profiles along the Y-axis and the X-axis, respectively. The solid curves refer to the sublaminates with symmetric lay-ups, while the dashed curves refer to those with unsymmetric lay-ups. It is seen that, along the X-axis, the curvature of the profile attains much larger absolute values in the vicinity of the boundary point $(a, 0)$ than around the central point. In contrast, along the Y-axis the curvature of the profile attains relatively small absolute values at the boundary point $(0, b)$ compared to the central point.

Since the curvature of the deformed middle surface of the plate directly affects the normal bending moment at a boundary point, which in turn contributes significantly to an opening action of the delaminated layer from the base laminate (provided that the boundary curvature is positive so that the deflection is non-negative), the concentration of the normal curvature near the boundary point $(a, 0)$, and its attenuation near the point $(0, b)$, tend to

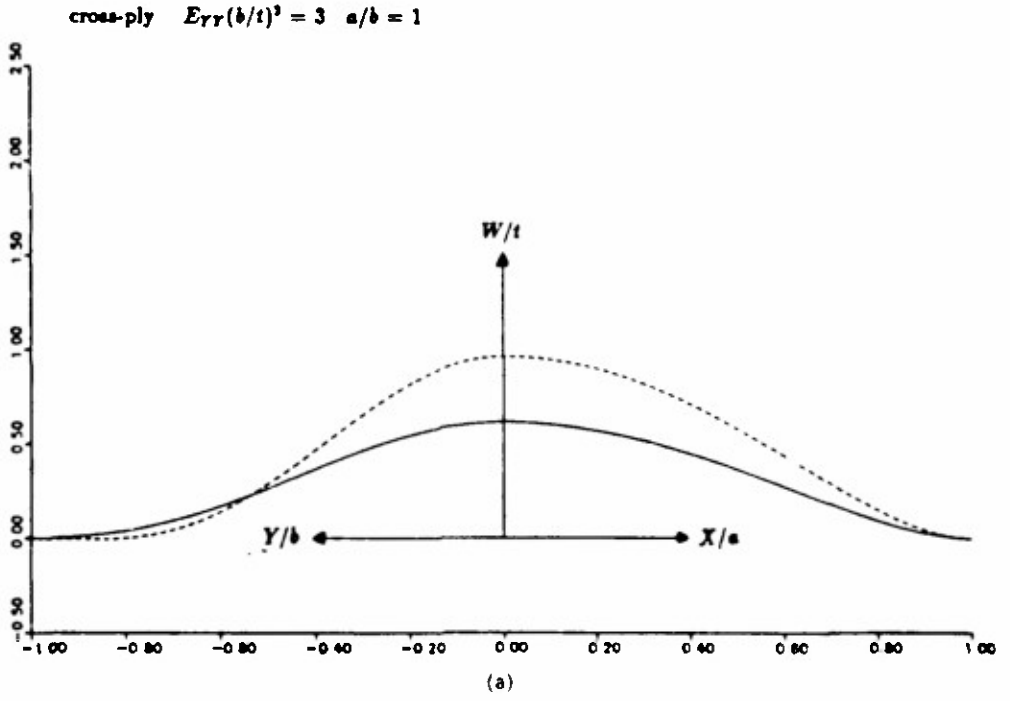

(a)

Fig. 10. Deflection profiles of cross-ply laminates (normalized strain load = 3.0)

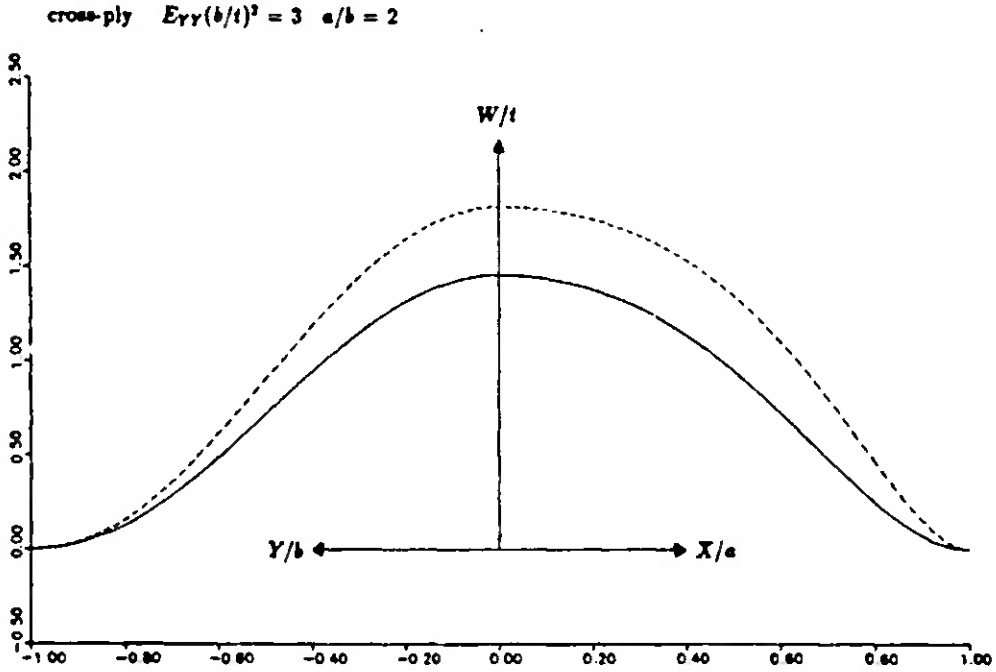

(b)

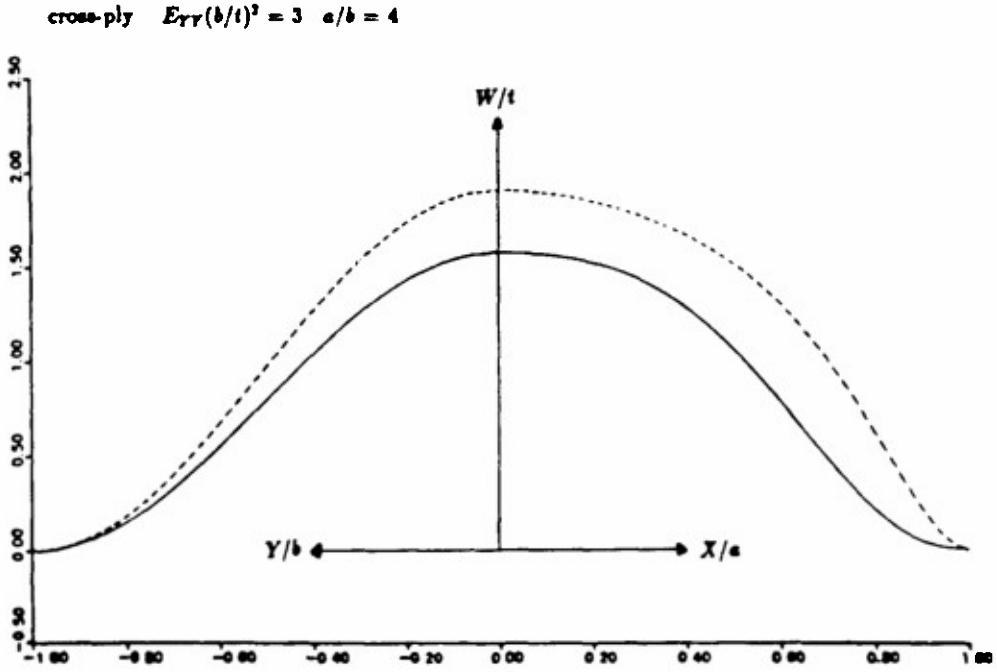

(c)

Fig. 10.—*continued*

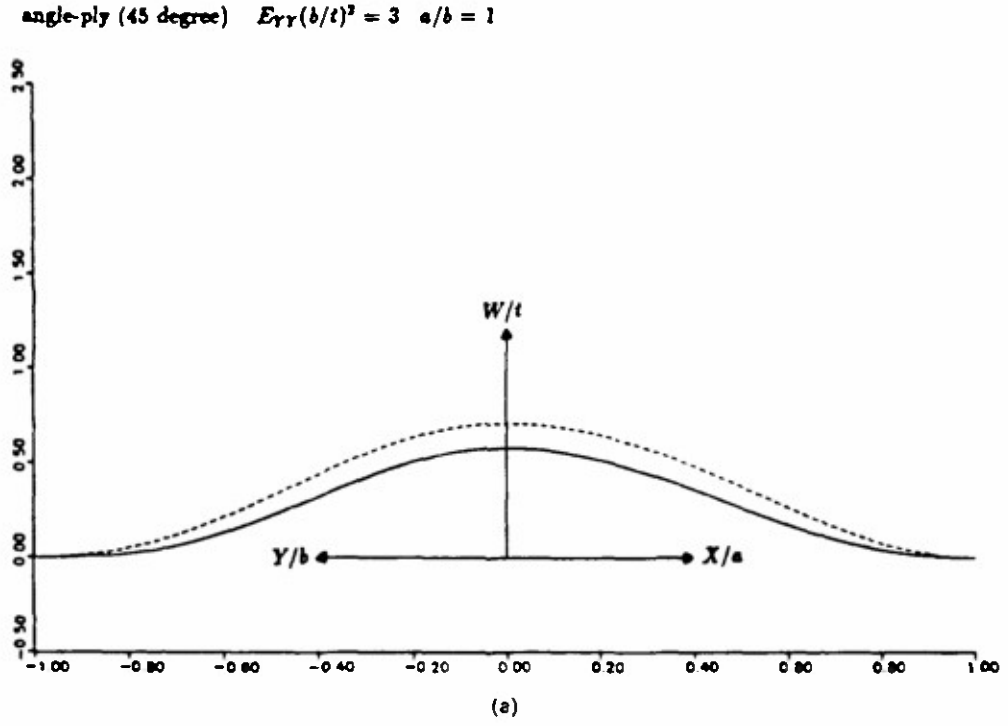

(a)

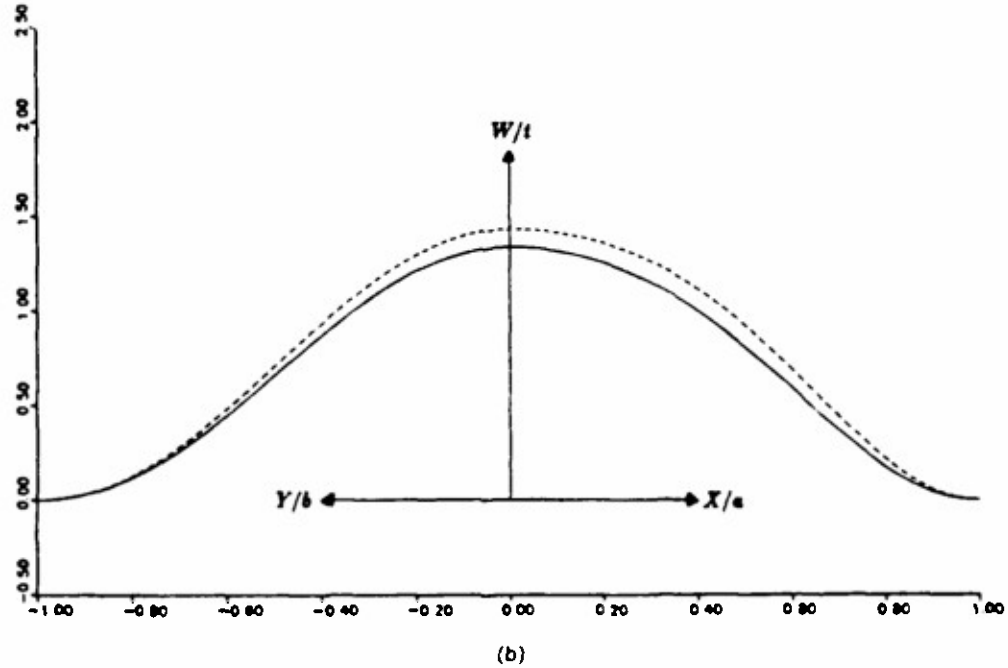

(b)

Fig. 11. Deflection profiles of 45° angle-ply laminates (normalized strain load = 3.0).

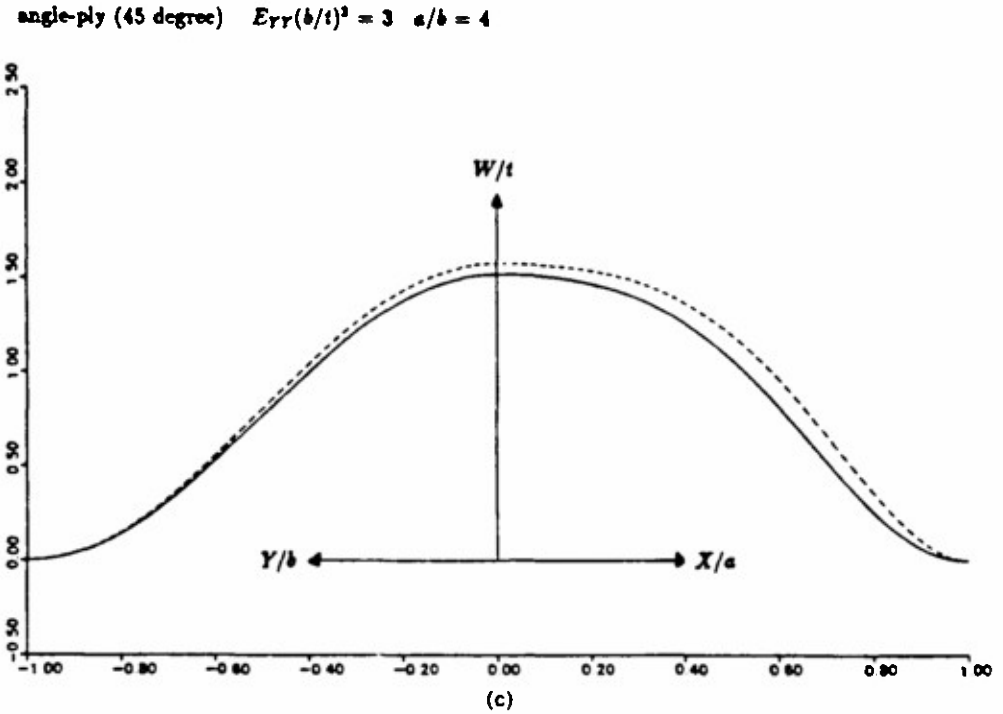

(c)

Fig. 11.—*continued.*

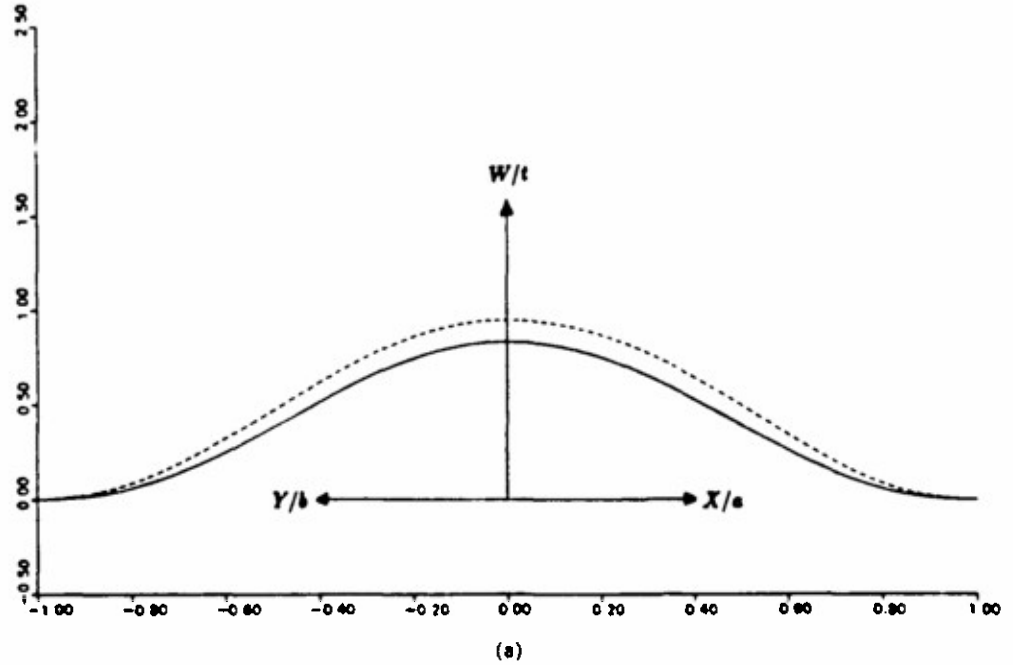

(a)

Fig. 12. Deflection profiles of 30° angle-ply laminates (normalized strain load = 2.0).

angle-ply (30 degree) $E_{YY}(b/t)^3 = 2$ $a/b = 2$

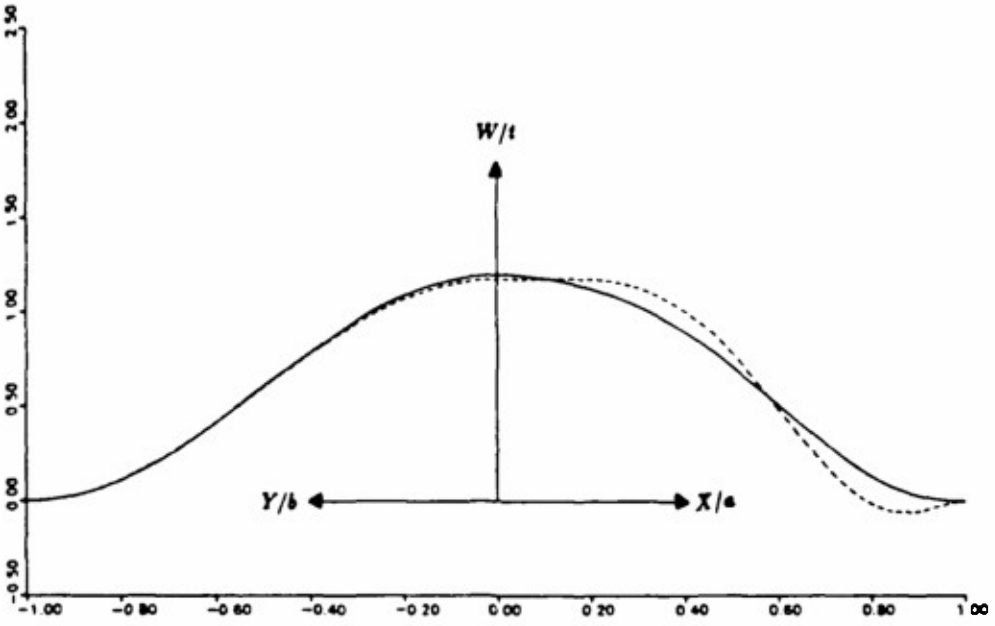

(b)

angle-ply (30 degree) $E_{YY}(b/t)^3 = 2$ $a/b = 4$

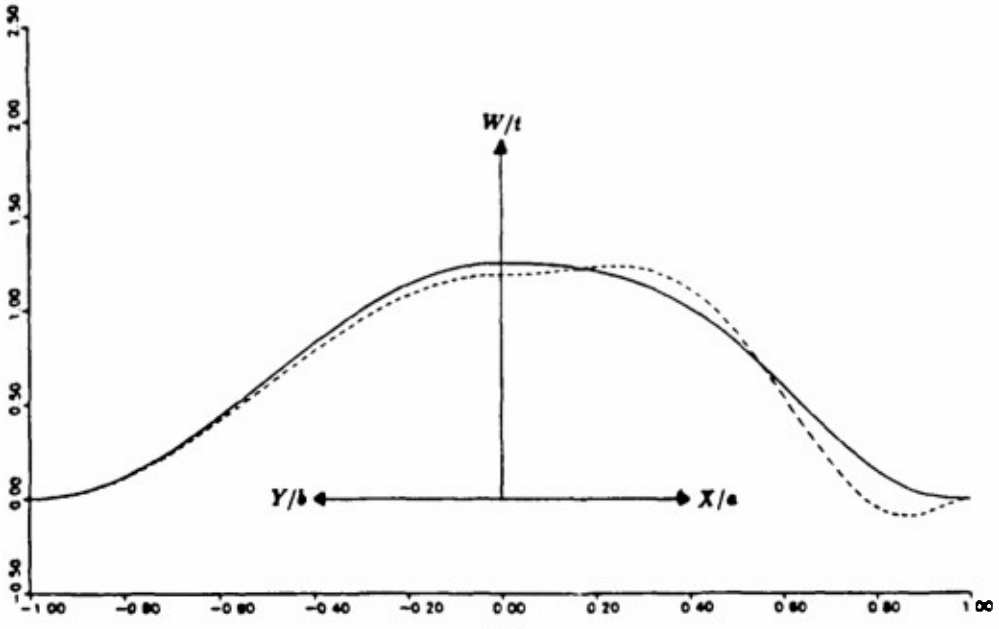

(c)

Fig. 12.—*continued.*

facilitate the growth of the delamination along the X-direction, i.e. the direction perpendicular to that of the compressive loading axis. However, this conclusion is only valid when the aspect ratio is not large. When the growth of the delamination in the transverse direction results in a sufficiently large a/b, the normal curvature at $(a, 0)$ becomes small relative to that at $(0, b)$, because of the longer length of the X-axis in the profiles.

It is interesting to note that the postbuckling deflections of the unsymmetric 30° angle-ply sublaminates with aspect ratios 2 and 4 show multiple wave patterns in the X-direction (see the second and third figures in Fig. 12). This is perhaps essentially due to the relatively small bending stiffness of such sublaminates in the X-direction. Furthermore, these solutions show negative deflection in the vicinity of the boundary point $(a, 0)$ while the solutions of unsymmetric cross-ply sublaminates with $a/b = 1$ show negative deflection near the boundary point $(0, b)$. Since negative deflections imply partial contact of the sublaminate with the base laminate, such mathematical solutions must be modified to take account of the contact condition. However, this difficult task is not attempted in the present work.

The deflection profiles of the 45° angle-ply sublaminates are similar to those of the cross-ply sublaminates with the same aspect ratio. However, the results for sublaminates with symmetric and unsymmetric lay-ups are closer in the 45° case than in the cross-ply case, because the bending–stretching coupling effect in unsymmetric sublaminates is relatively small in the former case compared to the latter case. Furthermore, local contact between the sublaminate and the base plate does not occur in the postbuckling deformation of 45° angle-ply sublaminates for any one of the three aspect ratios.

3.4. *Global and pointwise energy release rates*

For thin-film delaminates with a general shape, the energy-release rate at each point of the delamination boundary may be evaluated in terms of the normal and shearing in-plane forces and the normal bending moment and the twisting moment at that boundary point. The results for the pointwise energy release rates at the two boundary points $(a, 0)$ and $(0, b)$ are shown in Figs 13 and 14, respectively, in terms of the imposed strain load. As the imposed strain increases, the energy release rate at $(a, 0)$ grows more rapidly for the delaminations with smaller a/b, although the bifurcation strains for such delaminations are

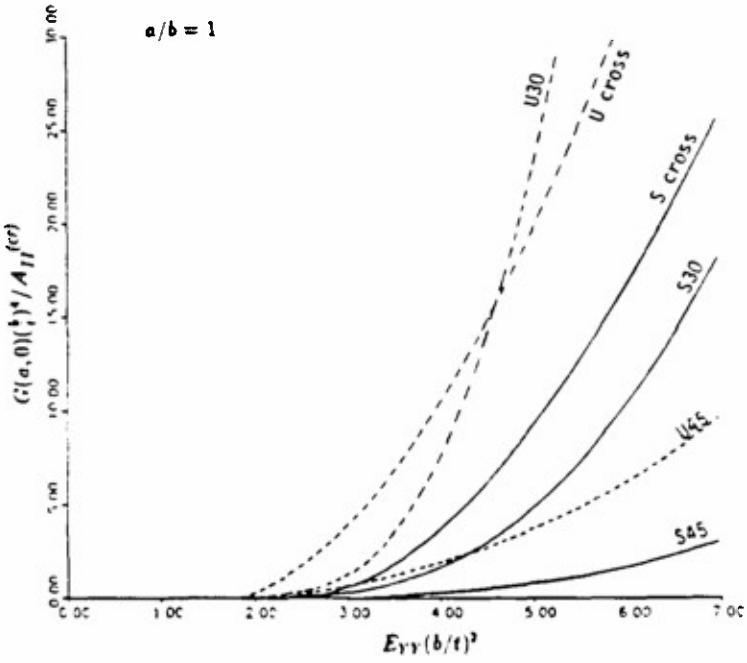

(a)

Fig. 13. Strain-energy release rate at $(a, 0)$.

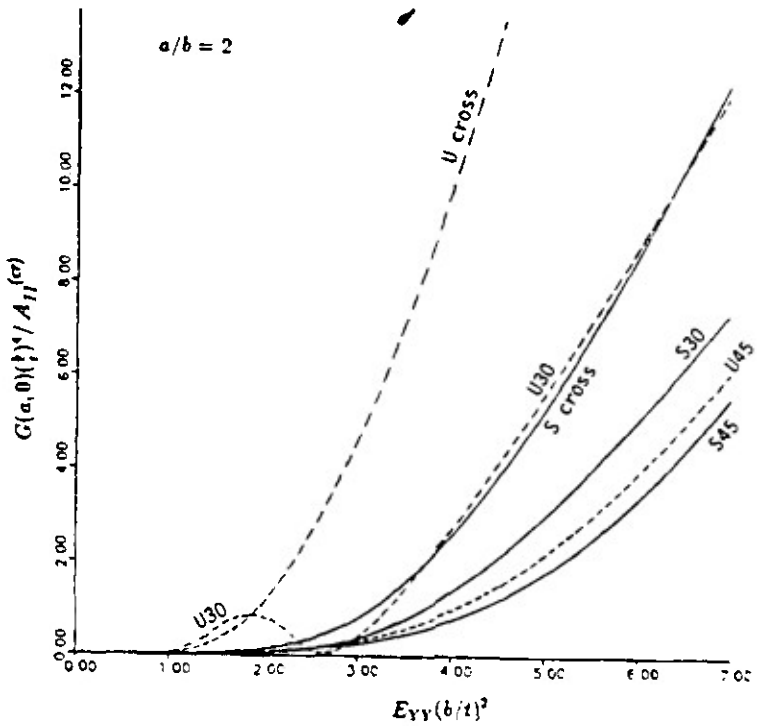

(b)

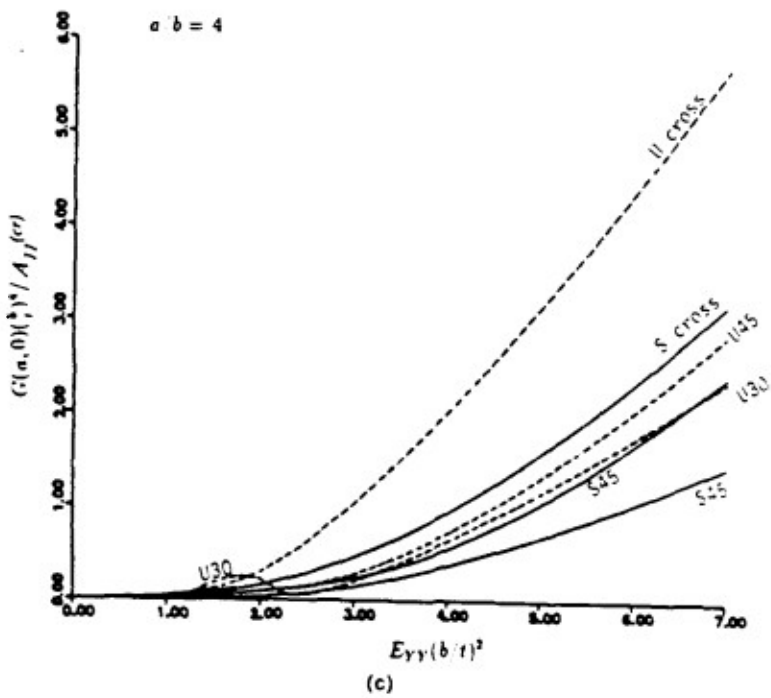

(c)

Fig. 13.—*continued*

greater. In contrast, the energy release rate at $(0, b)$ grows more rapidly, in general, for delaminations with larger a/b. For the circular delamination, the value at $(a, 0)$ dominates over the value at $(0, b)$. If the pointwise energy release rate is used as the criterion of delamination growth, then for a delamination model with a near circular initial shape subjected to an increasing compressive load along the Y-axis, postbuckling delamination growth tends to proceed first along the X-axis until the aspect ratio becomes sufficiently large so that the local energy release rates at $(a, 0)$ and $(0, b)$ become equalized. Afterwards, stable delamination growth may continue under an increasing load in such a manner that the energy release rates at all points of the moving delamination boundary are equal, i.e. equal to the critical value for growth. In unstable, dynamic delamination growth, the local energy release rates at different points of the moving boundary need not be equal because the growth criterion may depend on the crack moving speed.

It should be mentioned that, in case of anisotropic elliptical sublaminates, the maximum and minimum values of the boundary forces and moments and of the energy release rates generally do not occur at the point $(a, 0)$ or $(0, b)$. Consequently, postbuckling growth of an initially elliptical delamination generally proceeds in such a manner that the shape of the delamination becomes non-elliptical. Therefore, a procedure for predicting the delamination growth behavior based on evaluating the *global* energy release rates associated with growth along fixed co-ordinate directions is generally not applicable to two-dimensional delaminations in an anisotropic base plate. In such a procedure, the global energy release rates are obtained for an *assumed* manner of growth by evaluating the potential energies of the delamination model in two successive states of growth and by differentiating the results numerically with respect to the increasing semi-axial lengths of the ellipse. These global energy release rates are fundamentally different from the pointwise energy release rates used in the present study. Indeed, as shown by the present results, their relation to the strain load is very much different from that of the pointwise energy release rates. In cases where the consideration of global energy release rate may be justified, the use of the pointwise and global energy release rates are likely to yield somewhat different predictions with regard to the delamination growth behavior.

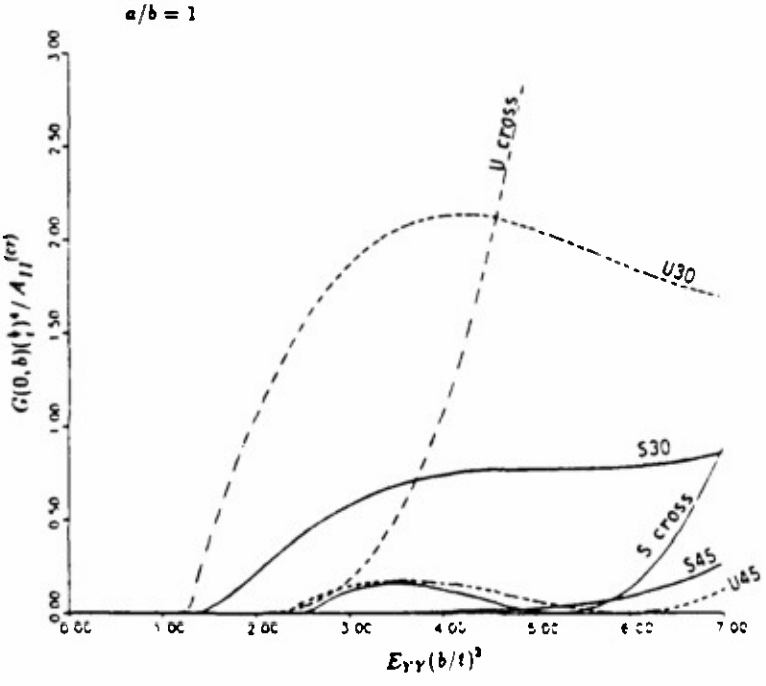

(a)

Fig. 14. Strain-energy release rate at $(0, b)$

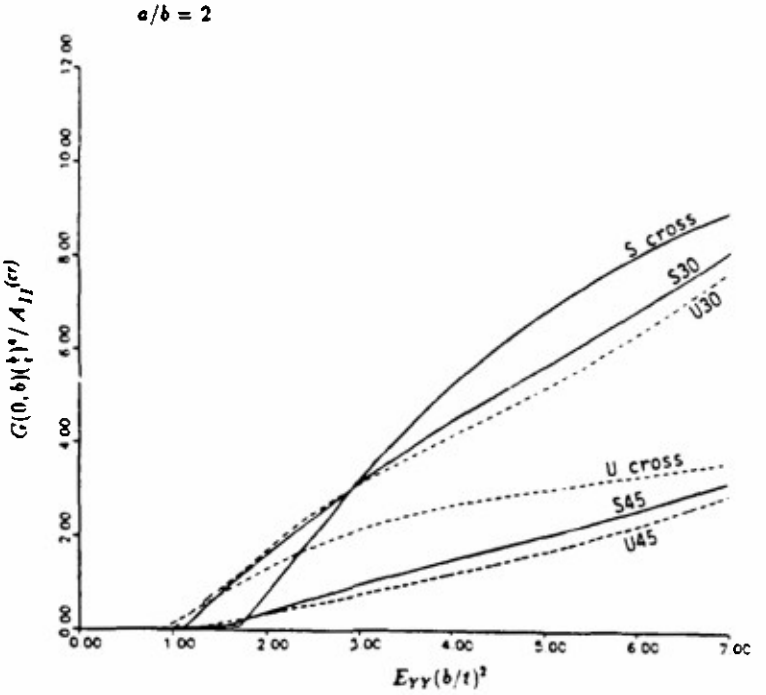

(b)

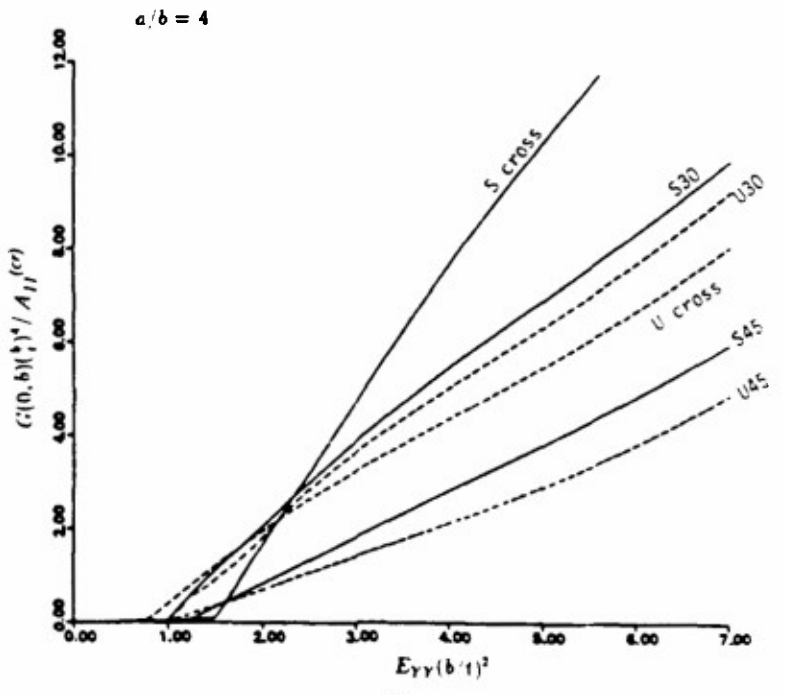

(c)

Fig. 14.—*continued*

4. CONCLUSIONS AND ADDITIONAL REMARKS

Several conclusions with far-reaching implications for the analysis and understanding of sublaminate buckling and crack growth associated with two-dimensional models may be drawn from the results of the present study. Some of these conclusions have been suggested in previous publications (Yin, 1989; Storakers, 1989). They are substantiated, in the present work, by examining Rayleigh–Ritz postbuckling solutions of elliptical sublaminates and by comparing solutions of the various orders.

(1) The bifurcation loads of thin-film elliptical delaminations may be calculated accurately by a Rayleigh–Ritz analysis involving a small number of undetermined coefficients. The results are better than those obtained by alternative methods [for example, Woinowsky-Krieger (1937) and Kassapoglou (1988)].

(2) The postbuckling behavior of a strip delamination model is rather exceptional because the non-linear von Karman equations reduce to a *linear* ordinary differential equation in the case of plane strain buckling. The solutions of strip models do not show non-uniformity of the in-plane deformation in the sublaminate and concentration of curvature of the deformed middle surface around boundary regions. These effects are significant and have important implications on the postbuckling and growth behavior of two-dimensional delamination models.

(3) The non-linear and boundary effects mentioned above cannot be determined, or determined with sufficient accuracy, by a linearized postbuckling analysis or by a Rayleigh–Ritz analysis involving lower-order polynomial expansions of the displacements. Predictions of the force and moment resultants in the sublaminate and of the delamination growth behavior based on Rayleigh–Ritz solutions of order lower than (5, 4) are generally unreliable.

(4) As the orders of polynomials in the displacement expansions increase, the deflection, forces, moments and energy release rates associated with the Rayleigh–Ritz solutions of circular delaminations in axisymmetric deformation converge towards the corresponding results obtained by direct integration of the von Karman equations (Yin, 1985). The convergence confirms the validity of the latter solution, whose results are significantly different to the solution obtained by the perturbation method (Bottega and Maewal, 1983). Rayleigh–Ritz solutions of the order (5, 4) deliver good results over a range of strain loads up to about three times the bifurcation strain. Solutions of the order (7, 6) yield better results over a much wider range of the strain load. On the other hand, solutions of the order (5, 6) are nearly indistinguishable from those of the order (5, 4). The results suggest that higher degree polynomials should be used in the expansions of the in-plane displacements so as to allow adequate modeling of the non-uniformity of the in-plane deformation.

(5) The computational effort involved in solving the non-linear algebraic equations associated with the Rayleigh–Ritz method is small compared to solving the same problem by non-linear finite-element modeling since the number of degrees of freedom required in the latter method maybe considerably larger. In implementing the Rayleigh–Ritz method, the major task consists of algebraic manipulations and integrations for obtaining the potential energy function. Given specific polynomial expansions of the displacements, this task needs to be performed only once in obtaining the functions L_{ij}, M_{ij} and N_{ij} (see eqn (6) in Part I of this paper). When these functions are determined, the potential energy functions and the governing algebraic equations for elliptical delaminations with different thicknesses, aspect ratios and stiffness matrices may be obtained in a straightforward manner. Consequently, the Rayleigh–Ritz method is ideally suited for a parametric study of the postbuckling behavior of elliptical laminates with diverse geometrical and material configurations.

A recent study of buckling, postbuckling and failure of elliptical delaminations has appeared which is also based on the perturbation method (Kassapoglou, 1988). While the work does not present sufficiently detailed results on postbuckling deformation to make a comparison with the present solutions feasible, it yields bifurcation loads with relatively

large errors (several percent). Generally speaking, any method of analysis which fails to provide very accurate results for the bifurcation load cannot be expected to yield acceptable results for the postbuckling deformation, because the buckling problem is a linearized problem whereas the postbuckling problem is strongly non-linear. It therefore appears that, unless higher-order perturbed equations are used, the perturbation method is not a promising approach for obtaining accurate solutions beyond an initial stage of postbuckling deformation.

In selecting the order of Rayleigh–Ritz solutions used in the present study we have taken into account the limitation on the validity of the solutions imposed by the thin-film assumption and the omission of the transverse shear effect. Polynomial expansions of the displacements are truncated at the order where further improvement in the accuracy of the solutions is believed to be within the error caused by these two assumptions. Recently, the effect of transverse shear deformation on the buckling and postbuckling behavior has been studied for strip delamination models (Kardomateas and Schmueser, 1988; Chen, 1989) and thin-film elliptical sublaminates (Peck, 1989). The results depend essentially on the slenderness of the delaminated layer and the base plate. Analytical solutions for strip delamination models, obtained by the use of a shear correction factor, indicate that the transverse shear effect may appreciably reduce the buckling load and significantly increase the energy release rate under a given postbuckling axial load.

Peck (1989) used a higher-order laminated plate theory in conjunction with the Rayleigh–Ritz method to calculate the buckling loads and postbuckling solutions of elliptical sublaminates. This provides a better approach to the assessment of the transverse shear effect in laminated plates than the use of a single shear correction factor (independent of the elastic anisotropy, orientation and lay-up of the constituent plies). It should be mentioned, however, that since the significance of the transverse shear effect increases with the thickness of the sublaminate, the effect may be more important in the delaminated portion of the base plate than in a thin delaminated layer. Hence an adequate evaluation of the transverse shear effect in delamination problems may require a complete analysis of the delamination model without using the thin-film assumption.

REFERENCES

Bottega, W. J. and Maewal, A. (1983). Delamination buckling and growth in laminates. *J. Appl. Mech.* **50**, 184–189.

Chai, H. and Babcock, C. D. (1985). Two-dimensional modelling of compressive failure in delaminated laminates. *J. Comp. Mater.* **19**, 67–98.

Chai, H., Babcock, C. D. and Knauss, W. G. (1981). One dimensional modelling of failure in laminated plates by delamination buckling. *Int. J. Solids Structures* **17**, 1069–1083.

Chen, H.-P. (1989). A variational principle consistent shear deformation theory on compressive delamination buckling and growth. *Proc. AIAA/ASME/ASCE/AHS/ASC 31st SDM Conference*, Long Beach, CA, 1208–1217.

Jane, K. C. (1989). Buckling, Postbuckling Deformation and Vibration of a Delaminated Plate. Ph.D. Thesis, Georgia Institute of Technology, Atlanta, GA.

Kardomateas, G. A. (1989). Large deformation effects in the postbuckling behavior of composites with thin delamination. *AIAA Jl* **27**, 624–631.

Kardomateas, G. A. and Schmueser, D. W. (1988). Buckling and postbuckling of delaminated composites under compressive loads including transverse shear effects. *AIAA Jl* **26**, 337–343.

Kassapoglou, C. (1988). Buckling, post-buckling and failure of elliptical delaminations in laminates under compression. *Comp. Struct.* **9**, 139–159.

Peck, S. O. (1989). Compressive Behavior of Delaminated Composite Plates. Ph.D. Thesis, Stanford University, Palo Alto, CA.

Shivakumar, K. N. and Whitcomb, J. D. (1985). Buckling of a Sublaminate in a Quasi-Isotropic Composite Laminate. *J. Comp. Mater.* **19**, 2–18.

Simitses, G. J., Sallam, S. N. and Yin, W.-L. (1985). Effect of delamination of axially loaded homogeneous laminated plates. *AIAA Jl* **23**, 1437–1444.

Storakers, B. (1989). Nonlinear aspects of delamination in structural members. In *Theoretical Mechanics. Proc. XVIIth Int. Congr. Theor. Appl. Mech.*

Yin, W.-L. (1985). Axisymmetric buckling and growth of a circular delamination in a compressed laminate. *Int. J. Solids Structures* **21**, 503–514.

Yin, W.-L. (1986). Cylindrical buckling of laminated and delaminated plates. *Proc. AIAA/ASME ASCE AHS 27th SDM Conference*, San Antonio, Texas, 165–179.

Yin, W.-L. (1988). The effects of laminated structure on delamination buckling and growth. *J. Comp. Mater.* **22**, 502–517.

Yin, W.-L. (1989). Recent analytical results in delamination buckling and growth. In *Interlaminar Fracture in Composites* (Edited by A. E. Armanios), pp. 253–266. Trans Tec., Switzerland.

Yin, W.-L. and Fei, Z. (1984). Buckling load of circular plate with a concentric delamination. *Mech. Res. Comm.* **11**, 337–344.

Yin, W.-L. and Fei, Z. (1988). Delamination buckling and growth in a clamped circular plate. *AIAA Jl* **26**, 438–445.

Yin, W.-L., Sallam, S. N. and Simitses, G. J. (1986). Ultimate axial load capacity of a delaminated beam-plate. *AIAA Jl* **24**, 123–128.

Appendix F

"Free-Edge Effects in Laminates Under Extension, Bending and Twisting, Part I: A Stress Function Approach"

By Wan-Lee Yin

Proceedings AIAA/ASME/ASCE/AHS/ASC 32nd Structures, Structural Dynamics, and Materials Conference

April 1991, Baltimore, MD, pp. 985-995

AIAA-91-0959-CP

Free-Edge Effects in Laminates Under Extension, Bending and Twisting. Part I: A Stress Function Approach

W.-L. Yin *
Georgia Institue of Technology
Atlanta, Georgia 30332

ABSTRACT

A variational method involving Lekhnitskii's stress functions is used to determine the free-edge interlaminar stresses in a multi-layered strip of laminate subjected to arbitrary combinations of axial extension, bending and twisting loads. The stress functions in each layer are approximated by polynomial functions of the thickness coordinate. The equilibrium equations, the traction-free boundary conditions and the continuity conditions of the interlaminar stresses are exactly satisfied in the present analysis, while the compatibility equations and the interfacial continuity of the displacements are enforced in the sense of the mean by applying the principle of complementary virtual work. Solutions are calculated for symmetric four-layer cross-ply and angle-ply laminates and the rasults are found to be in excellent agreement with rafined finite-element solutions using special hybrid-stress elements in corner regions.

1. Introduction

Composite laminates are prone to severe interlaminar stresses along a free edge. Theoretical studies based on the assumptions of layerwise homogeneity and linear elastic behavior suggest that a singularity of the stress field generally exists at the intersection of a frae edge with an interface between two dissimilar materials [1-3]. From a practical point of view, the presence of a stress singularity and its effect on the region outside the immediate neighborhood of the singularity are of greater importance than the precise mathematical form of the singularity (deduced by strictly applying the simplifying assumptions of layerwise homogeneity and linear elasticity to a corner region of microstructural dimension, and thereby producing physically unrealistic local results). This is because, from the same viewpoint, a singularity actually indicates a region of severe macroscopic stress gradient in which the stress field is affected significantly by nonlinear and inelastic material response and microscopic heterogeneity. This is especially true if, as in the case of free edges of laminates composed of thin plies, the regions of high stress gradient are only several times larger than the characteristic length of the microstructure -- the diameter of the reinforcing fibers and the spacing between adjacent fibers.

It follows from this reasoning that, when assessing the detrimental effects of free-edge interlaminar stresses, one should not pay too much attention to the minute details of the local stress near a mathematical singularity (as predicted by simplifying constitutive assumptions and layerwise homogenization). Obviously, any quantity calculated by discretizing the structure (using finite-difference or finite-element modeling), with values depending significantly on the way and the degree of refinement of discretization, is not an appropriate or reliable measure of the criticality of stress. One should instead rely on global quantities -- quantities which manifest the overall mechanical effects and characteristics of a small, severely stressed region, and quantities whose values do not change appreciably with refinement in material and geometrical modeling over that region. Examples of such global measures include the well-known path-independent integrals. They also include the maximum values of certain stress functions and their first-order derivatives along an interface, which are introduced in the present work.

This is the first of a series of two papers concerned with developing an efficient yet reasonably accurate analysis procedure for the free-edge interlaminar stresses in a multi-layered laminate subjected to axial antension, bending, twisting, or any combination of such strain-controlled loadings. Our raquirements for efficiency and accuracy are such that the final analysis procedure calls for extremely simple input data, that it may be implemented on a personal computer, and that the results of the analysis should be as adequate for the practical purposes of laminate analysis, design and optimization as the solutions obtained from elaborate finite-element analysis. The dual objectives may be achieved without trying to determine the nature of the stress singularity in an extremely small region, but instead by assessing its effects upon the surrounding region via a variational approach.

The first paper of the series (Part I) is concerned with a laminate composed of a relatively small number of anisotropic layers. In this work, example solutions under all three loading cases are computed for four-layer symmetric laminates, including the classical problems of cross-ply and angle-ply laminates. Laminates consisting of a large number of layers require a sublamiante/layer modeling in which the two interior layers adjacent to a particular interface are considered as anisotropic elastic media and all the remaining plies are grouped into an upper sublaminate and a lower sublaminate. The details of such a formulation and the method of analysis are developed in a forthcoming paper (Part II of the series).

Approximate solutions of the free-edge interlaminar stress problem may be obtained by directly solving the governing differential equations (e.g., using finite difference method or series expansion in conjunction with boundary collocation) or by using a variational approach. Direct solutions which accurately represent the interlaminar stresses near the free edge are not easy to obtain or ascertain because of the difficulty to enforce and to validate the convergence of

* Professor, School of Civil Engineering; Member, AIAA. Phone (404) 894-2773

such solutions. Among the existing works using a variational approach, a large number were based on the displacement formulation. More recently, the displacement/stress hybrid formulation has also been used. In contrast, the stress formulation is used in the present study (for all layers of the laminate in Part I of the paper and for the two interior layers of the model in Part II).

In the present analysis, Lekhnitskii's stress functions are introduced in each layer and the traction-free boundary conditions as well as the interfacial continuity of interlaminar stresses are strictly enforced, while the compatibility of strain and the interfacial continuity of displacements are enforced in the sense of weighted integrals through the use of the principle of complementary virtual work. This ensures that the approximate solutions of the present approach satisfies exactly the equilibrium equations everywhere (including all corner regions with steep stress gradients) and the continuity of the interlaminar stresses across entire interfaces (including short segments adjacent to the free edge). In contrast, such conditions are only satisfied in the sense of the mean in a variational approach based on the displacment formulation. With the concentration of the stress gradient and intense interlaminar stresses near the free edge, the application of the stationary potential energy principle to assumed displacement functions or their associated element shape functions may produce results for the stresses that significantly violate the equilibrium equations in corner regions and violate the interfacial continuity conditions in end segments which, although small, are of particular importance. Spilker [4,5] found that, if in corner regions one uses hybrid finite elements which do not satisfy free-edge boundary conditions exactly, then large errors and lack of convergence may result in the pointwise values of certain stress components even though the solutions converge in the sense of weighted integrals and satisfy the free-edge condition in the same sense. In finite-element solutions based on a purely displacement formulation, the danger of this anomalous behavior is always present because exact satifaction of the traction-free boundary conditions cannot be strictly enforced. Therefore, certain results provided by such solutions may be unreliable or even misleading. Indeed, for the classical problem of a symmetric, cross-ply, four-layer laminate under axial extension, a careful comparison indicates significant discrepancies in the stress fields near the free edge and in their trend of convergence among the various existing numerical solutions which do not strictly enforce the free-edge condition. The solutions examined include finite-difference solutions, stress-based solutions using the boundary collation or other approxiamate free-edge conditions, and a number of finite-element solutions using a displacement or hybrid formulation. The possibility of anomalous behavior does not arise in the present procedure of solution because all equilibrium equations, free-edge boundary conditions and interfacial continuity of tractions are satisfied exactly rather than in the sense of the mean. Although the present analysis requires only a very small fraction of computational effort compared to refined, displacement-based finite-element solutions, the results are found to be in better agreement with Spilker's finite-element solutions [4,5] which used special free-edge elements that satisy the traction-free conditions exactly.

Besides the constitutive assumption of linear elasticity, the only approximation used in the present analysis is that the stress functions in each layer are polynomial functions of the thickness coordinate. No a priori assumption is made concerning the dependence of the stress functions on the coordinate parallel to the interface. Rather, it follows as a consequence of the principle of complementary virtual work that the form of dependence is governed by a system of linear ordinary differential equations with constant coefficients. This system of equations together with homogeneous boundary conditions (resulting from the free-edge condition) define an eigenvalue problem. The solution of the eignevalue problem is a combination of a particular solution and eigenfunctions which hava exponential forms with real or complex exponents. The particular solution corresponds to the limiting stress fields away from the free edge (constant in each layer but generally vary from layer to layer) and is peculiar to each one of the three strain loading case -- axial extension, bending and twisting. On the other hand, the eigenvalues and eigenfunctions are the same for all three cases. When the task of solving the eigenvalue problem is completed, the solutions for the interlaminar stresses corresponding to the three distinct cases of strain loading may be obtained easily by taken different combinations of the eigenfunctions with the particular solution (peculiar to each case) so as to satify the homogeneous boundary conditions. Thus the present approach has the additional advantage that the solutions to all three cases may be obtained simultaneously. In contrast, implementation of the finite-element and other numerical solution procedures usually must be repeated for each distinct loading case.

We note that the assumption of polynomial dependence of the stress functions on the thickness coordinate in each layer may be justified for laminates consisting of thin plies. Although the present analysis uses lower-degree polynomial representations, more refined analysis may be implemented, in principle, with the use of higher degree polynomials. However, such refinement will only appreciably affect the resulting stress near the free edge. If the thickness of each ply is only one order of magnitude greater than the fiber diameter, then a higher-order polynomial representation of the fluctuations of the macroscopic stresses in the thickness direction has dubious physical significance.

It is pointed out in Sec. 8 of this paper that, along an interface, the torsion stress function Ψ and the first-order derivatives of the Airy stress function F are related to the stress resultants and the moment resultants of the interlaminar normal and shearing stresses over end segments of the interface. Since the maximum values of these derivatives are global measures of the criticality of the interlaminar stresses near the free edge, they may be used as parameters in the fracture criteria for the initiation of delamination growth along the interface.

2. Elasticity of an orthotropic layer referred to the global coordinates of the laminate

Consider a laminated strip of thickness $2y^*$ with two parallel free edges at $x = \pm a$ and consisting of n+1 unidirectional, fiber-reinforced composite layers separated by n planar interfaces. Tha

layers and their interfaces will be numbered from the bottom up. Thus the i-th layer is bounded below by the (i-1)-th interface, $y = y_{i-1}$, bounded above by the i-th interface, $y = y_i$, where $y = 0$ is the middle plane of the laminate (Fig. 1). The layer has the thickness $h_i = y_i - y_{i-1}$. Each unidirectional composite layer will be regarded in the present analysis as a homogeneous, orthotropic, linearly elastic medium with the extensional elastic modulus E_1 along the fiber direction and moduli E_2 and E_3 along the other two orthotropic directions. Other material moduli needed to characterize the elasticity of the layer are ν_{23}, ν_{31}, ν_{12}, G_{23}, G_{31} and G_{12}. It is more convenient for the present analysis to use the compliance coefficients S_{ij} (i,j = 1, ..., 6), defined by the following constitutive relation for the layer

$$\begin{Bmatrix} \epsilon_1 \\ \epsilon_2 \\ \epsilon_3 \\ \epsilon_4 \\ \epsilon_5 \\ \epsilon_6 \end{Bmatrix} = \begin{bmatrix} S_{11} & S_{12} & S_{13} & 0 & 0 & 0 \\ S_{21} & S_{22} & S_{23} & 0 & 0 & 0 \\ S_{31} & S_{32} & S_{33} & 0 & 0 & 0 \\ 0 & 0 & 0 & S_{44}/2 & 0 & 0 \\ 0 & 0 & 0 & 0 & S_{55}/2 & 0 \\ 0 & 0 & 0 & 0 & 0 & S_{66}/2 \end{bmatrix} \begin{Bmatrix} \sigma_1 \\ \sigma_2 \\ \sigma_3 \\ \tau_{23} \\ \tau_{12} \\ \tau_{13} \end{Bmatrix} \quad (1)$$

where $\epsilon_4 = \gamma_{23}/2$, $\epsilon_5 = \gamma_{13}/2$ and $\epsilon_6 = \gamma_{12}/2$. If the elastic properties of the layer are considered transversly isotropic in the plane perpendicular to the fiber direction, then $E_2 = E_3$, $\nu_{12} = \nu_{13}$ and $G_{12} = G_{13}$. Furthermore,

$$S_{11} = 1/E_1\ , \qquad S_{22} = S_{33} = 1/E_2\ ,$$
$$S_{12} = S_{13} = -\nu_{12}/E_1 = -\nu_{21}/E_2\ ,$$
$$S_{23} = -\nu_{23}/E_2\ , \qquad S_{44} = 1/G_{23}\ ,$$
$$S_{55} = S_{66} = 1/G_{12}$$

The thickness direction of all layers (i.e., the y-axis) is an orthotropic direction and this direction will be taken as the 3-direction in every layer. Within the plane of the layer, the fiber direction is oriented at a constant angle θ with repect to the z-direction (the direction parallel to the free edges). Transformation of the stress components from the (z, x, y) coordinate system to the orthotropic material system (1, 2, 3) has the form

$$\begin{Bmatrix} \sigma_1 \\ \sigma_2 \\ \sigma_3 \\ \tau_{23} \\ \tau_{13} \\ \tau_{12} \end{Bmatrix} = \begin{bmatrix} \cos^2\theta & \sin^2\theta & 0 & 0 & 0 & \sin 2\theta \\ \sin^2\theta & \cos^2\theta & 0 & 0 & 0 & -\sin 2\theta \\ 0 & 0 & 1 & 0 & 0 & 0 \\ 0 & 0 & 0 & \cos\theta & -\sin\theta & 0 \\ 0 & 0 & 0 & \sin\theta & \cos\theta & 0 \\ -\frac{1}{2}\sin 2\theta & \frac{1}{2}\sin 2\theta & 0 & 0 & 0 & \cos 2\theta \end{bmatrix} \begin{Bmatrix} \sigma_z \\ \sigma_x \\ \sigma_y \\ \tau_{xy} \\ \tau_{yz} \\ \tau_{zz} \end{Bmatrix}$$

The tensorial strain components transform in exactly the same manner. For simplicity we denote the matrix of transformation in the last equation by $TH(\theta)$ and the matrix of Eq. (1) by SS. Then $TH(-\theta)$ is the inverse matrix of $TH(\theta)$. Furthermore,

$$\begin{Bmatrix} \epsilon_z \\ \epsilon_x \\ \epsilon_y \\ \gamma_{xy}/2 \\ \gamma_{yz}/2 \\ \gamma_{zz}/2 \end{Bmatrix} = TH(-\theta).SS.TH(\theta) \begin{Bmatrix} \sigma_z \\ \sigma_x \\ \sigma_y \\ \tau_{xy} \\ \tau_{yz} \\ \tau_{zz} \end{Bmatrix} \quad (2)$$

where the matrix $TH(-\theta).SS.TH(\theta) = MM(\theta)$ has the form

$$\begin{bmatrix} a_{11} & a_{12} & a_{13} & 0 & 0 & a_{16} \\ a_{12} & a_{22} & a_{23} & 0 & 0 & a_{26} \\ a_{13} & a_{23} & a_{33} & 0 & 0 & a_{36} \\ 0 & 0 & 0 & a_{44}/2 & a_{45}/2 & 0 \\ 0 & 0 & 0 & a_{45}/2 & a_{55}/2 & 0 \\ a_{16}/2 & a_{26}/2 & a_{36}/2 & 0 & 0 & a_{66}/2 \end{bmatrix}$$

From the first row of Eq. (2) one obtains

$$\sigma_z = (\epsilon_z - a_{12}\sigma_x - a_{13}\sigma_y - a_{16}\tau_{zz})/a_{11}$$

Substituting into the right hand side of Eq. (2), and replacing the first row of Eq. (2) by the preceding expression for σ_z, one has

$$\begin{Bmatrix} \sigma_z \\ \epsilon_x \\ \epsilon_y \\ \gamma_{xy} \\ \gamma_{yz} \\ \gamma_{zz} \end{Bmatrix} = \begin{bmatrix} 1/a_{11} & -a_{12}/a_{11} & -a_{13}/a_{11} & 0 & 0 & -a_{16}/a_{11} \\ a_{12}/a_{11} & \beta_{22} & \beta_{23} & 0 & 0 & \beta_{26} \\ a_{13}/a_{11} & \beta_{23} & \beta_{33} & 0 & 0 & \beta_{36} \\ 0 & 0 & 0 & \beta_{44} & \beta_{45} & 0 \\ 0 & 0 & 0 & \beta_{45} & \beta_{55} & 0 \\ a_{16}/a_{11} & \beta_{26} & \beta_{36} & 0 & 0 & \beta_{66} \end{bmatrix} \begin{Bmatrix} \epsilon_z \\ \sigma_x \\ \sigma_y \\ \tau_{xy} \\ \tau_{yz} \\ \tau_{zz} \end{Bmatrix} \quad (3)$$

where the coefficients

$$\beta_{ij} = a_{ij} - a_{1i}a_{1j}/a_{11} \qquad \text{for } i,j = 1 \quad (4)$$

were introduced by Lekhnitskii ([6], p. 109).

3. Generalized plane deformation of a laminated strip

For a homogeneous anisotropic elastic medium of cylindrical shape with the generators parallel to the z-direction, Lekhnitskii investigated the class of infinitesimal deformations for which the stress tensor is independent of the z-coordinate. He found that the class consists of deformations whose displacement components have the form ([6], pp. 107-108)

$$\begin{aligned} w(z,x,y) &= (Ax - By + C)z + W(x,y) + \omega_1 y - \omega_2 x + w_o \\ u(z,x,y) &= -Az^2/2 - \theta yz + U(x,y) + \omega_2 z - \omega_3 y + u_o \\ v(z,x,y) &= Bz^2/2 + \theta xz + V(x,y) + \omega_3 x - \omega_1 z + v_o \end{aligned} \quad (5)$$

Such deformations will be called "generalized plane deformations". Starting from a plane deformation U(x,y) and V(x,y), one may obtain generalized plane deformations by superposing rigid-body translations, rotations, shearing along the z-axis (characterized by the function W(x,y)), uniform extension and twisting along the same axis (the constants C and θ), and uniform bending deformation with respect to the y- and x-axes (the constants A and B, respectively).

In the present work, we study the interlaminar stresses in a thin laminated strip bounded by two parallel free edges ($x = \pm a$) under mechanical loads at the two ends ($z = 0, \ell$). The end loads are such that the resulting stress in the strip depends only on x and y but not on the axial coordinate z. Hence in each layer of the laminated strip, the displacement functions have the form given by Eq. (5). In order to satisfy the interfacial continuity of the displacements, either exactly or in an averaged sense, it is necessary that the set of constants A, B, C and θ be the same for all layers.

It is well-known that intense interlaminar stresses are localized in the vicincity of the free edges. Along a free edge $x = a$, the in-plane normal and shearing stress resultants N_z and N_{zz} vanish, and so does the normal bending moment M_x. The non-vanishing force and moments are N_z, M_z and M_{zz}, and their corresponding kinematical variables are the axial extensional strain $\epsilon_z^o = C$, the bending curvature $k_z = B$, and the twisting curvature $k_{zz} = \theta$. Bending with respect to the y-axis introduces large bending strains near the free edges, and this usually does not happen unless the thickness and

width of the laminated strip ($2y^*$ and $2a$) are comparable in magnitude. Furthermore, this bending action, characterized by the constant A in Eq. (5), produces a nearly constant axial strain $a \cdot A$ in the vicinity of the free edge $x = a$. Hence its local effect on the interlaminar stresses near the free edge of a thin laminate may be accounted by absorbing the additional strain $a \cdot A$ into the uniform extensional strain C. Consequently, we shall set $A = 0$ in Eq. (5). It follows that, considered as a thin laminate, the local states of loading and deformation near $x = a$ are characterized by the free-edge condition and the three constant parameters B, C and θ.

4. Stress functions; interface and boundary conditions

A stress field in the i-th layer satisfying the differential equations of equilibrium may be expressed in terms of a pair of stress functions $\overset{(i)}{F}(x,y)$ and $\overset{(i)}{\Psi}(x,y)$ in the following manner:

$$\overset{(i)}{\sigma_x} = \overset{(i)}{F}_{,yy}, \qquad \overset{(i)}{\sigma_y} = \overset{(i)}{F}_{,xx}, \qquad \overset{(i)}{\tau_{xy}} = -\overset{(i)}{F}_{,xy}$$
$$\overset{(i)}{\tau_{xz}} = \overset{(i)}{\Psi}_{,y}, \qquad \overset{(i)}{\tau_{yz}} = -\overset{(i)}{\Psi}_{,x} \tag{6}$$

Obviously, an arbitrary bilinear function of x and y and an arbitrary constant may be added to the first and the second stress function, respectively, without affecting the resulting stress field in the layer. The first row of Eq. (3) yields

$$\overset{(i)}{\sigma_x} = (\epsilon_x - a_{12}\overset{(i)}{F}_{,yy} - a_{13}\overset{(i)}{F}_{,xx} - a_{16}\overset{(i)}{\Psi}_{,y})/a_{11} \tag{7}$$

The continuity of the normal and shearing stresses across the i-th interface $y = y_i$ requires that, along that interface,

$$(\overset{(i+1)}{F} - \overset{(i)}{F})_{,xx} = 0, \quad (\overset{(i+1)}{F}_{,y} - \overset{(i)}{F}_{,y})_{,x} = 0,$$
$$(\overset{(i+1)}{\Psi} - \overset{(i)}{\Psi})_{,x} = 0$$

Hence we may appropriately choose an additive bilinear function and an additive constant for the stress functions in the (i+1)-th layer so that, along the interface $y = y_i$,

$$\overset{(i+1)}{F} = \overset{(i)}{F}, \qquad \overset{(i+1)}{F}_{,y} = \overset{(i)}{F}_{,y}, \qquad \overset{(i+1)}{\Psi} = \overset{(i)}{\Psi} \tag{8}$$

Furthermore, without loss of generality the stress functions in the bottom layer may be chosen in such a way that, over the lower surface of the laminate, $y = -y^*$, one has

$$\overset{(1)}{F} = 0, \qquad \overset{(1)}{F}_{,y} = 0, \qquad \overset{(1)}{\Psi} = 0 \tag{9}$$

By integrating σ_x and τ_{xz} through the thickness of all layers, and making use of the continuity of $F_{,y}$ and Ψ across the interfaces, one finds that the stress resultants N_x and N_{xz} are equal to the values of $F_{,y}$ and Ψ, respectively, on the upper surface of the laminate. Let the values be denoted by G^* and Ψ^*, i.e.,

$$N_x = \sum_i \int \overset{(i)}{\sigma_x} dy = \sum_i \int \overset{(i)}{F}_{,yy} dy = \sum_i \overset{(i)}{F}_{,y} \Big|_{y=y_{i-1}}^{y=y_i} = F_{,y}\Big|_{-y^*}^{y^*} = G^*$$

$$N_{xz} = \sum_i \int \overset{(i)}{\tau_{xz}} dy = \sum_i \int \overset{(i)}{\Psi}_{,y} dy = \Psi^*$$

Now the stress moment M_x is given by

$$M_x = -\sum_i \int y \overset{(i)}{\sigma_x} dy = -\sum_i \int y \overset{(i)}{F}_{,yy} dy = -\sum_i \int (y \overset{(i)}{F}_{,y})_{,y} \cdot \overset{(i)}{F}_{,y}) \, dy = F^* - y^* G^*$$

where F^* is the value of the stress function on the top surface. For the case considered in the present work, N_x, N_{xz} and M_x all vanish because of the free-edge conditions. Hence,

$$F^* = G^* = \Psi^* = 0. \tag{10}$$

Finally, vanishing of the traction vector along the free edges $x = \pm a$ implies that

$$F_{,yy} = -F_{,xy} = \Psi_{,y} = 0$$

Integration with respect to the thickness coordinate yields the following results on $x = \pm a$,

$$F = F_{,x} = \Psi = 0. \tag{11}$$

Equations (9), (10) and (11) imply that, for the present problem, the stress functions in the layers may be chosen in such a way that F, Ψ and the normal derivative of F vanish on the boundary surfaces $x = \pm a$ and $y = \pm y^*$ and are continuous across all layer interfaces.

5. The principle of complementary virtual work

A variation in the stress field in the i-th layer satisfies the equilibrium equations

$$\delta\sigma_{ij,j} = 0$$

as well as the free-edge condition and the continuity of δF, $\delta F_{,y}$ and $\delta\Psi$ across the upper and lower interfaces. Hence,

$$0 = \iiint u_i \delta\sigma_{ij,j} \, dxdydz = \iiint [(u_i \delta\sigma_{ij})_{,j} - u_{i,j}] dxdydz$$
$$= \iint u_i \delta\sigma_{ij} n_j \, dA - \iiint \tfrac{1}{2}(u_{i,j} + u_{j,i}) \delta\sigma_{ij} \, dxdydz \tag{12}$$

Since the stresses in all layers are independent of the axial coordinate z, it is sufficient to consider only those variations of the stresses which are also independent of z. Furthermore, one need only consider an interval of the laminated strip of unit length along the axial direction, $0 \le z \le 1$. By summing Eq. (12) over all layers, and making use of the traction-free boundary conditions and the interfacial continuity of the interlaminar stresses, one obtains

$$\sum \iint (\Delta u \delta\tau_{xz} + \Delta v \delta\tau_{yz} + \Delta w \delta\sigma_z) dxdy - \sum \int ([u]_I \delta\tau_{xy} + [v]_I \delta\sigma_y + [w]_I \delta\tau_{yz}) dx = \sum \iint \epsilon_{ij} \delta\sigma_{ij} \, dxdy \tag{13}$$

where the double integrals are summed over all layers and the single integrals are summed over all interfaces $y = y_I$. The bracket symbol, $[\ ]_I$, denotes the jump of the quantity inside the bracket across the I-th interface. Δu, Δv and Δw stand for the differences of the displacements at $z = 1$ and $z = 0$. They may be obtained from Eq. (5) with $A = 0$:

$$\Delta u = -\theta y+\omega_2, \quad \Delta v = B/2+\theta x-\omega_1, \quad \Delta w = C-By$$

Equations (6) and (7) yield, in each layer,

$$\delta\tau_{xx} = \delta\Psi_{,y}, \qquad \delta\tau_{yz} = -\delta\Psi_{,x},$$

$$\delta\sigma_z = -(a_{12}\delta F_{,yy}+a_{13}\delta F_{,xx}+a_{16}\delta F_{,xy})/a_{11} \qquad (14)$$

Hence the double integrals on the left hand side of Eq. (13) yield, after integration by parts,

$$-\Sigma\,(Ba_{16}/a_{11}-2\theta)\iint \delta\Psi\,dxdy + B\,\Sigma\,[a_{12}/a_{11}]_I\int\delta F_I\,dx$$

$$+\Sigma\,(C-By_I)\int([a_{12}/a_{11}]_I\delta G_I+[a_{16}/a_{11}]_I\delta\Psi_I\,dx$$

$$-\Sigma\int[\omega_2]_I\delta\Psi_I\,dx$$

while the single integrals in Eq. (13) yield

$$-\Sigma\int([u_{,x}]_I\delta G_I+[v_{,xx}]_I\delta F_I+[u_{,z}+w_{,x}]_I\delta\Psi_I)\,dx$$

$$+\Sigma\int[\omega_2]_I\delta\Psi_I\,dx$$

Here F_I, G_I and Ψ_I stand for the values of F, $F_{,y}$ and Ψ, respectively, on the I-th interface. Substituting the preceding results into Eq. (13) and using the interfacial continuity of the tangential strains ϵ_x, γ_{xz} and the curvature $v_{,xx}$, one obtains

$$\Sigma\iint\epsilon_{ij}\delta\sigma_{ij}\,dxdy+\Sigma\,(Ba_{16}/a_{11}-2\theta)\iint\delta\Psi\,dxdy$$

$$-\Sigma\,(C-By_I)\int([a_{12}/a_{11}]_I\delta G_I+[a_{16}/a_{11}]_I\delta\Psi_I\,dx$$

$$-B\,\Sigma\,[a_{12}/a_{11}]_I\int\delta F_I\,dx=0. \qquad (15a)$$

The following expression for the first term of the preceding equation may be obtained from Eqs. (3) and (14):

$$\Sigma\iint\epsilon_{ij}\delta\sigma_{ij}\,dxdy=\Sigma\iint(F_{,yy},\ F_{,xx},\ -F_{,xy},$$

$$-\Psi_{,x},\ \Psi_{,y})\begin{bmatrix}\beta_{22}&\beta_{23}&0&0&\beta_{26}\\ \beta_{23}&\beta_{33}&0&0&\beta_{36}\\ 0&0&\beta_{44}&\beta_{45}&0\\ 0&0&\beta_{45}&\beta_{55}&0\\ \beta_{26}&\beta_{36}&0&0&\beta_{66}\end{bmatrix}\begin{Bmatrix}\delta F_{,yy}\\ \delta F_{,xx}\\ -\delta F_{,xy}\\ -\delta\Psi_{,z}\\ \delta\Psi_{,y}\end{Bmatrix}dxdy \qquad (15b)$$

6. Polynomial approximations of the stress functions

In a variational method of solution, the stress functions F and Ψ in all layers are to be determined within a class of admissible stress functions satisfying the traction-free boundary conditions (Eqs. (9)-(11)) and the interfacial continuity of F, $F_{,y}$ and Ψ. The criterion of selection is that Eq. (15) should be satisfied for arbitrary admissible variations δF and $\delta\Psi$. The criterion ensures, in an averaged sense, the compatibility of strain and the interfacial continuity of the displacements. If the layers constituting the laminate are very thin, one may approximate the stresses in each layer by polynomial functions of the thickness coordinate. Then the class of admissible stress functions consists of polynomial functions of y, with the coefficients depending on x.

In the i-th layer, we define the nondimensional thickness coordinate η by

$$\eta = (y-y_{i-1})/(y_i-y_{i-1})$$

In the classical plate theory the in-plane stresses vary linearly in the thickness direction. This feature is approximately valid in each thin layer of a laminated plate, except in regions close to the free edges. Hence the stress function $F(x,y)$ in each layer may be approximated by a polynomial function of degree three in the normalized thickness coordinate η. Now the stress function in the i-th layer must assume values $F_i(x)$ and $F_{i-1}(x)$, respectively, on the interfaces $y=y_i$ and $y=y_{i-1}$, and the y-derivative of the stress function must assume values $G_i(x)$ and $G_{i-1}(x)$ on these interfaces. Hence the cubic polynomial approximation of the stress function in the i-th layer must have the following expression

$$\overset{(i)}{F}(x,\eta) = (1-3\eta^2+2\eta^3)F_{i-1}(x)+(\eta-2\eta^2+\eta^3)h_iG_{i-1}(x)$$

$$+(3\eta^2-2\eta^3)F_i(x)+(\eta^3-\eta^2)h_iG_i(x) \quad (i=2,3\ldots n) \qquad (16a)$$

The cubic polynomial approximations of the stress functions in the bottom and top layers are given, respectively, by

$$\overset{(1)}{F}(x,\eta) = (3\eta^2-2\eta^3)F_1(x)+(\eta^3-\eta^2)h_1G_1(x) \qquad (16b)$$

and

$$\overset{(n+1)}{F}(x,\eta) = (1-3\eta^2+2\eta^3)F_n(x)+(\eta-2\eta^2+\eta^3)h_{n+1}G_n(x) \qquad (16c)$$

The stress functions given by Eqs. (15a,b,c) yield an interlaminar peeling stress σ_y having a cubic dependence on the thickness coordinate in each layer, an interlaminar shearing stress τ_{xy} with a quadratic dependence on η, and an in-plane stress σ_x with a linear dependence on η. For the sake of consistency the interlaminar shearing stress τ_{yz} and the in-plane shearing stress τ_{xz} will be approximated, respectively, by quadratic and linear functions of η. Then, according to Eq. (6), the stress function Ψ depends quadratically on y. It follows that

$$\overset{(i)}{\Psi}(x,\eta) = (1-\eta^2)\Psi_{i-1}(x)+\eta^2\Psi_i(x)+(\eta-\eta^2)h_iH_{i-1}(x)$$

$$(i=2,\ldots n) \qquad (17a)$$

$$\overset{(1)}{\Psi}(x,\eta) = \eta^2\Psi_1(x)+(\eta-\eta^2)h_1H_0(x) \qquad (17b)$$

$$\overset{(n+1)}{\Psi}(x,\eta) = (1-\eta^2)\Psi_n(x)+(\eta-\eta^2)h_{n+1}H_n(x) \qquad (17c)$$

where $\Psi_i(x)$ is the value of the stress function Ψ on the i-th interface and $H_i(x)$ is the value of $\Psi_{,y}$ on the upper side of the same interface (notice that, although Ψ is continuous across each interface, $\Psi_{,y}$ is generally discontinuous). Equations (16) and (17) imply that the stress functions in all layers are completely determined by 3n functions $F_i(x)$, $G_i(x)$, $\Psi_i(x)$ $(i=1,2,\ldots n)$ and n+1 functions $H_i(x)$ $(i=0,1,\ldots n)$, where $H_0(x)$ is the value of $\Psi_{,y}$ on the bottom surface $y=-y^*$.

7. An eigenvalue problem for the functions F_i, G_i, Ψ_i and H_i

Let the set of 4n+1 functions F_i, G_i, Ψ_i and H_i be arranged as the components of a column vector $\{X\}$ according to

$$X_i = F_i(x), \qquad X_{i+n} = G_i(x), \qquad X_{i+2n} = \Psi_i(x),$$

$$(i=1,2,\ldots n)$$

$$X_{i+3n+1} = H_i(x), \qquad (i = 0,1,\ldots n)$$

Then, by substituting Eqs. (16) and (17) into Eq. (15), performing the integration with respect to η, and integrating by parts with respect to x, we obtain

$$\{\delta X\}^t \cdot \left(([W]\frac{d^4}{dx^4} + [V]\frac{d^2}{dx^2} + [U])\{X\} - \{b\} \right) = 0 \qquad (18)$$

where $\{\delta X\}^t$, a row vector, is the variation of the transpose of $\{X\}$ and the column vector $\{b\}$ has the components

$$b_1 = B[a_{12}/a_{11}]_i \ , \qquad b_{i+n} = (C-By_i)[a_{12}/a_{11}]_i$$

$$b_{i+2n} = (C-By_i)[a_{16}/a_{11}]_i + 2h_{i+1}(2\theta - B\,\overset{(i+1)(i+1)}{a_{16}}/a_{11})/3$$

$$+ h_i(2\theta - B\overset{(i)\ (i)}{a_{16}}/a_{11})/3 \qquad (i = 1,2,\ldots n)$$

$$b_{i+3n+1} = (2\theta - B\,\overset{(i+1)\ (i+1)}{a_{16}}/a_{11})\ h_{i+1}^2/6 \qquad (i = 0,1,\ldots n)$$

As mentioned previously, $[a_{12}/a_{11}]_i$ denotes the jump of a_{12}/a_{11} across the i-th interface.

The matrices [U], [V] and [W] of Eq. (18) are constant real symmetric matrices and are completely determined by the integral expressions in Eq. (15b), i.e., by the first variation of the strain energy of the layers. It is clear from Eq. (15b) that the fourth-order derivatives in Eq. (18) arise only from the integrals $\Sigma\iint \overset{(i)(i)}{\beta_{33}} \overset{(i)}{F}_{,xx}\delta\overset{(i)}{F}_{,xx}\,dxdy$, i.e., they only invlovie the stress functions $\overset{(i)}{F}$ but not $\overset{(i)}{\Psi}$. Hence, by virtue of the representation of Eq. (16), the coefficient matrix [W] of the operator d^4/dx^4 has nonzero elements only in a 2n x 2n square submatrix in the upper left corner (i.e., in the rows and columns corresponding to the unknown functions F_i and G_i, i= 1,2,...n).

The elements of the three matrices have extremely complex expressions and it is inpractical to obtain these expressions without using symbolic algebraic programs. In the present work, the matrices [U], [V] and [W] are obtained from Eqs. (15b), (16) and (17) by using MAGSYMA [7]. The symbolic program is also used to obtain the compliance coefficients β_{ij} of each layer from Eqs. (1), (2) and (4).

Equation (18) is satisfied for arbitrary variations δH_0, δF_1, δG_1, $\delta\Psi_1$, ... and δH_n if and only if

$$([W]\frac{d^4}{dx^4} + [V]\frac{d^2}{dx^2} + [U])\{X\} = \{b\} \qquad (19)$$

Equation (19) and the homogeneous boundary conditions at the free edges

$$F_i(\pm a) = F_i'(\pm a) = G_i(\pm a) = G_i'(\pm a)$$

$$= \Psi_i(\pm a) = H_i(\pm a) = 0 \qquad (i = 1,2,\ldots n) \qquad (20)$$

$$H_0(\pm a) = 0$$

define an eigenvalue problem where the eigenvalues are the roots of the characteristic equation [8]

$$\text{Determinant}([W]\,\lambda^4 + [V]\,\lambda^2 + [U]) = 0 \qquad (21)$$

The primes in Eq. (20) indicate differentiation with respect to x. Since the nonzero elements of [W] are limited to a 2n x 2n submatrix, the characteristic equation is a polynomial equation of order 2x2n+2n+1 = 6n+1 in the variable λ^2. Hence there are 6n+1 pairs of (real and complex) eigenvalues, with each pair consisting of eigenvalues which differ only in algebraic sign. Considered as an equation for λ^2, the characteristic equation yields no solutions λ^2 with negative real parts. Hence there are no purely imaginary eigenvalues. Notice that the total number of eigenvalues, 12n+2, is equal to the number of boundary conditions in Eq. (20).

The (real or imaginary) eigenvector corresponding to each eigenvalue may be determined from the homogeneous differential equation associated with Eq. (19). The eigenfunctions have the form $\{c\}\exp(\pm\lambda_k x)$, where $\{c\}$ is a constant vector with real or complex components depending on whether λ_k is a real or complex eigenvalue.

Equation (19) has a constant particular solution $[U]^{-1}\{b\}$. The general solution of the equation may be obtained by combining the particular solution with a linear combination of the eigenvectors. The coefficients of the eigenvectors must be chosen so that all boundary conditions of Eq. (20) are satisfied. If the width of the strip, 2a, is sufficiently large compared to the thickness, then the eigenfunctions associated with the eigenvalues having negative (positive) real parts make negligible contribution to the solution in the right (left) half of the strip, since such eigenfunctions decay rapidly away from the left (right) free edge. In other words, the solutions for the left and right parts of the strip are approximately uncoupled.

In the case of a cross-ply laminate with the material axes parallel and perpendicular to the free edges, the solution space of the eigenvalue problem decomposes orthogonally into subspaces of dimensions 8n and 4n+2. The two subspaces are associated, respectively, with the two stress functions F and Ψ. We observe that, in the case of cross-ply laminates, the elastic compliance coefficients β_{26}, β_{36} and β_{45} vanish in every layer. Hence there is no coupling between the two stress functions F and Ψ in the variational equation associated with Eq. (15b). Furthermore, since a_{16} also vanishes in each layer of a cross-ply laminate, the last 2n+2 elements of the vector {b} in Eq. (18) do not depend on the loading parameters B and C while the first 2n elements of {b} do not depend on the twisting deformation θ. Consequently, Eq. (18) decouples into a system of 2n fourth-order differential equations for the functions F_i and G_i and another system of 2n+1 second-order equations for the functions Ψ_i and H_i. The first system of equations determines the solutions under axial extension and bending loads while the second system of equations determines the solutions under the twisting load.

B. Physical meanings of the functions $F_i'(x)$ and $G_i(x)$ and $\Psi_i(x)$

The functions $F_i(x)$, $\Psi_i(x)$, $G_i(x)$ and $H_i(x)$ in Eqs. (16) and (17) are the values of the stress functions and their y-derivatives along the i-th interface. They are related to the resultant forces and moments of the normal and shearing interlaminar strasses over interfacial intervals of varying lengths adjacent to the free edge. Let the origin of the axial coordinate x be shifted to the left

free edge of the strip. Then, over the interval [0, x] of the i-th interface in the new coordinate system, we have

$$\int \sigma_y \, dx = \int F_i'' \, dx = F_i'(x), \tag{22a}$$

$$\int \tau_{xy} \, dx = - \int G_i' \, dx = - G_i(x) \tag{22b}$$

$$\int \tau_{yz} \, dx = - \int \Psi_i' \, dx = - \Psi_i(x) \tag{22c}$$

Similarly,

$$\int x \, \sigma_y \, dx = x F_i'(x) - F_i(x),$$

$$\int x^2 \, \sigma_y \, dx = x^2 F_i'(x) - 2xF_i(x) + 2\int F_i \, dx$$

$$\int x \, \tau_{xy} \, dx = - x \, G_i(x) + \int G_i \, dx,$$

$$\int x \, \tau_{yz} \, dx = - x \, \Psi_i(x) + \int \Psi_i \, dx,$$

In particular, the maximum absolute values of G_i and Ψ_i, reached at the centerline of the strip, are equal to the resultant forces of the interlaminar shearing stresses τ_{xy} and τ_{yz}, respectively, over one half of the i-th interface. Generally, G_i and Ψ_i increase or decrease monotonically from zero to their maximum or minimum values at the centerline of the strip. If G_i or Ψ_i attains a large value in a very short distance from the free edge, then an intense interlaminar shearing stress (of mode I or III, respectively) occurs in a very short interval from the free edge. This situation is susceptible to delamination failure under the shear fracture mode.

The behavior of the function $F_i'(x)$ has a similar implication for the interlaminar normal stress. This function generally increases from zero at the free edge to a maximum value in a short distance from the free edge. It then decays slowly to zero at the midpoint of the beam. If F_i' increases from zero to a large maximum value in a very short interval from the free edge, then an intense tensile interlaminar normal stress acts in that short end interval, and the resultant tensile force is balanced by an equal compressive force distributed over the remaining portion of the half interface. This situation is susceptible to delamination failure under the peeling fracture mode.

The maximum values of the functions G_i, Ψ_i and F_i' and the charecterietic lengths of their regions of eteep gradient are meaningful measures of the criticality of the interlaminar stresses in the i-th interfece near the free edge. There are good reasone to suggest the use of these maximum values and characteristic lengths as parameters in the interlaminar fracture criteria for the peeling and ehearing modes of failure. These parameters may be easily calculated by the present method of enalysis. Being global measures, their values are less effected by the crudeness or refinement of the epproximate analysis than the pointwise values of the interlaminar stressee ere. That is, a relatively eimple enalysis (involving low-order polynomial approximations of the streaa functions) may provide unreliable reaults for the detailed interlaminar etrees dietributions elong the interfaces but may etill yield accurate reeults for the maximum values of G_i, Ψ_i and F_i' as well as the charateristic lengths of their regions of steep gradient. Aside from the question of accuracy end convergence, extremely detailed results of the interlaminar stresses near a singular point have dubious physical meaning in view of the microscopic heterogeneity of plies and the randomness inherent in the micro-struture.

9. The case of symmetric laminates

In the case of a symmetric laminate the middle plane $y = 0$ is a plane of symmetry. All stiffness and compliance coefficients are even functions of y. In particular, there is no disticontinuity in a_{12}/a_{11} or a_{16}/a_{11} across the plane $y = 0$ if that plane is artificially regarded as an interface. Hence there are no contributions to the single integrals of Eq. (15a) from the interface $y = 0$.

For a symmetric laminate loaded under a uniform axial strain only (i.e., $B = \theta = 0$ and $\epsilon_x = G \neq 0$), the deformation and stress in the laminate are symmetric with respect to the middle plane. Hence F is an even function of y while $F_{,y}$ and Ψ are odd functions. In particular, $G = \Psi = 0$ on the middle plane $y = 0$. Setting $B = \theta = 0$ in Eq. (15a), one finds that the regions of the laminate above and below the middle plane make equal contributions to the sum of integrals. Consequently, we need only compute the double integrals over the upper region and the single integrals over all interfaces above the middle plane.

The same conclusion is also valid for a symmetric laminate subjected to bending and twisting ($C = 0$ but B and θ not both zero). Under such loading cases F is an odd function of y while $F_{,y}$ and Ψ are even functions. In particular, $F = \Psi_{,y} = 0$ on $y = 0$ (notice that although $\Psi_{,y}$ is generally discontinuous across an interface, it is continuous across $y = 0$ because the stiffness coefficients have no discontinuity across the middle plane of a symmetric laminate). Because e_{16}/a_{11} is an even function of y while the jumps $[a_{12}/a_{11}]$ and $[a_{16}/a_{11}]$ are odd functions of y, the sum of integrals in Eq. (15a) receive equal contributions from the regions above and below the middle plane.

The preceding conclusions imply that, for the solution of the interlaminar stress problem of a symmetric laminate, the dimension of the vectors {X} and {b} may be reduced considerably. The unknown functions F_i, G_i, Ψ_i and H_i essociated with the interfaces in the lower half of the laminate may be dropped. Let the interfaces in the region $y \geq 0$, including the interface $y = 0$, be renumbered in the ascending order, starting with interface 0 on $y = 0$. Then, for the uniform axial strain load (i.e., $C \neq 0$ and $B=\theta=0$), the required set of unknown functions include F_i, G_i, Ψ_i and H_i for $i \geq 1$ and the functions F_0 end H_0. Under bending and twisting loads (i.e., $C = 0$), F_0 and H_0 are replaced by G_0 and Ψ_0.

For the classical problem of a symmetric, four-layer laminate under an axial strain load, the functions G_0 and Ψ_0 on the middle plane vanish identically. There is only one interface in the upper half of the laminate and the two layers in the upper region (renumbered as layers 1 and 2) have the expressions:

$$F^{(i)}(x,\eta) = (1-3\eta^2+2\eta^3)F_0(x)+(3\eta^2-2\eta^3)F_1(x)$$

$$+(\eta^3-\eta^2)h_1G_1(x) \, , \tag{23a}$$

$$\overset{(2)}{F}(x,\eta) = (1-3\eta^2+2\eta^3)F_1(x)+(\eta-2\eta^2+\eta^3)h_2C_1(x) \ , \quad (23b)$$

$$\overset{(1)}{\Psi}(x,\eta) = \eta^2\Psi_1(x)+(\eta-\eta^2)h_1H_0(x) \ , \quad (23c)$$

$$\overset{(2)}{\Psi}(x,\eta) = (1-\eta^2)\Psi_1(x)+(\eta-\eta^2)h_2H_1(x) \ , \quad (23d)$$

The vectors {X} and {b} of Eq. (19) become, respectively,

$$\begin{Bmatrix} F_0(x) \\ F_1(x) \\ G_1(x) \\ \Psi_1(x) \\ H_0(x) \\ H_1(x) \end{Bmatrix} \quad \text{and} \quad \begin{Bmatrix} 0 \\ 0 \\ C[a_{12}/e_{11}]_1 \\ C[a_{16}/a_{11}]_1 \\ 0 \\ 0 \end{Bmatrix} \quad (24)$$

In the cases of bending and twisting loads one has C = 0. The functions F_0 and H_0 vanish identically end the stress functions in layer 1 have the expressions

$$\overset{(1)}{F}(x,\eta) = (\eta-2\eta^2+\eta^3)h_1G_0(x) + (3\eta^2-2\eta^3)F_1(x)+(\eta^3-\eta^2)h_1G_1(x)$$

$$\overset{(1)}{\Psi}(x,\eta) = (1-\eta^2)\Psi_0(x)+\eta^2\Psi_1(x)$$

The stress functions in layer 2 are still given by Eqs. (23b) and (23d). The vectors {X} and {b} of Eq. (19) reduce, respectively, to

$$\begin{Bmatrix} F_1(x) \\ G_0(x) \\ G_1(x) \\ \Psi_0(x) \\ \Psi_1(x) \\ H_1(x) \end{Bmatrix} \quad \text{and} \quad \begin{Bmatrix} B[a_{12}/a_{11}]_1 \\ 0 \\ -Bh_1\,[e_{12}/e_{11}]_1 \\ 2(2\theta-B\overset{(1)}{a}_{16}/\overset{(1)}{e}_{11})h_1/3 \\ -Bh_1[a_{16}/a_{11}]_1+(2\theta-B\overset{(1)}{a}_{16}/\overset{(1)}{e}_{11})h_1/3+ \\ 2(2\theta-B\overset{(2)}{a}_{16}/\overset{(2)}{e}_{11})h_2/3 \\ (2\theta-B\overset{(2)}{a}_{16}/\overset{(2)}{a}_{11})h_2^2/6 \end{Bmatrix}$$

10. Results for symmetric four-layer laminates

For convenience of comperison with the existing solutins in the literature, approximate solutions have been obtained by the present method for laminates composed of identicel unidirectionel plies with the thickness h and with the elestic moduli

$$E_{11} = 20 \times 10^6 \text{ psi}, \quad E_2 = E_3 = 2.1 \times 10^6 \text{ psi},$$
$$\nu_{12} = \nu_{13} = \nu_{23} = 0.21,$$
$$G_{12} = G_{13} = G_{23} = 0.85 \times 10^6 \text{ psi}.$$

Unless otherwise steted, the distence between the pair of free edges is w = 2a = 16h.

We first consider s four-layer symmetric cross-ply laminate with the ply configuretion $[0/90]_s$. For the reason mentioned previously, the differentiel equations governing such e laminate, Eq. (19), is uncoupled into three fourth-order equetions for F_0, F_1 end G_1 end three second-order equations for Ψ_1, H_0 and H_1. The second set of equations (and the associated homogeneous boundary conditions) alone determine the functions Ψ_0, Ψ_1 and H_1 in the case of a twisting load (the function H_0 vanishes identically according to the previous symmetry arguments). The first set of equations determine the functions F_0, F_1 and G_1 in the case of an axial strain load and the functions F_1, G_0 and G_1 in the case of a bending load. The resulting interlaminar stresses on the 0/90 interface are shown in Figs. 2-4 for the three cases of strain loads. The solution for a unit bending deformation is close to that for a unit axial strain except for a reversal of algebraic signs. This may be expected because a negative unit bending curvature yields a positive unit axial strain at the interface y = h. Figure 4 shows that a unit twisting deformation produces a mode 3 interlaminar stress τ_{yz} whose magnitude is much greater than the mode 1 and mode 2 interlaminar stresses produced by a unit axial strain and a unit bending deformation. However, it follows from Eq. (5) that, for a laminate with a large width to thickness ratio, the work required to produce a unit twisting deformation is also much greater than that required to produce a unit bending deformation or a unit axial strain.

In the case of symmetric angle-ply laminates the solution space of the governing equations is not orthogonally decomposable. Hence all three components of interlaminer stresses generally arise in each one of the loading ceses. The results are shown in Figs. 6-8 for a $[45/-45]_s$ laminate. Here again a unit twisting deformation produces a very large mode 3 interlaminar stress. For the case of an axial strein load, the in-plane stresses on the lower surface of the top layer are shown in Fig. 5.

The present results for the cross-ply and angle-piy laminates are compared with several most elaborate numerical solutions in the existing literature. While the existing solutions generally show over-all egreement, there are significant discrepancies in the pointwise values (and particularly in the peak values) of the interlaminar stresses. In order to avoid the difficulty of discriminating a number of partially overlapping curves in the same figure, we use Table 1, instead of graphs, to show the comparison of certain key features of the various solutions, including the solutions obtained by the present method, for the $[0/90]_s$ laminate under a unit axial strain load. Each pair of values in the table (enclosed in a set of parentheses) show a maximum or minimum value of σ_y or τ_{xy} and the distance from the free-edge of the point where the extremal value occurs. Since the values are measured from the graphs of the original papers, they may include errors introduced in plotting or in taking measures from the graphs. Furthermore, in the case of finite-element solutions the maximum value of the interlaminar normal stress σ_y (which occurs at the free edge) depends significantly on mesh refinement and may become very large as the mesh size further decreases.

Although the present analysis requires only a small fraction of computational effort in comparison with most other numerical solutions, the results obtained are by no means inferior. In fact, compared to most other solutions in Table 1, the present solution yields extremal values of σ_y which are in better agreement with Spilker's solutions using special free-edge finite elements to ensure exact satisfaction of the traction-free boundary

conditions [4,5]. A similar comparison of the results for the $[45/-45]_s$ laminates also indicates that the solution of the present method agree well with the existing refined solutions to the extent that the latter solutions are in agreement among themselves.

	$-\max \tau_{xy}$	$\max \sigma_y$	$-\min \sigma_y$
Present	(.21, .32h)	(.29, 0)	(.036, 2.0h)
Ref. [4,5]	(.11, .85h)	(.29, 0)	(.034, 2.3h)
Ref. [9]	(.22, .18h)	(.43, 0)	(.032, 2.3h)
Ref. [10]	(.11, .82h)	--------	(.018, 2.4h)
Ref. [11]	----------	(1.0, 0)	(.028, 2.1h)
Ref. [12]	----------	(.29, 0)	(.048, 2.1h)
Ref. [13]	----------	(.31, 0)	(.020, 1.9h)
Ref. [14]	(.23, .20h)	(.30, 0)	(.029, 1.9h)
Ref. [15]	(.23, .13h)	(.30, 0)	(.034, 1.7h)

Table 1: Comparison of the various solutions of the $[0/90]_s$ laminate

It was mentioned previously that the characteristic equation (21) has two sets of eigenvalues which differ only in algebraic sign. The eigenfunctions corresponding to eigenvalues with positive (negative) real parts decay exponentially away from the right (left) free edge of the laminate. If the ratio w/h is large, then the first (second) set of eigenfucntions make negligible contribution to the solution away from the right (left) free edge. Consequently, the solutions in the left and right halves of the laminate are approximately decoupled. Hence the interlaminar stress distribution near a free edge is dependent on w/h only if this ratio is small. This conclusion is substantiated by the results for $[0/45]_s$ laminates with w/h = 4, 8, 16 and 50 loaded under an axial strain (Fig. 9) and a twisting deformation (Fig. 10). The interlaminar stress distributions approach limiting pattern as w/h increases. The results apparently contradict a previous conclusion of Murthy and Chamis [16] concerning the effect of laminate width.

11. Summary and Conclusion

(1) A systematic approximate method is developed for determining the interlaminar stresses in a laminated strip with two parallel free edges subjected to an axial strain, a bending deformation or a twisting deformation. The method is based on the use of Lekhnitskii's stress functions. The approximate solutions of the present method satisfy exactly the equilibrium equations in each layer, the traction-free boundary conditions over the top and bottom surfaces and the free edges, and the continuity conditions of interlaminar stresses across all interfaces. The compatibility condition for the strain and the interfacial continuity of the displacements are enforced in an averaged sense by extremizing the complementary energy functional with respect to the class of statically admissible stress fields whose stress functions in individual layers are polynomial functions of the thickness coordinate. This results in an eigenvalue problem associated with a linear system of ordinary differential equations having constant coefficients. The eigenfunctions have exponential forms with real or complex exponents. The solution of the stress functions are obtained by appropriately combining the eigenfunctions with a constant particular solution (peculiar to each one of the three loading cases) in such a way as to satisfy the homogeneous boundary conditions at the free edges. When the task of solving the eigenvalues problem has been completed, the interlaminar stresses corresponding to all three loading cases can be determined simultaneously. The case of a unit twisting deformation generally yields a very large mode 3 interlaminar shearing stress compared to the stresses caused by a unit axial strain and unit bending deformation. However, a unit twisting deformation also requires a much greater external work if the width-to-thickness ratio of the laminate is large.

(2) Sample solutions are obtained for symmetric four-layer laminates. By exploiting symmetric conditions, the eigenvalue problem is reduced in size. For an angle-ply laminate the charateristic equation is a polynomial equation of degree 9 in the square of the eigenvalue. In the case of cross-ply laminates the eigenvalue problem is decomposable into orthogonal subspaces of solutions. Using the present method, a complete analysis of a symmetric four-layer laminate takes only a fraction of a minute on an IBM personal computer and requires extremely simple preparation of input data, while the results for the interlaminar stresses are comparable in accuracy to refined finite-element solutions involving several hundreds of degrees of freedom (with the possible use of special corner elements). If the laminate has a large number of layers, a sublaminate/layer approach developed in the sequel of this paper (Part II) may be used to reduce the size of the eigenvalue and to obtain approximate solutions.

(3) The present method achieves the dual objectives of efficiency and accuracy because the representations of the stress functions in the analysis are not chosen arbitrarily or purely for computational reasons (as in choosing the shape functions in finite-element modeling). They are based on the eigenfunctions as determined by the complementary virtual work principle. Besides the assumption of linear elasticity, the assumed polynomial dependence of the stress function upon the thickness coordinate in each layer is the only approximation made in the present analysis. Additional and miscellaneous assumptions with obscure meaning and dubious implication are categorically avoided. This feature provides an important computational advantage because, as found by Spilker [4,5], the replacement of exact traction-free boundary condition by approximating conditions may significantly affect the convergence and the outcome of finite-element solutions in a corner region.

(4) In the i-th interface, the maximum values of the first order partial derivatives of the stress function and the characteristic lengths of their regions of steep gradient provide useful measures of the criticality of the interlaminar stresses near the free edge. These values are less affected by the degree of refinement of the approximate analysis method than the detailed distributions of the interlaminar stresses are. They may be used as parameters in the fracture criteria for the initiation of delamination failure.

Acknowledgment The author is grateful to the U. S. Army Research Office for partial financial support during the conduct of this research work under grant E-20-633 to Georgia Institute of Technology.

References

[1] Bogy, D. B., "Edge-bonded dissimilar orthogonal elastic wedges under normal and shear loading" ASME J. Appl. Mech., Vol. 35, pp. 460-466 (1968).

[2] Wang, S. S. and Choi, I., "Boundary-layer effects in composite laminates -- I. Free-edge stress singularities, -- II. Free-edge stress solutions and basic characteristics," ASME J. Appl. Mech., Vol. 49, pp. 541-560 (1982).

[3] Zwiers, R. I., Ting, T. C. T. and Spiker, R. L., "On the logarithmic singularity of free-edge stress in laminated composites under uniform extension," ASME J. Appl. Mech., Vol. 49, pp. 561-569 (1982).

[4] Spilker, R. L., "Edge effects in symmetric composite laminates: Importance of satisfying the traction-free-edge condition," J. Composite Materials, Vol. 14, pp. 2-20 (1980).

[5] Spilker, R. L., "A traction-free-edge hybrid-stress element for the analysis of edge effects in cross-ply laminates," Computers & Structures, pp. 167-179 (1980).

[6] Lekhnitskii, S. G., Theory of elasticity of an anisotropic elastic body. Holden-Day, San Franscisco, 1963.

[7] VAX UNIX MACSYMA Reference Manual, Version 11. Symbolic, Inc., 1985.

[8] Ince, E. L., Ordinary Differential Equations. Dover, New York, 1956, pp. 144-148.

[9] Wang, A. S. D. and Crossman, F. W., "Some new results on edge effect in symmetric composite laminates," J. Composite Materials, Vol. 11, pp. 92-106 (1977).

[10] Renieri, G. D. and Herakovich, C. T., "Nonlinear analysis of laminated fibrous composites," Report VPI-E-76-10, Virginia Polytechnic Institute (1976).

[11] Wang, J. T. S. and Dickson, J. N., "Interlaminar stresses in symmetric composite laminates," J. Composite Materials, Vol. 12, pp. 390-402 (1978).

[12] Pipes, R. B., Solutions of certain problems in the theory of elasticity for laminated anisotropic systems. Ph.D. Thesis, Univ. of Texas, Arlington, March 1972.

[13] Raju, I. S. and Crews, J. H., Jr., "Interlaminar stress singularities at a straight free edge in composite laminates," Computers & Structures, Vol. 14, pp 21-28 (1981).

[14] Chang, C.-C., Sandhu, R. S., Sierakowski, R. L. and Wolfe, W. E., "Continuous strain finite-element analysis of free edge effect in laminated composite specimens," J. Composites Tech. & Res., Vol. 10, pp. 54-64 (1988).

[15] Pagano, N. J., "Stress fields in composite laminates," Int. J. Solids Structures, Vol. 14, pp. 385-400 (1978).

[16] Murthy P. L. N. and Chamis, C. C., "Free-edge delamination: laminate width and loading conditions effects," J. Composites Tech & Res., Vol. 11, pp. 15-22 (1988).

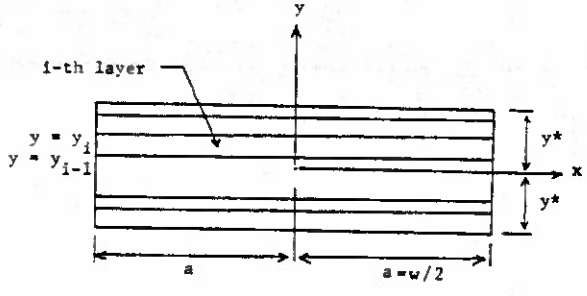

Fig. 1: A multi-layered laminate

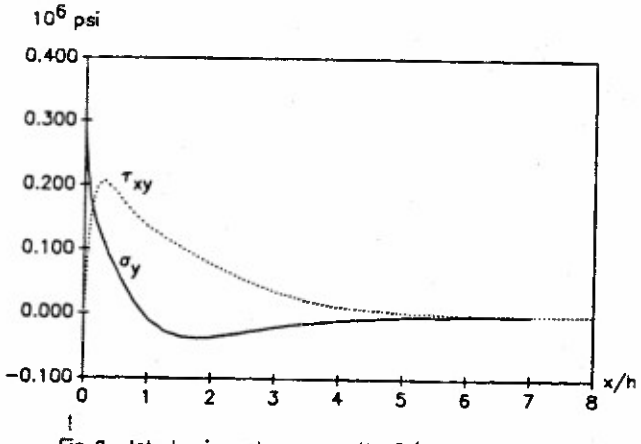

Fig. 2: Interlaminar stresses on the 0/90 interface in a [0/90/90/0] laminate under unit axial strain load

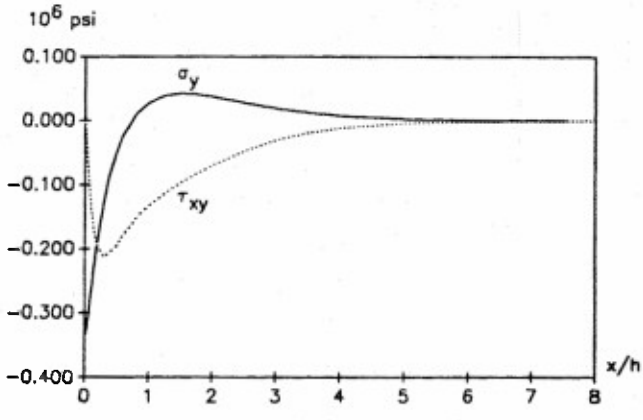

Fig.3: Interlaminar stresses on the 0/90 interface in a [0/90/90/0] laminate under unit bending deformation

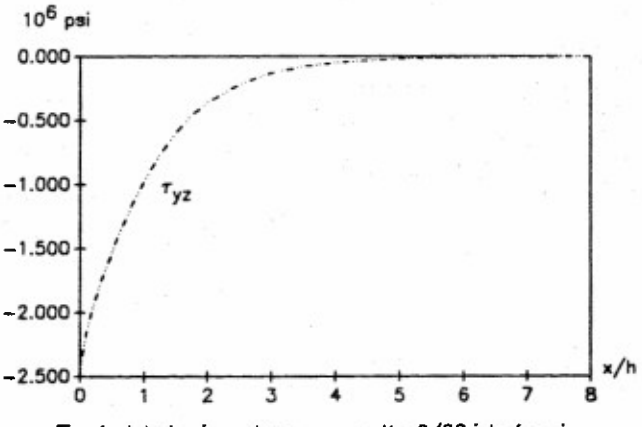

Fig. 4: Interlaminar stress τ_{yz} on the 0/90 interface in a [0/90/90/0] laminate under unit twisting deformation

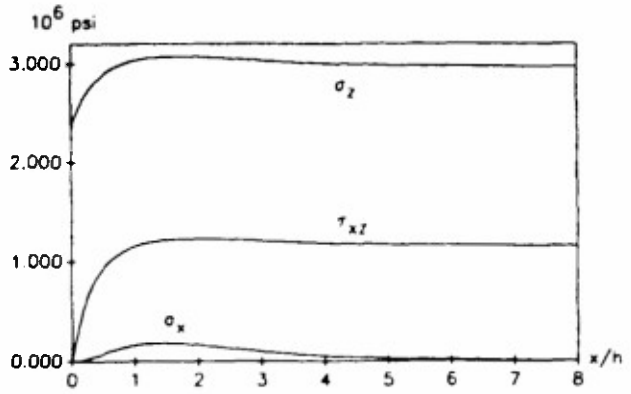

Fig. 5: In-plane stresses on the lower face of the top layer in a [45/−45/−45/45] laminate under unit axial strain

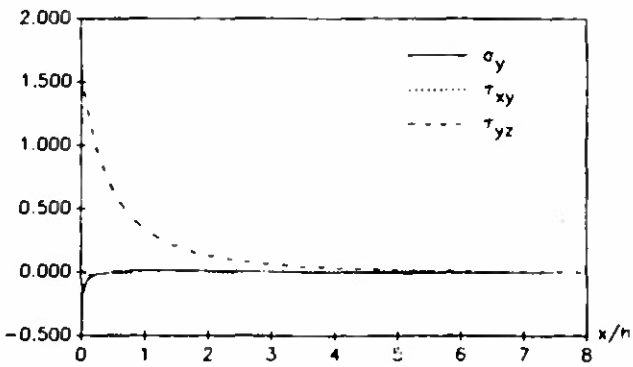

Fig. 6: Interlaminar stresses on the 45/−45 interface in a [45/−45/−45/45] laminate under unit axial strain

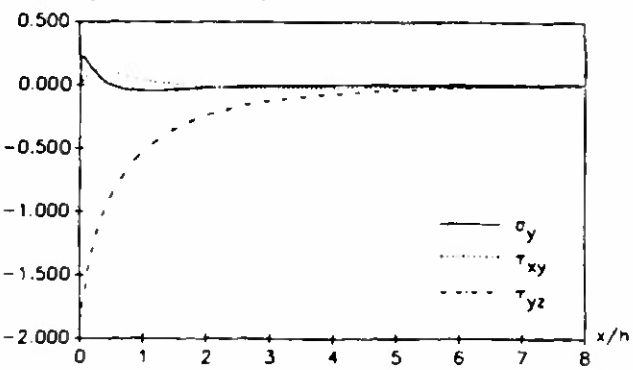

Fig. 7: Interlaminar stresses on the 45/−45 interface in a [45/−45/−45/45] laminate under unit bending

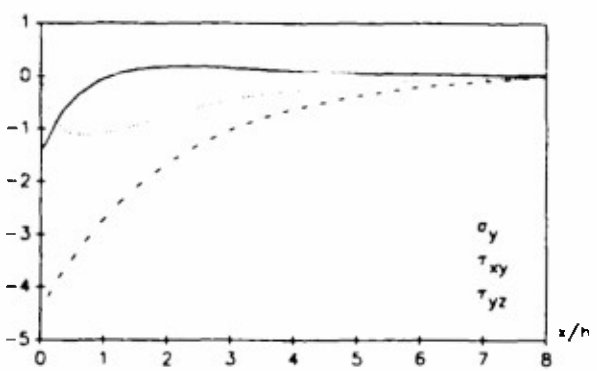

Fig. 8: Interlaminar stresses on the 45/−45 interface in a [45/−45/−45/45] laminate under unit twisting

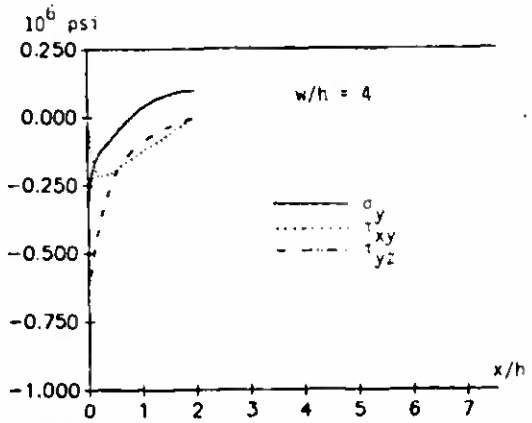

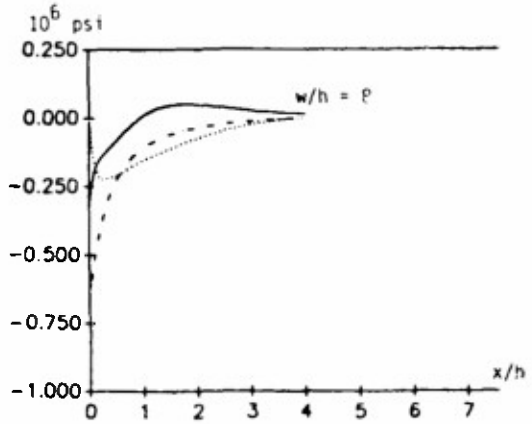

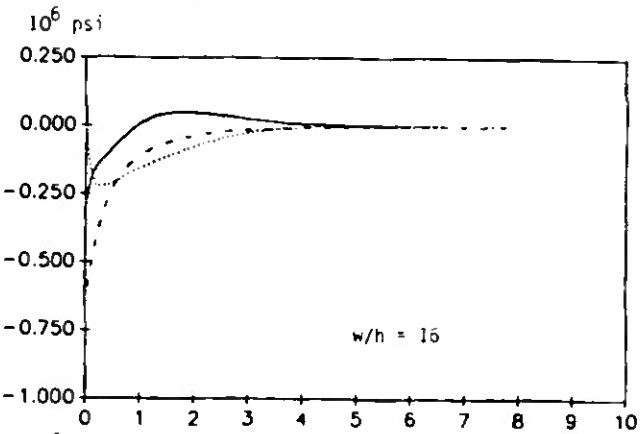

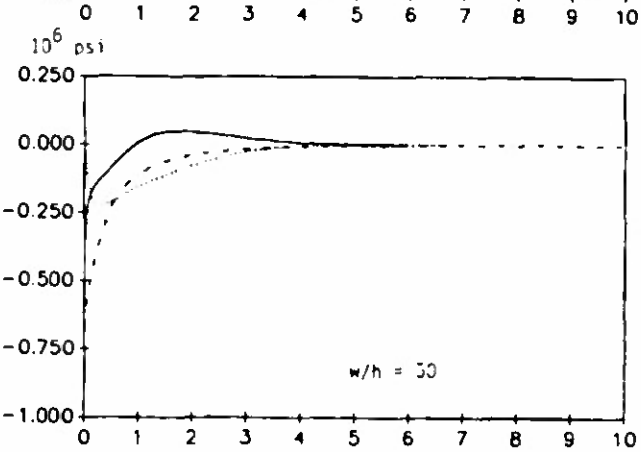

Fig. 9: Effect of laminate width on interlaminar stresses in a $[0/45]_s$ laminate under unit axial strain

Appendix G

"Thermal Stresses and Free-Edge Effects in Laminated Beams:

A Variational Approach Using Stress Functions"

By Wan-Lee Yin

ASME Journal of Electronic Packaging

Vol. 113, pp. 68-75 (April 1991)

Thermal Stresses and Free-Edge Effects in Laminated Beams: A Variational Approach Using Stress Functions

Wan-Lee Yin
Professor.
School of Civil Engineering
Georgia Institute of Technology,
Atlanta, GA 30332

A variational method involving stress functions is used to determine the interlaminar stresses and the free-edge effects in a laminated beam under a temperature loading. The stress function in each layer is approximated by a cubic polynomial function of the thickness coordinate. The equilibrium equations, the traction boundary conditions, and the continuity conditions of the interlaminar stresses are exactly satisfied in this analysis, while the compatibility equations and interfacial continuity of the tangential strains are enforced in an averaged sense by applying the principle of complementary virtual work. The method is highly efficient and accurate. A thermal stress analysis for a three-layer beam using only eight eigenfunctions yield results that are comparable in accuracy to finite-element solutions involving thousands of degrees of freedom.

1 Introduction

Studies of the thermal stresses in bimetallic or laminated beams and plates may be found in the literature of applied mechanics and composite materials (see, for example, Timoshenko (1925), Boley and Testa (1969), Hess (1969), Wang and Crossman (1977), Grimado (1978), Wang and Choi (1979), Chen and Nelson (1979), Chen et al. (1982), Chang (1983), Saganuma et al. (1984), Blech and Kantor (1984), Kuo (1989) and Cho et al.). In recent years, thermal stress problems of multilayer beams and plates have received a considerable amount of attention in the field of electronic packaging. A number of papers have appeared and various approximate methods have been proposed, at different levels of sophistication, to determine the free-edge interlaminar stresses induced by thermal expansion and mechanical loads (Taylor and Yuan (1962), Reinhart and Logan (1973), Roll (1976), Olsen and Ettenberg (1977), Vims and Kerps (1982), Suhir (1986a,b; 1988), and Gerstle and Chambers (1987)). However, certain approximate solutions based on ad hoc assumptions yield results that are insufficiently accurate. Other simple solutions or formulas may provide only one component of the interlaminar stress or may fail to satisfy certain free-edge boundary condition. Although elaborate numerical solutions using refined finite-element modeling have been obtained for special geometrical and material configurations, there is a need to develop efficient and reasonably accurate approximate methods of solution for predicting the interlaminar stresses and free-edge effects in laminated beams and plates with arbitrary ply configuration under various types of loading.

In a recent paper (Yin, 1991), the author presented an approximate method of analysis for calculating the free-edge interlaminar stresses in a laminated strip subject to three fundamental types of mechanical loading: extension along the longitudinal axis of the strip, bending of the axis, and twisting of the strip. In the analysis, Lekhnitskii's stress functions (Lekhnitskii, 1963) were introduced in each layer of the laminate, and both stress functions and the normal derivative of one function were required to vanish on the boundary surfaces, and to be continuous across all interfaces. The stress functions were approximated by polynomial functions of the thickness coordinate. A system of ordinary differential equations governing the coefficient functions of the polynomials were obtained by means of the complementary virtual work principle. Solution of the associated eigenvalue problem yields the stress functions and the interlaminar stresses. The application of the method has been extended to laminates with a large number of layers by a combined layer/sublaminate approach (Yin, 1989).

The method is adopted, in this paper, to determine the interlaminar stresses in the free expansion of a laminated beam under a temperature loading. Although the method is generally applicable to laminated beams composed of anisotropic elastic layers, for simplicity we restrict the present analysis to the case where all layers are isotropic. In this special case only one stress function (Airy's stress function) is needed in each layer.

The problem is first decomposed into a constrained thermal expansion problem (with zero axial displacements at the two ends of the beam) and a complementary problem. The latter

Contributed by the Electrical and Electronic Packaging Division and presented at the Winter Annual Meeting, Dallas, Texas, November 26-30, 1990 of THE AMERICAN SOCIETY OF MECHANICAL ENGINEERS. Manuscript received by the Electrical and Electronic Packaging Division October 3, 1990; revised manuscript received December 10, 1990.

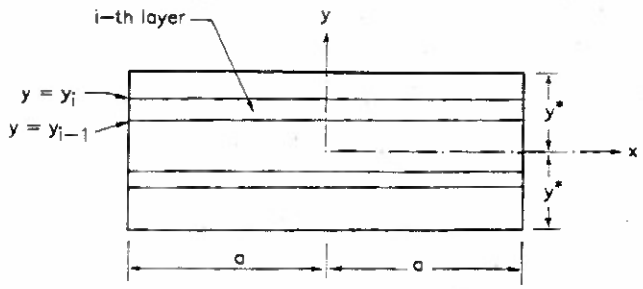

Fig. 1 A multilayered beam

problem is further decomposed into a trivial problem characterized by a uniform axial extension superposed on pure bending, and a third problem characterized by rapid decay of the interlaminar stresses away from the free edge. The last problem is solved by the eigenfunction analysis.

The analysis method is applied to two configurations of a three-layer beam for which refined finite-element solutions have been recently presented by Glaser (1989). Comparison of the results shows excellent agreement in the interlaminar normal stress and some discrepancy in the interlaminar shearing stress. While the finite-element solution involves over 10,000 degrees-of-freedom, the present analysis requires very simple data input, and very little computational effort even on a personal computer. Furthermore, the eigenvalues and eigenfunctions are dependent only on the geometry and material of the model, and are independent of the thermal loading. Once the eigenfunction analysis for a given model has been performed, repeated solutions for different temperature distributions involve only different combinations of the eigenfunctions, and may be achieved with extreme ease.

It is pointed out in Section 7 of this paper that the first-order partial derivatives of the stress function along an interface are related to the resultant forces and moments of the interlaminar normal and shearing stresses over end segments of the interface. Since the maximum values of these derivatives are global measures of the criticality of the interlaminar stresses near the free edge, they may be used as parameters in the fracture criteria for the initiation of delamination failure.

2 Stress Functions in a Multi-layer Beam

Consider a laminated beam of length $2a$ and consisting of $n+1$ homogeneous, isotropic, linearly elastic layers separated by n planar interfaces. We assume that mechanical loads are applied only to the two ends of the beam, so that the top and bottom surfaces of the beam are completely free from traction. The layers and their interfaces will be numbered from the bottom up. Thus the ith layer is bounded below by the $(i\text{-}1)$th interface and bounded above by the ith interface. This layer has the thickness h_i, and is composed of a material with Young's modulus E_i and Poisson's ratio ν_i. The axial coordinate x and the thickness coordinate y are introduced with the origin located at the center of the beam (Fig. 1). Any plane stress field in the ith layer satisfying the differential equations of equilibrium may be expressed in terms of a stress function in the following manner:

$$\sigma_x^{(i)} = F^{(i)}_{,yy}, \quad \sigma_y^{(i)} = F^{(i)}_{,xx}, \quad \tau_{xy}^{(i)} = -F^{(i)}_{,xy} \tag{1}$$

Obviously, an arbitrary bilinear function of x and y may be added to the stress function without affecting the resulting stress field in the layer.

The continuity of the normal and shearing stresses across the ith interface $y = y_i$ requires that, along that interface,

$$(F^{(i+1)} - F^{(i)})_{,xx} = 0, \quad (F^{(i+1)}_{,y} - F^{(i)}_{,y})_{,x} = 0.$$

Hence we may appropriately choose an additive bilinear function for the stress function in the $(i+1)$th layer so that, along the interface $y = y_i$,

$$F^{(i+1)} = F^{(i)}, \quad F^{(i+1)}_{,y} = F^{(i)}_{,y} \tag{2}$$

Furthermore, by combining with an additive bilinear function, the stress function in the bottom layer and its y-derivative may both be made to vanish identically over the bottom surface.

By integrating the axial stress through the thickness of all layers, and making use of the continuity of $F_{,y}$ across the interfaces, one finds that the resultant axial force is equal to the value of $F_{,y}$ on the top free surface. Let this value be denoted by G^*, i.e.,

$$\sum_i \int \sigma_x^{(i)}\, dy = \sum_i \int F^{(i)}_{,yy}\, dy = \sum_i F^{(i)}_{,y} \Big|_{y=y_{i-1}}^{y=y_i} = F_{,y} \Big|^{y=y^*} = G^*$$

where y^* is half the total thickness of the beam. Now the resultant bending moment in the beam is given by

$$M = -\sum_i \int y\, \sigma_x^{(i)}\, dy =$$

$$-\sum_i \int y\, F^{(i)}_{,yy}\, dy = -\sum_i \int \{(y\, F^{(i)}_{,y})_{,y} - F^{(i)}_{,y}\}\, dy$$

$$= F^* - y^* G^*$$

where F^* is the value of the stress function on the top free surface. Since the beam is subjected only to end loads, the axial load and the bending moment are independent of x. Consequently, G^* and F^* are both constants.

3 Reduction to a Problem With Zero End Force and End Moment by Decomposition

At this stage, we shall decompose a general traction boundary-value problem of a laminated beam with stress-free top and bottom surface (Problem A) into a similar problem with $F^* = G^* = 0$ (Problem B) and another problem in which the stress functions in all layers are independent of x (Problem C).

In Problem C, the only nonvanishing stress component is the axial stress. Since the shearing stress vanishes identically, the shearing strain also vanishes and, consequently, the axial strain ϵ_x varies linearly through the entire thickness of the beam, i.e.,

$$\epsilon_x = \epsilon_0 - \kappa y$$

where ϵ_0 is the axial strain on the middle plane and κ is the curvature of the deformed axis. Hence, in the ith layer we have

$$\sigma_x^{(i)} = E_i \epsilon_0 - E_i \kappa y \tag{3}$$

It follows that

$$G^* = \sum \int \sigma_x\, dy = Q\epsilon_0 - R\kappa \tag{4}$$

$$F^* - y^* G^* = -\sum \int y \sigma_x dy = -R\epsilon_0 + S\kappa \tag{5}$$

where

$$Q = \sum E_i h_i, \quad R = \sum E_i (y_i^2 - y_{i-1}^2)/2,$$

$$S = \sum E_i (y_i^3 - y_{i-1}^3)/3 \tag{6}$$

with the summations carried over all layers. Solving equations (4) and (5) for ϵ_0 and κ in terms of F^* and G^*, and substituting the results into equation (3), we obtain a solution corresponding to a uniform axial extension superposed on pure bending. When this solution is subtracted from Problem A, the remaining problem is a traction boundary-value problem with

$F^* = G^* = 0$, i.e., a problem characterized by vanishing resultant axial force and resultant bending moment (Problem B).

In the following analysis, we proceed to obtain an approximate solution of Problem B.

4 Polynomial Approximations of the Stress Functions

In the ith layer, we define the nondimensional thickness coordinate η by

$$\eta = (y - y_{i-1})/(y_i - y_{i-1})$$

The stress function in the ith layer may be approximated by a polynomial function of the normalized thickness coordinate η. In the classical beam theory the bending stress varies linearly in the thickness direction. This feature is approximately valid in each thin layer of a laminated beam, except in regions close to the two ends of the beam. Hence the stress function in each layer may be approximated by a polynomial function of degree three in the normalized thickness coordinate η. Now the stress function in the ith layer must assume values $F_i(x)$ and $F_{i-1}(x)$, respectively, on the interfaces $y = y_i$ and $y = y_{i-1}$, and the y-derivative of the stress function must assume values $G_i(x)$ and $G_{i-1}(x)$ on these interfaces. Hence the cubic polynomial approximation of the stress function in the ith layer must have the following expression

$$F^{(i)}(x,\eta) = (1 - 3\eta^2 + 2\eta^3)F_{i-1}(x) + (\eta - 2\eta^2 + \eta^3)h_iG_{i-1}(x) + (3\eta^2 - 2\eta^3)F_i(x) + (\eta^3 - \eta^2)h_iG_i(x) \quad (i = 2, \ldots, n) \tag{7}$$

The cubic polynomial approximations of the stress functions in the bottom and top layers are given, respectively, by

$$F^{(1)}(x,\eta) = (3\eta^2 - 2\eta^3)F_1(x) + (\eta^3 - \eta^2)h_1G_1(x) \tag{8}$$

and

$$F^{(n+1)}(x,\eta) = (1 - 3\eta^2 + 2\eta^3)F_n(x) + (\eta - 2\eta^2 + \eta^3)h_{n+1}G_n(x) + (3\eta^2 - 2\eta^3)F^* + (\eta^3 - \eta^2)h_{n+1}G^* \tag{9}$$

The stress functions given by equations (7)-(9) yield an interlaminar peeling stress σ_y having a cubic dependence on the thickness coordinate in each layer, an interlaminar shearing stress τ_{xy} with a quadratic dependence on η, and an axial stress σ_x with a linear dependence on η. In the next section we will be concerned with the *reduced problem*, for which the resultant axial force and resultant bending moment vanish, i.e., the problem with $F^* = G^* = 0$ (Problem B).

5 Complementary Virtual Work Principle for Pure Traction Boundary-Value Problems

In pure traction boundary value problems (including thermal stress problems where the entire boundary of the beam is free from traction) the total complementary energy of the beam is

$$\Omega = (1/2)\sum_i \int_{-a}^{a}\int_{y_{i-1}}^{y_i} \{(1/E_i)[F_{,yy}^2 + F_{,xx}^2 - 2\nu_i F_{,yy}F_{,xx} + 2(1+\nu_i)F_{,xy}^2]\,dx\,dy \tag{10}$$

Over the two end sections of the beam, we have

$$\delta\sigma_x = (\delta F)_{,yy} = 0, \quad \delta\tau_{xy} = -(\delta F_{,x})_{,y} = 0,$$

Integrating the last two equations in the thickness direction, and using the continuity conditions of equation (2), we obtain

$$\delta F = 0, \quad \delta F_{,x} = 0 \quad (\text{at } x = \pm a) \tag{11}$$

By substituting the cubic polynomial approximations of the stress functions for each layer into equation (10), and performing the integration with respect to the normalized thickness coordinate, we obtain an integral expression with respect to x only. By taking the first variation of the resulting expression, performing integration by parts, and making use of equation (11), we obtain a system of ordinary differential equations with constant coefficients of the following form

$$\left([A]\frac{d^4}{dx^4} - [B]\frac{d^2}{dx^2} + [C]\right)\begin{Bmatrix} F_1 \\ G_1 \\ \cdot \\ F_n \\ G_n \end{Bmatrix} = \{0\} \tag{12}$$

where $[A]$, $[B]$, and $[C]$ are $2n$ by $2n$ constant symmetric matrices. The traction boundary conditions at the two ends of the beam provide specified values of F_i, G_i and their first derivatives. This defines an eigenvalue problem where the eigenvalues are the roots of the characteristic equation

$$\text{Determinant}([A]\lambda^4 + [B]\lambda^2 + [C]) = 0 \tag{13}$$

Although the total number of real and complex eigenvalues is $8n$, half of the eigenvalues differ from the other half only in algebraic sign, because the characteristic equation contains only even powers of the eigenvalue λ. Considered as an equation for λ^2, the characteristic equation yields no solutions λ^2 with negative real parts. Hence there are no purely imaginary eigenvalues.

The eigenvector corresponding to each eigenvalue may be easily determined from equation (12). All eigenfunctions decay or grow exponentially in the positive x-direction. The manner of decay or growth is monotone or oscillatory depending on whether the eigenvalue is real or complex. The solution to Problem B is a linear combination of the eigenvectors with the coefficients so chosen that all boundary conditions for F_i and G_i and their first derivatives are satisfied at the two ends of the beam. If the length of the beam is sufficiently large compared to the thickness, then the eigenfunctions associated with eigenvalues having negative (positive) real parts make negligible contribution to the solution in the right (left) half of the beam, since such eigenfunctions decay rapidly away from the left (right) end of the beam. In other words, the solutions for the left and right parts of the beam are approximately uncoupled.

It should be remarked that, for an inelastic material under an incremental loading, differential equations similar to equation (12) may still be obtained from the principle of complementary virtual work even though the complementary energy function may not exist. Hence the applicability of the present method is not restricted to elastic bodies.

6 Thermal Stress in the Free Expansion of a Three-Layer Beam

Consider the thermal expansion of a three-layer beam when the ith layer ($i = 1, 2, 3$) is subjected to a temperature increment T_i from its stress-free state. Let us first replace this problem by a constrained thermal stress problem in which the two ends of the beam are not allowed to expand in the axial direction but may expand freely in the thickness direction. If the material of the ith layer has the thermal expansion coefficient α_i, then the solution to the constrained thermal stress problem is simply an axial stress field uniform in each layer:

$$\sigma_x^{(i)} = -E_i\alpha_iT_i = -C_i \quad (i = 1, 2, 3) \tag{14}$$

This trivial solution, however, requires compressive tractions at the two ends. Hence the solution must be combined with a purely mechanical solution which completely relieves the preceding compressive tractions at the two ends. The latter solution is characterized by the stress functions of equations (7)-

(9) with $n = 2$, in which the functions $F_1(x)$, $F_2(x)$, $G_1(x)$, and $G_2(x)$ are determined by the governing differential equations of equation (12) and the following end conditions:

$$G_1(\pm a) = h_1C_1, \quad G_2(\pm a) = h_1C_1 + h_2C_2, \quad F_1(\pm a) = h_1^2C_1/2$$
$$F_2(\pm a) = (h_1^2C_1 + h_2^2C_2)/2 + h_1h_2C_1 \tag{15}$$

Furthermore, the constants F^* and G^* in equation (9) are given by

$$G^* = h_1C_1 + h_2C_2 + h_3C_3,$$
$$F^* = (h_1^2C_1 + h_2^2C_2 + h_3^2C_3)/2 + h_1h_2C_1 + h_1h_3C_1 + h_2h_3C_2 \tag{16}$$

Equation (15) and (16) are obtained by integrating equation (14) with respect to the thickness coordinate.

As shown in Section 3, the traction boundary-value problem with nonvanishing F^* and G^* may be decomposed into a similar problem with vanishing F^* and G^* (Problem B) and another problem characterized by a uniform axial extension combined with pure bending (Problem C). The solution of Problem B satisfies the differential equations of equation (12) and assumes the boundary values given by the difference of equation (15) and the following data:

$$G_1(\pm a) = E_1h_1\{\epsilon_0 - \kappa(y_0 + y_1)/2\}$$
$$F_1(\pm a) = (E_1h_1^2/6)\{3\epsilon_0 - \kappa(2y_0 + y_1)\}$$
$$G_2(\pm a) = G_1(\pm a) + E_2h_2\{\epsilon_0 - \kappa(y_1 + y_2)/2\}$$
$$F_2(\pm a) = F_1(\pm a) + (E_2h_2^2/6)\{3\epsilon_0 - \kappa(2y_1 + y_2)\} + E_1h_1h_2\{\epsilon_x - \kappa(y_0 + y_1)/2\} \tag{17}$$

where

$$y_0 = -y^* = -(h_1 + h_2 + h_3)/2$$

The preceding expressions may be obtained from equations (3)–(9) and (16).

For the three-layer beam, the 4 by 4 constant symmetric matrices $[A]$, $[B]$ and $[C]$ of equation (12) are shown in the Appendix.

7 Physical Meanings of the Functions $F_i'(x)$ and $G_i(x)$

The functions $F_i(x)$ and $G_i(x)$ in equations (7)–(9) are the values of the stress function and of its y-derivative along the ith interface. They are related to the resultant force and moment of the normal and shearing interlaminar stresses over interfacial intervals of varying lengths adjacent to the free edge. Let the origin of the axial coordinate x be shifted to the left end of the beam. Then, over the interval $[0, x]$ of the ith interface in the new coordinate system, we have

$$\int \sigma_y dx = \int F_i'' dx = F_i'(x),$$
$$\int \tau_{xy} dx = -\int G_i' dx = -G_i(x)$$

Similarly,

$$\int x\, \sigma_y dx = x\, F_i'(x) - F_i(x),$$
$$\int x^2\, \sigma_y dx = x^2 F_i'(x) - 2xF_i(x) + 2\int F_i\, dx$$
$$\int x\, \tau_{xy}\, dx = -x\, G_i(x) + \int Gi\, dx,$$

In particular, the maximum absolute value of G_i, reached at the midpoint of the beam, is equal to the resultant force of the interlaminar shearing stress over one half of the ith interface. Generally, G_i increases or decreases monotonically from zero to its maximum or minimum value at the midpoint of the beam. If G_i reaches a large value in a very short distance from the free edge, then an intense interlaminar shearing stress occurs in a very short interval from the free edge. This situation is susceptible to delamination failure under the shear fracture mode.

The behavior of the function $F_i'(x)$ has a similar implication for the interlaminar normal stress. This function generally increases from zero at the free edge to a maximum value in a short distance from the free edge. It then decays slowly to zero at the midpoint of the beam. If F_i' increases from zero to a large maximum value in a very short interval from the free edge, then an intense *tensile* interlaminar normal stress acts in that short end interval, and the resultant tensile force is balanced by an equal compressive force distributed over the remaining portion of the half interface. This situation is susceptible to delamination failure under the peeling fracture mode.

The maximum values of the functions G_i and F_i' and the characteristic lengths of their regions of steep gradient are meaningful measures of the criticality of the interlaminar stresses in the ith interface near the free edge. There are good reasons to suggest the use of these maximum values and characteristic lengths as parameters in the interlaminar fracture criteria for the peeling and shearing modes of failure. These parameters may be easily calculated by the present method of analysis. Being global measures, their values are less affected by the crudeness or refinement of the approximate analysis than the pointwise values of the interlaminar stresses are. That is, a relatively simple analysis may provide unreliable results for the detailed interlaminar stress distributions along the interfaces but may still yield accurate results for the maximum values of G_i and F_i' as well as the characteristic lengths of their regions of steep gradient.

8 First Example

The preceding method of analysis is applied to two configurations of a three-layer laminated beam for which finite-element solutions have been given by Glaser (1989). The parameters for the first configuration are:

$h_1 = 2.032$ mm, $E_1 = 68.95$ GPa,
$h_2 = 0.0508$ mm, $E_2 = 13.0$ GPa,
$h_3 = 0.508$ mm, $E_3 = 120.66$ GPa,

$\nu_1 = 0.33$ $\alpha_1 = 23.6 \times 10^{-6}/°C$
$\nu_2 = 0.3$ $\alpha_2 = 11.7 \times 10^{-6}/°C$
$\nu_3 = 0.28$ $\alpha_3 = 3.2 \times 10^{-6}/°C$

The half length of the beam is 15.24 mm. For this configuration, Glaser used a total of 6440 plane stress quadrilateral elements involving 13,206 degrees of freedom. He also used submodeling and mesh refinement to refine his solutions and compared the results.

In the present analysis, we substitute the preceding parameter values into the matrices $[A]$, $[B]$ and $[C]$ as given in the Appendix. From the characteristic equation, equation (13), we obtain four pairs of complex conjugate roots for the square of the eigenvalue (in the unit mm^{-2}):

$2.326 \pm 2.882\, i$, $15.748 \pm 7.950\, i$, $138.02 \pm 333.50i$,
$1692.4 \pm 2548.1\, i$

It is clear that all eigenfunctions $\exp(-\lambda x)$ decay rapidly away from one or the other end of the beam. Indeed, since the first four eigenvalues are given by $\pm 1.736 \pm 0.829\, i$, at the midpoint of the beam (15.24 mm from the two ends) the associated eigenfunctions decay to $\exp(-15.24 \times 1.736)$ times their maximum values at one or the other end of the beam. Consequently, all eigenfunctions associated with the eigenvalues having positive (negative) real parts make negligible contributions to the solution in the left (right) half of the beam.

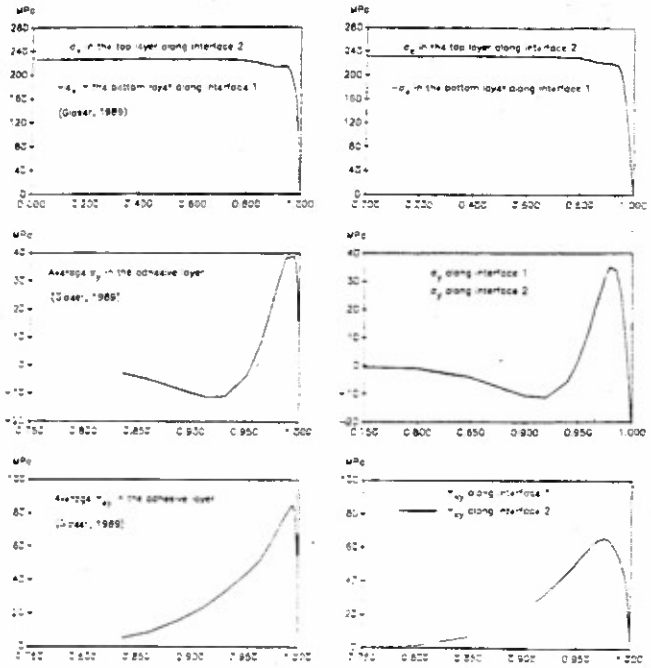

Fig. 2 Results of the first example: comparison of the present solution with Glaser's finite element solution

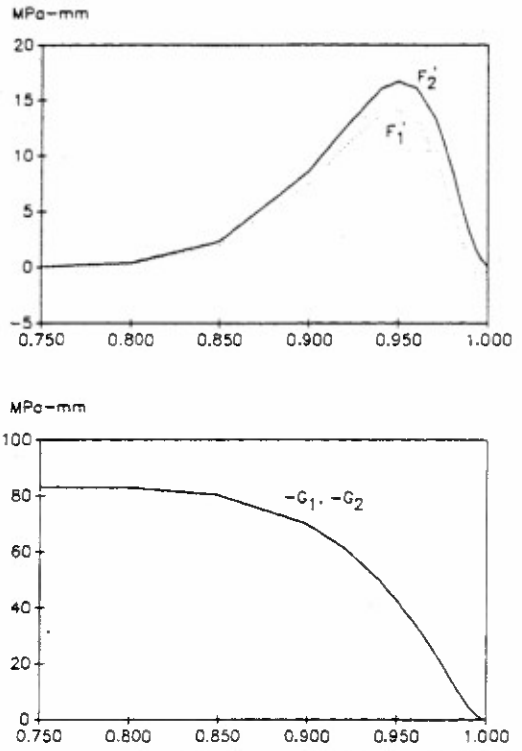

Fig. 3 Interfacial values of the first derivatives of the stress function

When the laminate is subjected to a uniform temperature increment 240°C, the solution of equation (14) for the *constrained* thermal expansion problem is given by

$$-C_1 = -390.53 \text{ MPa}, \quad -C_2 = -36.50 \text{ MPa}, \quad -C_3 = -92.67 \text{ MPa}$$

Now equations (14) and (15) yield

$$G_1 = 0.7936 \text{ MPa-m}, \quad F_1 = 806.26 \times 10^{-6} \text{ MPa-m}^2,$$

$$G_2 = 0.7954 \text{ MPa-m}, \quad F_2 = 846.62 \times 10^{-6} \text{ MPa-m}^2,$$

$$G^* = 0.8425 \text{ Mpa-m}, \quad F^* = 1262.65 \times 10^{-6} \text{ MPa-m}^2$$

From equation (6) we obtain

$$Q = 202.06 \text{ MPa-m}, \quad R = 25.190 \times 10^{-3} \text{ MPa-m}^2, \quad S = 127.32 \times 10^{-6} \text{ MPa-m}^3$$

From equations (4) and (5) we obtain ϵ_0 and κ associated with the solution of Problem C (characterized by a uniform axial extension combined with pure bending which relieves the resultant axial force and bending moment of the constrained thermal solution):

$$\epsilon_0 = 4.447 \times 10^{-3}, \quad \kappa = 2.225 \text{ radian/m}$$

Combining the axial stresses from equations (3) and (14), we obtain $\sigma_x = -196.9$ MPa in the bottom layer at Interface 1, and $\sigma_x = 232.5$ MPa in the top layer at Interface 2. These results are nearly exact in an interior segment of the beam because the *exact* solution of Problem C (which exactly complements the preceding two simple but exact solutions) decays rapidly away from the two ends. Glaser's finite-element solution yields corresponding results of -195.0 MPa and 229.1 MPa, respectively (the unit used by Glaser for these results, GPa, was possibly an error). Hence the discrepancy between the axial stress of the present analysis and that of the finite-element solution is less than 1.5 percent and, since the present result is nearly exact, the discrepancy reflects the error in the finite-element solution.

To obtain the axial stress and the interlaminar stresses in the vicinity of the free edge, the solutions of the constrained thermal expansion problem and of Problem C must be combined with the solution of Problem B. The last solution may be obtained by appropriately combining the eigenfunctions as described in the preceding section. The final results are shown in the three plots in the right column of Fig. 2. The corresponding plots in the left column of the figure show the finite-element results obtained by Glaser. The agreement is very good for the axial stress and the interlaminar normal stress. The interlaminar shearing stress obtained in the present analysis is smaller than the finite-element result in a very short interval (shorter than one quarter of the laminate thickness) adjacent to the free edge. Elsewhere, the agreement in the interlaminar shearing stress is also excellent.

The first derivatives of the stress function along the two interfaces are shown in Fig. 3. As previously mentioned, along each interface the values of $F_i'(x)$ and $G_i(x)$ are the resultant normal force and the resultant shearing force, respectively, acting across an end segment of the interface of length $(a-x)$. F_i' attains its maximum value at a point x^* on the interface where the interlaminar normal stress changes its sign. This point ($x^* \approx 0.95a$ for the present solution) is generally very close to the free edge. The *average* value of the interlaminar normal stress over the end segment $[x^*, a]$ equals $F_i'(x^*)/(a-x^*)$. This average value is a measure of the criticality of the interlaminar normal stress near the free edge. The interlaminar shearing stress does not change sign in the interval $[0, a]$. Hence its integral, $G_i(x)$, changes monotonically from 0 at the free edge to its maximum (absolute) value at the midpoint of the beam, $x=0$. Half of the change takes place in a very short interval $[x^{**}, a]$ near the free edge. The *average* interlaminar shearing stress over this short end interval is given by $G_i(x^{**})/(a-x^{**}) = G_i(0)/2(a-x^{**})$. This value is a measure of the criticality of the interlaminar shearing stress near the free edge. One finds that x^* is very close to x^{**}. Hence the two end segments of the ith interface used as the basis for averaging the interlaminar normal and shearing stresses are not significantly different.

9 Comments on the Solution Near the Free Edge

The reason for the more significant discrepancy in the in-

terlaminar shearing stress compared to the interlaminar normal stress (in the close vicinity of the free edge) is that, in the present analysis, τ_{xy} varies quadratically across the thickness of each layer whereas σ_y has a cubic variation. In the polynomial approximation of the stress function (equations (7) to (9)), the coefficient functions $F_i(x)$ and $G_i(x)$ as determined by the complementary virtual work principle predict better the *average* shearing stress across the thickness of each layer, and less satisfactorily its maximum value, which is reached along an adjacent interface. This reasoning suggests that the results for the interlaminar shearing stress may be improved if the third-order polynomial approximations for the stress functions are replaced by fourth-order polynomials in the thickness coordinate. The validity of this suggestion is supported by the superiority of the present result for the interlaminar normal stress (which has a cubic variation in η) compared to the interlaminar shearing stress.

The details of the interlaminar normal stresses as shown in the second plot in the right column of Fig. 2 are only captured by the finite-element solution with mesh refinement. Thus, when higher order polynomials are used to represent the stress functions, the present analysis may provide results as good as or better than finite-element solutions using more than 10,000 degrees-of-freedom, with a significant saving of programming labor and computational time.

It is well known that an exact analysis with strict adherence to the constitutive relations of linear elasticity (even at physically unattainable high levels of stress) yields a singularity at the intersection of the free edge with an interface. Such a stress singularity cannot be determined by the present approximate method or by the usual finite-element analysis. Yet the predicted magnitude of the interlaminar normal stress at the free edge is sometimes taken as a measure for assessing the accuracy of an approximate analysis. The rationale appears to be that since an exact analysis based on linear elasticity predicts infinite peeling stress at the free edge, one approximate solution might be better than another if, in the absence of other significant differences, the first solution yields a greater peeling stress at the free edge.

But the mere fact that an approximate analysis fails to determine a stress singularity should not be considered as a weakness of that analysis, because stress values exceeding a certain bound are physically unattainable. Progressive refinement in the finite-element modeling or in the present scheme of analysis (by raising the degree of the polynomial representation for the stress function) may result in increasingly larger values of the free-edge peeling stress. However, such refined solutions do not necessarily provide more or better information concerning the actual stress distribution near the free edge.

Along the free edge, σ_y according to the exact elasticity solution approaches infinity as one approaches an interface. Hence, along an interface, $\sigma_{y,x}$ approaches infinity at the free edge. But this limiting behavior of $\sigma_{y,x}$ presents a distorted picture of the real situation because it is a mathematical consequence of an unrealistic constitutive assumption. We notice that τ_{xy} and σ_y are related by the equilibrium equation $\tau_{xy,x} + \sigma_{y,y} = 0$. If an over-refined numerical or finite-element solution yields unrealistically large local values of $\sigma_{y,x}$, then it also yields unrealistically large values of $\tau_{xy,y}$, i.e., of the gradient of the interlaminar shearing stress in an end region of the interface. Therefore, while the higher gradients and larger values of τ_{xy} as predicted by over-refined approximate analyses may be closer to the exact elasticity solution with stress singularity, they may also present a distorted picture of the actual pattern of the interfacial shearing stress in a real material.

10 Second Example

The second configuration of the three-layer laminate to be analyzed was originally considered by Chen et al., 1982 (see their Example 1). For this configuration, the half length of the beam is 250 mm and the values of the geometrical and material parameters are

$$h_1 = 50.0 \text{ mm}, \quad E_1 = 68.9 \text{ GPa},$$
$$h_2 = 1.0 \text{ mm}, \quad E_2 = 30.0 \text{ GPa},$$
$$h_3 = 50.0 \text{ mm}, \quad E_3 = 206.9 \text{ GPa},$$
$$\nu_1 = 0.33, \quad \alpha_1 = 13.0 \times 10^{-6}/^\circ\text{F},$$
$$\nu_2 = 0.33, \quad \alpha_2 = 2.5 \times 10^{-6}/^\circ\text{F},$$
$$\nu_3 = 0.25, \quad \alpha_3 = 6.5 \times 10^{-6}/^\circ\text{F}.$$

In this case, the characteristic equation has two real roots and three pairs of complex conjugate roots for the square of the eigenvalue (in the unit mm^{-2}):

$$.004226, \quad .012193, \quad .001691 \pm .001675 \text{ i},$$
$$.003524 \pm .14678 \text{ i}, \quad 1.95065 \pm 4.2027 \text{ i}$$

Chen et al. considered a fictitious uniform temperature increment of 10^6°F. As indicated above, virtually exact results for the axial stress in the main body of the beam (away from the two ends) may be obtained by an elementary analysis neglecting the contributions of the eigenfunctions. This yields the values -255.6 GPa and 558.7 GPa, respectively, in the lower layer at Interface 1 and in the upper layer at Interface 2. The corresponding values from Glaser's finite-element solution are -254.1 GPa and 554.1 GPa. Glaser reported the values of -248.3 GPa and 537.9 GPa, respectively, for the solutions of Chen et al., although results with four-digit precision were not provided in their original paper and can only be conjectured by extrapolating the curves in Fig. 4 of the paper. A comparison of the results indicates discrepancies smaller than one percent with the finite-element solution and larger than three percent with the solution of Chen et al. (as given by Glaser).

The results for the interlaminar normal and shearing stresses in the vicinity of the free edge are shown in Fig. 4. The present results are somewhat in better agreement with the finite-element solution than the results of Chen et al.

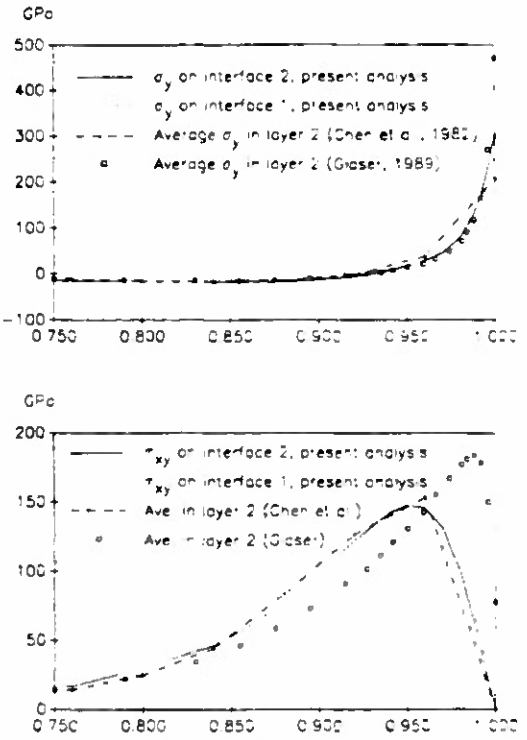

Fig. 4 Results of the second example

In the analysis of Chen et al., linear variation of the axial stress with respect to the thickness coordinate was assumed in the two thick layers 1 and 3 but not in the thin middle layer. Chen et al. did not introduce stress functions. However, they obtained quadratic variation of τ_{xy} and cubic variation of σ_y (with respect to the thickness coordinate in layers 1 and 3) from the assumed linear variation of the axial stress by integrating the equilibrium equations in each of the two layers. In the thin middle layer, they introduced the additional assumption that the shearing stress τ_{xy} does not vary in the thickness direction. Under this additional assumption, one equilibrium equation (which the authors used) forces the transverse normal stress σ_y to depend linearly on the thickness coordinate and the other equilibrium equation (which they did not use) requires that the axial stress in the middle layer be independent of x—a conclusion which is clearly incompatible with the free-edge boundary condition.

It may be shown that the additional assumption of Chen et al. for the thin middle layer, when combined with the free-edge boundary condition $\sigma_x = 0$, is mathematically equivalent to imposing the following expression for the functions F_2 and G_2 of the present analysis in terms of the functions F_1 and G_1:

$$G_2(x) = G_1(x), \quad F_2(x) = F_1(x) + h_2\, G_1(x)$$

As a result, the number of unknown functions in the eigenvalue problem is reduced from four to two and the order of the characteristic equation is lowered from 16 to 8. As an equation for the square of the eigenvalue, the characteristic equation in the analysis of Chen et al. has two real roots and one pair of complex conjugate roots. The simplified analysis and the underlying assumption are justifiable for a laminate with a very thin middle layer.

11 Summary and Conclusion

A systematic approximate method for obtaining the plane stress solutions of a laminated beam subjected to temperature loadings has been developed in this paper. The method is based on the use of stress functions. This ensures that the resulting approximate solution for the stress field satisfies exactly the equilibrium equations in each layer, the traction-free boundary conditions over the entire boundary of the beam, and all interfacial continuity conditions for the interlaminar stresses. The compatibility conditions for the strain and the interfacial continuity of the displacement are enforced in an averaged sense by extremizing the complementary energy functional with respect to the class of statically admissible stress fields whose stress functions in individual layers are cubic polynomial functions of the thickness coordinate. This results in an eigenvalue problem associated with a linear system of ordinary differential equations having constant coefficients. An appropriate combination of the eigenfunctions which satisfies the traction-free boundary conditions at the two ends yields the interlaminar stresses in the beam. In the main body of the beam away from the two ends, the axial stress is practically independent of the axial coordinate and its values can be determined, almost exactly, by combining two trivial solutions, the first being a constrained thermal expansion solution and the second being a solution corresponding to a uniform axial extension superposed on pure bending.

The present method achieves the dual objectives of efficiency and accuracy because the representations of the stress functions in the analysis are not chosen arbitrarily or purely for computational reasons (as in choosing the shape functions in finite-element modeling). They are based on the eigenfunctions as determined by the complementary virtual work principle. Polynomial expansion of the stress functions with respect to the thickness coordinate may be justified on the ground that the thickness of each layer is very small compared to the beam length. Besides the assumption of linear thermoelasticity, the assumed polynomial dependence of the stress function upon the thickness coordinate in each layer is the only approximation made in the present analysis. Additional and miscellaneous assumptions with obscure meaning and dubious implication are categorically avoided. This feature makes the present approximate analysis particularly appealing from a mathematical point of view.

Using the present method, a thermal stress analysis of a three-layer beam involves only eight real and complex eigenfunctions and yields results that are comparable in accuracy to finite-element solutions with more than 10,000 degrees of freedom. Compared to the finite-element analysis, the present method requires extremely simple data input and very little resources of computer time, storage and power (execution of the analysis for the two example problems in this paper took a fraction of a minute on an IBM personal computer with 640K memory). Furthermore, refinement and improvement in the approximate solutions may be achieved by increasing the degree of the polynomial representations of the stress functions. However, as was argued in Section 9 of this paper, there are good reasons to refrain from over-refining the approximate solutions. Although an exact analysis based on linear elasticity yields a stress singularity at the intersection of the free edge with an interface, this limiting behavior may provide a distorted picture of the actual patterns of the interlaminar normal and shearing stresses along an interface between real materials.

In the ith interface, the maximum values of the first order partial derivatives of the stress function (i.e., the maximum values of $F_i'(x)$ and $G_i(x)$) and the characteristic lengths of their regions of steep gradient provide useful measures of the criticality of the interlaminar stresses near the free edge. These values are less affected by the degree of refinement of the approximate analysis method than the detailed distributions of the interlaminar stresses are. They may be used as parameters in the fracture criteria for the initiation of delamination failure.

Acknowledgment

This work was made possible by a grant from the Army Research Office to Georgia Institute of Technology. The author gratefully appreciates the financial support.

References

Blech, J. J., and Kantor, Y., 1984, "An Edge Problem Having No Singularity at the Corner," *Computers Struc.*, Vol. 18, pp. 609–617.

Boley, B. A., and Testa, R. B., 1969, "Thermal Stresses in Composite Beams," *Int. J. Solids Struct.*, Vol. 5, pp. 1153–1169.

Chang, Fo-Van, 1983, "Thermal Contact Stresses of Bi-Metal Strip Thermostat," *Appl. Math. J. Mech.*, Vol. 4, Tsing-hua University, Beijing, China, pp. 363–376.

Chen, D., Cheng, S., and Gerhardt, T. D., 1982, "Thermal Stresses in Laminated Beams," *J. Thermal Stresses*, Vol. 5, pp. 67–84.

Chen, W. T., and Nelson, C. W., 1979, "Thermal Stress in Bonded Joints," *IBM J. Res. Devel.*, Vol. 23, pp. 178–188.

Cho, K. N., Striz, A. G., and Bert, C. W., "Thermal Stress Analysis of Laminates Using Higher Order Theory in Each Layer," *J. Thermal Stresses*, in print.

Gerstle, F. P., Jr., and Chambers, R. S., 1987, "Analysis of End Stresses in Glass-Metal Bimaterial Strips," *Technology of Glass, Ceramic, or Ceramic-Glass to Metal Sealing*, Eds. Moddeman, W. E., Merten, C. S. and Kramer, D. P., ASME, New York, MD-Vol. 4, pp. 47–59.

Glaser, J. C., 1989, "Thermal Stresses in Compliantly-Joined Materials," ASME Winter Annual Meeting, Paper No. 89-WA/EEP-14, San Francisco, CA, December 1989, 7 pages.

Grimado, P. B., 1978, "Interlaminar Thermoelastic Stresses in Layered Beams," *J. Thermal Stresses*, Vol. 1, pp. 75–86.

Hess, M. S., 1969, "The End Problem for a Laminated Elastid Strip—II. Differential Expansion Stresses," *J. Composite Mater.*, Vol. 3, pp. 630–641.

Kuo, An-Yu, 1989, "Thermal Stresses at the Edge of a Bimetallic Thermostat," ASME *Journal of Applied Mechanics*, Vol. 56, pp. 585–589.

Lekhnitskii, S. G., 1963, *Theory of Elasticity of an Anisotropic Elastic Body*, trans. P. Fern, Holden-Day, San Francisco.

Olsen, G. H., and Ettenberg, M., 1977, "Calculated Stresses in Multilayered Heteroepitaxial Structures," *J. Appl. Phys.*, Vol. 48, pp. 2543-2547.

Reinhart, F. K., and Logan, R. A., 1973, "Interface Stress of $Al_xGa_{1-x}As$-GaAs Layer Structures," *J. Appl. Phys.*, Vol. 44, pp. 3171-3175.

Roll, K., 1976, "Analysis of Stress and Strain Distribution in Thin Films and Substrates," *J. Appl. Phys.*, Vol. 47, pp. 3224-3229.

Saganuma, K., Okamoto, T., and Koizumi, M., 1984, "Effect of Interlayers in Ceramic-Metal Joints with Thermal Expansion Mismatches," *J. Amer. Cer. Soc.*, Vol. 67, pp. C256-C257.

Suhir, E., 1986a, "Stresses in Bi-metal Thermostats," ASME *Journal of Applied Mechanics*, Vol. 53, pp. 657-660.

Suhir, E., 1986b, "Stresses in Adhesively Bonded Assemblies Used in Electronic Packaging," *Mat. Res. Soc. Symp. Proc.*, Vol. 72, "Electronic Packaging Materials Science II," pp. 133-138.

Suhir, E. 1988, "An Approximate Analysis of Stresses in Multilayered Elastic Thin Films," ASME *Journal of Applied Mechanics*, Vol. 55, pp. 143-148.

Taylor, T. C. and Yuan, F. L., 1962, "Thermal Stress and Fracture in Shear-constrained Semiconductor Device Structure," *IRE (Inst. of Radio Engeneers) Trans. on Elec. Dev.*, ED-9, pp. 303-308.

Timoshenko, S., 1925, "Analysis of Bi-metal Thermostats," *J. Opt. Soc Amer.*, Vol. 11, pp. 233-255.

Vims, L. and Kerps, D., 1982, "Simple Stress Formula for Multilayered Thin Films on a Thick Substrate," *J. Appl. Phys.*, Vol. 53, pp. 1536-1537.

Wang, A. S. D., and Crossman, F. W., 1977, "Edge Effects on Thermally Induced Stresses in Composite Laminates," *J. Composite Mat.*, Vol. 11, pp. 300-312.

Wang, S. S., and Choi, I., 1979, "Boundary Layer Thermal Stresses in Angle-ply Composite Laminates," *Modern Developments in Composite Materials and Structures*, J. R. Visson, ed., pp. 315-341.

Yin, W.-L., 1989, "*Free-edge Interlaminar Stresses in a Laminated Strip Subjected to Axial Extension, Bending, and Twisting*," Final Report for Task No. 7, NASA Contract No. NAS1-17925, April 1989.

Yin, W.-L., 1991, "Interlaminar Stress Analysis Based on Stress Functions and the Complementary Energy Principle," *2nd Pan American Congr. Appl. Mech. Proc.*, Vina del Mar, Chile, January 1991.

APPENDIX

For a laminated beam composed of three isotropic elastic layers, the symmetric matrices $[A]$, $[B]$ and $[C]$ of Eqs. (12) and (13) are given by

$$[A] = \begin{bmatrix} \frac{13}{70}\left(\frac{h_1}{E_1}+\frac{h_2}{E_2}\right) & \frac{11}{420}\left(\frac{h_2^2}{E_2}-\frac{h_1^2}{E_1}\right) & \frac{9}{140}\frac{h_2}{E_2} & -\frac{13}{840}\frac{h_2}{E_2} \\ & \frac{1}{210}\left(\frac{h_2^3}{E_2}+\frac{h_1^3}{E_1}\right) & \frac{13}{840}\frac{h_2^2}{E_2} & -\frac{1}{280}\frac{h_2^3}{E_2} \\ & & \frac{13}{70}\left(\frac{h_2}{E_2}+\frac{h_3}{E_3}\right) & \frac{11}{420}\left(\frac{h_3^2}{E_3}-\frac{h_2^2}{E_2}\right) \\ & & & \frac{1}{210}\left(\frac{h_2^3}{E_2}+\frac{h_3^3}{E_3}\right) \end{bmatrix}$$

$$[B] = \begin{bmatrix} -\frac{6}{5}\left(\frac{1}{E_1h_1}+\frac{1}{E_2h_2}\right) & \frac{1}{10}\left(\frac{1}{E_1}-\frac{1}{E_2}\right)-\frac{1}{2}\left(\frac{\nu_1}{E_1}-\frac{\nu_2}{E_2}\right) & \frac{6}{5}\frac{1}{E_2h_2} & -\frac{1}{10E_2} \\ & -\frac{2}{15}\left(\frac{h_1}{E_2}+\frac{h_2}{E_2}\right) & \frac{1}{10E_2} & \frac{1}{30}\frac{h_2}{E_2} \\ & & -\frac{6}{5}\left(\frac{1}{E_2h_2}+\frac{1}{E_3h_3}\right) & \frac{1}{10}\left(\frac{1}{E_2}-\frac{1}{E_3}\right)-\frac{1}{2}\left(\frac{\nu_2}{E_2}-\frac{\nu_3}{E_3}\right) \\ & & & -\frac{2}{15}\left(\frac{h_2}{E_2}+\frac{h_3}{E_3}\right) \end{bmatrix}$$

$$[C] = \begin{bmatrix} 6\left(\frac{1}{E_1h_1^3}+\frac{1}{E_2h_2^3}\right) & 3\left(\frac{1}{E_2h_2^2}-\frac{1}{E_1h_1^2}\right) & -\frac{6}{E_2h_2^3} & \frac{3}{E_2h_2^2} \\ & 2\left(\frac{1}{E_1h_1}+\frac{1}{E_2h_2}\right) & -\frac{3}{E_2h_2^2} & \frac{1}{E_2h_2} \\ & & 6\left(\frac{1}{E_2h_2^3}+\frac{1}{E_3h_3^3}\right) & 3\left(\frac{1}{E_3h_3^2}-\frac{1}{E_2h_2^2}\right) \\ & & & 2\left(\frac{1}{E_2h_2}+\frac{1}{E_3h_3}\right) \end{bmatrix}$$

Appendix H

"Refined Variational Solutions of

the Interfacial Thermal Stresses in a Laminated Beam"

By Wan-Lee Yin

ASME Winter Annual Meeting

December 1991, Atlanta, GA

THE AMERICAN SOCIETY OF MECHANICAL ENGINEERS
345 E. 47 St., New York, N.Y. 10017

WA/EEP-33

Refined Variational Solutions of the Interfacial Thermal Stresses in a Laminated Beam

W.-L. Yin [1]
Georgia Institute of Technology
Atlanta, Georgia 30332

Abstract

Efficient and accurate solutions of the interlaminar stresses in a layered beam under a temperature loading are obtained by a variational method based on the principle of complementary virtual work. Stress functions are introduced in each layer and they are approximated by polynomial expansions of the *fifth* or lower degrees in the thickness coordinate. Comparison of the solutions of the various orders with the existing numerical and analytical solutions indicates that the variational solutions converge rapidly as the degree of the polynomial expansion increases and that even the lower-order variational solutions yield satisfactory results for the interlaminar stresses. Over end segments of the interface adjacent to the free edge, the resultant forces of the interlaminar normal and shearing stresses are given by the first-order derivatives of the stress functions. These global measures of the severity of interlaminar peeling and shearing action are predicted accurately by the lowest-order variational solution.

1. Introduction

Bimetal thermostats and multi-layered beams and laminates are often subjected to severe interfacial stresses under mechanical and temperature loads. Mismatches in the thermal and elastic properties of the adjacent layers generally result in a stress singularity at the intersection of an interface with a free edge. The problem has received a considerable amount of attention because of its importance to the technology of composite materials and to electronic packaging. Besides theoretical analysis of the stress singularity based on elasticity solutions, numerical solutions using finite-difference or finite-element methods have been obtained to determine the interfacial stress distribution near the free edge. Furthermore, simplified mechanistic approaches have been developed to provide efficient approximate solutions and quantitative measures of the criticality of the free-edge effects.

In a recent work (Yin, 1991a), the author developed a general scheme for the determination of interlaminar thermal stresses in laminated beams. The approach was based on the complementary virtual work principle with the use of stress functions. Besides the assumption of linear thermoelastic constitutive relation, the only approximation introduced in the analysis was that the stresses (and hence the stress functions) in each layer are polynomial functions of the thickness coordinate. No *a priori* assumption was made concerning the variation of the stresses along the axial direction. The resulting approximate solutions satisfy, *exactly*, the equilibrium equations in each layer, the free boundary conditions on exterior surfaces, and interfacial continuity of the tractions across all interfaces. Compatibility of the strain and interfacial continuity of the displacements are enforced in an averaged sense by minimizing the complementary energy. This computationally simple and efficient method was applied to the problem of a three-layer beam. The stress functions in the successive layers were taken to be cubic functions of the thickness coordinate. The interlaminar normal and shearing stresses were calculated and found to be in close agreement with the results of a very elaborate finite-element solution (Glaser, 1989), except in an extremely short interval at the end of the interface.

Stress functions that are cubic polynomial functions of the thickness coordinate in each layer yield an axial stress that has a linear variation across the thickness of the layer. Such stress functions are, therefore, the lowest order polynomial approximations needed to account for the effect of bending of the beam. That this lowest-order variational solution provides accurate results for the interlaminar stresses, except in extremely short intervals adjacent to the free edge, indicates the efficacy of the present method. More accurate solutions for the interfacial stresses may be obtained by the present approach using higher-order polynomial expansions of the stress functions. By comparing the variational solutions of increasing orders among themselves or with the elasticity solution, one may discern the general trend of convergence and assess the accuracy and reliability of the present method.

[1] Professor, Engineering Science and Mechanics Program.

In this paper, refined variational solutions based on fourth-order and fifth-order polynomial expansions of the stress function (in terms of the thickness coordinate in each layer) are obtained for three-layer and two-layer beams. The additional terms in the expansion provide a better representation of the stress field near the free edge. The resulting solutions for the three-layer beam are in excellent agreement with Glaser's finite element solutions even in the immediate neighborhood of the free edge. The results for the two-layer bimetal thermostat converge rapidly, in the sense appropriate to variational calculus, to an approximate elasticity solution (Kuo, 1989) which was obtained by using the Fourier transform method and the knowledge of the stress singularity associated with two joined quarter-spaces (Bogy, 1968, 1970).

The first derivatives of the stress functions (with respect to the axial and the thickness coordinates) are the integrals of the interfacial normal and shearing stresses (i.e., the resultant normal and shearing forces) over end intervals of varying lengths. It has been suggested (Yin, 1991a) that these integrals are more appropriate measures of the criticality of the interlaminar stresses than conventional measures such as the stress intensity factors, because stress singularities do not occur in a real material whereas the resultant forces of the interlaminar stresses over short end segments of the interface provide realistic indications of the severity of the local actions of peeling and shearing. For the two- and three-layer beams studied in the present work, a comparison of the variational solutions based on the third to the fifth-order polynomial expansions of the stress functions indicates that, although the results for the interlaminar stresses show appreciable discrepancies near the free edge, those for the derivatives of the stress functions are in much better agreement. Consequently, if the derivatives of stress functions are used in the fracture criteria of laminated beams, the variational solutions based on lower-order polynomial stress functions are adequate for providing realiable failure predictions even though such solutions do not yield accurate local interlaminar stress distributions in an extremely small neighborhood of the free edge. This indicates another important advantage of the stress-function-based variational approach besides its superior efficiency and extreme ease of data input.

2. Decomposition of the Thermal Expansion Problem of a Layered Beam

In a previous paper (Yin, 1991a), the thermal expansion problem of a layered beam of a finite length was decomposed into three component problems: (1) a *constrained* thermoelastic prohlem with a vanishing axial strain and a layerwise constant thermal stress field, (2) a mechanical problem characterized by a uniform axial extension combined with pure bending and (3) another mechanical problem with a self-equilibrating system of end tractions which, when superposed on the previous two solutions, completely relieves the tractions at the two free ends of the beam. The first two problems are easily solved and the solutions do not show interlaminar stresses. The interlaminar stresses associated with the third, non-trivial problem are determined hy solving an eigenvalue problem. In the present paper, a more direct decomposition of the original problem into two (rather than three) subproblems is achieved by conceptually extending the layered beam into one of infinite length. The second subproblem in the present decomposition is identical to the third suhprohlem in the original decomposition.

Consider a layered beam, of axial length 2a, consisting of n + 1 distinct, homogeneous, isotropic layers. The layers are separated by n parallel interfaces at $y = y_i$ (i = 1, 2, ... n), where the origin of the (x, y) coordinate system is chosen at the center of the heam, and the x-coordinate runs along the longitudinal direction. The beam is stress-free in some reference temperature and is subjected to a temperature increment T(y) which depends only on the y-coordinate. Our problem is to determine the thermal stresses along the interfaces of the beam.

We consider, instead of the layered beam of finite length 2a, an otherwise identical beam with infinite length under the same temparature load T(y). The infinitely long beam is free to bend and to extend along the axial direction. Consequently, the deformation of the infinite beam is characterized by a constant axial membrane strain ϵ_o and a constant curvature κ, i.e., the initially straight beam extends and bends uniformaly into a circular beam. Since the infinite beam exists only in imagination, over-lapping of the deformed beam with itself due to multiple winding around the circle may be ignored. It is clear that all cross-sections of the infinite beam are subjected to a zero shearing stress ($\tau_{xy} = 0$) and to the same distribution of the axial stress $\sigma_x(y)$, which is generally discontinuous across the interfaces $y = y_i$, and which has vanishing force and moment resultants because the beam is free to extend and to bend. In other words, the stress distribution $\sigma_x(y)$ across each cross-section is a self-equilibrating system. We now consider a segment of the infinite beam of initial length 2a. The segment is maintained in the given state of deformation hy the temperature load T(y) and the end traction $\sigma_x(y)$. If an equal but opposite system of end tractions $-\sigma_x(y)$ is superimposed on the segment, then the segment becomes traction-free over its entire boundary. Consequently, the solution of the original thermal stress problem for the finite beam may be decomposed into (1) a trivial solution with a total strain field characterized by a unifnrm axial strain ϵ_o on the middle axis and a uniform bending curvature κ (part of the strain field is due to the thermal strain associated with the temperature load and the other part is caused by the mechanical load at the two ends) and (2) a complementary mechancial solution due soley to the reversed end tractions $-\sigma_x(y)$. Our analysis is mainly concerned with the solution of the complementary mechanical problem. Once the solution of the complementary problem is obtained, it is combined with the trivial solution of the thermal expansion of an infinitely long beam to obtain the final solution for the interlaminar thermal stresses in a finite beam.

3. Polynomial Stress Functions

The layers and their interfaces will be numbered from the hottom up. Thus the i-th layer is bounded below by the (i-1)-th interface and bounded ahove hy the i-th interface. This layer has the thickness $h_i = y_i - y_{i-1}$, and is composed of a material with Young's modulus E_i, Poisson's ratio ν_i, and coefficient of thermal expansion α_i. Any plane stress field in the i-th layer satisfying the differential equations of equilibrium may he expressed in terms of a stress function in the following manner:

$$\sigma_x^{(i)} = F^{(i)}_{,yy}, \qquad \sigma_y^{(i)} = F^{(i)}_{,xx}, \qquad \tau_{xy}^{(i)} = -F^{(i)}_{,xy} \tag{1}$$

where the commas indicate partial differentiation. It has been pointed out (Yin, 1991a) that, because of the interfacial continuity of the interlaminar stresses, the stress functions in the successive layers may he chosen in such a way that F and $F_{,y}$ are both

continuous across the interfaces, i.e.,

$$\overset{(i+1)}{F} = \overset{(i)}{F}, \qquad \overset{(i+1)}{F}_{,y} = \overset{(i)}{F}_{,y} \tag{2}$$

along the interface $y = y_i$. Furthermore, the stress function in the bottom layer and its y-derivative may both be made to vanish identically over the bottom surface. It has also been shown that $F_{,y}$ and F on the top surface are related to the force and moment resultants of the end traction $\sigma_x(y)$. Since these force and moment resultants vanish in the case of the complementary mechanical problem, F and $F_{,y}$ also vanish on the top surface.

In the i-th layer, we define the non-dimensional thickness coordinate η by

$$\eta = (y - y_{i-1})/(y_i - y_{i-1})$$

and approximate the stress function in the layer by a polynomial expansion in the non-dimensional variable η:

$$\begin{aligned}\overset{(i)}{F}(x,\eta) &= (1 - 3\eta^2 + 2\eta^3)\, F_{i-1}(x) + (\eta - 2\eta^2 + \eta^3)\, h_i G_{i-1}(x) \\ &\quad + (3\eta^2 - 2\eta^3)\, F_i(x) + (\eta^3 - \eta^2)\, h_i G_i(x) \\ &\quad + \eta^2(1 - \eta)^2 P_i(x) + \eta^2(1 - \eta)^3 Q_i(x) \quad (i = 2, \ldots, n)\end{aligned} \tag{3}$$

where $F_i(x)$, $G_i(x)$, $P_i(x)$ and $Q_i(x)$ are undetermined coefficient functions. It is easily verified that $F_i(x)$ and $G_i(x)$ coincide, respectively, with the first and second quantities in Eq. (2), i.e., they are the values of the stress function and its y-derivative along the i-th interface. In the bottom and top layers, Eq. (3) is replaced, respectively, by the following expressions

$$\begin{aligned}\overset{(1)}{F}(x,\eta) &= (3\eta^2 - 2\eta^3)F_1(x) + (\eta^3 - \eta^2)h_1 G_1(x) \\ &\quad + \eta^2(1 - \eta)^2 P_1(x) + \eta^3(1 - \eta)^2 Q_1(x)\end{aligned} \tag{4}$$

and

$$\begin{aligned}\overset{(n+1)}{F}(x,\eta) &= (1 - 3\eta^2 + 2\eta^3)F_n(x) + (\eta - 2\eta^2 + \eta^3)h_{n+1} G_n(x) \\ &\quad + \eta^2(1 - \eta)^2 P_{n+1}(x) + \eta^2(1 - \eta)^3 Q_{n+1}(x)\end{aligned} \tag{5}$$

The stress functions used in a previous study (Yin, 1991a) did not include the coefficients of the quartic and quintic terms in η (P_i and Q_i).

Substituting the preceding expressions of the stress functions into the total complementary energy of the beam

$$\begin{aligned}\Pi = (1/2) \sum_i \iint (1/E_i) \{&F_{,yy}^2 + F_{,xx}^2 - 2\nu_i F_{,yy} F_{,xx} \\ &+ 2(1 + \nu_i) F_{,xy}^2\}\, dx\, dy\end{aligned} \tag{6}$$

we obtain, by the usual procedure of variational calculus, the Euler equation associated with the first variation of Π:

$$([A]\frac{d^4}{dx^4} + [B]\frac{d^2}{dx^2} + [C])\{X\} = \{0\} \tag{7}$$

where [A], [B] and [C] are $4n+2$ by $4n+2$ real symmetric matrices and where the column vector $\{X\}$ has the components $P_1(x)$, $Q_1(x)$, $F_1(x)$, $F_2(x)$, ..., $F_n(x)$, $G_n(x)$, $P_{n+1}(x)$ and $Q_{n+1}(x)$.

If the temperature load T(y) varies linearly in each layer, then the end traction $-\sigma_x(y)$ of the complementary mechanical problem also varies linearly in each layer. In this case the the functions P_i and Q_i ($i = 1, 2, \ldots, n+1$) vanish at the end points $x = \pm a$ while the boundary values of the functions G_i and F_i ($i = 1, 2, \ldots, n$) at these end points may he easily obtained by integrating $-\sigma_x(y)$ once and twice with respect to the thickness coordinate. These boundary condi-tions together with the *homogeneous* boundary condition for the derivatives of the functions F_i, G_i, P_i and Q_i provide enough conditions for uniquely determining the unknown coefficients in the general solution of the governing differential equation, Eq. (7).

Because of the lengthy algehraic manipulations required to derive the coefficient matrices [A], [B] and [C] of Eq. (7) in terms of the geometrical and material parameters of the beam, the task of derivation was implemented with the use of the symbolic computational program MACSYMA. The program also translated the resulting expressions of the matrices into Fortran expressions. The expressions were subsequently integrated into a Fortran program which reads the geometrical and material parameters and the temperature load, evaluates the matrices [A], [B] and [C], computes all real and complex eigenvalues and the corresponding eigenvectors associated with Eq. (7), forms the appropriate linear combination of the eigenvectors so as to satisfy the end conditions for the functions F_i, G_i, P_i and Q_i (deduced from the end traction $-\sigma_x(y)$, which is in turn caused by the thermal load), and finally calculates the interlaimar stresses along the interfaces by evaluating the derivatives of the functions $F_i(x)$ and $G_i(x)$. The execution of the program for a two- or three-layer beam requires only a fraction of a minute on an IBM PC-XT and a few seconds on a 386 PC. Data input is extremely simple. It consists of a few lines of numbers, including the number of layers in the beam (at present limited to three but may he increased by modifying the program), the elastic moduli and the thermal expansion coefficients of the successive layers, and the temperature load in each layer (assumed to be constant or to vary linearly within each layer). Comparison of the results generated by the program with the existing results of finite-element and analytical solutions for the same problem show very close agreement, as shown in the following section of this paper. The program, therefore, appears to be ideally suited for simple, inexpensive and reliahle computation of the interlaminar thermal stresses in the practical analysis of a layered beam.

4. Refined Variational Solutions of Three-Layer and Two-Layer Beams

Glaser (1989) presented a finite-element solution of the thermal stresses in a three-layer heam of length 2a suhjected to a uniform temperature increment 240°C. The middle layer of the heam is a thin layer of adhesive. The geometrical and material parameters of the problem are given as follws:

$h_1 = 2.032$ mm, $E_1 = 68.95$ GPa, $\nu_1 = .33$, $\alpha_1 = 23.6 \times 10^{-6}$/°C,
$h_2 = .0508$ mm, $E_2 = 13.0$ GPa, $\nu_2 = .30$, $\alpha_2 = 11.7 \times 10^{-6}$/°C,
$h_3 = .508$ mm, $E_3 = 120.66$ GPa, $\nu_2 = .28$, $\alpha_2 = 3.2 \times 10^{-6}$/°C,

where h_i, E_i, ν_i and α_i denote, respectively, the thickness,

Young's modulus, Poisson's ratio and the thermal expansion coefficient of the i-th layer.

For this problem, variational solutions are obtined by the preceding solution scheme using polynomial expansions of the fifith order in the thickness coorinate, and the results are shown by solid curves in Figs. 1-4, where the axial coordinate x originates from the center of the beam and is normalized with respect to the half-length a = 15.24 mm. These results are in better agreement witb Glaser's finite-element solution (shown by the scatterd open square marks in the figures) than the previous varational solution based on cubic polynomial stress function (Yin, 1991a, indicated by broken curves). Appreciable discrepancies between the third-order and fifth-order variational solutions are confined to a very short end interval of the interface with a length smaller than the thicknesses of the adjacent layers.

We next consider a bimetal thermostat previously studied by Suhir (1986, 1989) and more recently by Kuo (1989), which has the following geometrical and material parameters:

h_1 = 2.54 mm, E_1 = 70.38 GPa, ν_1 = .345, α_1 = 23.6 x 10^{-6}/°C,
h_2 = 2.54 mm, E_2 = 324.7 GPa, ν_2 = .293, α_2 = 4.9 x 10^{-6}/°C.

Results for the interlaminar and axial stresses (normalized with respect to $E_2\alpha_2\Delta T$, where ΔT = 240° C is the uniform temperature load) based on polynomial stress functions of the third, fourth and fifth orders are obtained and shown in Figs. 5-8. In these figures the origin of the axial coordinate has been chosen at the left end of the beam and the coordinate is normalized with respect to the layer thickness $h = h_1 = h_2$. The three sets of results for the interlaminar normal stress σ_y are all in close agreement. The peak value of the interlaminar shearing stress τ_{xy} increases with the order of the polynomial representation for the stress function, and the results suggest that, as the order increases indefinitely, the variational solutions of τ_{xy} along the interface converge to a limiting distribution which has an infinite limiting value as x approaches zero from the interior of the interface. This limiting behavior does not contradict the boundary condition of zero traction at the free edge because the intersection of the interface witb the free edge is a singular point of the stress field where the limiting values of the stresses τ_{xy} and σ_x are not unique but depend generally on the path of approach to the singular point. Analytical solutions which take into account the nature of the stress singularity do predict unbounded interlaminar normal and shearing stresses at the free edge (Kuo, 1989). Except in an extremely short interval (equal in length to a fraction of the layer thickness) adjacent to the free edge, the interlaminar stresses obtained from the variational solutions are generally in close agreement with those of the analytical solution.

Figures 7 and 8 show, respectively, the axial stresses σ_x on the lower and upper sides of the interface in the bimetal thermostat. The stresses vanish at the free edge due to the boundary condition of vanishing traction. In contrast, the elasticity solution yields unbounded values of σ_x at the free edge (Kuo, 1991). However, significant discrepancies among the variational solutions and between the variational solutions and the elasticity solution are once again restricted to an immediate neighborhood of the free edge. Outside this neighborhood, the variational solutions converge rapidly to the elasticity solution.

Figures 9 and 10 show the first derivatives of the stress functions along the interface. Let the origin of the axial coordinate x he shifted to the left end of the beam. Then, over the interval [0, x] of the interface in the new coordinate system, we have

$$\int \sigma_y \, dx = \int F'' \, dx = F'(x), \tag{8}$$

$$\int \tau_{xy} \, dx = -\int G' \, dx = -G(x). \tag{9}$$

In Fig. 9, the maximum value of $|F'|$ occurs at $x = x^* \approx 0.3h$, where h is the common thicknesses of the two layers. The interlaminar normal stress is negative in the short end intervals of length x^* and positive in the remaining portion of the interface. According to Eqs. (8) and (9), the resultant normal and shearing forces across the short segment $[0, x^*]$ of the interface are equal, respectively, to the maximum value of F' and to the value of -G at x^*. Although the three variational solutions of different polynomial orders yield significantly different results for the interlaminar stresses within the short segment, both the length of the segment, x^*, and the resultant normal and shearing forces, $F'(x^*)$ and $-G(x^*)$, are nearly independent of the order of the polynomial approximation. In other words, although the lowest-order variational solution does not provide accurate results for the interlaminar stresses in the immediate vicinity of the free edge, it does yield highly accurate results for the resultant normal and shearing forces over the short end interval of the interface where σ_y maintains the same algebraic sign. If the two-layer thermostat were subjected to a negative temperature increase, then the value of $F'(x^*)$ would be positive rather than negative and this maximum value of F' would indicate the resultant peeling action over the short end interval where the peeling stress is positive. The approximation in the variational solution results essentially in changing the distribution of interlaminar stresses in the short interval so that the solutions are continuous at x = 0 and compatible with the free-edge boundary conditions (although the elasticity solution is discontinuous at the singular point). This smoothing or redistribution of the interlaminar stresses, however, does not appreciably change the resultant normal and shearing forces in the interval $[0, x^*]$.

In real materials, stress singularities do not occur and singular interlaminar stress distributions based on the assumption of linear elasticity are invariably changed by the nonlinearity and inelastic response of the material including the effect of plasticity. Therefore, precise knowledge of the mathematical nature of the stress singularity, considered as an end result of the analysis in itself, is practically useless or irrelevant [1]. Although linear elasticity provides an elegant theory and a useful tool to the mechanician, one should only extract from it results that make sense and give rational interpretations of these results. From this point of view, a singularity of the stress field merely indicates a region of severe stress and steep stress gradient. Precise knowledge of the stress distribution within this region, if desirable, must be obtained by using more realistic models of the material behavior. However, by extending the implication of the St. Venant's principle to inelastic deformations, the elasticity solution can provide certain indications of the mutual action between a

[1] Of course, this remark is not a criticism of proper uses of singularity solutions in mechanics -- not as end results in themselves, but as intermediate mathematical tools for constructing final solutions, in the sense that Green's functions are used in the potential theory and the boundary-element analysis.

severely stressed region and the larger surrounding region. The parameters x^*, $F'(x^*)$ and $G(x^*)$, obtained in the present analysis, are *global* measures of the interaction between an end region around the interface and the surrounding region. These global measures have equal status as other precisely defined glohal measures, e.g., the path-independent integrals used frequently in fracture mechanics. Since the first derivatives of the stresses functions at $x = x^*$ have explicit physical meanings (as resultant peeling and shearing forces over the segment $[0, x^*]$) and since their values can be obtained accurately hy lower-order variational solutions, these derivatives may be especially suitable as parameters in the failure criteria for interfacial fracture.

5. Conclusion

In the present work, we obtained variational solutions of the thermal expansion problem of two-layer and three-layer beams using high-order polynomial expansions of the stress functions with respect to the thickness coordinate. The solutions are compared with the existing analytical and numerical solutions. The results indicate rapid convergence of the variational solutions of successive orders to the elasticity solution. For most practice purposes, even the lowest-order variational solution, obtained in an earlier paper (Yin, 1991a), yields acceptable results of the interlaminar stresses. As the order of the polynomial expansion increases, the interlaminar stresses approach limiting patterns that have unbounded values as one approaches the free edge from the interior of an interface. These limiting patterns are also consistent with the elasticity solution. However, because analytical functions are used as approximating functions in the variational method, and because the free-edge condition is strictly imposed, the variational solutions of τ_{xy} and σ_x must vanish and must be continuous at the intersection of the interface with the free-edge. In contrast, the elasticity solution bas a singularity at the intersection. Hence the stress field reaches different limits depending upon the path of approach to the singularity. If one requires that τ_{xy} and σ_x along the interface be continuous at the free e 'ge, then the boundary-value problem of elasticity has no solution. The preceding differences between the elasticity solution and the variational solutions in the extremely small immediate neighborhood of the singularity have no physical significance because stress singularities do not occur in real materials.

Althouh the interlaminar stresses obtained from the variational solutions of different orders show significant discrepancies in a short interval adjacent to the interface, their resultant forces over the interval are in excellent agreement. These resultant forces are given by the first derivatives of the stress functions. They are global measures of the mutual action between a region of stress concentration around an end segment of the interface and the larger surrounding region. Like other global measures examplified by path-independent integrals, they are appropriate parameters in the failure criteria for interfacial fracture.

The variational method of solution used in the present work is efficient and reliahle. The computer program, presently developed for the analysis of two-layer beams with or without a thin adhesive layer, is extremely easy to use, because of the simplicity of data input. Furthermore, the method can be extended to deal with more general heams and laminates composed of anisotropic layers and suhjected to a comhination of thermal and mechanical loads, including extension, bending and twisting of the laminates (Yin, 1991b), so long as the geometry and stresses are constant in the z-direction (the direction perpendicular to the x-y plane). A multi-layered beam or laminate can be analyzed by a substructure approach in which two interior layers adjacent to a given interface are treated as distinct elastic media while the remaining layers are grouped into upper and lower sublaminates. Such general problems with practical importance defy analytical methods of solution and even finite-element modeling (without using a substructure approach) when the number of layers becomes large. The present analysis method, when properly modified, provides the answers with a minimum amount of computational effort.

Acknowledgment This work was made possible by a grant from the Army Research Office to Georgia Institute of Technology. The author gratefully appreciates the financial support.

References

Bogy, D. B., 1968, "Edge-Bonded Dissimilar Orthogonal Elastic Wedges Under Normal and Shear Loading," *ASME J. Appl. Mech.*, Vol. 35, pp. 460-466.

Bogy, D. B., 1970, "On the Problem of Edge-Bonded Elastic Quarter-Planes Loaded at the Boundary," *Int. J. Solids Struct.*, Vol. 6, pp. 1287-1313.

Glaser, J.C., 1989, "Thermal Stresses in Compliantly-Joined Materials," ASME Winter Annual Meeting, Paper No. 89-WA/EEP-14, San Francisco, CA, December 1989, 7 pages.

Kuo, A.-Y., 1989, "Thermal Stresses at the Edge of a Bimetallic Thermostat," *ASME J. Appl. Mech.*, Vol. 56, pp. 585-589.

Suhir, E., 1986, "Stresses in Bi-Metal Thermostats," *ASME J. Appl. Mech.*, Vol. 53, pp. 657-660.

Suhir, E., 1989, "Interfacial Stresses in Bimetal Thermostats," *ASME J. Appl. Mech.*, pp. 595-600.

Yin, W.-L., 1991a, "Thermal Stresses and Free-Edge Effects in Laminated Beams: A Variational Approach Using Stress Functions," *ASME J. Electronic Packaging*, Vol. 113, pp. 68-75.

Yin, W.-L., 1991b, "Free-Edge Effects in Laminates Under Extension, Bending and Twisting, Part I: A Stress Function Approach", *Proc. AIAA/ASME/ASCE/AHS/ASC 32nd SDM Conference*, pp. 985-995, April, 1991, Baltimore, MD.

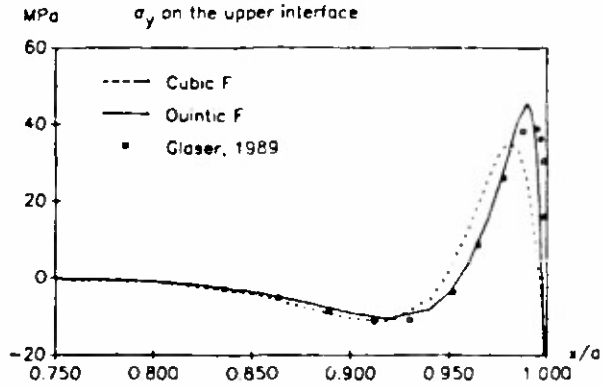

Figure 1

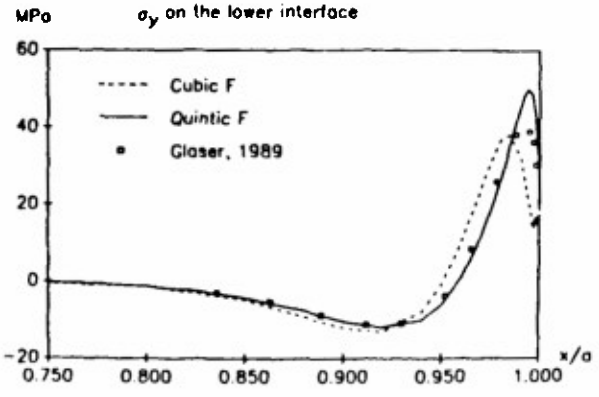

Figure 2

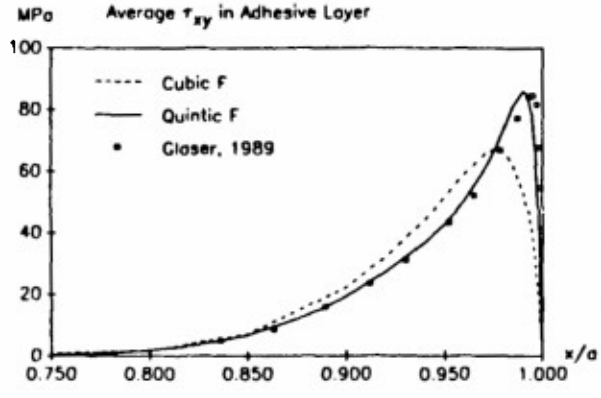

Figure 3

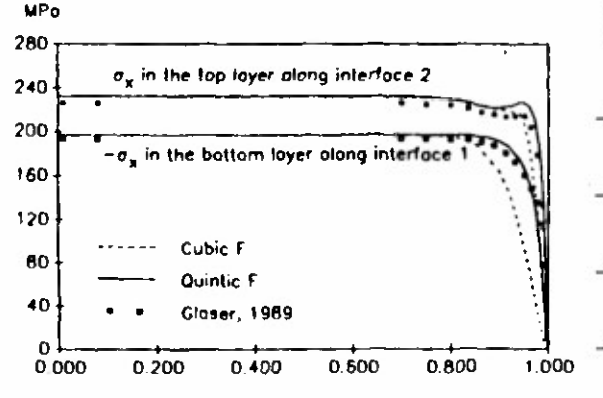

Figure 4

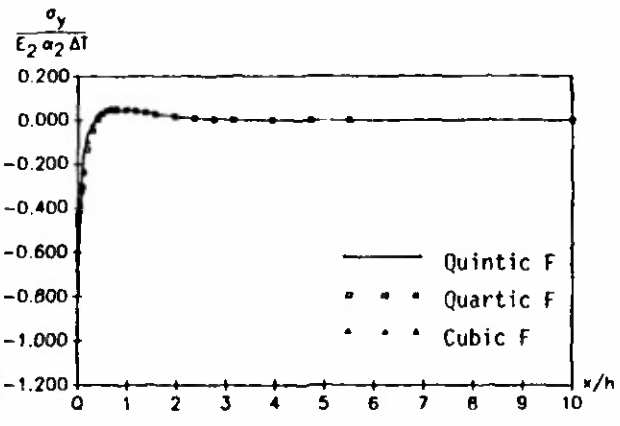

Figure 5

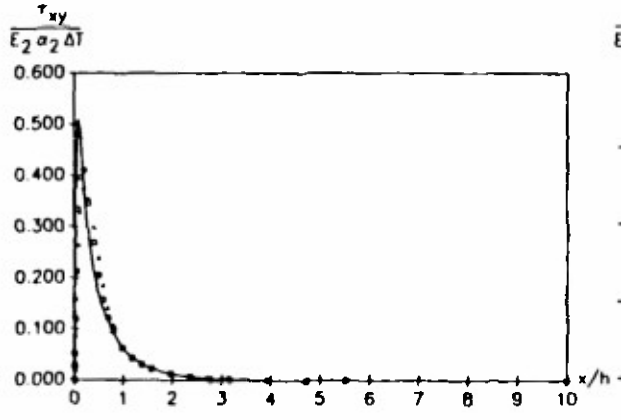

Figure 6

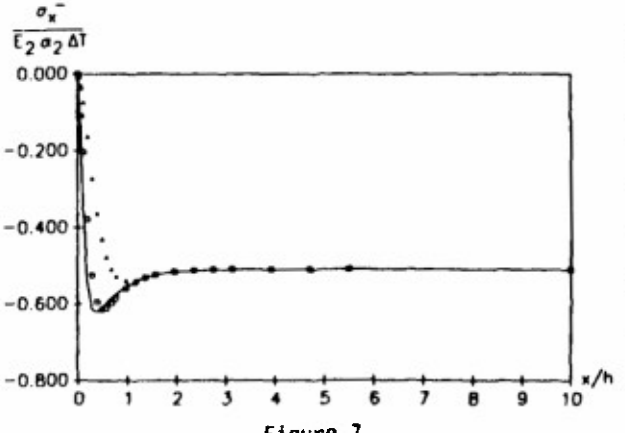

Figure 7

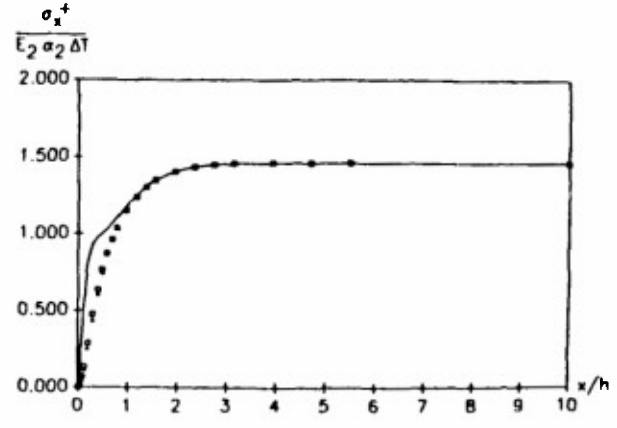

Figure 8

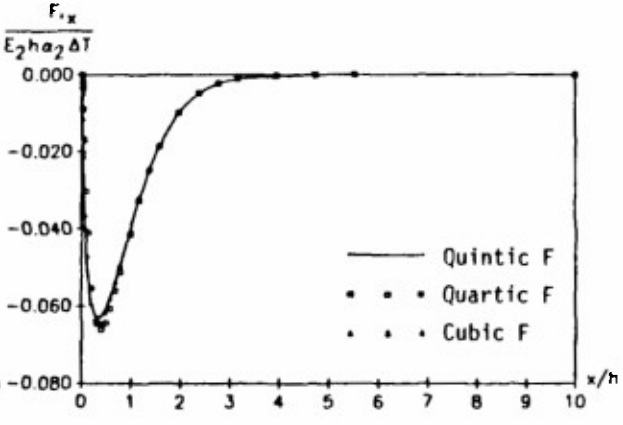

Figure 9

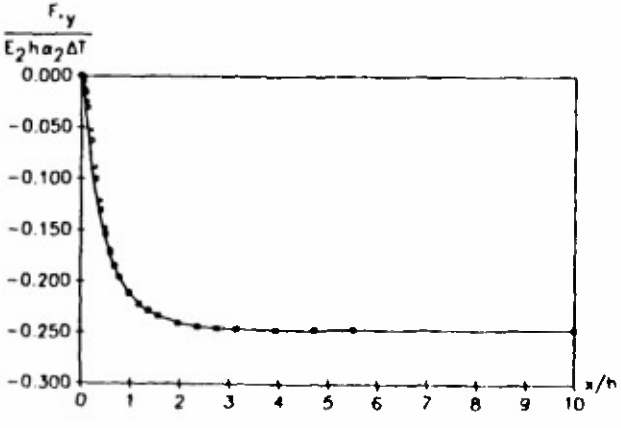

Figure 10